Missouri S&T Library and Learning Resources

Scholars' Mine

Doctoral Dissertations | Student Theses and Dissertations

Fall 2013

Gas dynamics and heat transfer in a packed pebble-bed reactor for the 4th generation nuclear energy

Rahman Abdulmohsin

Follow this and additional works at: https://scholarsmine.mst.edu/doctoral_dissertations

 Part of the Chemical Engineering Commons

Department: Chemical and Biochemical Engineering

Recommended Citation

Abdulmohsin, Rahman, "Gas dynamics and heat transfer in a packed pebble-bed reactor for the 4th generation nuclear energy" (2013). *Doctoral Dissertations*. 2178.
https://scholarsmine.mst.edu/doctoral_dissertations/2178

This thesis is brought to you by Scholars' Mine, a service of the Missouri S&T Library and Learning Resources. This work is protected by U. S. Copyright Law. Unauthorized use including reproduction for redistribution requires the permission of the copyright holder. For more information, please contact scholarsmine@mst.edu.

GAS DYNAMICS AND HEAT TRANSFER IN A PACKED PEBBLE-BED REACTOR FOR THE 4TH GENERATION NUCLEAR ENERGY

by

RAHMAN ABDULMOHSIN

A DISSERTATION

Presented to the Faculty of the Graduate School of the

MISSOURI UNIVERSITY OF SCIENCE AND TECHNOLOGY

In Partial Fulfillment of the Requirements for the Degree

DOCTOR OF PHILOSOPHY

in

CHEMICAL ENGINEERING

2013

Approved by
Muthanna Al-Dahhan, Advisor
Athanasios Liapis
Pathasakha Neogi
Joseph Smith
Gary Mueller

© 2013
Rahman Abdulmohsin
All Rights Reserved

ABSTRACT

Proper analyses of axial dispersion and mixing of the coolant gas flow and heat transport phenomena in the dynamic core of nuclear pebble-bed reactors pose extreme challenges to the safe design and efficient operation of these packed pebble-bed reactors.

The main objectives of the present work are advancing the knowledge of the coolant gas dispersion and extent of mixing and the convective heat transfer coefficients in the studied packed pebble-beds. The study also provides the needed benchmark data for modeling and simulation validation. Hence, a separate effect pilot-plant scale and cold-flow experimental setup was designed, developed and used to carry out for the first time such experimental investigations. Advanced gaseous tracer technique was developed and utilized to measure in a cold-flow packed pebble-bed unit the residence time distributions (RTD) of the gas phase. A novel sophisticated fast-response and non-invasive heat transfer probe of spherical type was developed and utilized to measure in a cold-flow packed pebble-bed unit the solid-gas convective heat transfer coefficients. The non-ideal flow of the gas phase in pebble bed was described using one-dimensional axial dispersion model (ADM), tanks-in-series (T-I-S) model and central moments analyses (CMA) method. Some of the findings of this study are:

- The flow pattern of the gas phase does not much deviate from the idealized plug-flow condition which depends on the gas flow rate and bed structure of the pebble-bed.
- The non-uniformity of gas flow in the studied packed pebble bed can be described adequately by the axial dispersion model (ADM) at different Reynolds numbers covers laminar and turbulent flow conditions. This has been further confirmed by the results of tanks in series (T-I-S) model and the central moment analyses (CMA).
- The obtained results indicate that pebbles size and hence the bed structure strongly affects axial dispersion and mixing of the flowing coolant gas while the effect of bed height is negligible in packed pebble-bed. At high range of gas velocities, the change in heat transfer coefficients with respect to the gas velocity reduces as compared to these at low and medium range of gas velocities.
- The increase of coolant gas flow velocity causes an increase in the heat transfer coefficient and the effect of gas flow rate varies from laminar to turbulent flow regimes at all radial positions of the studied packed pebble-bed reactor.
- The results show that the local heat transfer coefficient increases from the bed center to the wall due to the change in the bed structure and hence in the flow pattern of the coolant gas.
- The results and findings clearly indicate that one value as overall heat transfer coefficient cannot represent the local heat transfer coefficients within the bed and hence correlations to predict radial and axial profiles of heat transfer coefficient are needed.

ACKNOWLEDGMENTS

First and foremost, thanks and praises to GOD for his kindness and blessing.

I would like to express my sincere gratefulness to my advisor, Prof. Muthanna Al-Dahhan. He has catalyzed my work with his enthusiasm, encouragement and advice, and I thank him for giving me the chance of pursuing my studies at Missouri S&T. He has taught me how to think when facing research problems and how to tackle it. His technical and non-technical advice was invaluable to me in my professional and personal life. I also would like to thank him for helping me to attend different conferences from which I gained valuable experience.

I want to extend my thanks to all members of my dissertation examination committee, for their time and for serving on my committee. They have provided very critical comments and brought-up helpful fundamental questions during my proposal which I seriously considered later and which brought up new perspectives to this work.

This work would have not been possible without the continuous financial support of the very high temperature reactor (VHTR) consortium [U.S. Department of Energy (DOE)-Nuclear Energy Research Initiative (NERI) project (NERI-08-043)] and the fellowship from Graduate Assistantship Areas of National Need (GAANN) program for last year.

I am thankful for all Dr. Al-Dahhan's research group for all the enjoyable discussions we had on different scientific and non-scientific issues. I would also like to thank those who helped me with the manufacturing and the building of the experimental setups, Mr. Dean Lenz. His technical support was invaluable.

Special thanks are due back home to all my family members for their support and encouragement throughout the years. Finally, a warm thanks to my lovely wife, Rania, who stood by my side during the ups and downs, for believing in me and for supporting my ideas and dreams. She was always the breath of fresh air that sailed me through my long Ph.D. Journey. No words can describe her, so, thanks or better SHOKRAN!

Rahman Abdulmohsin

Missouri University of Science and Technology, Rolla / MO-USA, November 2013

TABLE OF CONTENTS

LIST OF ILLUSTRATIONS

LIST OF TABLES

NOMENCLATURE

Symbol	Description
C	concentration of the tracer in the gas phase, mol/m^3
C_{inj}	concentration of the injection tracer, mol/m^3
C_{in}	dimensionless tracer concentration in the gas phase at the plenum outlet
C_{in}^*	dimensionless convoluted tracer concentration in the gas at plenum outlet
C_{out}	dimensionless tracer concentration in the gas phase at the reactor outlet
C_{out}^*	dimensionless convoluted tracer concentration in the gas at reactor outlet
d_h	effective (hydraulic) pebble diameter, m
d_p	pebble diameter, m
D_{AB}	molecular diffusion coefficient, m^2/s
D_c	column diameter, m
D_{ax}	effective axial dispersion coefficient of the gas phase, m^2/s
L	length of the bed (not the column), m
M	total mass of injected tracer, gm
n	total number of experimental data points, Eqn. 5.2
N	the data point number, Eqn.5.4
Q	volumetric flow rate of injected tracer, cm^3/s
t	time, s
t_m	mean residence time of the bed, s
V_T	total bed volume, cm^3
V	interstitial gas velocity (= V_g/ε), m/s
V_g	superficial gas velocity based on empty column, m/s
z	axial distance along the bed, m
Z	axial distance along the bed, m

Greek Letters

β	constant in Eqn. 2.8
Υ	tortuosity factor
τ_o	residence time in the plenum, s

ε_b	voidage of bed (porosity), dimensionless
ε_b	average (mean) voidage of bed , dimensionless
μ	dynamic viscosity of the fluid, Kg.m/s
ρ	density of fluid, kg/m^3

Dimensionless Groups

Nu	Nusselt number ($=hd_p/k$), dimensionless
Nu_h	effective Nusselt number [$=hd_h/k= \varepsilon Nu/(1-\varepsilon)$], dimensionless
Pe_D	dispersive Peclet number ($= V_g d_p/\varepsilon D_{ax}$), dimensionless
Pe_M	molecular Peclet number ($=Re_P Sc= V_g d_p/\varepsilon D_{AB}$), dimensionless
Pr	Prandtl number ($=\mu C_p/k$), dimensionless
Re	Reynolds number ($= \rho V_g d_p/\mu$) , dimensionless
Re_P	particle Reynolds number ($=\rho V_g d_p/\varepsilon\mu = Re/\varepsilon$), dimensionless
Re_h	effective Reynolds number [$=\rho V d_h/\mu=Re/(1-\varepsilon)$], dimensionless
Sc	Schmidt number ($=\mu/\rho D$), dimensionless

List of Abbreviations

AARE	average absolute relative error
ADM	axial dispersion model
CFD	computational fluid dynamics
CMA	central moments analyses
CSTR	continuous stirred tank reactor
Gen IV	4^{th} generation of nuclear reactors
GIF	generation IV international forum
GFR	gas-cooled fast reactor
HTGR	high temperature gas-cooled reactor
HTR	high temperature reactor
HTTF	heat transfer test facility
HWA	hot-wire anemometry
IEO	International Energy Outlook
INEEL	Idaho National Engineering and Environmental Laboratory

INL	Idaho National Laboratory
KTA	German nuclear safety standard commission (Kerntechnischer Ausschuss)
LDA	laser doppler anemometry
LFR	lead-cooled fast reactor
MIR	matched index of refraction
MIT	Massachusetts Institute of Technology
MSR	molten salt reactor
NGNP	next generation nuclear plant
NMR	nuclear magnetic resonance
PBR	pebble bed reactor
PEBBED	multi-scale simulation and optimization of BPRs code
PFR	plug-flow reactor
PIV	particle image velocimetry
PMMA	polymethyl-methacrylate
RTD	residence time distribution
SCWR	supercritical-water-cooled reactor
SFR	sodium-cooled fast reactor
US DOE	Untied States department of energy
VDI	German Engineers Association (Verein Deutscher Ingenieur)
VHTR	very high temperature reactor

1. INTRODUCTION AND OBJECTIVES

1.1. OVERVIEW

The world energy demand is rising sharply with increasing population and a higher standard of living. According to the International Energy Outlook (IEO) 2011, the total world energy consumption is projected to increase by 53% by 2035 (Figure 1.1, Part a), if the present laws and policies remain unchanged (EIA, 2011). If the present energy mix remains the same and if it is simply expanded proportionally to meet the future demand, the adverse effects due to the production of greenhouse gas on global climate change will be intensified. To fulfill the future demand without producing the adverse effects on the global climate and environment, energy supply must be increased in the total energy mix which should come from safe, clean, and cost-effective energy sources.

Commercial nuclear energy is proving to be the most environmentally "green" way of producing electrical power on a very large scale. Because of its environmental advantages, safety record and high power density, nuclear energy use will continue to be an integral part of the overall worldwide energy mix which will provide independent and stable energy security for many nations. In addition, nuclear energy minimizes the carbon dioxide emissions into the environment, which have become a recognized component contributing to global climate change. Therefore, nuclear power plays an important role in meeting energy needs while achieving security of supply and minimizing carbon dioxide emissions. Most nuclear reactors that are currently being planned are in Asia, where there are fast-growing economies and a rapidly rising electricity demand. More than fifteen countries rely on nuclear power for 25% or more of their electricity. Today there are some 439 nuclear power reactors operating in thirty countries and generating

14% of total electricity production (see Figure 1.1, Part b). This is the largest portion of the total electricity production that comes from non-greenhouse gas-producing sources (US DOE, 2002).

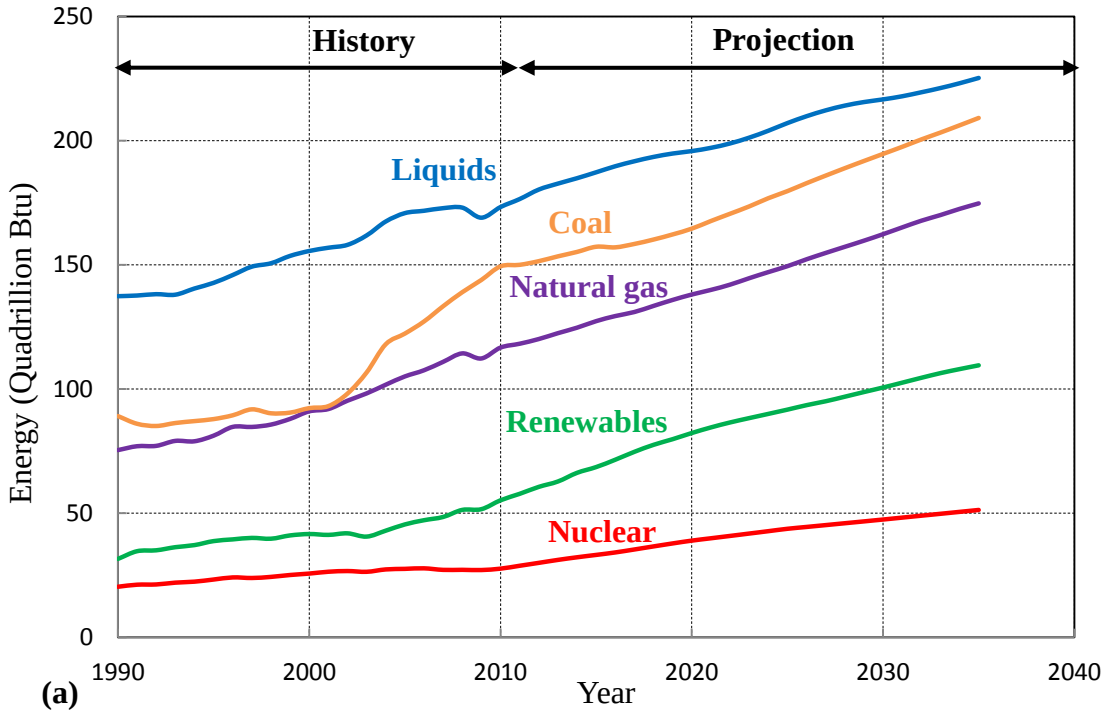

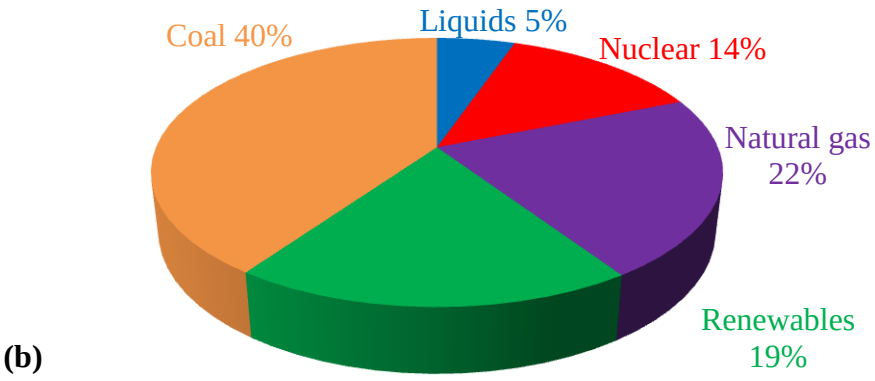

Figure 1.1. World Projected Energy Consumption and Electricity Production: (a) World Marketed Energy Use by Fuel Type; (b) Present Electricity Production by Fuel Type (EIA, 2011)

1.2. WHY IS A NEXT GENERATION NUCLEAR PLANT NEEDED?

To achieve sustainability, high economics and efficiency, enhanced safety, reliability, waste minimization, proliferation-resistance, and still be environmentally friendly, the Generation IV International Forum (GIF) was initiated in 2000 for the development of fourth generation (Gen IV) nuclear power plants (US DOE, 2002). The thirteen current members of the GIF guide the collaborative efforts of the world's leading nuclear technology nations to develop these nuclear energy systems. The technology roadmap produced by the GIF (EIA, 2011) for long-term research projects resulted in proposals for six nuclear reactor technologies called Gen IV nuclear reactors, as listed in Table 1.1. The six most promising reactor concepts were selected on the basis of their ability to provide a reliable and safe energy system together with reduced nuclear waste production and increased economic competitiveness.

The next generation nuclear plants (NGNP), or the 4^{th} generation (Gen IV) nuclear reactors, will fulfill the future energy demand and environmental needs. In addition, they can be used to produce hydrogen and process heat for industrial needs. The very high temperature reactor (VHTR) is one of these six advanced concepts for Gen IV nuclear reactors that are being considered for electric power, to process heat, and for hydrogen production. The VHTR is a continuation and optimization of the present high temperature gas-cooled reactor (HTGR) designs, with the aim of reaching a coolant outlet temperature of around 1000 °C or above, which would increase reactor performance. The core configuration of VHTR can be a pebble-bed type or a prismatic-block type, according to the fuel elements assembly. An annulus filled with mobile fuel-spheres is used in the core of the pebble-bed reactor (PBR), while a hexagonal prismatic fuel-blocks core configuration is used for the prismatic-block reactor. Both pebble- fuel type and

prismatic -block type are still considered for the NGNP design with a once-through low-enriched uranium fuel cycle at a high burn up value. Thus, the focus of this work is on studying the gas dispersion and heat transfer phenomena related to pebble-bed reactors.

Table 1.1. Gen IV Nuclear Reactors Selected by GIF

Gen IV System	Acronym	Neutron Spectrum	Coolant	Temperature (^{o}C)	Fuel Cycle	Size (MWe)
Gas-cooled fast reactor	GFR	fast	helium	850	closed	1200
Lead-cooled fast reactor	LFR	fast	lead	480–800	closed	300–1200 600–1000
Sodium-cooled fast reactor	SFR	fast	sodium	550	closed	30–150 300–1500 1000–2000
Molten salt reactor	MSR	thermal/ fast	fluoride salts	700–800	closed	1000
Supercritical-water-cooled reactor	SCWR	thermal/ fast	water	510–625	open/ closed	300-700 1000–1500
Very-high temperature reactor	VHTR	thermal	helium	900-1000	open	250–300

1.3. DESCRIPTION OF THE PEBBLE-BED REACTOR

The pebble bed reactor gets its name from the type of nuclear fuel it consumes, and it offers many advantages over conventional reactors. A pebble bed-type of very-high

temperature gas-cooled reactor (VHTR) is one of the most probable solutions (Goodjohn, 1991) and the most promising concepts (Koster et al., 2003) of the six classes of generation IV advanced technologies. The pebble bed reactor concept is adopted by many test and demonstration reactors, including the modular pebble bed reactor (MPBR) in the United States (Kadak and Berte, 2001) and the prototype reactor of the pebble bed modular reactor (PBMR) in South Africa (Koster et al., 2003; Terry et al., 2001), the 10-MWt high temperature reactor (HTR-10) in China (Wang and Lu, 2002; Xu and Sun, 1997), and the prototype pebble bed reactor at Jülich research centre in Germany that is known as Arbeitsgemeinschaft Versuchsreaktor (AVR, translates to experimental reactor consortium) early in the 1960s, (Schulten, 1978; Frewer et al., 1985; Lohnert and Reutler, 1983).

In general, the pebble bed reactor is a pyrolytic graphite-moderated and helium gas-cooled nuclear reactor that achieves a requisite high outlet temperature while retaining the passive safety and proliferation resistance requirements of Gen IV designs (Gougar et al, 2003). A schematic of a pebble bed reactor is shown in Figure 1.2.

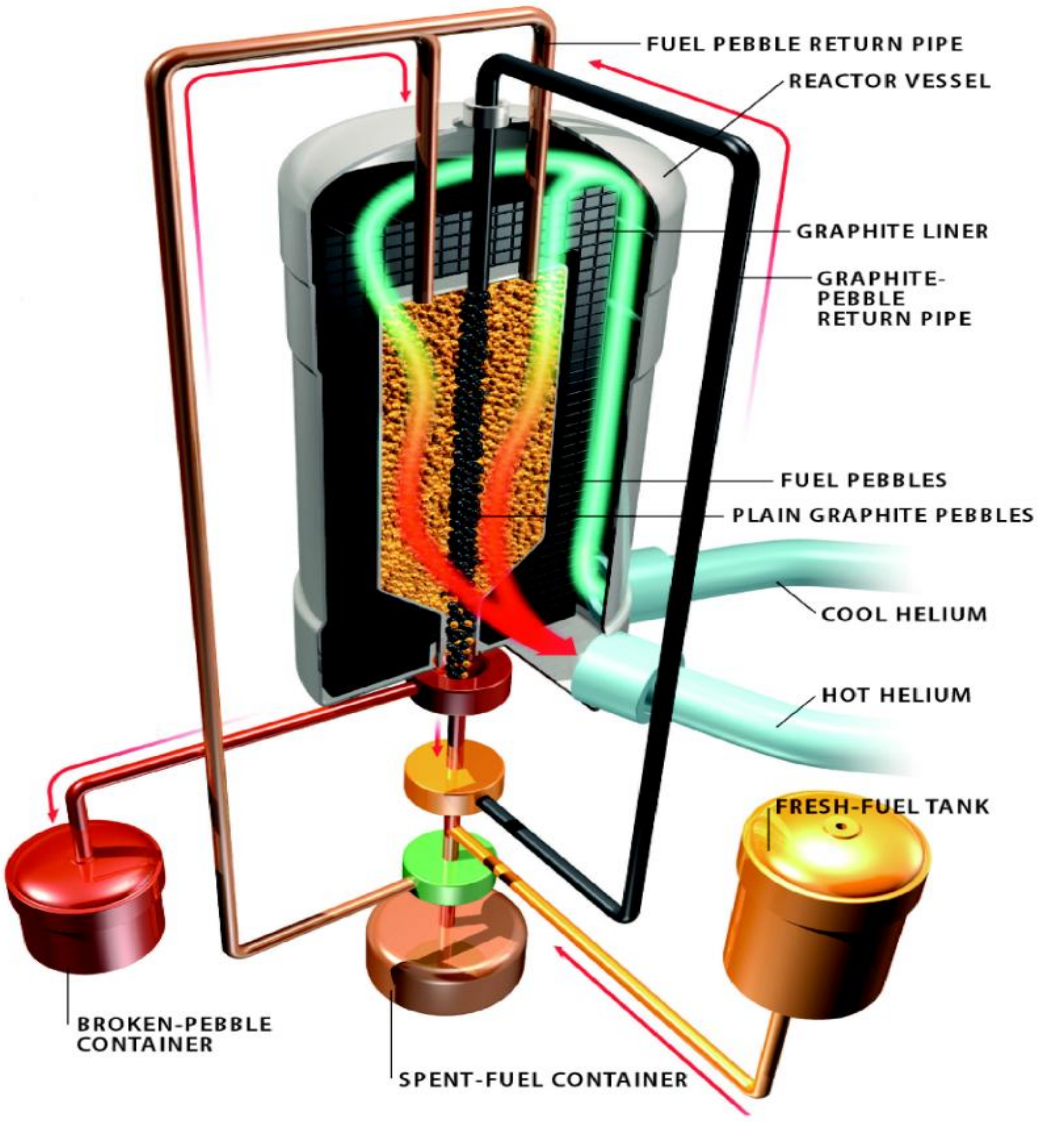

Figure 1.2. A Schematic Diagram of the Pebble-Bed Nuclear Reactor (Rycroft, 2007)

In this reactor, the core has a “double-zone” configuration, i.e., there are two cores, an inner blind core of graphite spheres at the center and an outer annular active core with fuel spheres. The graphite spheres acts both as a structural material and as a moderator. The fuel and graphite spheres, called pebbles, are approximately the size of a

tennis ball (usually about 6 cm in diameter). Both the fuel and graphite pebbles are made from graphite and other carbon based materials and they have almost a similar shape and average density (1.85 gm/cm^3), except that the fuel pebbles in a graphite matrix contain a large amount of uranium particles (about 11,000 particles) (Li et al, 2009). In the core of the nuclear pebble-bed reactor, hundreds of thousands of microspheres of coated particles (about 900-950 microns in diameter) known as TRISO (tri-structural isotropic) fuel particles are embedded within a graphite matrix to form a final fuel pebble and act as a pressure vessel. The TRISO coated fuel particles cause fission in a graphite pebble (Lee and Lee, 2009), and due to their high surface/volume ratio, TRISO fuel particles easily transfer heat from fuel to matrix graphite. A schematic sketch of a typical microstructure of the TRISO fuel particle is shown in Figure 1.3.

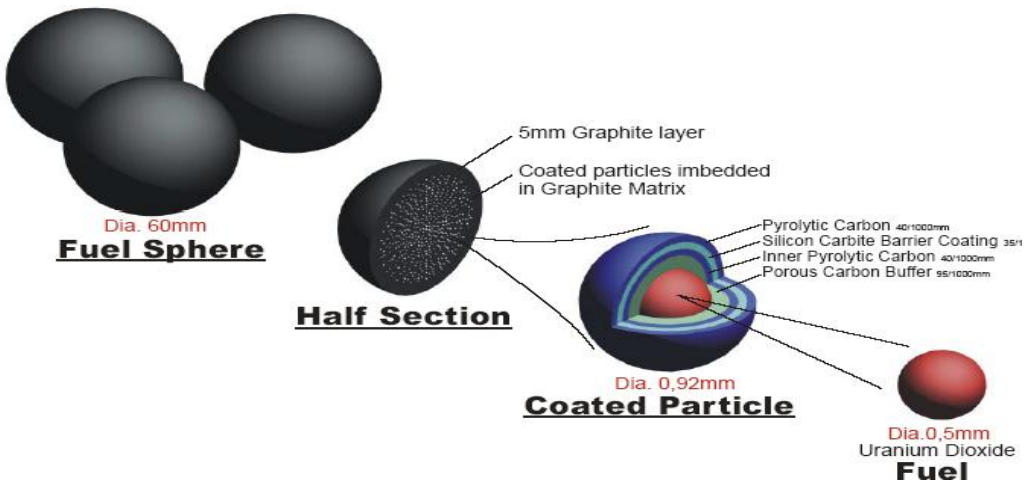

Figure 1.3. A Schematic Sketch of the Typical Microstructure for the TRISO Fuel Particles in Pebble-Bed Reactor

Each TRISO fuel particle consists of a spherical fuel kernel (~ 0.5 mm) composed of low-enriched uranium dioxide (UO_2), sometimes uranium oxycarbide (UCO) in the center, coated with four concentric layers of three isotropic materials. The four layers are: (1) a porous buffer layer made of carbon of low density that serves to capture any fission product particles emitted from the fuel kernel, (2) a dense inner layer of pyrolytic carbon (PyC) of high density, (3) a ceramic layer of polycrystalline silicon carbide (SiC) to retain fission products at elevated temperatures and to give the TRISO particles more structural integrity, (4) another dense outer layer of pyrolytic carbon (PyC). Microspheres of TRISO fuel particles are designed not to crack as a result of stress from processes (such as differential thermal expansion or fission gas pressure), even at temperatures beyond 1600°C.

The fuel and graphite pebbles move downward by gravitational force through the reactor core in the form of a very slowly moving pebble bed (at the rate of less than one pebble per minute). The pebbles stack inside the reactor, so older ones are removed from the bottom, inspected for burn-up and mechanical integrity, and re-circulated into the top of the reactor core until it achieves the specified high discharge burn up. While this unique feature of moving pebbles and dynamic core provide advantages of variations in packing, physics and heat removal and hence would allow more complete fission, the transport phenomena and physical processes involved are extremely complex mechanisms in this type of reactor (Abdulmohsin and Al-Dahhan, 2012). In the annular active core, heat generated from the nuclear fission reaction and decay heat from fission products inside the fuel spheres are removed by the forced circulation of the pressurized (typically up to 8.5 MPa) coolant helium gas (~ 500 ^{o}C inlet core temperature). The

elevated static pressure and the large pebble diameter cause high values of the Reynolds number (up to about 4.5×10^4) , under normal operating conditions, which exceed those usually occurring in the conventional technology by one order of magnitude. Helium gas is chosen as a coolant in VHTRs because of its excellent heat exchange properties and because it is both chemically and radiologically inert and, does not undergo a phase change. In addition, it is naturally available in sufficient quantities (Huda and Obara, 2008). It is worth mentioning here that an axial core down flow of the coolant removes the problem of bed levitation that would limit the power density of the reactor (Claxton, 1966). In a PBR core, the coolant flow structure, and hence the heat removed, appears to be strongly dependent on the distribution of the moving fuel pebbles. As the helium gas flows downward under high flow conditions (relatively high Reynolds numbers of about 50,000) through the reactor core and over these heated, randomly and closely distributed pebbles, combined with the high temperature integrity of the fuel and structural graphite, the coolant gas attains a very high temperature at the core outlet (~ 900^oC). This is one of the attractive features because the high operating temperature allows a higher thermal efficiency to be yielded (it is possible to extract up to about 50% or a little more) than what would be rendered by conventional nuclear plants (typically between 35-40%), and it can be used in various industrial processes. For example, the high temperature helium gas can be used for the production of industrial process heat and hydrogen, which in turn can be used for treating metals, processing food, as well as creating an alternative fuel source in the form of hydrogen fuel cells. In addition, the reactor can be cooled by natural circulation and still survive in accident scenarios, that might raise the temperature of the reactor to 1600 °C. The bed structure, coolant flow dynamics, pressure drop and heat

transport, which determine the thermal-hydraulic characteristics of a reactor, are among the essential phenomena that need to be well understood for proper design and safe performance of these reactors. The advantages and disadvantages of nuclear pebble bed reactors are summarized in Table 1.2.

Table 1.2. Advantages and Disadvantages of Pebble Bed Reactors

Pros	Cons
The moving fuel pebbles provide variations in packing, physics, and heat removal.	Moving bed of complex-flow structure and path.
Inherent safety due to fuel type and gas coolant; hence a negative temperature coefficient is achieved, which means that if the temperature rises, the nuclear reaction is slowed and the power is reduced.	Due to the system complexity, extremely complex transport and processes are involved.
High outlet gas temperature yields higher thermal efficiency.	Accurate analyses of flow-field and heat transport in the dynamic core pose an extreme challenge to the efficient design and safe operation.
High heat capacity and low power density	
Unlike conventional nuclear reactors, pebble bed reactors do not need to be shutdown in order to check on the integrity and consumption of uranium and to be refueled; this is due to on-line refueling.	
Promises to generate less nuclear waste	
The design produces a small reactor that can be built cheaply with short construction time and operated safely.	
The pebbles are supposed to survive temperatures of 1600 °C, far hotter than the worst foreseeable accident.	

1.4. MOTIVATION FOR THE PRESENT STUDY

In order to reliably simulate the thermal-hydraulics phenomena and hence the performance in the dynamic core of nuclear packed-pebble bed reactors, the coolant gas

dynamics and heat transport processes must be characterized (Abdulmohsin and Al-Dahhan, 2011a; 2011b; 2012). In addition, the experimental investigation of the thermal hydraulic characteristics of pebble beds is an issue of high importance while selecting the core geometry and evaluating the performance and safety of such kind of reactors (Rimkevicius and Uspuras, 2008). The efficiency of the pebble bed reactor is strongly dependent upon how the coolant removes the generated heat from the dynamic core of this reactor. Furthermore, the knowledge of dispersion and mixing in the longitudinal direction is most important when temperatures are rapidly changing with respect to time or axial coordinate due to nuclear reaction and interphase heat transport. *Unfortunately, there are no reported studies in the literature about the knowledge and quantification of the complex coolant gas flow structure and dynamics in pebble bed nuclear reactor.*

On the other hand, the local fuel temperatures depend not only on the local power generation but on the point heat removal rate. In other words, the heat removal has been considered as a one of the three fundamental safety functions in high temperature gas-cooled reactors (HTGRs). Hence, the detailed information and proper understanding of the transport of heat generated during nuclear fission from slowly moving hot fuel pebbles to the flowing coolant gas is crucial for the safe design and efficient operation of packed-pebble bed nuclear reactors. All three modes of heat transport (i.e., conduction, convection, and radiation) are important for the modeling and predicting the pebble-bed core temperature distribution. During nominal operation of the reactor at relatively high Reynolds numbers, the heat transfer mechanism is governed by the forced convection mode. At low Reynolds numbers (the case of an accident), effects of free convection, thermal radiation, heat conduction, and heat dispersion come into the same order of

magnitude as the contribution of the forced convection (Fenech, 1981). However, little information related to the pebble-to-coolant gas heat transfer is available in the literature and this process has not yet been fully understood (Stainsby et al, 2010; Abdulmohsin et at., 2011; Abdulmohsin and Al-Dahhan, 2012). In addition to that, detailed experimental investigations that benchmark the simulation methods, computer codes and theoretical approaches are still lacking. Furthermore, there are no cold-flow separate effects experimental setups that can be used with advanced measurement techniques capable of investigating the coolant gas dynamics and heat transport processes encountered in the core of the pebble bed.

Accordingly, using sophisticated measurement techniques, the present study systematically and simultaneously investigates in a pilot-plant scale cold-flow setup the gas dynamics, pressure drop, and heat transport. In addition, a comprehensive integral study assessing the impact of bed structure on gaseous coolant dynamics and heat transport processes will be conducted, which will provide crucial information from a safety perspective. While the obtained knowledge will advance the thorough understanding of the coolant gas dynamics and heat transport of packed pebble-bed nuclear reactors, the study will also provide the needed benchmark data for modeling and simulation validation. *Hence, such study will be among the first systematic investigation to be conducted simultaneously of coolant gas dispersion and mixing and heat transfer phenomena.*

1.5. OBJECTIVES OF THE PRESENT STUDY

The major thrust of this work is to advance the knowledge and the fundamental understanding of the dynamics of coolant gas and the heat transport phenomena in

packed pebble-bed nuclear reactors. In order to achieve this, the following tasks are set for this work:

1.5.1. Development of Separate Effects Experimental Setup and Sophisticated Measurement Techniques. A separate effect pilot-scale experimental setup will be designed, developed and used for carrying out the experimental investigations. This separate effects setup is a cold-flow model of a packed pebble-bed that is designed to conduct gas tracer measurements, pressure drop, and heat transfer investigations. Three sophisticated measurement techniques will be developed, which are a gaseous tracer technique, two types of heat transfer probes (rod and sphere mimicking the pebble), and a differential pressure transducer.

1.5.2. Gas Dynamics Study. This task consists of the following:

(a) Development and implementation of a sophisticated gaseous tracer technique that includes all the needed mathematical models and programs.

(b) Investigating the effects of the following variables in a 0.3 m diameter packed pebble-bed unit on the coolant gas dispersion and mixing phenomena, using the sophisticated gaseous tracer technique in which air is used as the gas phase while helium is used as the tracer:

1. Gas flow rate: a wide range of superficial gas velocities (0.01 m/s to 2 m/s), covering the conditions of both laminar and turbulent flow regimes.
2. Pebble size: pebbles of three different sizes (1.25 cm, 2.5 cm, and 5 cm).
3. Bed height: three beds of different heights (0.3 m, 0.6 m and 0.9 m).

In this task, an impulse of helium as a tracer is injected at various locations of the separate effects experimental set-up and the concentration is monitored at the outlet of the bed and at other locations as needed to deconvolute the dispersion in the external

volumes and parts of the bed. The measured residence time distributions (RTDs) will be analyzed to quantify the flow pattern and the gas dispersion and how these vary with the change in the variables mentioned above. This can be done by fitting the RTDs to the axial dispersion model (ADM) and the tank-in-series (T-I-S) model to quantify the level of dispersion.

In addition, a statistical central moment analysis-based method will be performed to analyze the residence time distributions of coolant gas in the studied packed-pebble bed reactor to estimate the mean residence time (1^{st} moment), degree of spreading or variance (2^{nd} moment) and asymmetry or skewness (3^{rd} moment), and to identify how far the flow is from the ideal plug flow and if there is any channeling, bypass, stagnancy, etc.

Since there is no study reported in the literature related to the RTD of the coolant gas in pebble bed reactors, there is no correlation that has been reported to predict the axial dispersion of the gas in pebble bed reactors. Therefore, the correlations reported in the literature for predicting of the axial gas dispersion in chemical packed bed reactors of small particles will be evaluated against the data obtained from this task for packed pebble-beds of large pebble diameter as a first attempt.

1.5.3. Pressure Drop Measurements. This task consists of the following:

(a) Development of a differential pressure transducer technique to measure pressure drop along the height of the pebbles.

(b) Investigating the effect of the following variables in a 0.3 m diameter packed pebble-bed unit on the pressure drop using air as the gas phase:

1. Gas flow rate: a wide range of superficial gas velocities (0.01 m/s to 2 m/s), covering laminar and turbulent flow regimes.
2. Pebble size: three beds of different particle sizes (1.25 cm, 2.5 cm, and 5 cm).

Based on the insight gained from the experimental measurements, the available reported correlations will be evaluated for their ability to predict the pressure drop in pebble bed reactors.

1.5.4. Heat Transfer Investigations. This task consists of the following:

(a) Development of two sophisticated and fast-response heat transfer techniques; one is of a rod-type (an invasive technique) as a first step and another one is of a spherical-type that mimics the pebbles of 5 cm in diameter (a non-invasive technique).

(b) Investigating the effects of the following variables in a 0.3 m diameter packed pebble-bed unit on the heat transfer coefficient and its radial profile at different axial positions using air as the gas phase:

1. Gas flow rate: a wide range of superficial gas velocities (0.01 m/s to 2 m/s), covering laminar and turbulent flow regimes.
2. Bed height: three beds of different heights (0.3 m, 0.6 m and 0.9 m).
3. Pebble size: three beds of different particle sizes (1.25 cm, 2.5 cm and 5 cm).

For pebble size of 5 cm, both rod and spherical-type probes have been used. However, for pebbles of 1.25 cm and 2.5 cm only the rod-type probe technique will be used.

Based on the insight gained from the experimental measurements the available reported empirical correlations will be assessed for their ability to predict the convective heat transfer coefficients in the studied pebble beds.

1.6. DISSERTATION STRUCTURE

This dissertation consists of the following sections:

1. Section 1 introduces the pebble bed reactors for the 4th Generation Nuclear Energy. The motivation for this study and objectives are presented as well.
2. Section 2 provides a general theoretical background and literature review of previous studies of pressure drop, gas dynamics, and heat transfer phenomena in pebble bed reactors.
3. Section 3 reports the results for the investigation of gas dynamics in the studied pebble bed reactors based on the axial dispersion model.
4. Section 4 presents the gas dispersion and mixing phenomena in the studied pebble bed reactors using the tanks-in-series model.
5. In Section 5, the time residence distribution in a in a pebble bed reactor is analyzed based on the central moment method.
6. Section 6 describes the investigations of the pressure drop in a in a pebble bed reactor.
7. Section 7 describes the investigations of the heat transfer coefficient in a in a pebble bed reactor.
8. Finally, Section 8 summarizes the concluding remarks of this study and provides the recommendations for future work on the topic.

In addition, two appendices are attached as follows: Appendix A gives more information and an outline of the operating procedures of the developed gaseous tracer technique. Appendix B provides more information and an outline of the operating procedures of the developed sophisticated heat transfer technique of a rod-type probe. Appendix B also gives the experimental results that were obtained by using the developed fast-response heat transfer technique of a rod-type probe.

2. THEORTICAL BACKROUND AND LITERTITURE REVIEW

2.1. OVERVIEW

Engineers and scientists have been studying packed beds of small particles before the turn of the 20th century, and extensive literature exists regarding the flow of gases, the transfer of heat and mass, and the pressure drop in fluids flowing through packed beds. As such, thousands of studies have been conducted to develop empirical, semi-empirical, and numerical analyses to describe these studies in such systems. However, for beds with large particles similar to those encountered in pebble bed reactors, there are unfortunately lacks of studies. The key phenomena of interest for the randomly packed pebble-bed reactors involve the variability in the packing structure throughout the bed, pressure drop across the bed, dispersion and mixing, and heat transport processes. Therefore, this section discusses and analyzes the background related to the focus of this work, particularly, the existing knowledge of the bed structure, fluid flow and pressure drop, coolant gas dispersion and mixing phenomena, and heat transfer characteristics of packed pebble-bed reactors. It is worth mentioning that the quantification of the bed structure is not a part of this study. Another study in our laboratory has focused on characterizing the bed structure using gamma-ray computed tomography (CT).

2.2. PHYSICAL CHARACTERISTICS OF PACKED PEBBLE-BEDS

It is well known that the statistical parameter of porous media is the porosity or void fraction (voidage). Therefore, the principle physical quantities of a randomly packed pebble-bed reactor must combine this statistical structural parameter (porosity) with the characteristics of particle size and mean interstitial velocity.

The thermal design of a packed pebble-bed reactor is based upon the mechanisms of heat transport, and the flow and pressure drop of the coolant throughout the pebble-bed (KTA Standards, 1981; Kugeler and Schulten, 1989; van Antwerpen et al., 2010). The mechanisms in turn are all sensitive to the porous structure or porosity variations of the packed bed (White and Tien, 1987). Therefore, before any rigorous analysis of the fluid flow and heat transfer are attempted, it is important to have a thorough understanding of the structural arrangement of the packed bed under consideration.

The bed voidage could be broadly categorized by two terms, that is, the average (mean) porosity of the bed (ε_b), and the local voidage ($\varepsilon(r)$). Traditionally, investigators have defined the local porosity or void fraction as the ratio of the void volume to the volume of the packing structure at a localized position within the packed bed (Meuller, 2012), and it has a numerical value between 0 (no voidage) and 1(no bed). For randomly packed pebble-beds, the void fraction can be expressed as:

$$\varepsilon(r) = \frac{\text{Local volume of voids in packing}}{\text{Local bulk volume of packing}} = \frac{V_T - V_S}{V_T} = 1 - \frac{V_S}{V_T} \tag{1a}$$

where V_S is the volume of the solid particles (pebbles), while V_T is the total volume of the bed.

The average radial porosity of the bed (ε_b) can be azimuthally averaged based on the cross-sectional area defined as:

$$\varepsilon_b = \frac{2}{R^2}\int_0^R \varepsilon(r) r dr \tag{1b}$$

where R is the radius of the packed pebble-bed.

In a packed bed, the porosity varies sharply near the wall, since at that location, geometry of the packing is interrupted (White and Tien, 1987). As a result, the velocity

profile inside a packed bed can be severely distorted near the wall, reaching a maximum in the near-wall region. This phenomenon is known as flow or wall channeling. Wall channeling can have a significant impact on heat and mass transfer in packed beds (White and Tien, 1987). However, in the case of the pebble bed nuclear reactor, this might lead to a reduction in wall temperature and also lead to a non-uniform temperature distribution at the outlet of the bed (du Toit, 2008). Knowledge of the porosity distribution within a packed bed is thus important to any proper analysis of the transport phenomena in the bed (Goodling et al., 1983); and this analysis must be made before any design changes can be recommended, for example, to improve the temperature distribution at the outlet of the reactor. Characterizing the bed structure of pebble beds has been quantified in our laboratory using gamma ray computed tomography (CT) as a part of another study (DOE report, 2012).

2.2.1. Mean Bed Porosity. As mentioned before, the total average (mean) porosity is a useful structural parameter in the design and guide to characterize of packing in fixed packed systems. In the gas-cooled pebble bed reactor, the core consists of randomly packed same size spherical pebbles with a homogeneous porosity except at the wall region. Near the wall, the porosity is higher due to the presence of the wall, and the porosity fluctuates toward the core region of the bed, where it becomes uniform. The following formula was recommended by Fenech (1981) and Achenbach (1982, 1995) to estimate the mean bed porosity (εb):

$$\varepsilon_b = \frac{0.78}{\left(D/d_p\right)^2} + 0.375 \qquad \text{for} \quad \left(D/d_p\right) > 2 \qquad (2)$$

where D is the diameter of the bed and d_p is the pebble diameter. The above formula represented the experimental results of Carman (1937) and Barthels (1972; 1977)

as quoted by Achenbach (1995). It is worth mentioning that the mean porosity is independent of the pebble diameter itself, but depends on the aspect ratio or the tube-to-pebble diameter ratio (D/d_p). It decreases as the aspect ratio increases, and it levels out to an average value of about 0.375 for a very high value of the aspect ratio ($D/d_p \to \infty$). The voidage varies radially through the bed toward the core region due to the wall effect, and the extent of this variation depends on the aspect ratio.

The distribution of the spherical pebbles in a packed pebble-bed reactor is no longer random near the wall because of the orientation forced by the presence of the wall. The high values of voidage near the wall, of course, cause a non-uniform velocity distribution across the core of the pebble bed. In the center of the bed, the velocity is lower than the mean velocity calculated from the overall mass flow, while close to the wall, the velocity is higher than the mean velocity. To estimate the magnitude of the wall effect, it is assumed that the core of the packed pebble-bed consists of two parts of different void fractions (Fenech, 1981). The near-wall region and the central region of the corresponding porosities, respectively, can be expressed as follows:

Near wall region:

$$\varepsilon_w = \frac{63.6}{\left[\left(D/d_p\right)+15\right]^2} + 0.43 \qquad \text{for} \quad \left(D/d_p\right) > 2 \tag{3a}$$

Central region

$$\varepsilon_c = \varepsilon_w - \frac{\varepsilon_w - \varepsilon_b}{\left[1-\left(d_p/D\right)\right]^2} \qquad \text{for} \quad \left(D/d_p\right) > 2 \tag{3b}$$

The near wall-region voidage (ε_w) correlation was developed based on approximating the experimental results of Benenati and Brosilow (1962), while the

central voidage (ε_c) correlation was developed based on the calculated values by means of the equation of conservation of mass (Fenech, 1981).

2.2.2. Radial Distribution of Bed Porosity. A number of empirical correlations and mathematical models to describe the radial variation in the porosity of packed beds of small particles have been proposed by various researchers. du Toit (2008) stated that the correlations to predict the variation in the porosity of packed beds can be classified into two categories, i.e., those that attempt to describe the oscillatory behavior of the variation in the porosity and those that attempt to describe the variation in the average porosity using an exponential expression. It should be noted that the porosity is considered to be uniform in the tangential direction, i.e., an axially symmetric approach. The correlations of the approaches are presented in the next sections:

2.2.2.1 Oscillatory porosity correlations. Various attempts at modeling the voidage variations are presented in the literature. Most of the more recent models describe both the oscillatory nature and damping of the voidage variations. Using the experimental data of Benenati and Brosilow (1962), Martin (1978) proposed the following correlation:

$$\varepsilon(x)=\begin{cases}\varepsilon_{\min}+(1+\varepsilon_{\min})x^2 & \text{for } -1\le x<0\\ \varepsilon_b+(\varepsilon_{\min}-\varepsilon_b)\exp\left(-\frac{x}{4}\right)\cos\left(\frac{\pi}{C}x\right) & \text{for } x\ge 0\end{cases} \tag{4a}$$

with

$$x=2\frac{R\text{-}r}{d_p}-1$$

$$C=\begin{cases}0.816 & D/d_p\to\infty\\ 0.876 & D/d_p=20.3\end{cases} \tag{4b}$$

where (ε_{min}) is the minimum porosity within the range from 0.20–0.26 , ε_b is the bulk porosity of the packed bed undisturbed by wall effects, and C is a constant.

Based on the findings of Roblee et al. (1958) and other investigators, Cohen and Metzner (1981) fitted the following set of correlations to represent the oscillatory variation of the porosity in the radial direction away from the wall of a cylindrical packed bed:

$$\begin{aligned} \frac{1-\varepsilon(x)}{1-\varepsilon_b} &= 4.5\left[x-\frac{7}{9}x^2\right] && \text{for } x \le 0.25 \\ \frac{\varepsilon(x)-1}{1-\varepsilon_b} &= a_1\exp(-a_2x)\cos(a_3x-a_4)\pi && \text{for } 0.25 < x < 8 \\ \varepsilon(x) &= \varepsilon_b && \text{for } 8 < x < \infty \end{aligned} \tag{5a}$$

with

$$x = \frac{R-r}{d_p} \tag{5b}$$

where ε_b is the average porosity of the bed. The authors determined the constants a_1 through a_4 to be: $a_1 = 0.3463$, $a_2 = 0.4273$, $a_3 = 2.4509$ and $a_4 = 2.2011$, while R refers to the outer radius of a cylindrical bed.

It is worth mentioning here that the models suggested by Martin (1978) and Cohen and Metzner (1981) are similar in the sense that they both contain a cosine term to describe the oscillations and an exponential term to describe the dampening. In addition, the influence of the column to particle diameter ratio on the period of oscillation was recognized and included in their models.

Mueller (1991, 1992) modeled the oscillations of the voidage with a zero order Bessel function of the first kind and described the dampening with an exponential term. Using his results and other existing data, Mueller (1992) derived an empirical correlation

that can be used to predict the variation in the porosity in the radial direction for fixed packed beds of uniformly sized spheres in cylindrical containers. The effect of the column to particle diameter ratio on the period of the oscillations was taken into account as the following:

$$\varepsilon(r) = \varepsilon_b + (1-\varepsilon_b) J_0\left(a\frac{r}{d_p}\right)\exp\left(-b\frac{r}{d_p}\right) \qquad \text{for } D/d_p \geq 2.02 \tag{6a}$$

with

$$a = \begin{cases} 7.45 - \dfrac{3.15}{D/d_p} & \text{for } 2.02 \leq D/d_p \leq 13 \\ 7.45 - \dfrac{11.25}{D/d_p} & \text{for } 13 < D/d_p \end{cases}$$

$$b = 0.315 - \frac{0.725}{D/d_p} \tag{6b}$$

$$\varepsilon_b = 0.365 + \frac{0.22}{D/d_p}$$

where ε_b is the average porosity of the bed.

Many versions of the correlation proposed by Mueller (1992) exist (Mueller, 1999, 2002, 2005). Mueller (2010) also formulated the local radial porosity area based on analytical equation formulas for a cylindrical system with mono-sized spherical particles. More recently, Mueller (2012) developed a new and simple method for calculating the radial porosity profile for mono-sized spheres in cylindrical containers. The new method was derived from geometrical and analytical analyses and uses arc lengths to calculate the radial porosity profile.

The same exponentially damped sinusoidal form that Martin (1978) posited was used by de Klerk (2003) in the development of his model. de Klerk determined the constants of the model by fitting the form of the correlation to the porosity data found in

the literature. The constants were then adjusted so that the correlation yielded sensible average bed porosities. The radial variation of porosity through a cylindrical packed bed of spherical particles can be written as follows:

$$\varepsilon(x)=\begin{cases}2.14x^2-2.53x+1 & \text{for } x\le 0.637\\ \varepsilon_b+0.29\exp(-0.6x)\cos\left[2.3\pi(x-0.16)\right]+0.15\exp(-0.9x) & \text{for } x>0.637\end{cases} \quad (7a)$$

with

$$x=\frac{\text{r-R}_i}{d_p} \qquad R_i\le r\le\frac{R_o+R_i}{2}$$
$$x=\frac{R_o-r}{d_p} \qquad \frac{R_o+R_i}{2}\le r\le R_o \quad (7b)$$

It is important to note that in Equation (7b), R_i refers to the inner radius of the annulus and R_o to the outer radius of an annular packed bed.

It is obvious that various authors have performed experiments to obtain different porosity correlations for the variation in the voidage of packed beds in the bulk and near-wall regions. Although many different experimental techniques have been used, the results in general are in agreement. A good overview of the experimental methods used by the various authors is given in de Klerk (2003). However, porosity results obtained from the analysis of numerically generated annular packed beds and physical experimental data obtained by du Toit (2008) were used to evaluate the different porosity correlations.

van Antwerpen et al., (2010) made an evaluation based on the comparison between the relevant correlations with the numerical results of du Toit (2008) for the heat transfer test facility (HTTF), as shown in Figure 2.1. du Toit emphasized that in the case of Cohen and Metzner (1981), the correlation between the dimensionless distance, x,

from both walls in the middle of the annulus is less than eight and the correlation therefore never achieves the bulk value for the porosity.

Theuerkauf et al. (2006) stated that due to the nature of the Bessel function employed by Mueller (1992), the predicted variation in the porosity next to the wall was not correct, which led to a significant over prediction of the porosity in the near-wall region. Thus, the correlation by Mueller (1992) was not included in the comparison by du Toit (2008) and was also not taken into account in the evaluation by van Antwerpen et al., (2010). du Toit (2008), stated that the correlation proposed by Martin (1978) was the most representative of du Toit's his numerical results. However, it was reported by Van Antwerpen et al., (2010) that the correlation proposed by de Klerk (2003) gave an even better prediction of the variation in the radial porosity than that of Martin.

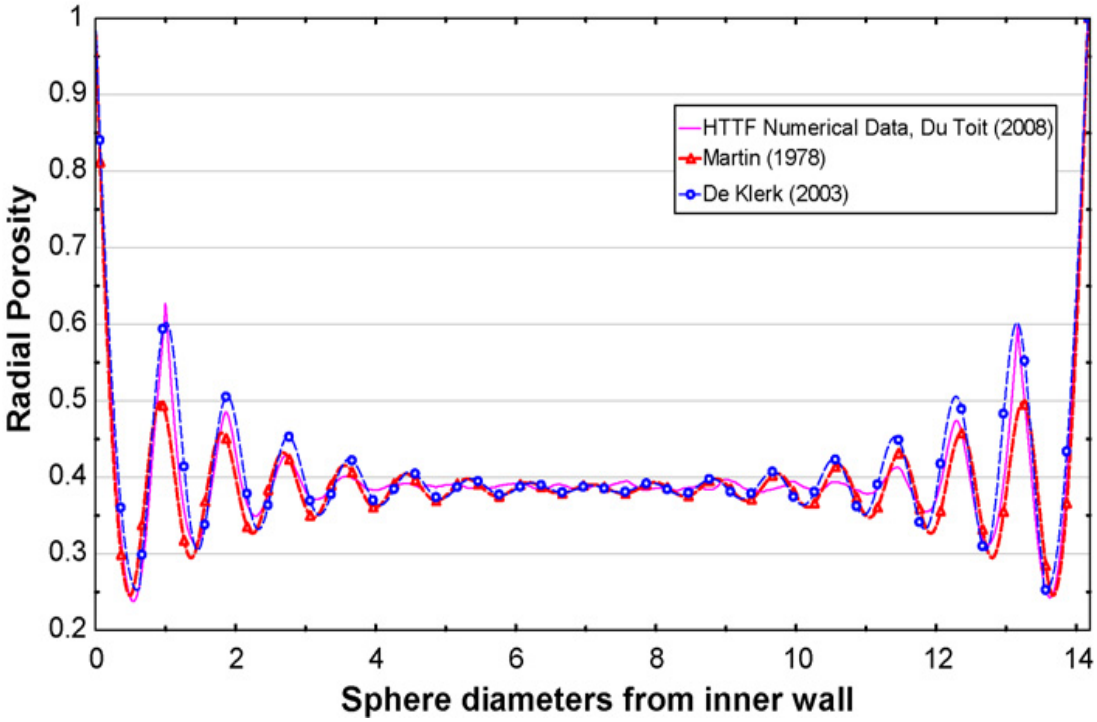

Figure 2.1. Comparison between Radial Oscillatory Porosity Correlations (van Antwerpen et al., 2010)

2.2.2.2 Exponential porosity correlations. In some simplified models, such as the model of Vortmeyer and Schuster (1983), it is assumed that the "average" porosity decays exponentially from unity at the wall to the bulk value further away from the wall. Following Cheng and Hsu (1986), Hunt and Tien (1990) and Sodre and Parise (1998), the radial porosity distribution for an annular packed bed can be written as follows:

$$\varepsilon(r)=\begin{cases}\varepsilon_o\left[1+C\exp\left(-N\dfrac{\mathrm{r\text{-}R_i}}{\mathrm{d_p}}\right)\right] & \text{for } \mathrm{R_i}\le \mathrm{r}\le\dfrac{\mathrm{R_o}+\mathrm{R_i}}{2}\\ \varepsilon_o\left[1+C\exp\left(-N\dfrac{\mathrm{R_o\text{-}r}}{\mathrm{d_p}}\right)\right] & \text{for } \dfrac{\mathrm{R_o}+\mathrm{R_i}}{2}\le \mathrm{r}\le\mathrm{R_o}\end{cases} \tag{8a}$$

where R_i is the inner radius of the annulus and R_o is the outer radius of the annulus. Vortmeyer and Schuster (1983), Cheng and Hsu (1986) and Hunt and Tien (1990) use the expression $\varepsilon_o = \varepsilon_b$, to represent the bulk porosity of the bed, while Sodre and Parise (1998) use $\varepsilon_o = \varepsilon_\infty$, to represent the porosity off an infinite bed. Most researchers use a value of C that gives a porosity of one at the wall, but Cheng and Hsu (1986) use C = 1. For spherical particles, Vortmeyer and Schuster (1983) and Cheng and Hsu (1986) use 2 as the value of N, but Hunt and Tien (1990) use N = 6. Sodre and Parise (1998) proposed that the value of N be obtained from the following:

$$N = \frac{2C\varepsilon_\infty d_p\left[1-\exp\left(-N\left(R_o-R_i\right)/2d_p\right)\right]}{\left(\bar{\varepsilon}-\varepsilon_\infty\right)\left(R_o-R_i\right)} \tag{8b}$$

where $\bar{\varepsilon}$ is the average bed porosity for the annulus given by the following:

$$\bar{\varepsilon} = 0.3517 + 0.387\frac{d_p}{2\left(R_o-R_i\right)} \tag{8c}$$

du Toit (2008) noted that the correlation derived by Sodre and Parise failed to fit with the results obtained by the other correlations and proposed that ε_∞ be substituted by ε_b in the bulk region of the annulus and substituted $\bar{\varepsilon}$ with the average porosity for the annulus obtained from the numerical results

Equation (8a) must be solved using an iterative procedure. In contrast, White and Tien (1987) proposed a radial porosity distribution of this form:

$$\varepsilon(r) = \begin{cases} \left[1+\left(\frac{1-\varepsilon_b}{\varepsilon_b}\right)\sqrt{1-\exp\left(-2\frac{r-R_i}{d_p}\right)}\right]^{-1} & \text{for } R_i \le r \le \frac{R_o+R_i}{2} \\ \left[1+\left(\frac{1-\varepsilon_b}{\varepsilon_b}\right)\sqrt{1-\exp\left(-2\frac{R_o-r}{d_p}\right)}\right]^{-1} & \text{for } \frac{R_o+R_i}{2} \le r \le R_o \end{cases} \tag{9}$$

van Antwerpen et al., (2010) have evaluated and made a comparison between the exponential porosity correlations (Equations 8-9), and numerical results of du Toit (2008) for the heat transfer test facility (HTTF), as shown in Figure 2.2. After a careful examination by du Toit it was found that the correlation proposed by Hunt and Tien (1990) gave the best representation of the "average" variation of porosity in the radial direction.

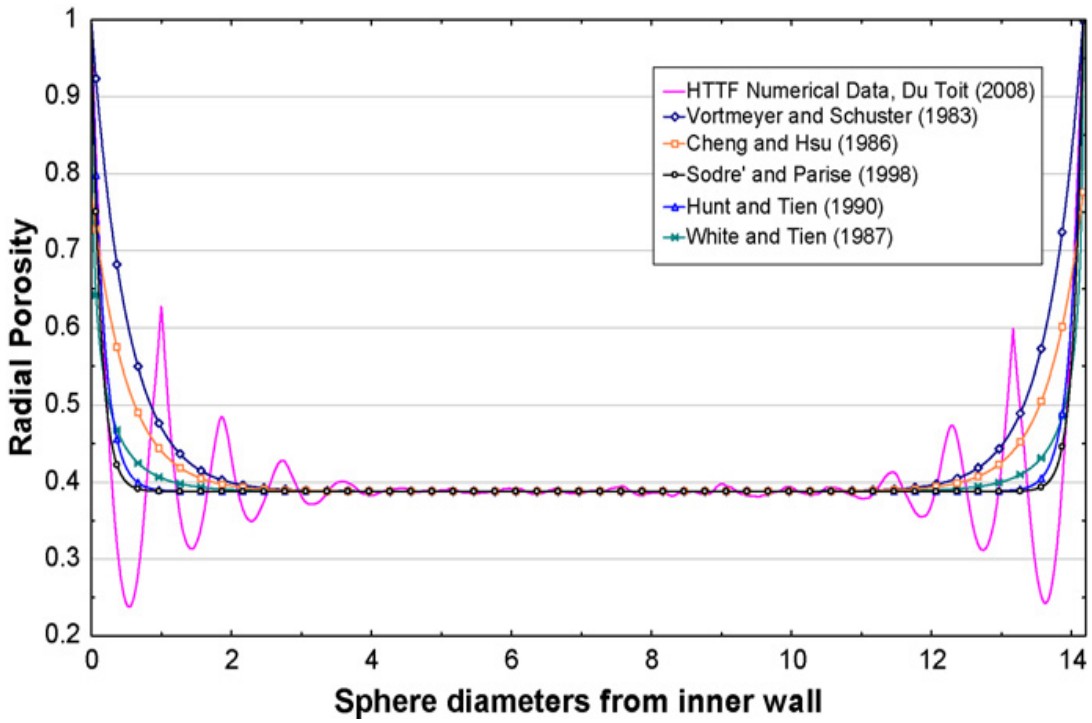

Figure 2.2. Comparison between Radial Exponential Porosity Correlations (van Antwerpen et al., 2010)

2.3. IDENTIFICATION OF FLUID FLOW REGIMES IN A PACKED BED

Resistance to fluid flow is usually obtained from pressure drop measurements in randomly packed beds. It is possible to distinguish four different flow regimes in packed pebble-bed reactors, based on the effective Reynolds number which is defined as:

$$\mathrm{Re_h} = \frac{\rho \mathrm{V d_h}}{\mu} = \frac{1}{(1-\varepsilon_b)}\mathrm{Re} \tag{10a}$$

where $\mathrm{d_h}$ is the equivalent hydraulic (effective) diameter which is the characteristic length of the packed pebble-bed and defined as follows:

$$\mathrm{d_h} = \mathrm{d_p}\frac{\varepsilon_b}{(1-\varepsilon_b)} \tag{10b}$$

while V is the interstitial velocity which is the characteristic or the mean velocity in the gaps between the pebbles and defined as follows:

$$\mathrm{V} = \frac{\mathrm{V_g}}{\varepsilon_b} \tag{10c}$$

In addition, Re is the Reynolds number and is defined on the basis of the total mass flow rate through the total cross-sectional area of the packing and on the diameter of the pebbles as follows:

$$\mathrm{Re} = \frac{\rho \mathrm{V_g d_p}}{\mu} \tag{10d}$$

The physical significance of these four different flow regimes is as follows:

1) For $\mathrm{Re_h} < 1$; a creeping-flow regime which is purely viscous. It follows Darcy's law; therefore, it is called darcian flow. In this regime, the viscous forces dominate over the inertia forces and only the local (pore-level) geometry influences the flow (Kaviany, 1995). This regime is also characterized by a linear relationship between pressure drop and mass flow (Achenbach, 1995). Therefore, it is sometimes referred to as the linear-laminar flow regime (Hlushkou and Tallarek, 2006).

2) For $1-10 < \mathrm{Re_h} < 150$; a steady laminar-flow regime in which the inertia effects begin to play an important role in the flow condition; therefore, it is called the inertial-flow regime.
3) For $150 < \mathrm{Re_h} < 300$; an unsteady laminar-flow regime in which both viscous and inertia forces are important. In this regime wake instability might be responsible for the transition from the laminar steady flow to unsteady flow. In this regime, the deviation from Darcy's law begins; hence, this is sometimes called the non-linear laminar flow regime (Hlushkou and Tallarek, 2006).
4) For $\mathrm{Re_h} > 300$; a turbulent-flow regime in which viscous effects are negligible. It is a highly unsteady chaotic flow; therefore, it is called an unsteady-and chaotic-flow regime. There is a failure of Darcy's law to describe the flow through fixed beds in this regime.

2.4. CHARACTERISTICS OF FLUID FLOW IN A PACKED BED

It is well known that the fluid flow problem in porous media is caused by transition between flow in channels and flow around submerged objects. According to the discontinuity of this system, an exact representation of the fluid flow distribution in porous media is impossible (Ziolkowska and Ziolkowski, 1993). For flow through packed bed reactors, it is desirable to be able to predict the flow rate obtainable for a given energy input (usually measured as pressure drop) or to be able to predict the pressure drop necessary to achieve a specific flow rate. Practically, the complexity of the flow pattern rules out a rigorous analytic solution to the problem; hence, an empirical or semi-empirical correlation has been suggested. Generally, in packed pebble-bed reactors, the

resistances of flow are usually described in terms of total pressure drop (ΔP) or the pressure drop coefficient, which is defined as:

$$\psi = \frac{\Delta P}{(\rho/2)V^2}\frac{d_h}{L} \tag{11}$$

The pressure loss due to friction between solid (pebbles) and gas phases in the core of the pebble bed can be expressed as the following (Fenech, 1981):

$$\Delta P = \psi \frac{L}{d_h}\frac{\rho}{2}V^2 = \psi \frac{L}{d_p}\frac{\rho}{2}V_g^2\left(\frac{1-\varepsilon_b}{\varepsilon_b^3}\right) \tag{12}$$

V_g is the superficial gas velocity based on the cross section of the empty column.

On the one hand, there are two main approaches for developing friction factor expressions for packed beds (Fan and Zhu, 1998; Bird et al., 2002). In the first approach, the packed bed is visualized as a bundle of tubes. In the second approach, the packed bed is regarded as a collection of submerged objectives. Based on these two approaches, the pressure drop in fixed packed beds has been described by two different models (Wirth, 2010). The first one is the model of the hydrodynamic diameter, and the second is the model of the flow around a single particle. The first model is older and leads to the relatively easy pressure drop equations, such as the classical Ergun-type equation (Ergun, 1952). It is more useful to mention here that, this model assumes the packing is statistically uniform, so there are no channeling or bypassing effects (although in the actual situation of a pebble bed reactor, channeling, bypassing, etc would occur). Thus and then the development given here does not apply to the randomly packed pebble-bed reactors. The second model is newer (Molerus, 1993), and it overcomes the assumption of statistical uniformity; therefore, it is more appropriate for randomly packed pebble-bed reactors.

On the other hand, the dimensionless pressure drop (ψ) is a function of the effective Reynolds number ($\mathrm{Re_h}$); therefore, several correlations were developed and verified using experimental data (Melese and Katz, 1984). The well-known Ergun equation expresses the friction factor in a packed bed as follows (Ergun, 1952):

$$\psi = \frac{150}{\mathrm{Re_h}} + 1.75 \qquad \text{for} \qquad \mathrm{Re_h} \le 5\times10^4 \tag{13}$$

where $\mathrm{Re_h}$ is a modified or effective Reynolds number that is based on the average interstitial velocity (V) and on the characteristic length scale of the pores (an equivalent hydraulic diameter, $\mathrm{d_h}$) follows by recalling Equation 10a:

$$\mathrm{Re_h} = \frac{\rho \mathrm{V d_h}}{\mu} = \frac{1}{(1-\varepsilon_b)}\mathrm{Re} \tag{10a}$$

The above equation is formed by adding the Carmen-Kozeny (Carman, 1937; Kozeny, 1927) equation for purely laminar-flow (viscous effect, $\mathrm{Re_h} < 1$) through a porous medium modeled as an assembly of capillaries, to the Burke-Plummer (Burke and Plummer 1928), equation derived for the fully-turbulent (inertia effect, $\mathrm{Re_h} \ge 300$) limit in a capillaric medium (Fan and Zhu, 1998). The first term in the expression (Equation 13) refers to viscous energy losses, of importance at low flow rates (i.e. streamline flow), and the second term refers to kinetic energy losses, of importance at high flow rates (i.e. turbulent flow).

Eisfeld and Schnitzlein (2001) compared their measurements with predictions of twenty-four different pressure drop correlations from the literature, and they pointed out that Reichelt's approach (Reichelt, 1972) of correcting the Ergun equation for the wall is the most promising one. Eisfeld and Schnitzlein developed an improved correlation that accounted for the effect of the wall as follows:

$$\psi = \frac{308 A_w^2}{Re_h} + \frac{2 A_w}{B_w} \qquad \text{for} \qquad Re_h \le 2\times 10^4 \tag{14a}$$

with the wall correction terms

$$A_w = \left[1 + \frac{2}{3} \frac{\left(d_p / D \right)}{(1-\varepsilon_b)} \right] \tag{14b}$$

$$B_w = \left[1.15 \left(\frac{d_p}{D} \right)^2 + 0.87 \right]^2 \tag{14c}$$

In fact, this is an Ergun-type equation where the contribution of confining walls to the hydraulic radius was accounted for analytically by the coefficient A_w. Additionally, the coefficient B_w is introduced, describing empirically the porosity effect of the walls at the high Reynolds number.

The German Nuclear Safety Standard Commission (Kerntechnischer Ausschuss - KTA) has been considered and analyzed about thirty papers relevant to the results of the randomly packed bed with spherical particles (Fenech, 1981). The KTA adopted the following empirical correlation for the applications of the high temperature packed pebble-bed nuclear reactors (KTA Standards, 1981):

$$\psi = \frac{320}{Re_h} + \frac{6}{Re_h^{0.1}} \qquad \text{for} \qquad Re_h \le 5\times 10^4 \tag{15}$$

The first term of the above equation (Equation 15), represents the asymptotic solution for laminar flow, while the second term represent the same for the turbulent flow.

The Association of German Engineers (Verein Deutscher Ingenieure-VDI) Heat Atlas provides the following correlation for the coefficient of loss of pressure through friction in fixed beds (Wirth, 2010):

$$\psi = \left(\frac{0.4}{\varepsilon_b} \right)^{0.78} \frac{317}{\mathrm{Re}_h} + \frac{6.17}{\mathrm{Re}_h^{0.1}} \tag{16}$$

Finally, it is very useful for modeling purposes to address here that the total pressure drop phenomenon within the flow due to the presence of the pebble bed can also be characterized by the dimensionless Euler number (Rousseau and van Staden, 2008) as follows:

$$\mathrm{Eu} = \frac{\Delta P}{\rho V^2} = \frac{1}{2} \psi \frac{L}{d_h} = \frac{1}{2} \psi \frac{L}{d_p} \left(\frac{1-\varepsilon}{\varepsilon} \right) \tag{17}$$

It can be interpreted as a measure of the ratio of pressure to inertial forces; a perfect frictionless flow corresponds to an Euler number of unity. Rousseau and van Staden (2008) also illustrate the relation between the Euler number and momentum transport via the momentum conservation equations for the axial and radial gas flow paths within the packed pebble-bed nuclear reactor.

2.5. GAS DISPERSION AND MIXING PHENOMENA

Dispersion is a well-known phenomenon in porous media primarily for heat and mass transfer processes. The dispersion coefficient is a property valid only under continuum assumptions. This is similar to viscosity in momentum transfer, heat conductivity in heat transfer, and the diffusion coefficient in mass transfer. The axial dispersion phenomenon in a pebble bed is a consequence of the combined contributions of both the molecular diffusion and the hydrodynamic mixing (convection) mechanisms in the spaces between the pebbles along the length of the pebble bed. At the macroscopic level, the individual contribution of each mechanism to the overall dispersion phenomenon depends mainly on the gas flow conditions and bed structure. Typically, the

axial dispersion and degree of mixing in the packed bed are characterized and quantified in terms of axial dispersion coefficients and dispersive Peclet numbers, respectively.

It is well known that the phenomenon of axial dispersion is indicated by the spread of residence times of the individual elements of a fluid stream passing through a packed bed. Even if it is possible theoretically in unpacked tubular reactors to quantify deviations from an ideal plug flow model by measuring fluid velocities in order to obtain a complete velocity distribution profile, this approach is never used in packed pebble bed reactors because it is physically impossible to realize it in practice. Therefore, simple knowledge of the residence time distribution (RTD) is necessary. The RTD can be obtained by studying the response of the system to a tracer impulse. Different approaches are available in the literature to obtain the parameters from the RTD (Levenspiel, 1999).

The main problem with the RTD method comes from possible interactions between process dynamical behavior and the dynamics of the sensor. As a result, the obtained measurements are the time convolution of the desired phenomenon and of an unexpected one. From a mathematical point of view, the time response of the sensors cannot be subtracted from the RTD since these are two dynamical systems in series. Therefore, convolution and deconvolution integral methods are used to analyze the RTD.

Unfortunately, in the reported studies, there is no detailed experimental measurements, knowledge and quantification of the coolant gas dispersion and its extent of mixing for pebble bed nuclear reactors. However, there are studies reported in the literature related to the dispersion of the gas and liquid phases and their mixing in the chemical/catalytical packed-bed reactor of smaller particles (1-3 mm in diameter) (Danckwerts, 1953; Kramers and Alberda, 1953; Levenspiel and Smith, 1957; Bischoff

and McCracken, 1966; Chao and Hoelscher, 1966; Edwards and Richardson, 1968; Gunn, 1969,1987; Tsotsas and Schlunder, 1988; Barjaktarovic et al., 2003; Guedes and Delgado, 2005). Recently, Delgado (2006) summarized and reviewed the literature on the phenomenon of dispersion (longitudinal and transverse) in packed beds. The author stated that there are several variables that need to be considered in the analysis of the dispersion in packed beds, such as the length of the packed bed, viscosity and density of the fluid, ratio of the column diameter to the particle diameter (aspect ratio), ratio of the column length to the particle diameter, particle size distribution, particle shape, velocity of the fluids, and operating temperature.

In spite of this large number of studies, the correlations reported in the literature for predicting the axial gas dispersion coefficient in packed beds of large particles are still not reliable. There are some correlations that predict the axial gas dispersion coefficient of chemical/catalytic packed bed systems of small particles in terms of dispersive Peclet numbers, as summarized in Table 2.1.

Early attempts to correlate and predict the dispersion coefficients in a packed bed of smaller particles were performed by Gunn and Pryce (1969) and Gunn (1969) using different approaches (Gunn, 2004). Gunn described dispersion in a randomly packed bed as a stochastic process, and the author also used the probability theory to incorporate both diffusion and mixing effects. The early analysis of Gunn (1969) of the tracer motion led to the following expression for the dispersive Peclet number:

$$\frac{1}{\mathrm{Pe_D}} = \left[\frac{\mathrm{Pe_M}}{4\alpha_1^2(1-\varepsilon_b)}\right](1-\mathrm{p})^2 + \left[\frac{\mathrm{Pe_M}}{4\alpha_1^2(1-\varepsilon_b)}\right]^2 \mathrm{p}(1-\mathrm{p})^3 \left\{\exp\left[-\frac{4\alpha_1^2(1-\varepsilon_b)}{\mathrm{p}(1-\mathrm{p})\mathrm{Pe_M}}\right]-1\right\} + \frac{1}{\tau}\frac{1}{\mathrm{Pe_M}} \tag{18}$$

The dimensionless groups are given by the following:

$$\left.\begin{aligned} Pe_D &= \frac{V_g d_p}{\varepsilon_b D_{ax}} && \text{dispersive Peclet number} \\ Pe_M &= \frac{V_g d_p}{\varepsilon_b D_{AB}} = Re_P Sc && \text{molecular (mass) Peclet number} \\ Re_P &= \frac{\rho V_g d_p}{\varepsilon_b \mu} = \frac{Re}{\varepsilon_b} && \text{particle Reynolds number} \\ Sc &= \frac{\mu}{\rho D_{AB}} && \text{Schmidt number} \end{aligned}\right\} \quad (18a)$$

where D_{ax} is the axial gas dispersion coefficient and D_{AB} is the molecular diffusion coefficient. While α_1 is the first root of the first order Bessel function and p is the fluid mechanical probability. According to the hypothesis of Gunn (1969), p is only a function of the Reynolds number ($Re = \rho V_g d_p/\mu$). Hence, later Gunn (1987) proposed a correlation for p as outlined in the following discussion.

Gunn (1969) proposed two limits for the dispersive Peclet number (Pe_D), by expanding the exponential term in Equation 18, and based on the value of the product of the particle Reynolds number, and Schmidt number which is called the molecular (mass) Peclet number (Pe_M). These two limits are:

For small values of Pe_M

$$\frac{1}{Pe_D} = \frac{1}{\tau}\frac{1}{Pe_M} \quad (19)$$

i.e., the dispersive Peclet number is due to molecular diffusion alone.

For large values of Pe_M

$$\frac{1}{Pe_D} = \frac{1-p}{2p} \quad (20)$$

i.e., the dispersive Peclet number is due to convection alone.

In Equation 18, τ is the tortuosity factor, which is defined as the ratio that compares the average length of the actual fluid flow paths through the packing to the packing heights (Lanfrey et al., 2010). This parameter was originally introduced to account for the sinuosity of the flow paths in the permeability model (Carman, 1956). The tortuosity factor is also lumped both tortuous zigzag flow paths and constricted points and can be approximated as $\tau \approx \sqrt{2}$ for a packed bed of spherical particles (Carman, 1956; Sherwood et al., 1975). Boudreau (2006) correlated the tortuosity factor to readily measure porosity through this simple relation:

$$\tau = \sqrt{1 - \ln\left(\varepsilon_b\right)^2} \tag{21a}$$

More recently, Lanfrey et al. (2010) developed a theoretical model for the tortuosity of a fixed bed randomly packed with identical spherical particles. They found that, the tortuosity was proportional to a packing structure factor, which could well capture the balancing effect between porosity and particle sphericity, as follows:

$$\tau = \frac{\varepsilon_b}{\left[\left(1-\varepsilon_b\right)^{4/3}\right]} \tag{21b}$$

As porosity decreased, the tortuosity increased and it did not depend on the particle size.

Gunn (1987) proposed a correlation for the fluid mechanical probability (p) needed for Equation 18 as a function of Re for packing of spherical particles as follows:

$$p = 0.17 + 0.33 \times \exp\left(-\frac{24}{Re}\right), \qquad Re = \frac{\rho V_g d_p}{\mu} \tag{22}$$

The above expression (Equation 22) suggests that p should have the value of 0.5 for $Re \to \infty$.

Gunn (1987) also proposed another simplified correlation for Pe_D, by assuming that diffusive and mixing components of dispersion are additive, and rewrote Equation 18 in the following form:

$$\frac{1}{Pe_D} = \frac{1}{\tau}\frac{1}{Pe_M} + \frac{1}{2} \tag{23}$$

Delgado (2006) evaluated Gunn's correlation (Equation 23) with available experimental data, as shown in Figure 2.3, and he pointed out that the experimental values of the dispersive Peclet number are generally higher than predicted by Equation (23). Delgado also pointed out that Equation (23) is inaccurate over part of the intermediate range of Pe_M and that there are significant deviations observed only in the range from $0.6 < Pe_M < 60$. It is important to state here that, Figure 2.3, shows that for low values of Pe_M (creeping flow regime), there seems to be a tendency for Pe_D to become independent of Sc. Reported that several correlations (Hiby, 1962; Evans and Kenney, 1966; Edwards and Richardson, 1968; Scott et al., 1974; Langer et al., 1978; Johnson and Kapner, 1990) have been proposed to represent the data reasonably in this intermediate range (see Figure 2.3).

Bischoff and Levenspiel (1962b) developed this semi-empirical correlation for dispersion in a packed bed as:

$$\frac{1}{Pe_D} = \frac{\varepsilon_b/\tau}{Pe_M} + \frac{0.45}{\left[1+7.3\left(Pe_M\right)^{-1}\right]} \tag{24}$$

Edwards and Richardson (1968) proposed an empirical correlation for axial dispersion of gases flowing through a fixed bed of small particles expressed as the following:

$$\frac{1}{\mathrm{Pe_D}} = \frac{1}{\tau}\frac{1}{\mathrm{Pe_M}} + \frac{0.5}{\left[1+\left(\beta / \mathrm{Pe_M}\right)\right]} \tag{25}$$

The term $[1+(\beta / \mathrm{Pe_M})]$ on the right-hand side of Equation (25) is an empirical correction factor that takes in to account that the radial (transverse) dispersion might take place at a low Reynolds number that reduces the axial (longitudinal) dispersion as introduced by the authors. Where β is a constant and it increases as the diffusivity of gas (D_{AB}) increases.

The best fit of their experimental results was obtained with a value of 9.7 for β and using the value of approximately $\sqrt{1.87}$ for τ. Equation (25) then becomes the following:

$$\frac{1}{\mathrm{Pe_D}} = \frac{0.73}{\mathrm{Pe_M}} + \frac{0.5}{\left[1+9.7\left(\mathrm{Pe_M}\right)^{-1}\right]} \tag{26}$$

Wen and Fan (1975) and Tsotsas and Schlunder (1988) deduced alternative correlations for the prediction of the dispersive Peclet number ($\mathrm{Pe_D}$) of gas flowing in packed beds of spherical particles as follows:

The correlation by Wen and Fan (1975) is expressed as below:

$$\frac{1}{\mathrm{Pe_D}} = \frac{0.3}{\mathrm{Pe_M}} + \frac{0.5}{\left[1+0.38\left(\mathrm{Pe_M}\right)^{-1}\right]} \tag{27}$$

The correlation by Tsotsas and Schlunder (1988) is expressed as:

$$\frac{1}{\mathrm{Pe_D}} = \frac{\gamma}{\mathrm{Pe_M}} + \frac{1}{1.14\left[1+10\left(\mathrm{Pe_M}\right)^{-1}\right]} \tag{28a}$$

The quantity γ is a function of bed porosity and can be approximated empirically by the following (Tsotsas and Martin, 1987):

$$\gamma = \frac{\varepsilon_b}{\tau} = 1-\left(1-\varepsilon_b\right)^{1/2} \tag{28b}$$

Tsotsas and Martin used $\gamma \approx 0.3$ for $\varepsilon_b = 0.4$.

Wakao and Kaguei (1982) gave an overview of the different experimental data and proposed the following correlation for axial dispersion in packed bed of spherical particles as the following:

$$\frac{1}{\mathrm{Pe_D}} = \frac{0.7}{\mathrm{Pe_M}} + \frac{1}{2} \tag{29}$$

Guedes de Carvalho and Delgado (2003) developed a mathematical expression that would represent their experimental data with good accuracy for the longitudinal dispersion in a chemical packed bed as the following:

$$\frac{1}{\mathrm{Pe_D}} = \frac{\mathrm{Pe_M}}{5}(1-\mathrm{p})^2 + \frac{\mathrm{Pe_M^2}}{25}\mathrm{p}(1-\mathrm{p})^3\left\{\exp\left[-\frac{5}{\mathrm{p}(1-\mathrm{p})\mathrm{Pe_M}}\right]-1\right\} + \frac{1}{\tau}\frac{1}{\mathrm{Pe_M}} \tag{30a}$$

with

$$\mathrm{p} = \frac{0.48}{\mathrm{Sc}^{0.15}} + \left(\frac{1}{2} - \frac{0.48}{\mathrm{Sc}^{0.15}}\right)\exp\left(-\frac{75\mathrm{Sc}}{\mathrm{Pe_M}}\right) \tag{30b}$$

It is important to bear in mind that Equation 30a is recommended only for random packings of spherical particles that are well-packed (Delgado, 2006), and it covers a wide range of values of $\mathrm{Pe_M}$ and Sc.

It is clear from the above correlations that dispersive Peclet numbers ($\mathrm{Pe_D}$) for gases flowing through packed beds depend on the variations in molecular Peclet numbers ($\mathrm{Pe_M}$), and hence, on the Schmidt number. Under extremely low flow rate conditions (creeping flow regimes) of coolant gas there are no reliable measurements because of experimental difficulties, and the dispersion phenomenon is related to the pure molecular diffusion mechanism. In other words, at the limit $\mathrm{Pe_M} \to 0$, axial dispersion takes place by molecular diffusion alone. At high flow rate conditions (turbulent flow regimes),

dispersion occurs purely by turbulent mixing, and it is obvious that upon increasing the velocity of the gas, the dispersive Peclet number tends to reach the limiting value of about 2. This value can be estimated theoretically using the equivalence of a packed bed (at $Pe_D \to \infty$) with a series of perfect mixers (Tsotsas and Schlunder, 1988).

Table 2.1. Summary of Selected Correlations for Axial Gas Dispersion in Chemical Packed Bed Reactors

Author	Correlation	Range
Gunn (1969)	$\frac{1}{Pe_D}=\left[\frac{Pe_M}{4\alpha_1^2(1-\varepsilon_b)}\right](1-p)^2+\left[\frac{Pe_M}{4\alpha_1^2(1-\varepsilon_b)}\right]^2 p(1-p)^3\left\{\exp\left[-\frac{4\alpha_1^2(1-\varepsilon_b)}{p(1-p)Pe_M}\right]-1\right\}+\frac{1}{\tau}\frac{1}{Pe_M}$ $p=0.17+0.33\times\exp\left(-\frac{24}{Re}\right)$	$0.4\le Re\le 420$ $Sc=0.88$ $0.368\le\varepsilon\le 0.37$
Bischoff and Levenspiel (1962b)	$\frac{1}{Pe_D}=\frac{\varepsilon_b/\tau}{Pe_M}+\frac{0.45}{\left[1+7.3(Pe_M)^{-1}\right]}$	$0.05\le Re\le 44000$ $\varepsilon=0.40$
Edwards and Richardson (1968)	$\frac{1}{Pe_D}=\frac{0.73}{Pe_M}+\frac{0.5}{\left[1+9.7(Pe_M)^{-1}\right]}$	$0.008\le Re\le 50$ $Sc=0.72$ $0.368\le\varepsilon\le 0.41$
Wen and Fan (1975)	$\frac{1}{Pe_D}=\frac{0.3}{Pe_M}+\frac{0.5}{\left[1+0.38(Pe_M)^{-1}\right]}$	$0.008 < Re < 400$ $0.28 < Sc < 2.2$
Wakao and Kaguei (1982)	$\frac{1}{Pe_D}=\frac{0.7}{Pe_M}+\frac{1}{2}$	$Re\ge 5$
Gunn (1987)	$\frac{1}{Pe_D}=\frac{1}{\tau}\frac{1}{Pe_M}+\frac{1}{2}$	$0.4\le Re\le 420$ $Sc=0.88$ $0.368\le\varepsilon\le 0.37$
Tsotsas and Schlunder (1988)	$\frac{1}{Pe_D}=\frac{0.3}{Pe_M}+\frac{1}{1.14\left[1+10(Pe_M)^{-1}\right]}$	$0.05\le Re\le 44000$ $\varepsilon=0.40$
Guedes de Carvalho and Delgado (2003)	$\frac{1}{Pe_D}=\frac{Pe_M}{5}(1-p)^2+\frac{Pe_M^2}{25}p(1-p)^3\left\{\exp\left[-\frac{5}{p(1-p)Pe_M}\right]-1\right\}+\frac{1}{\tau}\frac{1}{Pe_M}$ $p=\frac{0.48}{Sc^{0.15}}+\left(\frac{1}{2}-\frac{0.48}{Sc^{0.15}}\right)\exp\left(-\frac{75Sc}{Pe_M}\right)$	$0.02\le Re\le 89.1$ $57\le Sc\le 1938$ $0.37\le\varepsilon\le 0.385$

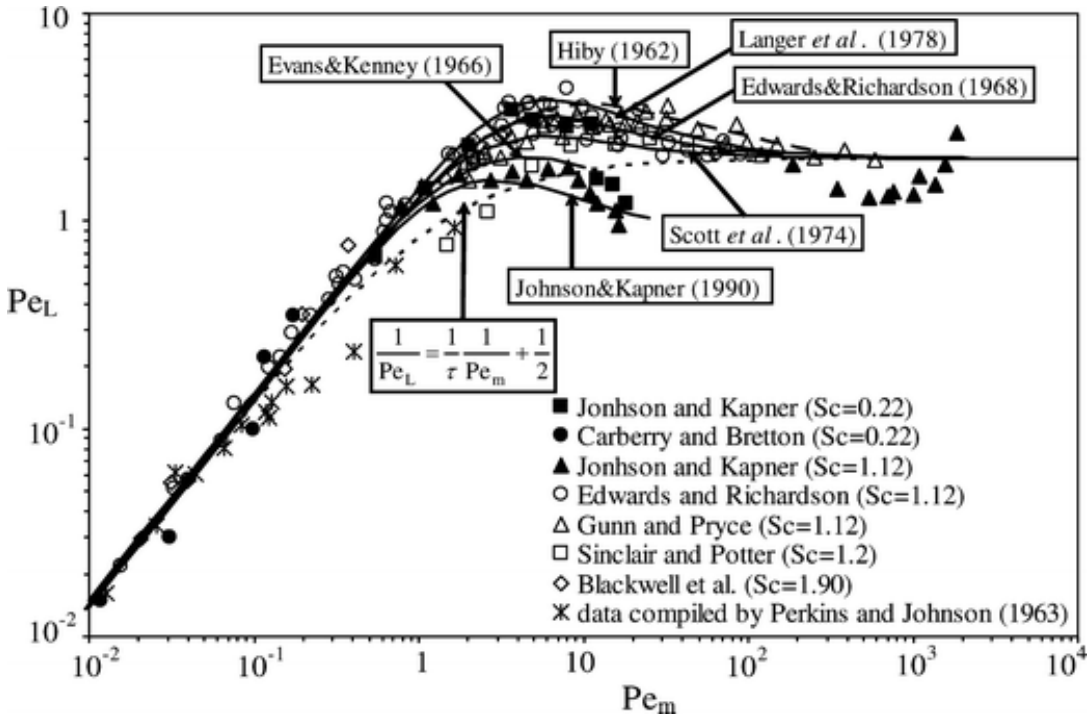

Figure 2.3. Some Experimental Data Points for Axial Dispersion in Gaseous Systems (Delgado, 2006), where $Pe_m = Pe_M$

2.6. HEAT TRANSFER CHARACTERISTICS

Heat transport in packed pebble beds is an extremely complex phenomenon where the contributions of the three modes of conduction, convection, and thermal radiation need to be accounted for. Moreover, the heat transfer modes might interact with one another. Therefore, the phrase, "packed pebble-bed heat transfer," is used to describe a variety of mechanisms where the following might occur:

1. Heat conduction through the solid pebble itself from one side of the pebble through to the other side.
2. Forced convection heat transfer due to the bulk flow and turbulent mixing of the coolant gas.

3. Conduction heat transfer through the point of physical contact between the individual pebbles in the bed. This mode can be further subdivided into the axial and radial directions that refer to the radial pebble-to-pebble conduction and axial pebble-to-pebble conduction, respectively.
4. Heat transfer by conduction across the stagnant gas surrounding the point of contact between pebbles.
5. Thermal radiation heat transfer between the surfaces of adjacent pebbles within the pebble bed.
6. Forced convection heat transfer from the hot pebbles to the coolant gas flowing through the bed, sometimes is referred to as the pebble-coolant heat transfer mode. In packed-pebble bed reactors, at normal operating conditions of elevated temperatures this mode will be an important process.
7. Radiation absorption by the coolant gas.
8. Heat transfer by natural convection in the coolant gas, this mode will be dominant at extremely low flow rates, which are the case when an accident occurs within the reactor.

All of these modes of heat transport phenomena are illustrated schematically in Figure 2.4. In the normal operation of the nuclear pebble bed reactor, two or more of the modes listed above might take place simultaneously in parallel or in series. It is obvious that the heat transport mechanism in packed pebble beds is extremely dependent on the fluid flow distribution in the core. As a result, the list above involves the following, broadly (Szomanski and Aust, 1968): (a) mechanisms that are independent on fluid flow (1, 3 and 4); and (b) mechanisms that depend of fluid flow (2, 5, 6, 7 and 8).

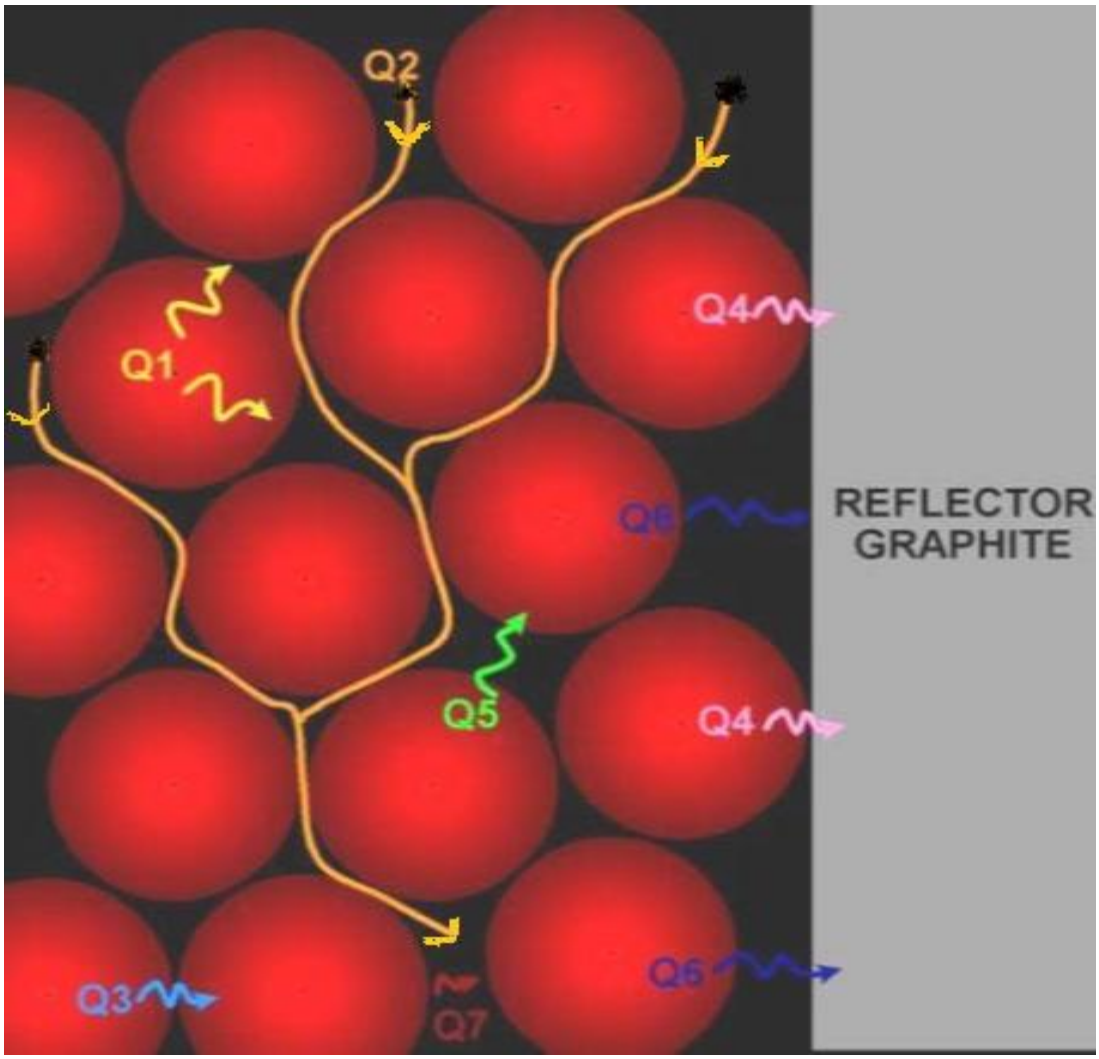

Figure 2.4. Schematic Sketch of the Heat Transfer Modes in the Dynamic Core of Packed Pebble Bed Reactors (Reitsma, 2012)

As mentioned earlier, for the proper modeling and predicting of the pebble-bed core temperature distribution, all of the three modes of heat transport (i.e., conduction, convection and radiation) are important. However, during nominal operation of the reactor (relatively high Reynolds numbers), the heat transfer mechanism is governed by forced convection between the hot pebbles to the coolant gas flowing through the bed.

This heat convection can be quantified and characterized in terms of the pebble coolant convective heat transfer coefficient or non-dimensional Nusselt number. At low Reynolds numbers (the case of accident), the effects of free convection, thermal radiation, heat conduction, and heat dispersion come into the same order of magnitude as the contribution of the forced convection (Fenech, 1981). Thermal radiation heat transfer inside the core is a complex mechanism and very difficult to characterize. The effective thermal conductivity is a lumped parameter that characterizes the conduction and radiation heat transfer mechanisms in a packed bed.

Generally in packed beds, the convective heat transfer is from the particles to the fluid flowing through the bed, sometimes it is referred to as the fluid-to-particle mode. The basic idea for the treatment of particle-to-fluid heat transfer is to consider the situation of the individual particle. In the literature, considerable efforts have been made to evaluate the heat transfer coefficient in chemical/catalytic packed bed reactors due to the importance of this parameter. An extensive review of experimental/theoretical works on particle-to-fluid heat transfer in the packed beds can be found in Wakao and Kaguei (1982), and more recently it was well summarized by Gnielinski (2010) and Tsotsas (2010). In fact, the heat transfer in packed beds is an extremely complex process, and there is, of course, no exact theory satisfactorily describes this phenomenon.

However, there are some correlations reported in the literature related to the convection heat transfer coefficient in gas-solid packed bed systems in terms of Nusselt numbers, as summarized in Table 2.2. Wakao and Kaguei (1982) give an overview of the different experimental data existing at that time and propose the following semi empirical correlation for heat transfer in a packed bed as the following:

$$Nu = 2 + 1.1 Pr^{1/3} Re^{0.6} \tag{31}$$

where the non-dimensional Prandtl number (Pr) is defined as follows:

$$Pr = \frac{\mu C_p}{k} \tag{31a}$$

Nu_h is an effective Nusselt number that is defined based on the average interstitial velocity and on the characteristic length scale for the pores (an equivalent hydraulic diameter, d_h) as follows:

$$Nu_h = \frac{h d_h}{k} = \frac{\varepsilon_b}{(1-\varepsilon_b)} Nu \tag{31b}$$

where the Nusselt number is defined based on pebble diameter (d_p) and is given by:

$$Nu = \frac{h d_p}{k} \tag{31c}$$

In this expression, h is the average convective solid-gas heat transfer coefficient in the pebble bed, and k is the thermal conductivity of flowing coolant gas.

Ranz (1952) and Rowe and Claxton (1965) earlier suggested alternative correlations for the prediction of the Nusselt number in packed beds, listed in Table 2.2. Kaviany (1995) stated that the above correlation (Equation 31) is a reliable one because it is based on a rigorous selection and adaptation of relevant experimental data. It is worthwhile to mention that the minimum Nusselt number (Nu=2) of the single sphere as the Reynolds number goes to zero ($Re \to 0$) represents the heat transfer by conduction only. This asymptotic value results from the solution of the unsteady state heat conduction equation for chemical packed bed reactors and it is subject to discussion in nuclear pebble bed reactors. Nelson and Galloway (1975) argued that, for $Re \to 0$ the heat transfer from spheres in the pebble bed cannot be related to that of a single sphere in an infinite surrounding since the boundary conditions are different. They showed that for dense packed systems which is the case of pebble bed nuclear reactors, the Nusselt

number (Nu) grows linearly with Re and declines to zero as Re approaches zero. Nelson and Galloway suggested the following correlation in densely packed beds:

$$\mathrm{Nu} = \frac{0.18}{\left(1-\varepsilon_{\mathrm{b}}\right)^{1/3}}\left[\frac{1}{\left(1-\varepsilon_{\mathrm{b}}\right)^{1/3}}-1\right]\mathrm{Re}\,\mathrm{Pr}^{2/3} \tag{32}$$

The average void fraction of the bed occurs as a parameter in Equation (32).

For high-temperature packed pebble-bed nuclear reactors, the theory explaining the convective solid-gas heat transfer coefficient is based on the assumption that the heat transfer of heated pebbles can be related to the heat transfer from a single sphere (pebble) by introducing an arrangement or form factor, f_{ε}, which depends on the void fraction (Gnielinski, 2010). Hence, Gnielinski (1978, 1981), evaluated the experimental results of about twenty authors and established a relationship among the Nusselt number, Reynolds number, Prandtl number and porosity of the packed-pebble bed, in the following form:

$$\mathrm{Nu} = f_{\varepsilon}\mathrm{Nu}_{\mathrm{sp}} \qquad \text{for} \qquad \mathrm{Re}/\varepsilon_{\mathrm{b}} \le 2\times10^{4} \tag{33}$$

where,

$$f_{\varepsilon} = 1+1.5(1-\varepsilon) \tag{33a}$$

$\mathrm{Nu}_{\mathrm{sp}}$ is the Nusselt number of a single sphere (pebble), which can be calculated, according to the following equation:

$$\mathrm{Nu}_{\mathrm{sp}} = 2+\sqrt{\mathrm{Nu}_{\mathrm{lam}}^{2}+\mathrm{Nu}_{\mathrm{turb}}^{2}} \tag{33b}$$

$\mathrm{Nu}_{\mathrm{lam}}$ and $\mathrm{Nu}_{\mathrm{turb}}$ are the Nusselt numbers of the single sphere for laminar and turbulent flow, respectively. They can be obtained from the equations valid for the flat plate by introducing a length scale as a characteristic streaming length which is equal to the sphere diameter in the case of spherical pebbles, thusly:

$$\mathrm{Nu}_{\mathrm{lam}} = 0.664\left(\mathrm{Re}/\varepsilon_{\mathrm{b}}\right)^{1/2}\mathrm{Pr}^{1/3} \tag{33c}$$

$$\mathrm{Nu}_{\mathrm{turb}} = \frac{0.037\left(\mathrm{Re}/\varepsilon_{\mathrm{b}}\right)^{0.8}\mathrm{Pr}}{1+2.443\left(\mathrm{Re}/\varepsilon_{\mathrm{b}}\right)^{-0.1}\left(\mathrm{Pr}^{2/3}-1\right)} \tag{33d}$$

In their modular pebble-bed reactor project (Terry, 2001), the Idaho National Engineering and Environmental Laboratory (INEEL) and the Massachusetts Institute of Technology (MIT), and also the Association of German Engineers (VDI) Heat Atlas (Gnielinski, 2010), provide the above equations (33-33d) as recommended correlations for the predication of pebble-to-gas heat transfer in the core of the high-temperature packed pebble-bed nuclear reactors.

Based on experimental data from several independent studies of heat convection in randomly packed pebble-beds, the German Nuclear Safety Standard Commission (KTA) proposed a correlation to determine the heat transfer coefficient of solid to flowing gas for a German high temperature reactor (HTR), as follows (KTA Standards, 1983):

$$\mathrm{Nu} = 1.27\left(\frac{\mathrm{Pr}^{1/3}}{\varepsilon_{\mathrm{b}}^{1.18}}\right)\mathrm{Re}^{0.36} + 0.033\left(\frac{\mathrm{Pr}^{1/2}}{\varepsilon_{\mathrm{b}}^{1.07}}\right)\mathrm{Re}^{0.86} \qquad \text{for} \quad 100 \le \mathrm{Re} \le 10^5 \tag{34}$$

The above correlation (Equation 34) is very similar to the one developed by Gupta et al. (1974) and also to that correlation recommended for the flow of gases through packed beds by Bird et al., (2002), that are listed in Table 2.2. According to Gougar (2006), the Idaho National Laboratory (INL) has adopted the KTA's correlation in their multi-scale and multi-dimensional simulation and optimization code for the design and analysis of pebble-bed high temperature reactors which is called the PEBBED code. A similar empirical heat transfer correlation was developed by Achenbach (1995) for a pebble bed heat transfer coefficient in which the Reynolds number range exceeds ranges used by other researchers by one order of magnitude, as follows:

$$\mathrm{Nu} = \left[\left(1.18\,\mathrm{Re}^{0.58}\right)^4 + \left(0.23\left(\mathrm{Re_h}\right)^{0.75}\right)^4 \right]^{1/4} \qquad \text{for} \qquad \mathrm{Re}/\varepsilon_b \le 7.7\times10^5 \qquad (35)$$

Finally, the convection heat transfer at the wall, in terms of the wall Nusselt number $\left(\mathrm{Nu_W}\right)$, for fluid flow in a packed pebble bed can be expressed as follows (Hahn and Achenbach, 1986):

$$\mathrm{Nu_W} = \left(1 - \frac{1}{\mathrm{D}/\mathrm{d_p}}\right)\mathrm{Re}^{0.61}\,\mathrm{Pr}^{1/3} \qquad \text{for} \qquad 100 \le \mathrm{Re} \le 2\times10^4 \qquad (36)$$

Table 2.2. Summary of Selected Correlations for the Heat Transfer Coefficient in Packed Pebble-Bed Reactors

Author	Correlation	Range
Ranz (1952)	$\mathrm{Nu} = 2 + 0.6\,\mathrm{Pr}^{1/3}\,\mathrm{Re}^{0.5}$	$\mathrm{Re} \geq 100$ $0.6 \leq \mathrm{Pr} \leq 400$
Rowe and Claxton (1965)	$\mathrm{Nu} = \mathrm{A} + \mathrm{B}\,\mathrm{Pr}^{1/3}\,\mathrm{Re}^{\mathrm{n}}$ $\mathrm{A} = \frac{2}{1-(1-\varepsilon_b)^{1/3}};\quad \mathrm{B} = \frac{2}{3\varepsilon_b}$ $\frac{2-3\mathrm{n}}{3\mathrm{n}-1} = 4.65\,\mathrm{Re}^{-0.28}$	$1 \leq \mathrm{Re} \leq 1\times10^5$ $0.71 \leq \mathrm{Pr} \leq 7.18$ $0.26 \leq \varepsilon_b \leq 0.632$
Gupta et al. (1974)	$\mathrm{Nu} = 2.876\left(\frac{\mathrm{Pr}^{1/3}}{\varepsilon_b}\right) + 0.3023\left(\frac{\mathrm{Pr}^{1/3}}{\varepsilon_b}\right)\mathrm{Re}^{0.65}$	$10 \leq \mathrm{Re} \leq 1\times10^5$ $0.71 \leq \mathrm{Pr} \leq 7.18$ $0.26 \leq \varepsilon_b \leq 0.935$
Gnielinski (1978; 1981)	$\mathrm{Nu} = f_\varepsilon \mathrm{Nu}_{\mathrm{sp}}$ $f_\varepsilon = 1 + 1.5(1-\varepsilon_b)$ $\mathrm{Nu}_{\mathrm{sp}} = 2 + \sqrt{\mathrm{Nu}_{\mathrm{lam}}^2 + \mathrm{Nu}_{\mathrm{turb}}^2}$ $\mathrm{Nu}_{\mathrm{lam}} = 0.664\left(\varepsilon_b\right)^{1/2}\mathrm{Pr}^{1/3}$ $\mathrm{Nu}_{\mathrm{turb}} = \frac{0.037\left(\mathrm{Re}/\varepsilon_b\right)^{0.8}\mathrm{Pr}}{1+2.443\left(\mathrm{Re}/\varepsilon_b\right)^{-0.1}\left(\mathrm{Pr}^{2/3}-1\right)}$	$\mathrm{Re}/\varepsilon_b \leq 2\times10^4$ $0.71 \leq \mathrm{Pr} \leq 10^4$ $\varepsilon_b = 0.387$
Wakao and Kaguei (1982)	$\mathrm{Nu} = 2 + 1.1\mathrm{Pr}^{1/3}\,\mathrm{Re}^{0.6}$	$15 \leq \mathrm{Re} \leq 8500$ $\varepsilon_b = 0.4$
KTA Standards (1983)	$\mathrm{Nu} = 1.27\left(\frac{\mathrm{Pr}^{1/3}}{\varepsilon_b^{1.18}}\right)\mathrm{Re}^{0.36} + 0.033\left(\frac{\mathrm{Pr}^{1/2}}{\varepsilon_b^{1.07}}\right)\mathrm{Re}^{0.86}$	$100 \leq \mathrm{Re} \leq 10^5$ $\mathrm{Pr} = 0.70$ $0.36 \leq \varepsilon_b \leq 0.42$
Hahn and Achenbach (1986)	$\mathrm{Nu}_{\mathrm{W}} = \left(1 - \frac{1}{\mathrm{D}/\mathrm{d}_{\mathrm{p}}}\right)\mathrm{Re}^{0.61}\,\mathrm{Pr}^{1/3}$	$100 \leq \mathrm{Re} \leq 2\times10^4$
Achenbach (1995)	$\mathrm{Nu} = \left[\left(1.18\,\mathrm{Re}^{0.58}\right)^4 + \left(0.23\left(\mathrm{Re}_h\right)^{0.75}\right)^4\right]^{1/4}$	$\mathrm{Re}/\varepsilon_b \leq 7.7\times10^5$ $\mathrm{Pr} = 0.71$ $\varepsilon_b = 0.387$
Bird et al. (2002)	$\mathrm{Nu} = 2.19\,\mathrm{Pr}^{1/3}\,\mathrm{Re}^{1/3} + 0.78\,\mathrm{Pr}^{1/3}\,\mathrm{Re}^{0.62}$	$1 \leq \mathrm{Re} \leq 1\times10^5$ $\mathrm{Pr} > 0.70$

2.7. EFFECT OF POROSITY ON PRESSURE DROP, AXIAL DISPERSION AND FORCED CONVECTIVE HEAT TRANSFER

In randomly packed pebble-bed reactors, the value of porosity influences appreciably the absolute magnitude of the pressure drop across the bed, the axial dispersion process and the convective heat transfer coefficient between solid and flowing coolant gas. In order to explain analytically the effect of voidage on pressure drop for a randomly packed pebble-bed of spherical particles (pebbles), the KTA's empirical correlation (Equation 15) is rewritten for the dimensionless pressure drop form (or it is called friction force coefficient), $\left(\psi = \left(\Delta P/\left(\rho/2\right)V^2\right)\left(d_h/L\right)\right)$, in terms of the Reynolds number as follows (KTA Standards, 1981):

$$\psi = \frac{320}{\left[\mathrm{Re}/\left(1-\varepsilon_b\right)\right]} + \frac{6}{\left[\mathrm{Re}/\left(1-\varepsilon_b\right)\right]^{0.1}} \qquad \text{for} \qquad \left[\mathrm{Re}/\left(1-\varepsilon_b\right)\right] \le 5\times10^4 \tag{38}$$

As mentioned earlier, the first term of Equation 38, represents the asymptotic solution for laminar flow, while the second term represents the solution for turbulent flow. Each of the terms can be written as (Fenech, 1981; Achenbach, 1995):

$$\psi = A\left(\frac{\mathrm{Re}}{1-\varepsilon_b}\right)^{-n} = A\left(1-\varepsilon_b\right)^n \mathrm{Re}^{-n} \tag{39}$$

where, n=1 represents the low Reynolds number range and n=0 represents the high one. The variation of pressure drop with porosity has been expressed by Fenech (1981) as per the following:

$$\frac{d\left(\Delta P\right)}{\Delta P} = \frac{\partial\left(\Delta P\right)}{\partial\varepsilon_b}\frac{d\varepsilon_b}{\Delta P} \tag{40}$$

Combining Equations (12) and (39), with Equation (40), yields:

$$\frac{d\left(\Delta P\right)}{\Delta P} = -\frac{\left[3-\varepsilon_b(2-n)\right]}{\left(1-\varepsilon_b\right)}\frac{d\varepsilon_b}{\varepsilon_b} \tag{41}$$

Here n=1 for laminar flow conditions, while n=0 for turbulent flow conditions (KTA Standards, 1981). These values of the exponent (n) come from the KTA correlation that is used for determining the friction force coefficient or the dimensionless pressure drop form (Equation 15).

It can be shown from Equation (41) that a positive relative variation of the void fraction ($d\varepsilon_b/\varepsilon_b$) causes a negative relative variation of the pressure drop [d (ΔP) /ΔP] multiplied by a factor that is dependent on the porosity (ε_b) and on the slop (n) of the Reynolds number. In other words, it is greater by a factor of [3- ε_b (2-n) / (1- ε_b)].

For a randomly packed bed of spherical particles, the values for real packings typically fall into the range, (ε_b =0.36-0.42) (Zhang et al, 2006). Therefore, the normal packing of typical voidage (ε_b) of around 0.4 represents a separate line between loose packing ($\varepsilon_b > 0.4$) and dense packing ($\varepsilon_b < 0.4$).

Using Equation (41), Figure 2.5 has been plotted to show the effect of void fraction on pressure drop. For example, at $\varepsilon_b = 0.4$, the percentage of error with respect to pressure drop is ~ 4 times. The error defined as undergone for the determination of porosity. In other words, an error of 1% in ε_b causes errors of ~ 4% in ΔP as per the equations above and Figure (2.5).

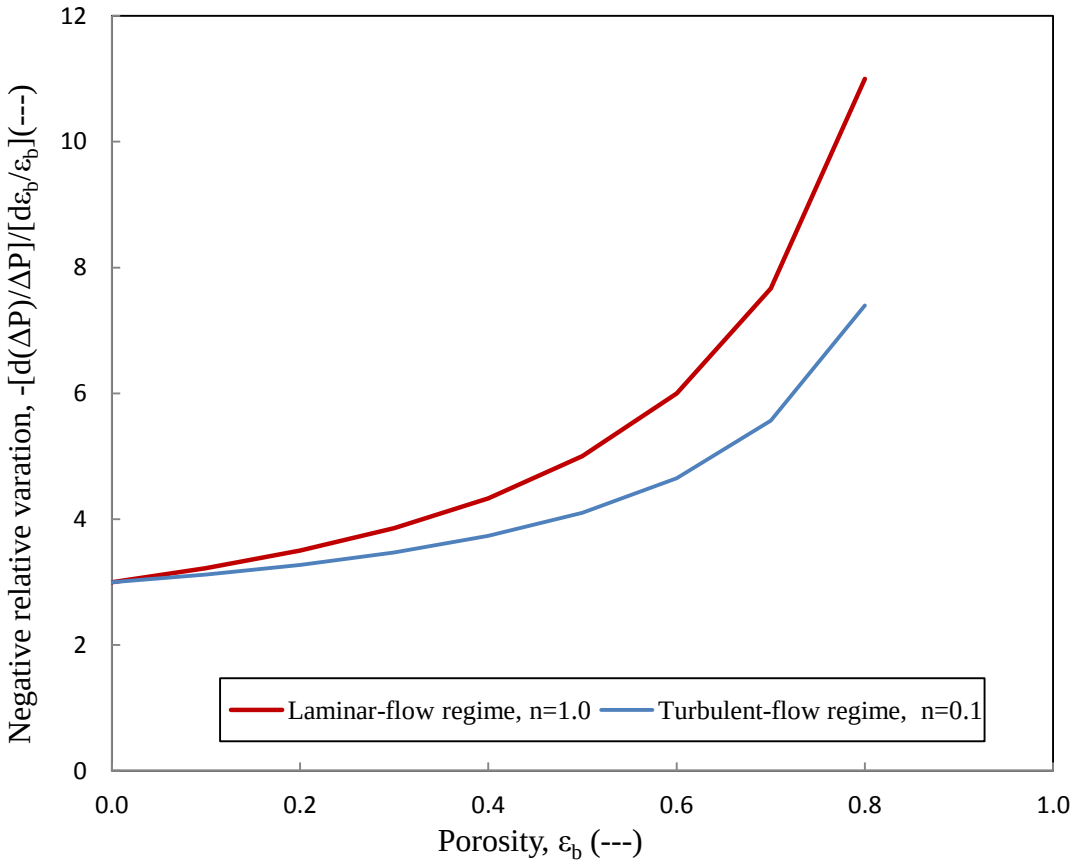

Figure 2.5. Effect of Void Fraction (Porosity) on the Pressure Drop in the Laminar and Turbulent Flow Regimes

The literature of axial dispersion phenomenon, as discussed in section 2.5, shows that the dispersive Peclet number (Pe_D) is a function of the Reynolds number (Re), the Schmidt number (Sc) and the porosity (ε_b) created by the packing. Therefore, the functional dependence of these groups can be expressed by the following:

$$Pe_D = f\left(\varepsilon_b; Re; Sc\right) \tag{42}$$

To explain the trend of the influence of porosity on the axial dispersion process, the early correlations of axial dispersion in packed beds, as showed in Table 2.1, have

been analyzed and accordingly **this work suggests the following correlation that describes the relationship of Pe_D with respect to Re , Sc and ε_b.**

$$\frac{1}{Pe_D} = A\left(\frac{1-\varepsilon_b}{\varepsilon_b}\right)^{-n}\left(\frac{Re}{1-\varepsilon_b}\right)^{-n} Sc^{-n} \tag{43}$$

This form represents a sum of the contribution of diffusion and convection terms.

As mentioned earlier, at low flow rates, axial dispersion is considered to be a function of the diffusion coefficient modified by a factor which accounts for the tortuosity and porosity created by the packing. As the flow velocity increases, dispersion becomes a function of the hydrodynamics using the same packing. Therefore, the exponent can be considered n=1 for low flow rate and n=0 for high flow rate.

By following the same approach of variation of pressure drop with porosity, the variation of axial dispersion with porosity can be presented in this work as follows:

$$\frac{d(1/Pe_D)}{(1/Pe_D)} = \frac{\partial(1/Pe_D)}{\partial\varepsilon_b}\frac{d\varepsilon_b}{(1/Pe_D)} \tag{44}$$

Combining the above equation together with Equation (43) yields:

$$\frac{d(1/Pe_D)}{(1/Pe_D)} = -\frac{(3-2n\varepsilon_b)}{(1-\varepsilon_b)}\frac{d\varepsilon_b}{\varepsilon_b} \tag{45}$$

Here n=1 for laminar flow conditions, while n=0 for turbulent flow conditions.

Regarding the effect of the voidage on the forced convective heat transfer, similar to those effects on the pressure drop (Equation 40) and the axial dispersion and mixing in terms of Pe_D (Equation 44), Fenech, (1981) reported the following expression:

$$\frac{d(Nu)}{Nu} = -\frac{(1-n\varepsilon_b)}{(1-\varepsilon_b)}\frac{d\varepsilon_b}{\varepsilon_b} \tag{46}$$

Here n=0 for laminar flow conditions while n=0.6 for turbulent flow conditions (Fenech, 1981).

It can be shown from the Equations (45 and 46) that a positive relative variation of the void fraction ($d\varepsilon_b/\varepsilon_b$) causes a negative relative variation of both the reciprocal Peclet number [$d\,(1/Pe_D) / (1/Pe_D)$] and the Nusselt number [$d\,(Nu)/Nu$] multiplied by the factors of [$(3- 2n\varepsilon_b)/(1- \varepsilon_b)$] and [$(1- n\varepsilon_b)/(1- \varepsilon_b)$], respectively. Using Equations 45 and 46, parts a and b of Figure 2.6 show the effect of void fraction on axial dispersion and convective heat transfer, respectively. For example, at $\varepsilon_b= 0.4$ the percentage of error with respect to the reciprocal Peclet number and the Nusselt number are ~ 4.3 times and ~ 1.5 times, respectively, the error undergone for the determination of porosity. In other words, an error of 1% in ε_b causes errors of ~ 4.3% and ~ 1.5% for $(1/Pe_D)$ and Nu, respectively.

Based on Figures 2.5 and 2. 6, the percentage of error for all relative variations rises with increasing porosity (ε_b) and decreasing as the exponent (n) increases. Hence, the strong dependence of the pressure drop, axial dispersion, and mixing and heat transfer on the void fraction underlines the importance of packing and refueling pebble beds carefully to avoid bypass and channeling coolant flow due to local variations in the packing density.

It is obvious that the fluid flow, pressure drop, axial dispersion and mixing and heat transport mechanisms are all sensitive and influenced by the porous structure of the packed-pebble bed reactor. Therefore, a proper understanding and characterization of the porous structure of the bed is of great importance for safe design and efficient operation of packed pebble-bed reactors. As a part of another graduate study thesis (DOE report, 2012), this has been addressed by quantifying the bed structure using gamma ray computed tomography (CT).

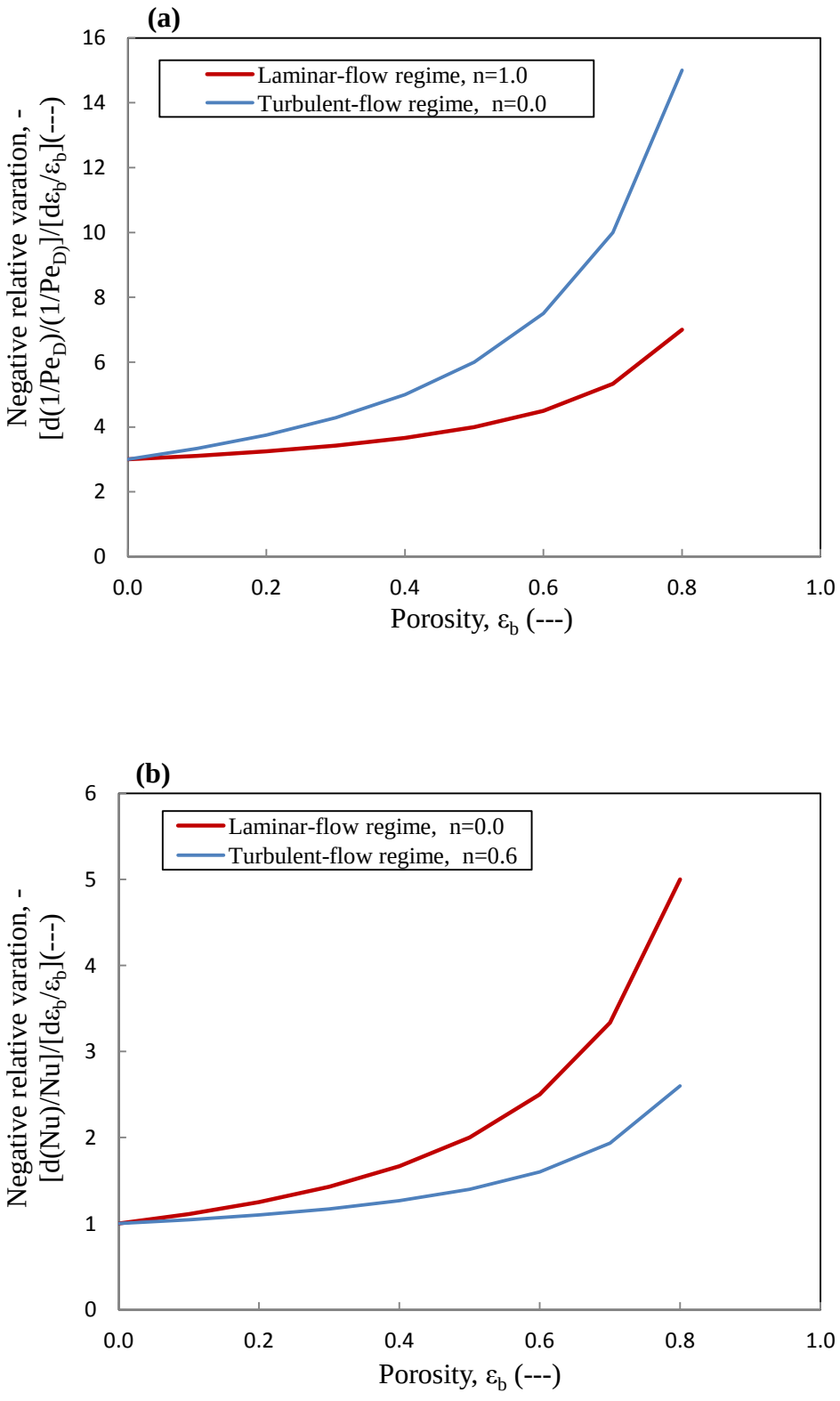

Figure 2.6. Effect of Void Fraction (Porosity) in the Laminar and Turbulent Flow Regimes on the following: (a) Convective Heat Transfer, and (b) Axial Dispersion and Mixing

3. GAS DISPERSION AND MIXING PHENOMENA IN THE PEBBLE BEDS DESCRIBED BY AXIAL DISPERSION MODEL (ADM)

3.1. MOTVATION

For the nuclear packed pebble-bed reactors, the key point of safety and reliability is the capability of removing the heat produced in the core in both normal operation and under accident conditions. The heat removed appears to be strongly depending on the distribution and structure of the coolant flow in the core. However, inefficient removal of the heat can have negative impact on the temperature gradient of the bed and hence on the reactor performance. In addition to that, the high local temperature gradients cause damaging hot spots that should be avoided in the core of pebble-bed reactors for proper design and safe operation. For this reason, a thermal-hydraulic analysis related to the investigation of gas phase dispersion and the extent of its mixing in pebble-bed reactors is of crucial importance. Furthermore, the efficiency of the reactor is dependent upon how the flowing gas through the bed is distributed. Hence, the ability to measure the gas distribution in a pebble-bed reactor is practically very useful in designing and operating these reactors. In general, moving bed where the particles are contacted with gas phase while they move downward have found applications in industry such as two phase flow catalytic hydro-processing of heavy oil as the catalyst are replaced on-stream. Despite these recent interests, there is still lack of understanding of the complex gas flow structure and mixing phenomena in these moving bed types of reactors.

In the open literatures, there are very few conducted studies related to the flow-field in the pebble beds. Among these studies, Hassan and Dominguez (2008) applied particle image velocimetry (PIV) along with matched index of refraction (MIR)

technique to measure the full-field velocity of the liquid phase in the interior region of a small sized (3cm x 3cm x 35 cm) packed bed. They packed the column randomly with 4.7 mm diameter of polymethyl-methacrylate (PMMA) beads of 1.18 g/cm^3 density which offer high light transmittance with a refractive of index and p-cymene (liquid phase) was selected instead of gas phase. They correlated the results of the liquid phase to that of the gas phase. Vertical liquid flow structures were identified in some of the pores (voids) between the spheres while there were some flows with preferential direction in some other pores. In general, it was observed that the flow in the pores is of a very complicated nature. Despite they used liquid phase instead of gas phase, the authors also concluded that the obtained data would be useful for enhancing the understanding of gas flow through packed bed and for the computational fluid dynamics (CFD) code validation. In the study of Lee and Lee (2009), flow field measurements were taken in a two-dimensional wind tunnel by particle image velocity (PIV) technique in very narrow flow channel between the pebbles and air was used as the gas phase. Also, small size (170mm x 170mm x 505 mm) pebble bed test section was used. The results showed that the presence of stagnation points within the fuel gaps might lead to having hot spots on the surface of the fuel particles. With only these two attempts, the hydrodynamics phenomena have not yet been well understood.

As mentioned earlier in Section 2, there are no detailed experimental measurements, detailed knowledge and quantification of the gas phase dynamics and its extent of mixing in nuclear packed pebble bed reactors. Furthermore, most of the reported experimental studies were restricted to understand the effect of operating conditions on the global parameters such as pressure drop and overall voidage of the bed

(Hassan, 2008). However, there are studies reported in literature related to the dispersion of gas and its mixing in two phase gas-solid flow packed bed reactor, as discussed in Section 2.

Accordingly, this work focuses on quantifying for the first time the dispersion and extent of mixing of the gas phase in a cold-flow pebble bed unit of 0.3 m diameter using an advanced gaseous tracer technique developed for this purpose. The deviation of the flow of the gas phase from plug flow characteristics in pebble bed is described using axial dispersion model (ADM) where such representation is valid if there is not much deviation from ideal plug-flow reactor (PFR) model. However, quantification of the bed structure using gamma-ray computed tomography has been part of other graduate study thesis in our research group. The effect of gas velocity on the axial dispersion coefficient has been investigated using a wide range of flow conditions which covers both laminar and turbulent flow regimes in the studied pebble bed. The effects of bed structure in terms of particle size and bed height have been investigated. The degree and extent of mixing in the pebble bed is characterized in terms of axial dispersion coefficient (D_{ax}) and dispersive Peclet numbers ($Pe_D=V_g d_p/\varepsilon_b D_{ax}$).

3.2. EXPERIMENTAL WORK

3.2.1. Separate Effects Experimental Setup. Since the velocity of the helium gas in real pebble bed is very high as compared to the pebbles moving slowly by gravity of ~ 4.5 mm/hr average speed. The entire pebble bed reactor can be considered as a fixed packed bed (du Toit, 2002) relative to the flowing gas phase.

Therefore, to simplify the experimental work yet to mimic the interaction between the gas phase and the solids, the pebble bed is made of fixed bed particles for the purpose of this study. The cold-flow unit of pebble bed, that has been developed as separate effects experimental set up to conduct proper gas tracer, pressure drop and heat transfer coefficient measurements, consists of a Plexiglas column of 0.3 m diameter and variable height of 0.3-0.92 m. The schematic diagram of the separate effect experimental setup is shown in Figure 3.1. Oil-free compressed air was used as the gas phase flowing downward while different sizes of glass bead particles were used as the pebbles in a fixed bed.

Three different sizes of glass beads type of pebbles of 1.25 cm (0.5 inch), 2.5 cm (1 inch), and 5 cm (2 inch) diameter with the same density (2.1 gm/cm^3) have been selected to form randomly packed beds. In the other words, the aspect ratios (bed-diameter to pebble-diameter, D/d_p) of 24, 12 and 6 have been used based on the pebble bed of 30 cm diameter, respectively. The typical value of void fraction (average porosity of the bed, ε_b) for random packing in each case is measured in our laboratory by direct balance method and found to be around 0.378, 0.385, and 0.397, respectively. In this method the total number of spheres packed into the cylindrical column is known in addition to the volume of the empty column. The empty column volume is calculated using the cylinder dimensions. Since the total number of spheres is known, the total volume occupied by the packing material is calculated using the volume of an average of a number of individual spheres. The voids volume is calculated by subtracting the volume of the empty column from the volume occupied by the spheres and hence the porosity or the void fraction can be estimated. This method assumed that the beads are perfect

spheres with tight tolerances in its diameter. In addition, the average porosities from present experiments were compared with recommended correlations in the literature, as discussed in Section 2.

The flow rate of the filtered dry air was adjusted by a pressure regulator and rotameters system, which consists of two rotameters (Omega HFL6715A-0045-14) connected in parallel. The range of each one of these rotameters was 15-150 SCFM at calibrated pressure of 100 psi and temperature of 70 ^{o}F. The superficial gas velocity (V_g) was varied within the range of 0.01 m/s to 2 m/s which covers both laminar and turbulent flow regimes. Table 3.1 summarizes the experimental setup dimensions and the operating conditions. A cone type upper plenum of 0.1 m height is mounted at the top of the bed to distribute the gas phase to the bed, as shown in Figure 3.2. It should provide good backmixing before the bed with small external volume. The gas is distributed to the bed using perforated plate with 140 holes of 3 mm diameter. These holes are arranged in a 2.25 cm square pitch, as shown in Figure 3.3. The opening area of the distributor is 2.7% of the total area. The design of distributor was checked at the entrance boundary between the plenum and the reactor by calculating the orifice Reynolds number. The orifice Reynolds numbers for the 0.01 m/s and 2 m/s superficial gas velocity ranged from 2,400 to 186,000 which means that the distributor operates in the jetting regime (Degaleesan, 1997). This indicates that the flow through the distributor holes is unidirectional and there is no possibility of mal-distribution of the gas to the bed and/or backmixing. Hence, the gas flow distribution on top of the reactor is ensured by a perforated plate. Finally, the bottom of the pebble bed consists of a plastic cone shape with an angle of 60^{o} horizontally and an exit opening of 5 cm for the gas phase.

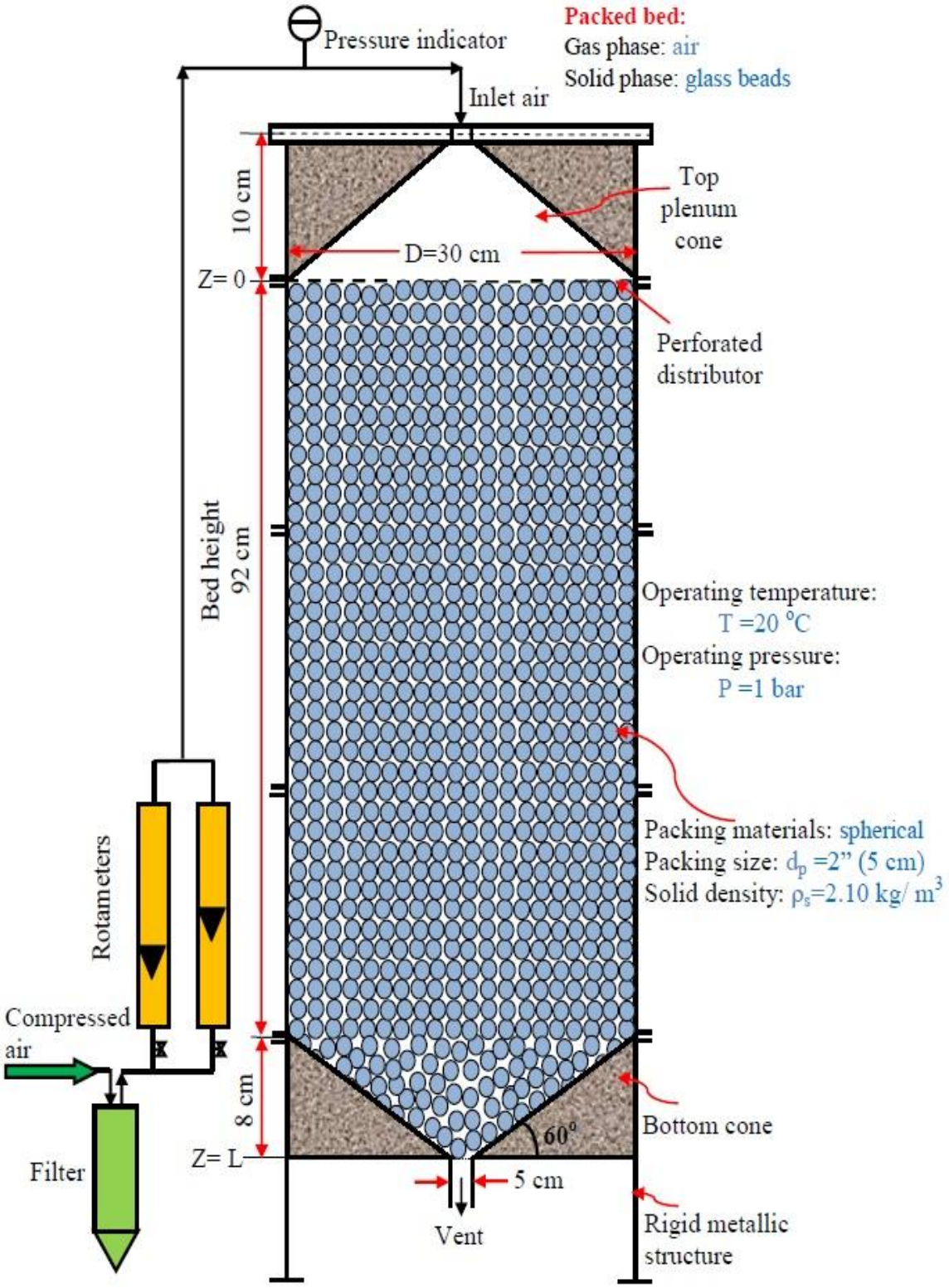

Figure 3.1. Schematic Diagram of the Separate Effect Experimental Set-Up; the Bed Height can be Varies into 1ft, 2ft and 3ft (92 cm) with Equally Spaced Flanges

Table 3.1. Experimental Setup and Operating Conditions

Parameter	**Range**
Packed bed diameter, m	0.3
Packed bed height, m	0.3-0.92
Gas phase	Air
Solid phase	Glass beads (marbles)
Packing shape	Spherical
Packing size, cm	1.25, 2.5 and 5
Aspect ratio	24, 12 and 6
Average bed porosity	0.378, 0.385, and 0.397
Superficial gas velocity, m/s	0.01-2.0
System pressure, kPa	101.33
System temperature, ^{o}C	21

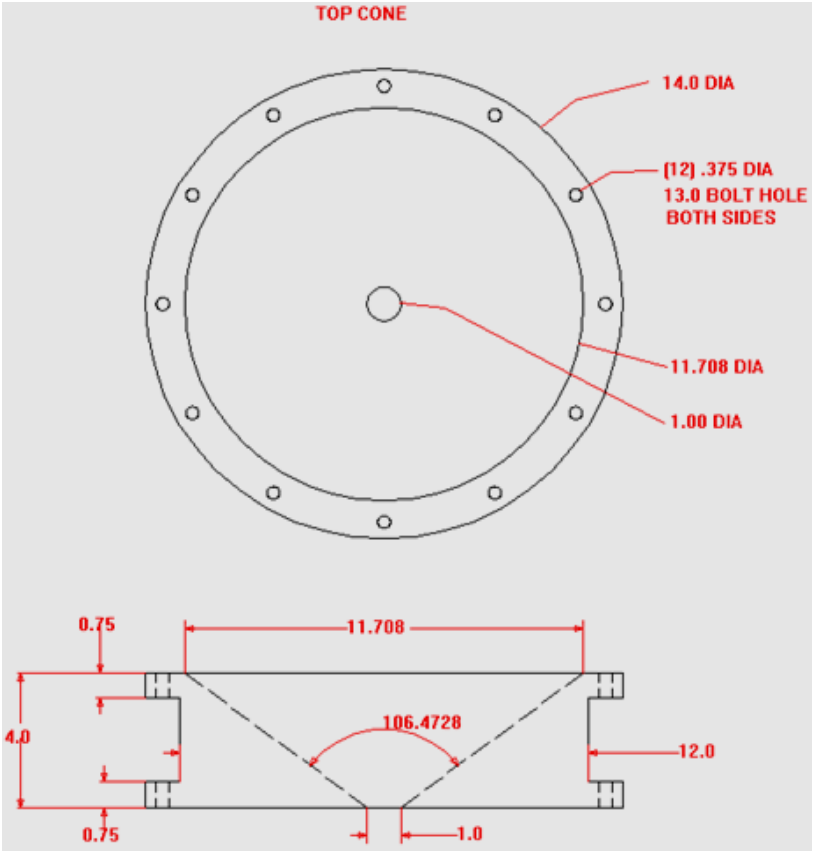

Figure 3.2. Schematic Diagram of the Upper Plenum Cone, Units are in Inches

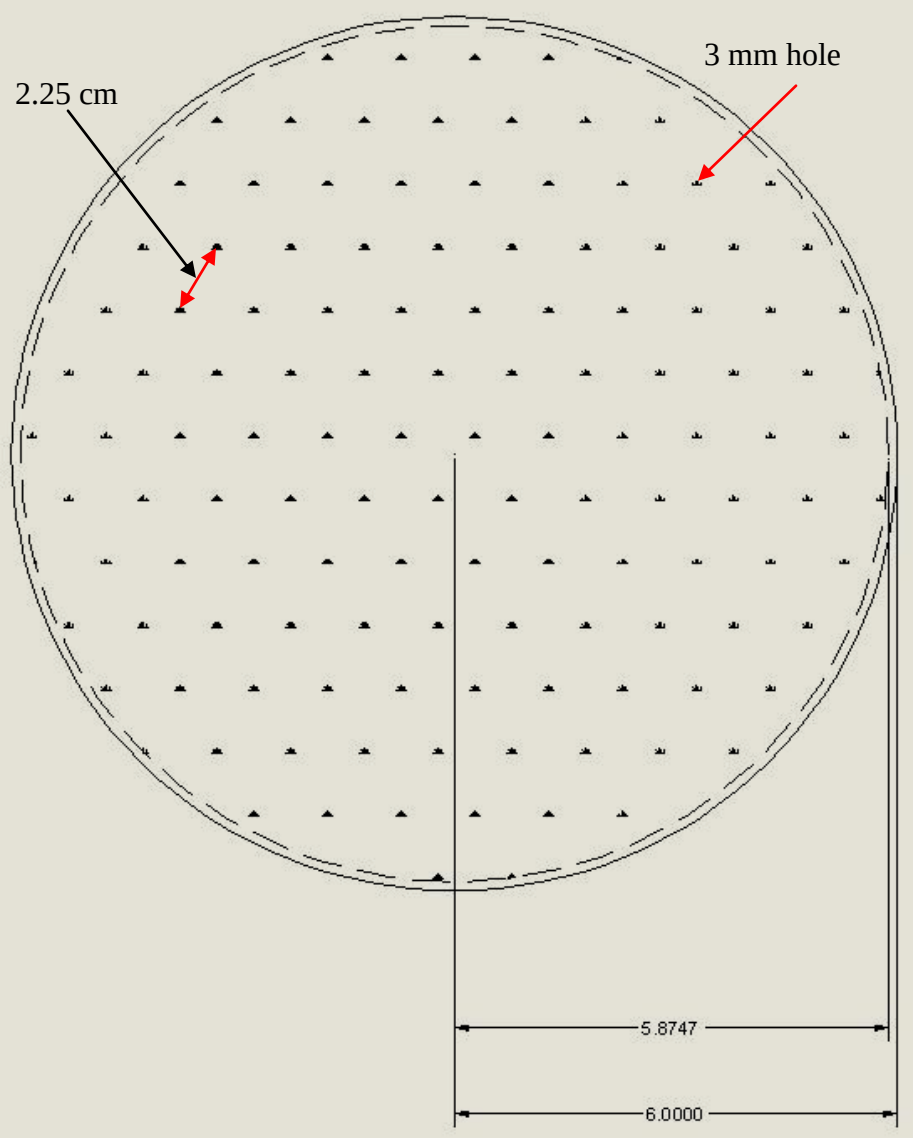

Figure 3.3. Schematic Diagram of the Air Perforated Distributor at the Exit of Upper Plenum (Figure 3.1), Units are in Inches

3.2.2. Development of Gaseous Tracer Technique. The well designed gaseous tracer technique that was developed by Han (2007) along with needed methodology of convolution and deconvolution to get the bed response has been adopted in this work. Hence, this technique was redeveloped and used as a part of this study to measure the RTD of the gas phase in the studied pebble bed. A photo of the pebble bed unit equipped with the gaseous tracer technique is shown in Figure 3.4. While the schematic diagram of the advanced gas dynamics experimental setup is shown in Figure 3.5.

The gaseous tracer unit consists of gas analyzer, gas pump, and PC with data acquisition (DAQ) system. The gas analyzer is a binary type (GOW-MAC 20 series) which contains a thermal conductivity detector (TCD). Here helium gas is used as a tracer in the air stream, where TCD was found to be suitable for helium concentration measurements. However, the unit is also equipped with flame ionization detector (FID) for other tracer gases. A vacuum pump (Model: GOW-MAC 59-300) is used to draw the gas sample out of the reactor and pass it to the detector. More information and an outline about the operating steps of the gas tracer technique are given in Appendix A. The response of the detector is then amplified, converted to digital signals, and recorded as time-series data at sampling frequency of 10 Hz which can be adjusted as well. As mentioned earlier, the technique is similar to the one developed by Han (2007) and implemented on characterizing the gas phase dispersion in bubble and slurry bubble columns. This method offers an advantage over other gas tracer techniques reported in the literature since it yields a proper estimation of the RTDs of the gas phase of the desired section of the bed as it accounts for the extra dispersion that occur due to the non-ideal tracer injection and the extra dispersion encountered in the plenum, sampling lines,

and analysis system which cause significant measurement errors. The tracer injection at the inlet of the upper cone plenum does not make a delta function at the gas distributor, which is the input boundary of the bed. Similarly, due to the extra dispersion caused by sampling lines and analytical components, response measured by the gas detection system does not exactly represent the actual tracer response at the point of sampling at the bed outlet. In order to compensate for the extra dispersion effects in the distributor, plenum zone, and sampling/analytical system a convolution integral method developed and implemented by Han (2007) was applied (Levenspiel, 1999; Han, 2007; Hamed, 2012) by which the extra dispersion is accounted for which will be discussed in the following sections.

In this work, specific arrangement was implemented to improve the accuracy of the gas tracer technique on its implementation on the developed pebble bed separate effects experimental setup. This arrangement was to place the detection system (thermal conductivity detector, TCD) close to the sampling points. This insured that the mean residence time and variance of the tracer in the sampling lines were as small as possible. The implementation of this arrangement caused a significant reduction in the mean residence time and the variance of the sampling lines and analytical system. This reduction allows more accurate estimation of the extent of gas mixing in the bed.

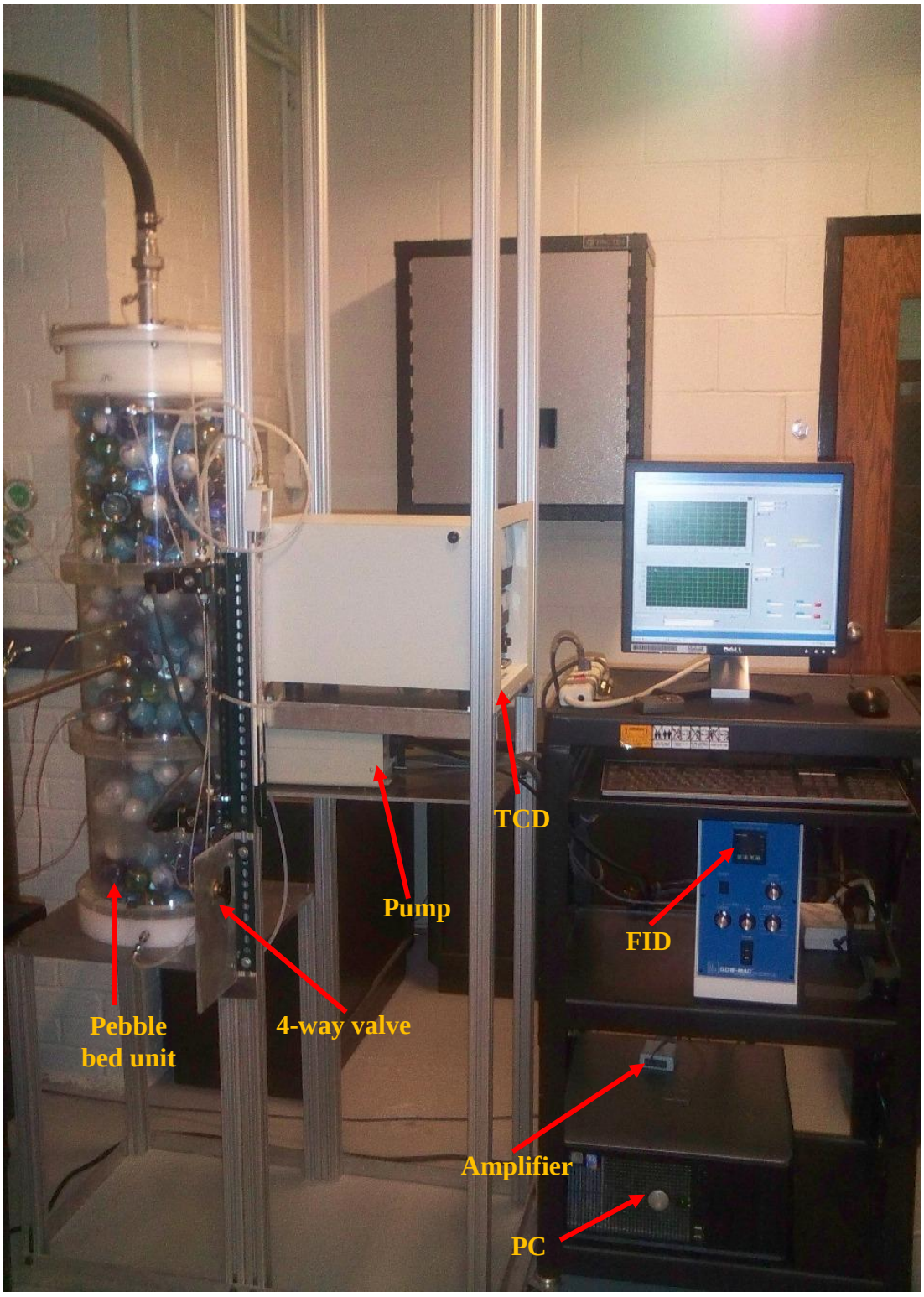

Figure 3.4. A Photo of the Pebble Bed Unit with an Advanced Gas Tracer Technique

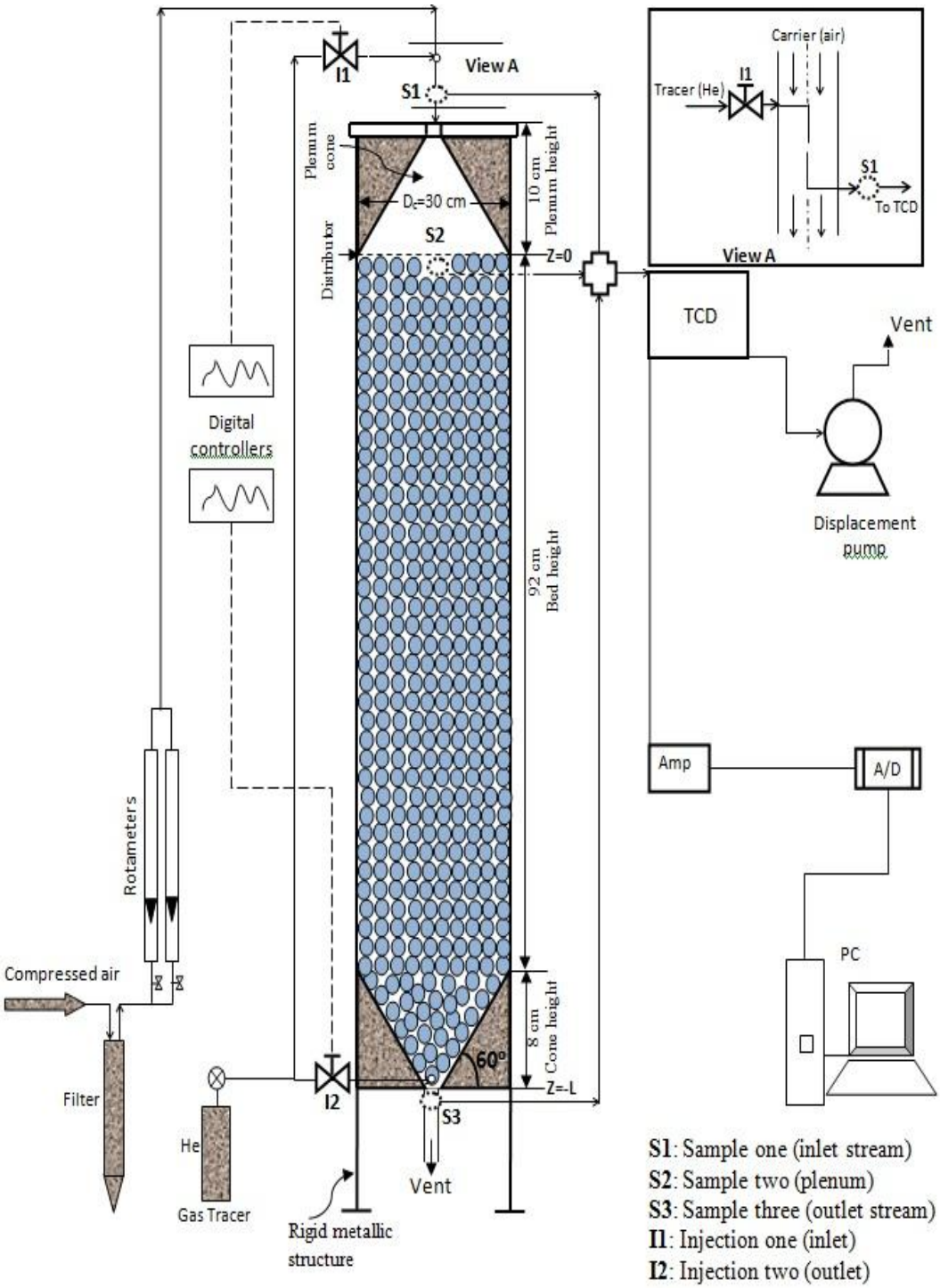

Figure 3.5. Schematic Diagram of the Advanced Gas Dynamics Experimental Set-Up

3.2.3. Development of Gaseous Tracer Measurements on the Cold-Flow Pebble Bed Setup.

The developed tracer technique involves two injecting ports and three sampling ports as shown in Figure 3.6. The tracer is injected at the center of the inlet gas line (I1) for the measurement of the overall response that includes the bed and external volumes and at the bottom conical cone of the bed outlet (I2) for the measurement of the response of the bottom sampling line (S3) where the overall response is measured at the bottom conical cone. There are three ports for sampling which are at: 1) the gas inlet (S1, view A, Figure 3.5) close to port I1 for the measurement of the response of the upper sampling line where the response of the upper plenum is measured at the exit of the upper distributor, 2) the pores of the gas distributor under plenum to measure the response of the upper plenum alone (S2), and 3) the neck of the conical bottom cone (S3) to measure the response of the bottom sampling line where the overall response is measured at the bottom. These injection and sampling ports are used as per Table 3.2. For each experiment one injection port and one related sampling port are used following the steps of experiments to be conducted to extract properly the response of the bed only (Table 3.2). A pulse input of tracer was introduced to the pebble bed at the injection point (I1) using a solenoid valve controlled by a digital timer where the injection time was adjusted at 0.05 s. Gas was sampled continuously at one of the indicated sampling ports through thin nylon tubes of 0.158 cm inner diameter under a vacuum generated by a vacuum pump. Using the pre-mentioned injection and sampling ports, four measurements (i-iv) were conducted at each experimental condition, as outlined in Table 3.2. This Table shows the trace injection ports, gas sampling locations used for the four tracer measurements and the zones to characterize their gas dispersion

with each measurement. In this work, each measurement was repeated 5–6 times and the average value is reported. Since the thermal conductivity detector, (TCD) is not connected directly to the experimental setup and it received the sample continuously and constantly through the vacuum pump; there is no any random fluctuations in the produced signal. For this reason, there is no need to filter the signal. The reproducibility of the measurements was within ±3%. The obtained response curves were normalized by the maximum value in each curve. Finally, gas phase axial dispersion inside the bed was quantified by model fitting and using a convolution integral method to deconvolute the tracer signals for parameters estimation, as discussed in the next sections.

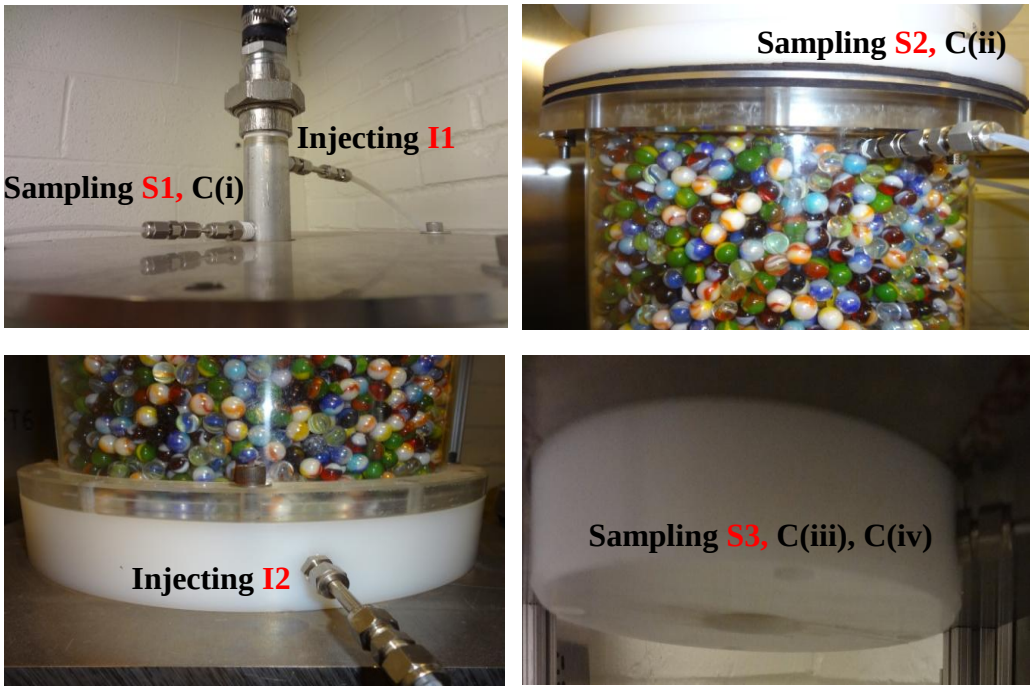

Figure 3.6. Photos of the Two Injection Ports and Three Sampling Ports

Table 3.2. The Designed Four Measurements for the Gaseous Tracer Technique

Measurement	Tracer injection	Sampling location	Tracer signal	Dispersion zones measured
(i)	I1	S1	$C_{(i)}$	Top sampling lines/ analytical system from S1
(ii)	I1	S2	$C_{(ii)}$	Plenum /distributor zone + sampling lines / analytical system from S2
(iii)	I2	S3	$C_{(iii)}$	Bottom sampling lines /analytical system from S3
(iv)	I1	S3	$C_{(iv)}$	Plenum/ distributor zone + packed bed zone + bottom sampling lines /analytical system from S3

I1 and **I2**: injection ports; **S1**, **S2** and **S3**: sampling ports. All locations indicated in Figures 3.5 and 3.6.

It is important and very useful to note that the application of the convolution integral method is valid only when the sub systems are completely independent (Levenspiel, 1999), which means that there is practically no back-mixing between them (i.e. convective unidirectional flow dominates at the boundaries between the sub systems). This assumption was confirmed in the design of the perforated distributor. Similar to the entrance boundary, no backmixing was observed at the outlet pipe between the two convoluted systems. This was made possible because the outlet small pipe (5 cm) could keep a high gas flow rate passing through it, preventing any back-mixing of the tracer.

3.3. THE METHODOLOGY OF DATA ANALYSIS

The experimental conditions are identified and positions of different tracer injection ports and sampling positions are described (Figure 3.5 and Table 3.2). The methodology, algorithms and programs of data analyses developed by Han (2007) have been extended to pebble bed in order to de-convolute the dispersion occurring in the external components from the overall dispersion (overall response).

It is also worth to mention here that the tracer experiments are delicate and their application methods need careful consideration and properly set. Hence, proper design and operation are essential which could be related to the injection time, tracer amount, rotameters readings, length of the tubes of sampling, location of the sampling points, the vicinity of the analytical system to set-up, etc. Therefore, in this work a methodology of many steps has been carefully taken to design the system and to process the obtained raw data and analyze properly the tracer responses from each compartment of the system, as shown in Figure 3.7. The methodology consists of two main steps as follows:

Step 1: Preparation of the raw data which is based on statistical procedures.

Step 2: Processing of the prepared data which is related to the convolution integral method and obtaining the only bed response and the axial dispersion coefficient.

The two main steps will be discussed in details in next sections.

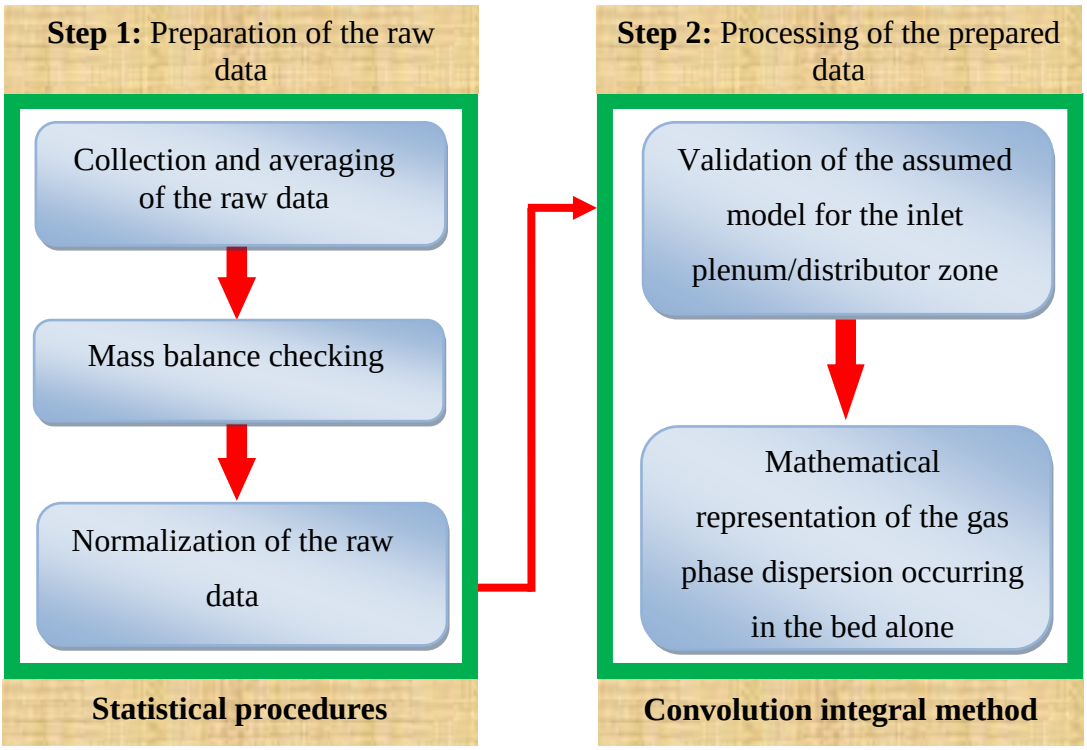

Figure 3.7. Schematic Diagram of the Procedures Used to Process the Obtained Data

3.4. STATISTICAL PROCEDURES FOR THE PREPARATION OF THE RAW DATA

In this first main step, i.e. preparation of the raw data, the statistical procedures were used to process the obtained raw data. This step is divided into three steps as discussed below. In addition, selected experiments are used to explain these steps. In these selected experiments air is used as the gas phase while helium is used as the gas tracer. The flow rate of air is kept at 0.02 m^3/s which is equivalent to a superficial gas velocity (V_g) of 20 cm/s based on 30 cm internal diameter of pebble bed.

3.4.1. Collection and Averaging of Raw Data. As shown in Table 3.2, a series of different experimental measurements (for different amount of injected helium depending on the volumetric flow rate of the related bed external components) are required in order to characterize the gas phase dispersion and mixing occurring in the bed zone alone. As mentioned before, in this work, each measurement was repeated 5–6 times and the average value is reported. Figure 3.8 shows the output signal of the tracer for six runs with the average one for the measurements of C(iv) (Table 3.2) at superficial gas velocity (Vg) of 30 cm/s. The reproducibility of these measurements was within ±1.5%.

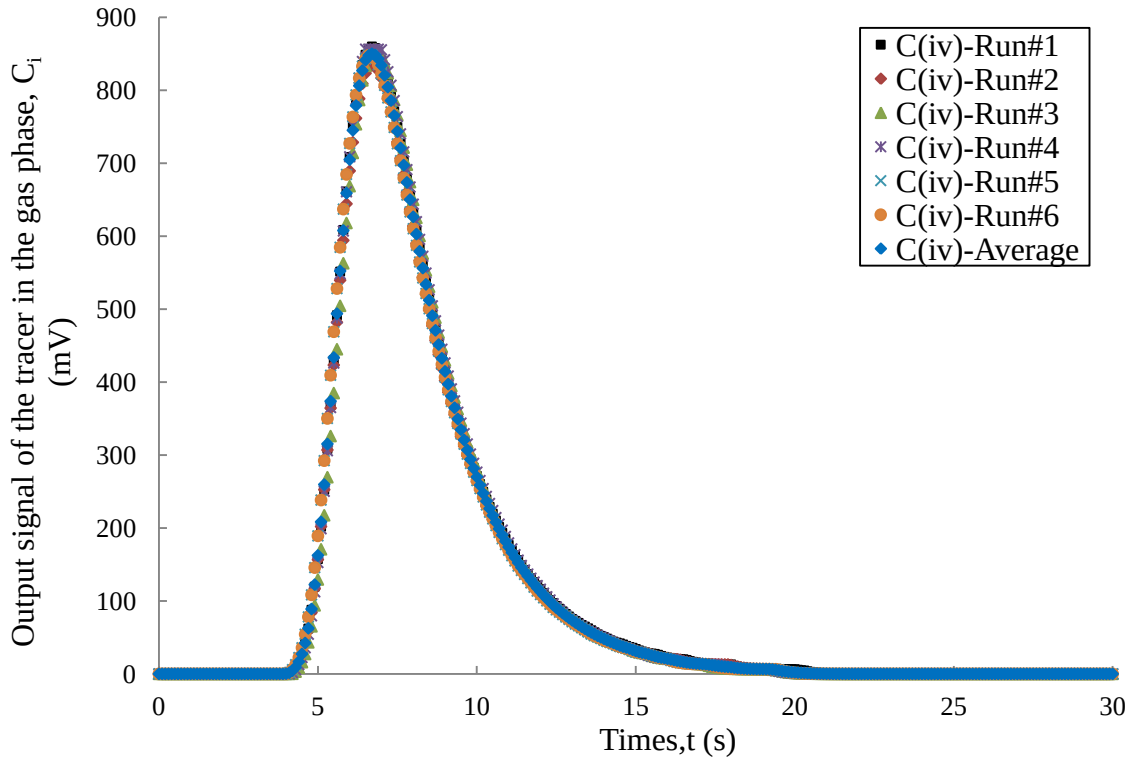

Figure 3.8. The Raw Data of Six Runs with the Average one for the Measurements C(iv) (Table 3.2) at Vg=30 cm/s and for 92 cm (1 ft) Height

3.4.2. Mass Balance Checking. Mass balance assessment needs to be carried out in order to ensure that the injected amount of tracer is going in and leaving the system and then are no tracer adsorption or leakage. Ideally, certain amount of gas tracer (helium gas) should be injected suddenly into the system in a shortest time possible (less than 1 sec) to achieve proper impulse input. At the same time, injected helium amount should be sufficient to get detected properly. The appropriate time interval of injection is found to be around 0.5 sec by trial and error. This time of injection has been used for all tracer injections. Based on total mass balance, the quantity of the injected tracer has been found to be 4.5g. This is equivalent to the injected mass flow rate of 9 g/sec or volumetric flow rate of 50 cm3/sec of helium tracer.

3.4.3. Normalization of the Raw Data. This is an important step in which the measured signals for the compartment ($C_{(i)}$- $C_{(iv)}$) of Table 3.2 are normalized by the maximum and minimum values in order to obtain a common scale to all signals which is from 0-1.0. The measured signals ($C_{(i)}$- $C_{(iv)}$) in (mV) are related to the helium concentrations. If it is approximated that within the studied range of helium concentration, there is a linear relationship between the helium concentration and the measured signal, the measured signal in terms of mV can be used directly to normalize the RTD which is equivalent to the normalized RTD obtained using the helium concentration, if a calibration curve is available. Since calibration curves are not available in this work, the output tracer signals for each measurement of Table 3.2 are normalized based on the measured signals in mV according to the following expression:

$$C_{norm} = \frac{C_i - C_{min}}{C_{max} - C_{min}} \approx \frac{C_i}{C_{max}} \tag{47a}$$

For the linearship between tracer concentrations (c_i) and the measured signals (C_i):

$$C_{norm} = \frac{C_i}{C_{max}} \approx \frac{c_i}{c_{max}} \quad (47b)$$

C_{norm} is the normalized value of the output signal of the tracer in the gas phase; it ranges from 0-1. In this study, normalized value (C_{norm}) is used as an equivalent to the dimensionless response or normalized concentration for all measurements listed in Table 3.2.

C_i is the value of the output tracer signal

C_{max} is the maximum value of the output tracer signal

C_{min} is the minimum value of the output tracer signal. Since C_{min} of the signal is close to zero (Figure 3.8), then Equation 47a is equivalent to the C_i / C_{max}.

This step is being done for qualitative comparison for dispersion of different compartment signals by converting them to the same scale of 0-1.0. The normalized signals will be used in the following steps. Figure 3.9 shows gas tracer normalized signals obtained for different sampling positions corresponding to the Table 3.2 and Figure 3.5.

It is obvious that the $C_{(i)}$ measurement response of upper sampling lines is less dispersed as compared to the $C_{(ii)}$ measurement. This confirms the occurrence of low dispersion in the sampling lines as compared to the plenum dispersion. This is necessary from proper data analysis point of view and to characterize properly the dispersion occurring in the plenum. The same trend is observed for the $C_{(iii)}$ measurement from the bottom sampling lines, due to the identical design of sampling lines. The aim is to decrease the dispersion occurring in the sampling lines, in order to properly estimate the dispersion occurring in the plenum/distributor and the pebble bed themselves.

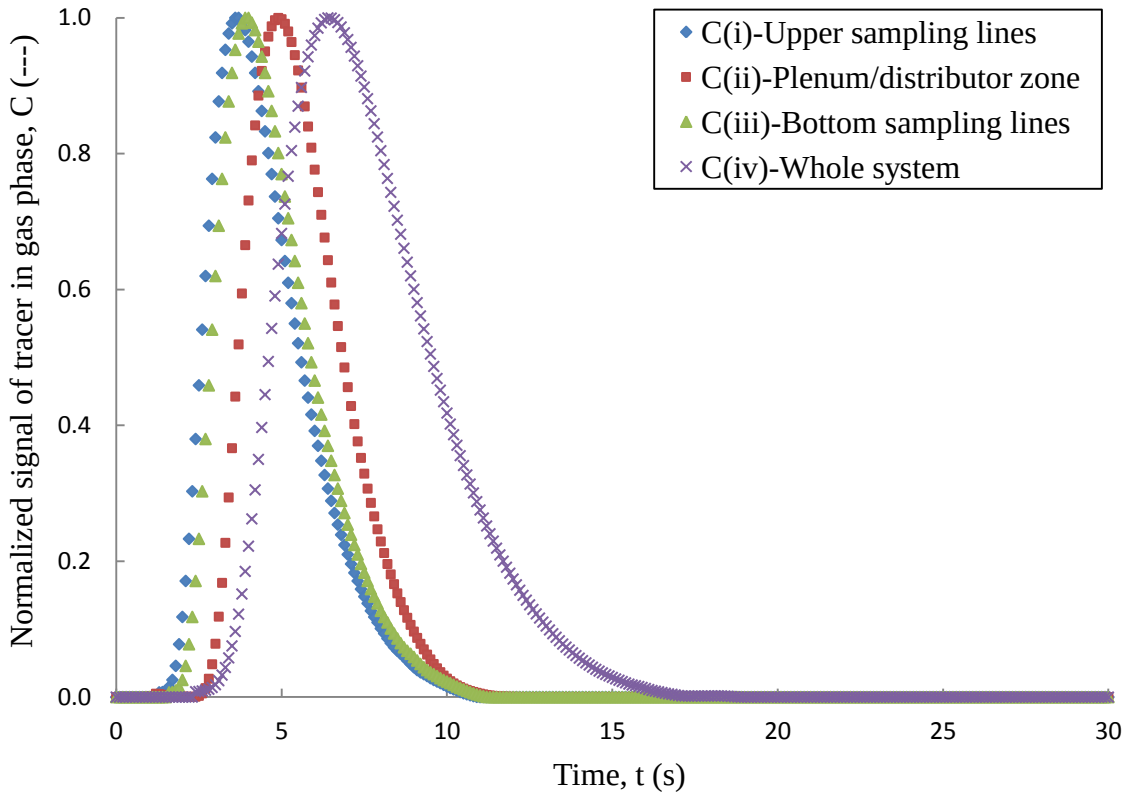

Figure 3.9. RTD Responses of the Gas Tracer Obtained for Different Sampling Positions at Vg=20 cm/s

It is important to mention here that as a check on the experimental method in this work, the sampling of tracer at location S2 for the measurement (ii) (response of the plenum/distributor) was done at the bottom of the pores of the gas distributor at different radial positions under plenum. The dimensionless radial positions as: $r/R = 0.0$ (center of the bed), 0.3, 0.6 and 0.9 (near wall of the bed). As shown in Figure 3.10, the results showed that there were no significant differences in the signal of tracer for the same packing. This is due to the very well mixed conditions achieved in the plenum upper distributor.

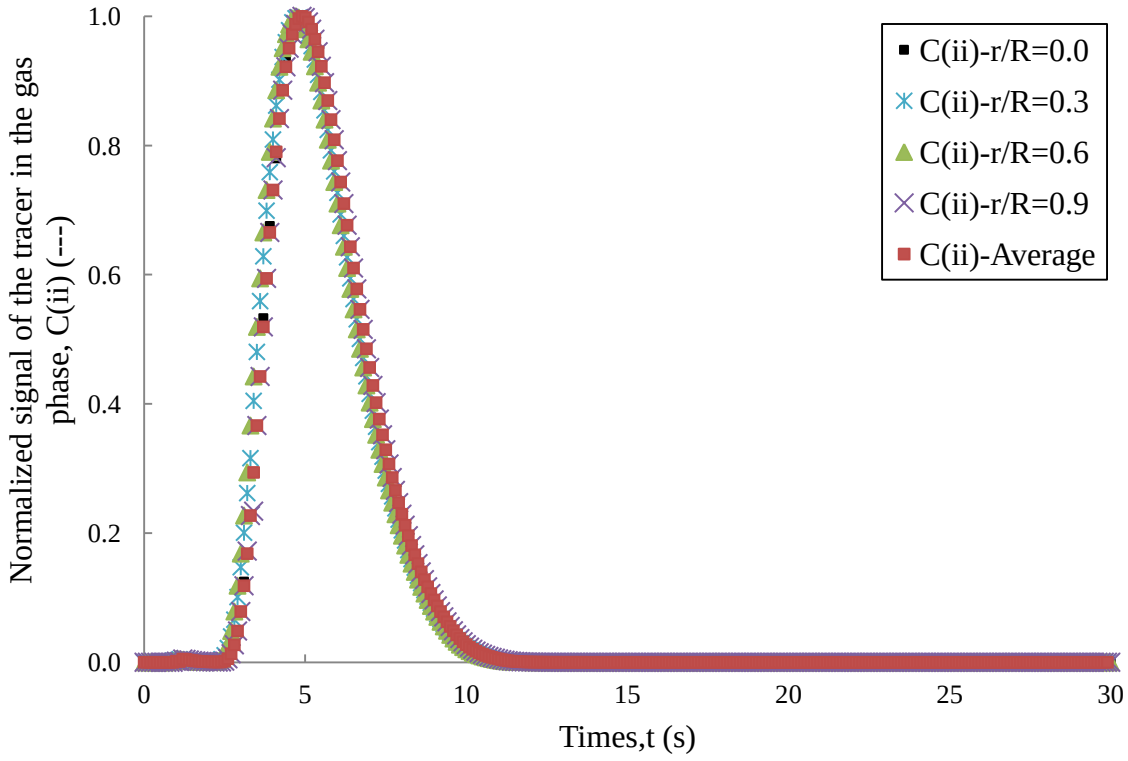

Figure 3.10. RTD Responses of the Plenum/Distributor for Different Sampling Radial Positions at Vg=20 cm/s

3.5. CONVOLUTION INTEGRAL METHOD TO DECONVOLUTE THE TRACER SIGNALS FOR PARAMETERS ESTIMATION

In order to experimentally measure the tracer signals of the bed alone and to obtain its residence time distribution (RTD), the tracer signal of the bed alone needs to be obtained and/or extracted from the whole tracer signal that includes the bed and the external compartments of the system, such as sampling/analytical lines on top and bottom side of the bed, top plenum and the distributor. From experimental success point of view, the external volume (i.e. top and bottom sampling/analytical lines and plenum/distributor zone) seen by tracer should be minimum. In fact, this is a critical step and it needs

carefully designed separate effects experiments that allow doing it. Hence, in this work such development have been achieved and implemented.

Another important issue of great interest, from a mathematical point of view, is that the time response (RTD) of the compartments cannot be subtracted from the whole single of the system since this is two or more dynamical systems in series. In fact, this is the main problem with the RTD method where stems from possible interactions between whole system dynamical behavior and dynamics of other compartments. As a result, the obtained measurements are the time convolution of the desired phenomenon and of unexpected ones. Therefore, the analysis is performed using the convolution integral method and assumed specific models developed and implemented by Han (2007). To do this, the following steps, as illustrated in Figure 3.11, need to be taken to analyze properly the tracer response from each compartment of the system:

1. Estimation of the gas dispersion in the plenum/distributor zone: in this step the tracer input signal to the bed is assumed to be the output response of the ideal continuous stirred tank reactor (CSTR) model that properly describes the plenum/distributor zone at the top of the bed. This will be validated first and then used to provide the input for the reactor model. The model validation will be based on the regression analyses and fitted by minimizing the averaged squared error in the time domain between the predicted and the measured tracer signals, as illustrated in Figures 3.11a and b.
2. Estimation of the axial dispersion of the gas phase in the bed zone: in this step the signal of the bed alone is analyzed using one-dimensional (1D) axial dispersion model (ADM) to estimate the value of the axial dispersion coefficient and then dispersive Peclet number, which quantifies the dispersion and the extent of the gas

mixing, respectively. This assumption will be validated first by experimental measurements, as shown in Figures 3.11c and d.

The details of the convolution integral method and the implementation of both ideal CSTR model for the plenum/distributor zone and one-dimensional ADM for the bed zone are discussed below.

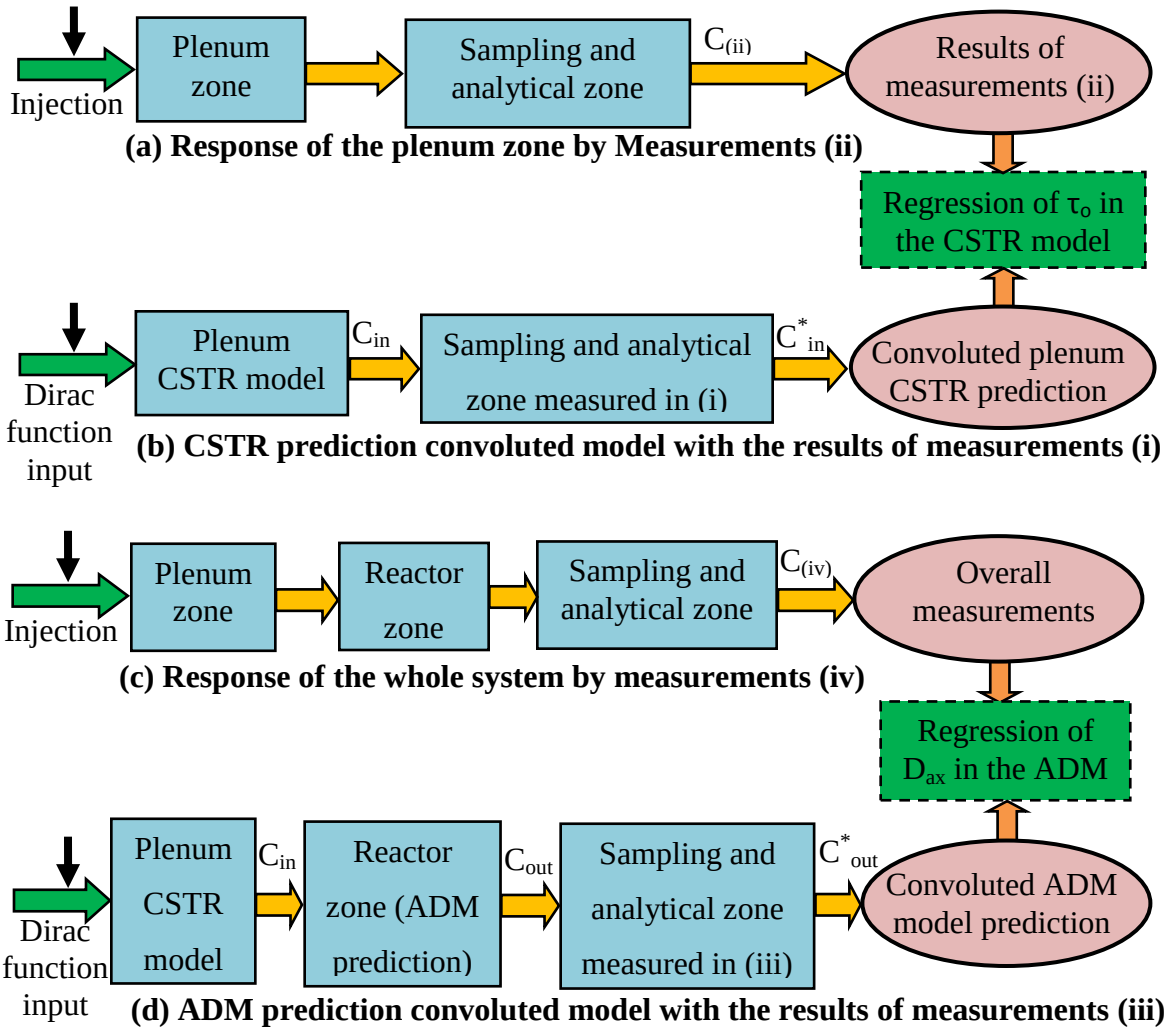

Figure 3.11. Schematic Diagram of the Convolution Integral Methods and CSTR and ADM Models Fit

3.5.1. Description of the Gas Dispersion in the Plenum/ Distributor Zone. The gas phase mixing occurring in the plenum and distributor zone is assessed using ideal CSTR model. The impulse injection at the inlet of the plenum can be expressed as follows:

$$\frac{dc}{dt} = -\frac{1}{\tau_o} c \tag{48a}$$

Where τ_0 is the residence time in the plenum, t is time at any instant and c is the theoretical outlet concentration of tracer in the gas phase. The initial condition (IC) is given by:

$$\text{I.C:} \qquad t = 0, \qquad c = c_{inj} \tag{48b}$$

Where c_{inj} is the injected tracer concentration in the inlet stream of the plenum. The solution of Equation 48a gives the plenum outlet tracer concentration in the gas phase at the distributor which is the inlet concentration to the bed (i.e. to the ADM model that is used to describe the bed), as shown schematically in Figure 3.12. This plenum/distributor output (ideal CSTR model) in a dimensionless form (C_{in}) is given below:

$$C_{in} = \frac{c}{c_{inj}} \approx \frac{c}{c_{max}} = e^{-\frac{t}{\tau_o}} \tag{48c}$$

Since

$$\frac{c_i}{c_{max}} \approx \frac{C_i}{C_{max}} \tag{47b}$$

Then

$$C_{in} = \frac{C}{C_{max}} = e^{-\frac{t}{\tau_o}} \tag{48d}$$

The parameter τ_0 of the CSTR model was estimated by regression using the measured response tracer at the plenum outlet (Figures 3.11a and b).

Measurements (i) and (ii) of Table 3.2, represent the dispersion occurring in the sampling lines and analytical system and in the plenum section. For measurement (i), the gaseous tracer input profile is assumed to be an ideal pulse function. This is a reasonable assumption; as the sampling tube for port S1 is placed close to the injection nozzle (Figure 3.5, View A). The length of the sampling lines from ports S1 and S2 were made equal to ensure same external volume for the measurements (i) and (ii) and hence, same dispersion. Measurement (i) ($C_{(i)}$) is used as the same input to the plenum to convolute the plenum as CSTR for the prediction of C_{in} (Han, 2007; Levenspiel,1999):

$$C_{in}^{*}(t) = \int_{0}^{t} C_{in}(t') C_{(i)}(t - t')\, dt' \tag{49}$$

It is important to mention here that the tracer entering the system ($C_{(ii)}$) at t' earlier than t of the outlet concentration $\left(C_{in}^{*}\right)$, more details about the theoretical basis of the convolution integral method are given by Levenspiel (1999).

The convoluted plenum CSTR prediction (C_{in}*) will be compared against the measured response of the measurement (ii) ($C_{(ii)}$), where τ_0 will be fitted by minimizing the averaged squared error in the time domain between the predicted C_{in}* and the measured $C_{(ii)}$ as follows:

$$\text{Error} = \frac{1}{n} \sum_{j=1}^{n} \left[C_{in}^{*}(t_j) - C_{(ii)}(t_j) \right]^2 \tag{50}$$

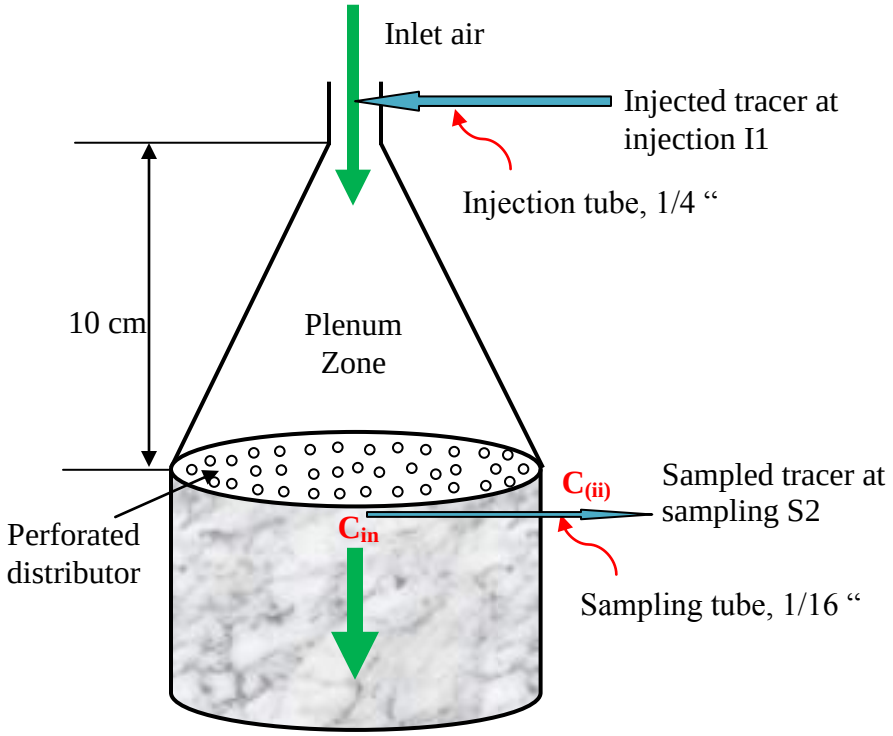

Figure 3.12. Schematic Diagram of Plenum/Distributor Zone

3.5.2. Description of the Gas Dispersion in the Bed Zone Using Axial Dispersion Model.

A mass balance around a differential segment of the bed, in absence of reaction and radial variations yields the axial dispersion model (ADM) or axially-dispersed plug-flow model as follows (Bischoff and Levenspiel, 1962a):

$$\frac{\partial c}{\partial t} = D_{ax}\frac{\partial^2 c}{\partial z^2} - V\frac{\partial c}{\partial z} \tag{51a}$$

Dividing Eqn 51a by c_{max} becomes:

$$\frac{\partial (c/c_{max})}{\partial t} = D_{ax}\frac{\partial^2 (c/c_{max})}{\partial z^2} - V\frac{\partial (c/c_{max})}{\partial z} \tag{51b}$$

Equation 51b can be re-written in dimensionless form in terms of the measured signal as follows:

$$\frac{\partial C_{out}}{\partial t} = D_{ax}\frac{\partial^2 C_{out}}{\partial z^2} - V\frac{\partial C_{out}}{\partial z} \tag{51c}$$

Where,

$$C_{out} = \frac{c}{c_{max}} \approx \frac{C}{C_{max}} \tag{51c}$$

Where c is the tracer concentration while C is equivalent mV signal. D_{ax} is the effective dispersion coefficient in the axial direction which is a lumped parameter attributable to the combined effects of molecular diffusion and hydrodynamic mixing where the last one is resulting from turbulent eddies and rotating vertices of the non-flow zones in the vicinity of the particles contact points.

In this dispersion model, the transport process occurs by two mechanisms: (i) dispersive transport arising from axial dispersion phenomena within the gas phase and (ii) convective transport arising from bulk flow in the axial direction. It is worth recalling that this model derived from the governing mass transport equation for the system with the effect of the velocity profile is lumped into the dispersion coefficient and the uniform velocity or mean interstitial velocity (V) is not arbitrary assumed or imposed.

The initial condition (IC) is given by:

$$\text{I.C:} \qquad t = 0 \qquad 0 \le z \le L \qquad C_{out} = 0 \tag{52a}$$

Danckwert's boundary conditions (BCs) for the closed-closed system were used as follows:

$$\text{B.C.1:} \qquad t < 0 \qquad z = 0 \qquad V_g C_{out} = V_g \varepsilon_b C_{in}\Big|_{z=0} - D_{ax} \frac{\partial C_{out}}{\partial z}\Big|_{z=0} \tag{52b}$$

$$\text{B.C.2:} \qquad t > 0 \qquad z = L \qquad \frac{\partial C_{out}}{\partial z}\Big|_{z=L} = 0 \tag{52c}$$

Here C_{in} is calculated using Equation 48c (c/c_{inj}) with the fitted value of τ_0 for each condition as discussed earlier. The superficial gas velocity (V_g) is known from the pre-set flow rate and the void fraction or average bed porosity (ε_b) was measured by direct balance method mentioned earlier.

The dispersion represented by the axial dispersion coefficient is determined by curve fitting of the experimental measured response of the bed alone in the time domain. The regression of the bed axial dispersion coefficient (D_{ax}) is schematically illustrated in Figures 3.11c and d. The dispersion in the sampling and analytical system from port S3 is obtained by the measurement (iii) (Table 3.2). The response of the whole system will be obtained by the measurement (iv). Using C_{in} obtained from Equation 43a as an input tracer profile to the ADM, the model yields an output profile of C_{out} at the bottom level, as sketch schematically in Figure 3.13. The output profile (C_{out}) is then convoluted with $C_{(iii)}$ to yield the convoluted predictions (C_{out}^{*}).

$$C_{out}^{*}(t) = \int_{0}^{t} C_{out}(t') C_{(iii)}(t - t')\, dt' \tag{53}$$

Then convoluted reactor model predictions (C_{out}^{*}) will be compared against the response of the whole system measured by measurement (iv) ($C_{(iv)}$), where D_{ax} is fitted by minimizing the averaged squared error in the time domain, defined as:

$$\text{Error} = \frac{1}{n} \sum_{j=1}^{n} \left[C_{out}^{*}(t_j) - C_{(iv)}(t_j) \right]^2 \tag{54}$$

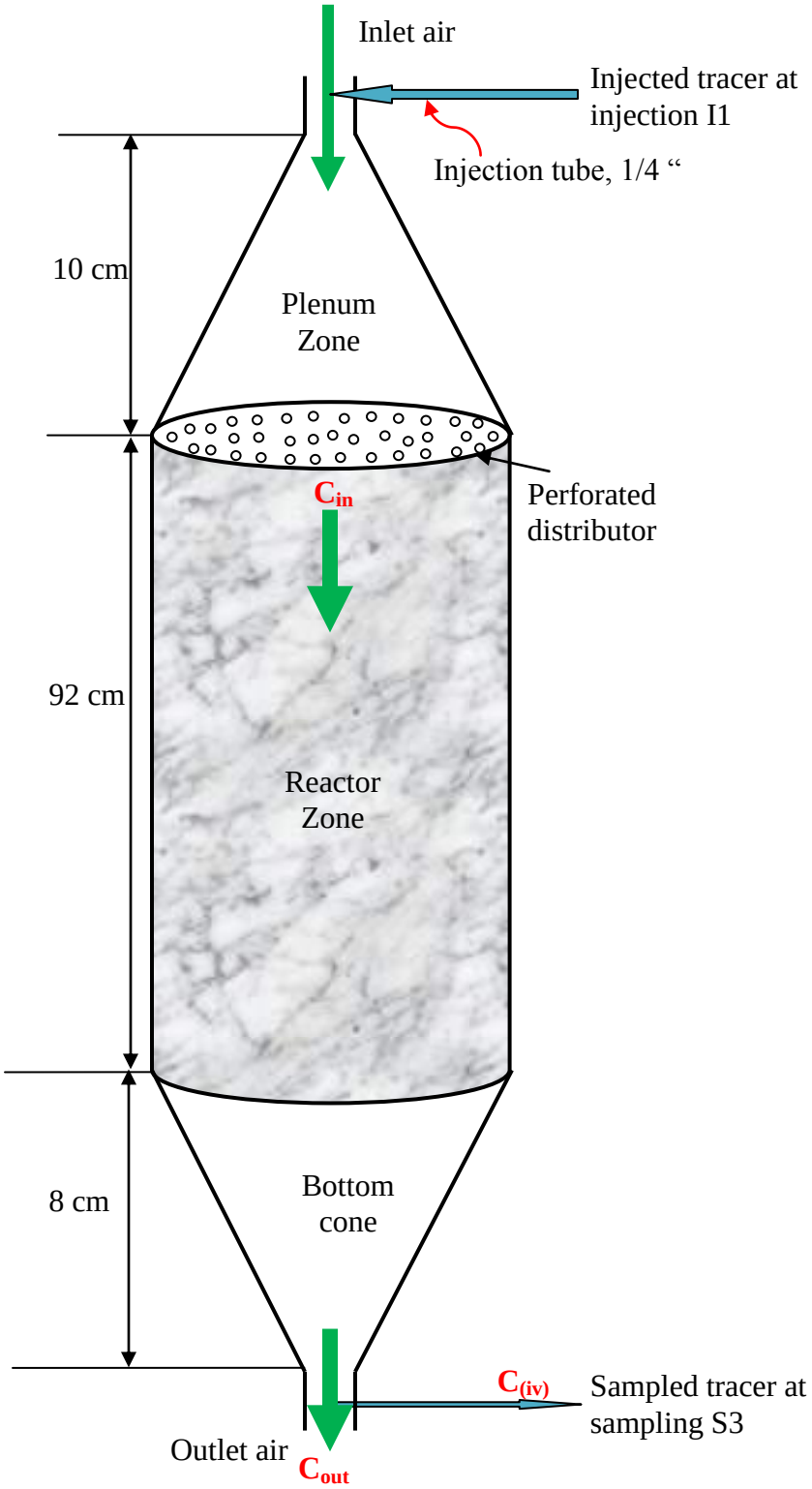

Figure 3.13. Schematic Diagram of Whole System of Different Zones

As discussed before, the dispersive Peclet number is a very useful parameter used to the measure the extent of mixing in bed. For this purpose, the axial dispersion model, Equation 51b, can be rewritten in dimensionless form as following:

$$\frac{\partial C_{out}}{\partial \theta} = \frac{1}{Pe_D}\frac{\partial^2 C_{out}}{\partial Z^2} - \frac{\partial C_{out}}{\partial Z} \tag{54a}$$

where

$$C_{out} = \frac{c}{c_{max}} \qquad \theta = \frac{tV}{d_p} = \frac{tV_g}{\varepsilon_b d_p} \qquad Z = \frac{z}{d_p} \tag{54b}$$

The dimensionless time, θ, corresponds physically to the number of displacements; that is, it is equal to the ratio of the total fluid volume introduced to the free volume of the bed (Liao and Shiau, 2004). While Pe_D is the dispersive Peclet number and physically represents the ratio of the rates of transport by convection to the transport by dispersion as:

$$Pe_D = \frac{\text{Rate of transport by convection}}{\text{Rate of transport by dispersion}} = \frac{Vd_p}{D_{ax}} = \frac{V_g d_p}{\varepsilon_b D_{ax}} \tag{54c}$$

The dispersive Peclet number represents the extent of mixing and is determined by obtaining D_{ax} by curve fitting of experimental measured response of the bed alone in the time domain using Equation 51b.

It is well known that all reactors in practice have some effects of axial dispersion which is in turn reducing the performance of the reactor. The criterion in assessing the dispersion effects can be derived by the introduction of two characteristic times as follows (Jess et al., 2013):

1. The residence time of the reactor (convection time, τ) which is given as follows:

$$\tau = \frac{\varepsilon_b V_T}{Q} = \frac{\varepsilon_b L}{V_g} \tag{55a}$$

where V_T is the total volume of the bed and Q is the volumetric flow rate of the gas phase.

2. The residence time for the axial dispersion (dispersion time, τ_{ax}) in a reactor of length, L, which is given by:

$$\tau_{ax} = \frac{d_p L}{D_{ax}} \tag{55b}$$

Combing the above two characteristic times (Equations 55 a and 55b) with the definition of the dispersive Peclet number (Equation 54c), gives the dispersive Peclet number (Pe_D) as the ratio of the characteristics dispersion time to convection time as follows:

$$Pe_D = \frac{V_g d_p}{\varepsilon_b D_{ax}} = \frac{\left(d_p L / D_{ax}\right)}{\left(\varepsilon_b L / V_g\right)} = \frac{\tau_{ax}}{\tau} \tag{56}$$

Jess et al., (2013) reported that the influence of the axial dispersion is negligible if the residence time of the reactor (τ) is smaller than the dispersion time (τ_{ax}) by about 50%, which can be mathematically expressed as:

$$\tau \leq 0.5\tau_{ax} \tag{57}$$

Based on the above criterion (Equation 57), it may be stated, as a rule of thumb, that the axial dispersion could be neglected with confidence as long as the dispersive Peclet number is equal or greater than twenty ($Pe_D \geq 20$).

It is worth to mention here that within an axially dispersed plug-flow model or axial dispersion model (ADM), there are three adjusted parameters of great interest which could be used to identify, characterize and model the reactor. There are defined as follows:

1. The axial dispersion coefficient (D_{ax}): It is a measure of how slow or rapid the spreading process is in the reactor.
    a. The low values of D_{ax} represent a slow spreading process of the species which is controlled by molecular diffusion. This gives a rise to large or more dispersion and the flow characteristics are far from plug flow conditions.
    b. The high values of D_{ax} characterize a rapid spreading process of the species which is hydrodynamically controlled. This gives a rise to small or less dispersion and the flow characteristics have small deviation or are closer to plug flow conditions.
2. The dispersive Peclet number (Pe_D): It is a measure of the degree of the axial dispersion and mixing process.
    a. The low values refer (due to low superficial gas velocity) to relatively more dispersion and/or poor extent of mixing in the reactor.
    b. The high values (due to high superficial gas velocity) indicate less dispersion and/or better extent of mixing in the reactor.
3. The dispersion number ($1/Pe_D$): It is a measure of how the reactor flow model will be identified, if it is close to the ideal plug-flow model.
    a. The low value of dispersion number (close to zero) indicates that the flow pattern of the reactor is close to the ideal plug-flow model.
    b. The high value of dispersion number (goes to infinity) indicates that the flow pattern of the reactor is close to the perfect mixed-flow model.

3.6. VALIDATION OF THE ASSUMED MODELS AND THE PARAMETERS FITTING

As mentioned before, the ultimate objective of the steps described in Figure 3.5 and Table 3.2, is to extract accurately the response of the bed alone from the total system response which includes sampling lines in top and bottom part of bed and top plenum/ distributor zone. Such steps demand to assume particular dispersion models for the plenum/ distributor zone and the reactor zone. The plenum/distributor zone at the top of the bed is assumed to follow ideal continuous stirred tank reactor (CSTR) model while the pebble bed reactor is assumed to follow 1-D axial dispersion model. These assumptions have been validated first by experimental measurements.

3.6.1. Validation of the Continuous Stirred Tank Reactor (CSTR) Model for the Top Plenum/Distributor Zone.

The dispersion and mixing occurring in the plenum/distributor compartment represented by measurement (ii) of Table 3.2, as shown in Figures 3.14 a and b, for both the laminar and turbulent flow regimes need to be assessed if CSTR model can describe it in order to be used in the convolution integral method to extract the response of the bed alone. In this step of validation, the first two measurements signals i.e. C(i) and C(ii) (Table 3.2) are used. First, the calculated dimensionless C_{in} from CSTR model (Equation 48c) is used to get C_{in}* from Equation 49 which is the convoluted plenum CSTR predictions, Figures 3.11 a and b.

This C_{in}* is compared with the C(ii) measurement which is the experimentally obtained response of the plenum plus distributor, and the top sampling system together (Figure 3.14). Then estimating τ_0 by fitting is carried out to match the convoluted plenum

CSTR predictions with the experimental results. This is done by minimizing the error (averaged squared type) defined in Equation 50.

A good match is observed between C(ii) measurement and the predicted C_{in}* (Figure 3.14) which indicates that the gas mixing occurring in the plenum and distributor can be modeled as a CSTR for both flow conditions of the laminar and turbulent flow regimes . The averaged squared error calculated using Equation 50 is found to be 7.6E-04 and 5.7E-04 for the laminar and turbulent flow, respectively. The C_{in} calculated from the plenum CSTR model with a fitted parameter (τ_o) is used as an input tracer profile to the reactor model (ADM) instead of an idealized delta function input. This is necessary in order to incorporate mixing occurring in the plenum and distributor before the pebble bed.

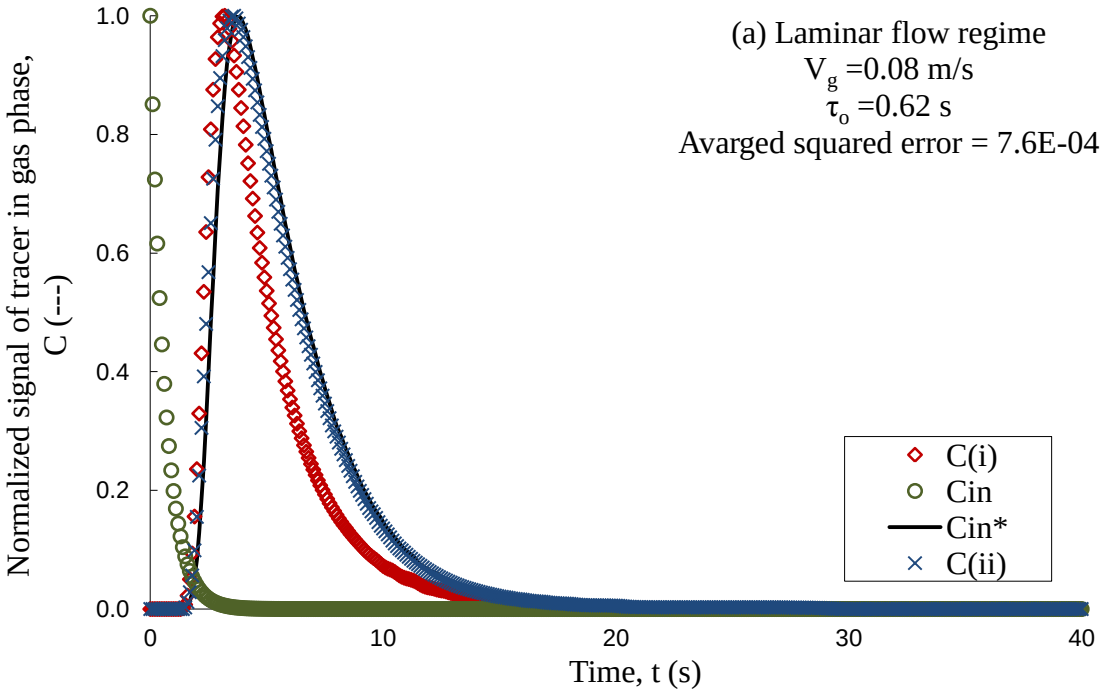

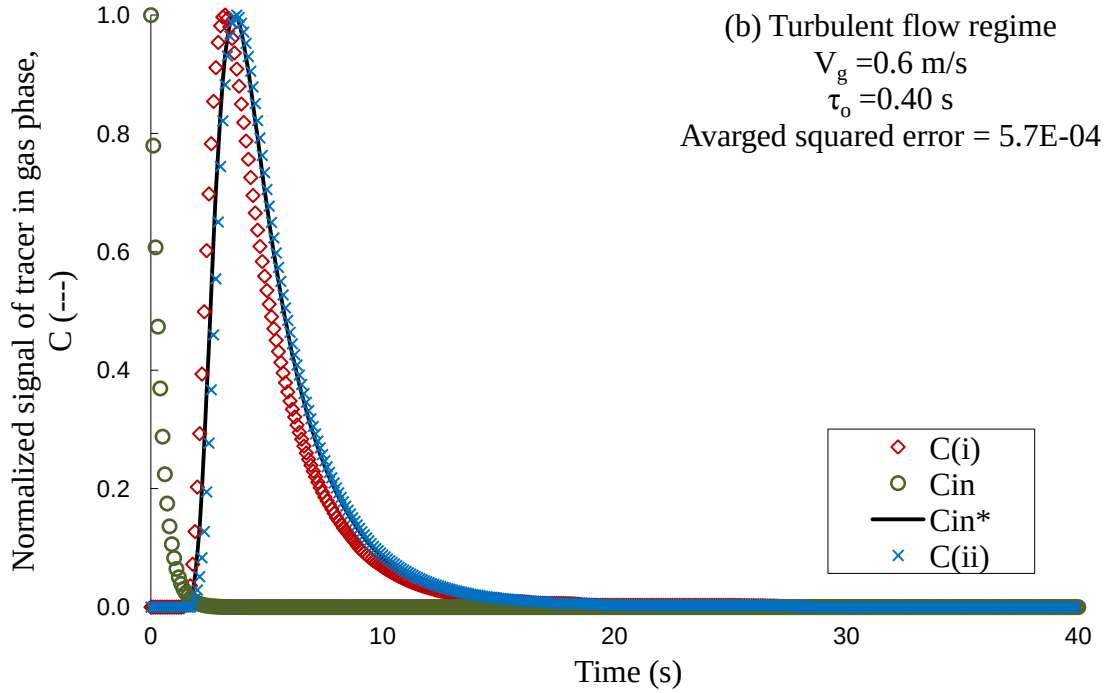

Figure 3.14. Responses of the Normalized Gas Tracer Signal at the Plenum/ Distributor Zone with CSTR Model Fit: a) Laminar Flow Regime; and b) Turbulent Flow Regime

3.6.2. Validation of the One-Dimensional Axial Dispersion Model (ADM) for the Pebble Bed Alone. Parts a and b of Figure 3.15 show the dispersion in the sampling lines and analytical system from port S3 and the response of the whole system which were obtained by the measurement (iii) and measurement (iv), respectively.

The C(iii) measurement is used as an input to convolute the reactor model prediction. Then, the C_{in} obtained from Equation 48c (CSTR model of the plenum) is used as an input tracer profile to the suggested reactor model. This yields an output profile (C_{out}) for the pebble bed, which is then convoluted with C(iii) based on Equation 53. The convoluted bed model predictions (C_{out}*) is then compared with the response of the whole system which is obtained by the C(iv) measurement. Finally, estimation of the axial dispersion coefficient (D_{ax}) by fitting is carried out to match the convoluted reactor model (i.e. ADM) predictions with experimental results as shown in the Figures 3.11 c and d . This is performed by minimizing the error, which is defined based on Equation 54 as the average of difference between squares of C_{out}* and $C_{(iv)}$. Figures 3.15a and b show $C_{(iv)}$ and C_{out}* in both the laminar and turbulent flow regimes, respectively.

The averaged squared errors calculated by Equation 54 are 3.9E-04 and 1.6E-03 for the laminar and turbulent flow regimes, respectively. A good match is observed between C_{out}* and $C_{(iv)}$ (Figure 3.15) for both flow cases which indicates that dispersion occurring in the pebble bed can be represented mathematically by one dimensional ADM at the studied conditions.

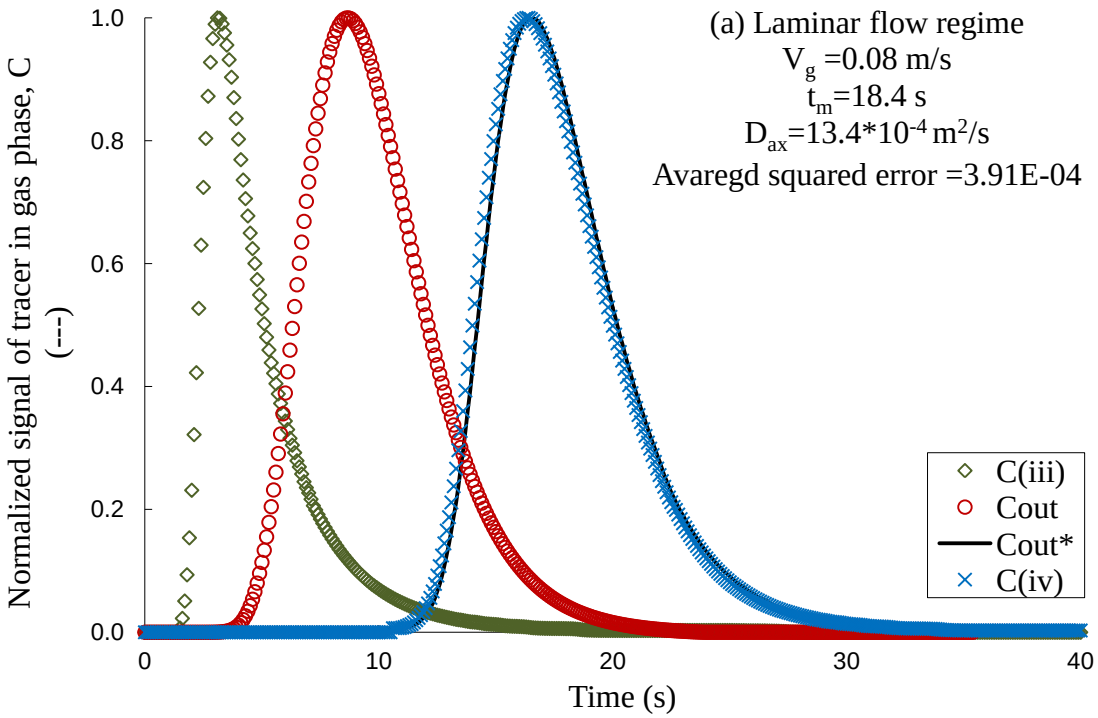

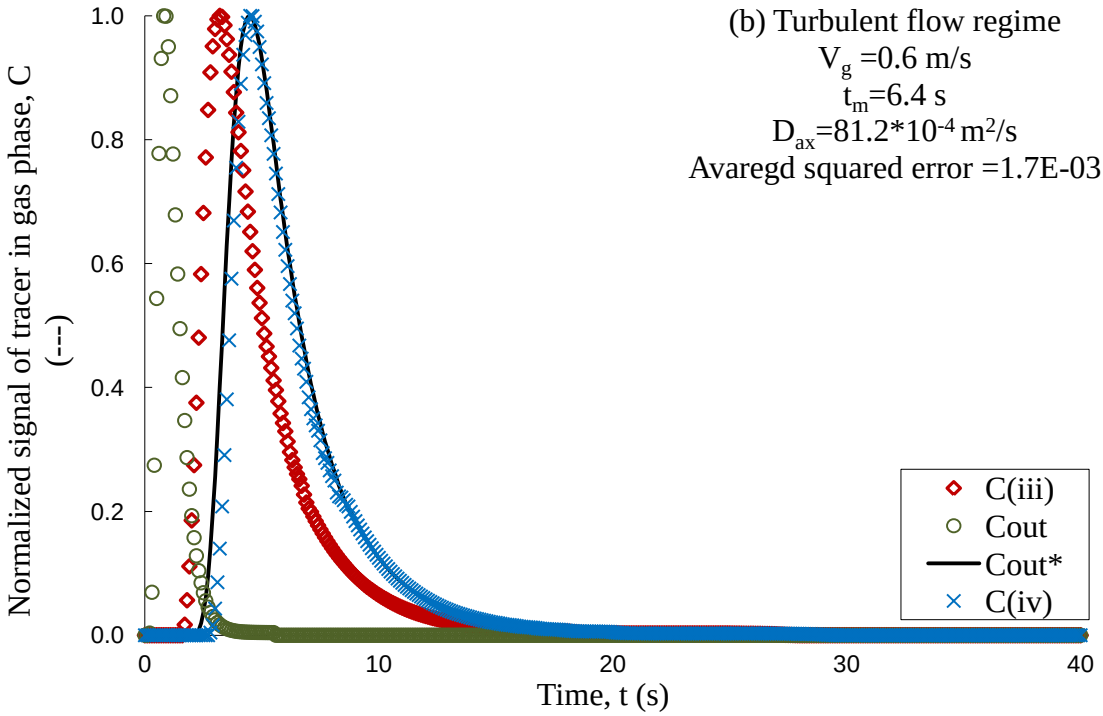

Figure 3.15. Responses of the Normalized Gas Tracer Signal at the Reactor Outlet with ADM Fit: a) Laminar Flow Regime; and b) Turbulent Flow Regime

Figures 3.15a and b illustrate also the effect of the gas velocity on the gas phase axial dispersion. For low Reynolds number (laminar flow) conditions, the gas dispersion is relatively larger (wide spreading), i.e more dispersion observed, as in Figure 3.15a and hence D_{ax} is small (low rate of dispersion causing relatively large dispersion). This is due to the wide variation in voidage distribution and low pressure drop in the bed. This effect in turn tends to increase mean residence time and would set up a radial gradient in gas velocity (yet to be validated experimentally). Peak width decreases with increasing the gas velocity in pebble bed, i.e less dispersion (narrow spreading) is observed at high gas velocities (turbulent flow regime), as shown in Figure 3.15b and hence D_{ax} is large. This is because increasing of gas velocity leads to an increase in the pressure drop along the bed and to fast dispersion (spreading) of species. This yields better distribution of the gas and hence reduction in its dispersion. More discussions relevant to the effect of gas velocity will be carried in the next section.

To check the effect of extra dispersion occurring in the plenum on the obtained values of D_{ax}, the D_{ax} are estimated using a delta function as an input to ADM instead of C_{in}. Larger D_{ax} values were obtained compared to those when C_{in} values were used as input. This suggests that ignoring the extra dispersion occurring in the plenum and sampling system introduces significant error of around 49.3% in the estimation of D_{ax} in the bed, as shown in Figure 3.16. This also has been reported in the study carried out in slurry bubble columns (Han, 2007).

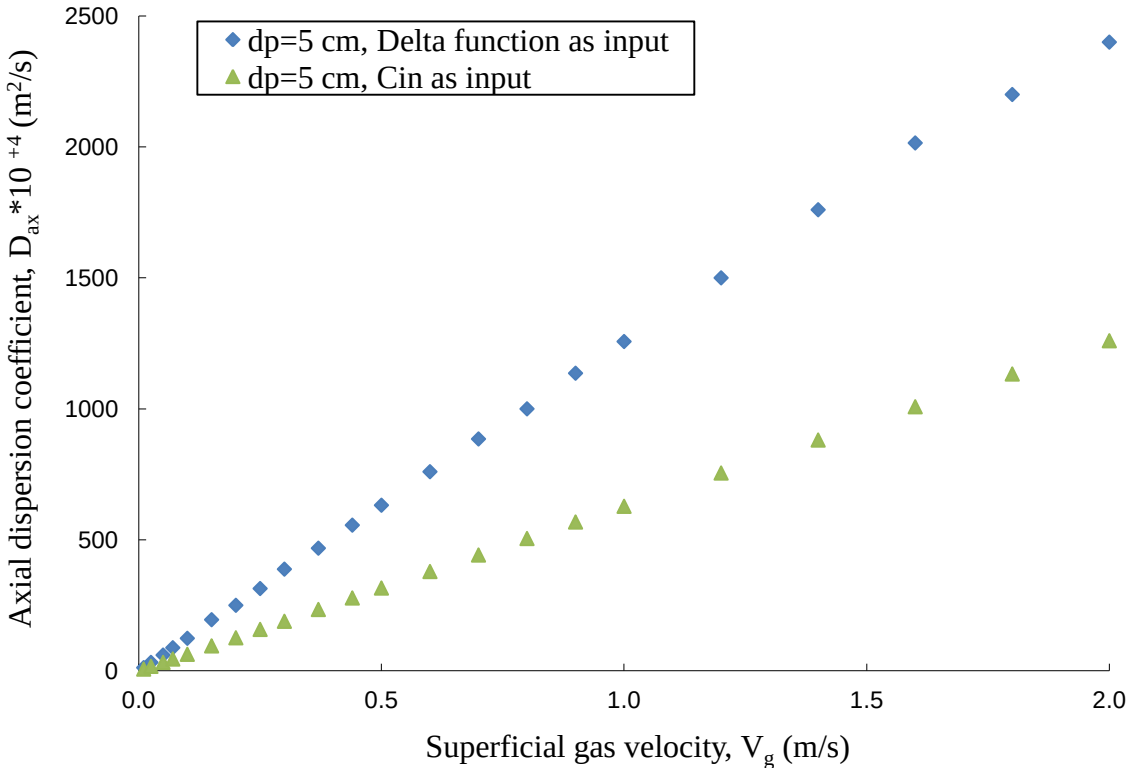

Figure 3.16. Effect of Extra Dispersion Occurring in the Plenum on the Obtained Values of the Axial Dispersion Coefficient for 3 ft Height

3.7. RESULTS AND DISCUSSION

3.7.1. Effect of Gas Flow on the Axial Gas Dispersion. The mechanism of axial dispersion phenomenon was mentioned earlier, in Section 2, as a consequence of combined contributions from both the molecular diffusion and the hydrodynamic mixing (convection) mechanisms in the spaces between the pebbles. At the macroscopic level, the individual contribution of each mechanism to the overall dispersion phenomenon depends mainly on the gas flow conditions and bed structure.

Figure 3.17a shows the effect of gas velocity on the measured axial dispersion coefficients in the studied packed bed for different particle sizes using bed height of 92cm. In this Figure, the trend indicates a noticeably increase in the obtained axial

dispersion coefficients with superficial gas velocity. Part a of Figure 3.17 demonstrates that the low values of axial dispersion coefficient indicate large dispersion and larger mean residence time (slower movement of fluid element, i.e low rate "slow" dispersion) in pebble bed at low range of gas velocities. While the higher values confirm small dispersion and smaller mean residence time (faster movement of fluid element, i.e high rate "fast" dispersion) in pebble bed at high gas velocities. This phenomenon could be interpreted that when the gas through a packed bed flows at a very low rate, there will be sufficient residence time for the molecular diffusion to equalize concentration within each pore space and also there will be slow or low rate dispersion of species at low gas velocity. In this case, axial dispersion is characterized by a region in which molecular diffusion dominates. Therefore, the axial dispersion is larger in the laminar flow regime. However, if the velocity is increased high enough (turbulent flow regime), it will eventually reach a velocity in the interstices at which there is insufficient residence time for diffusion to equalize concentration within each pore space and also there will be higher dispersion of species at high gas velocity. In this regime, axial dispersion is smaller and the value of the axial dispersion coefficient becomes larger and Pe_D ($V_g d_p/\varepsilon_b D_{ax}$) reaches plateau where the change in V_g gets comparable to the change in D_{ax}.

Gunn, (1987) assumed that diffusive and mixing components of dispersion are additive, as in the following expression which has been reported in Section 2 and is recalled here for clarity:

$$\frac{1}{Pe_D} = \frac{1}{\tau}\frac{1}{Pe_M} + \frac{1}{2} \tag{23}$$

with

$$\left.\begin{aligned} Pe_D &= \frac{V_g d_p}{\varepsilon_b D_{ax}} && \text{dispersive Peclet number} \\ Pe_M &= \frac{V_g d_p}{\varepsilon_b D_{AB}} = Re_P Sc && \text{molecular (mass) Peclet number} \\ Re_P &= \frac{\rho V_g d_p}{\varepsilon_b \mu} = \frac{Re}{\varepsilon_b} && \text{particle Reynolds number} \\ Sc &= \frac{\mu}{\rho D_{AB}} && \text{Schmidt number} \end{aligned}\right\} \quad (18a)$$

Where D_{AB} is the molecular diffusion coefficient, while, τ is the tortuosity factor.

This correlation (Equation 23) can be re-written in terms of the axial dispersion coefficients as in the following form:

$$\frac{D_{ax}}{D_{AB}} = \frac{1}{\tau} + \frac{1}{2}\frac{V_g d_p}{\varepsilon_b D_{AB}} \quad (58)$$

In order to explain the influence of gas velocity on the dispersion coefficient, it is important to consider the limiting case where the gas velocity goes to zero ($V_g \to 0$) in Equation 58. In this case the dispersion coefficient is affected by the area open to the molecular diffusion (D_{AB}) and hence increases slightly within the increase in average porosity of bed, which is increased as particle diameter increases. As the gas velocity increases, the contribution of convective dispersion increases and becomes dominating over that of molecular diffusion at high superficial gas velocity. This dominance will be still there and the axial dispersion coefficient continues to increase with superficial gas velocity. However, the Pe_D reaches plateau because the change in V_g (ΔV_g) becomes comparable to the change in D_{ax} (ΔD_{ax}).

To further explain the contribution of the molecular diffusion and the hydrodynamic mixing mechanisms, the degree and extent of longitudinal gas phase dispersion in the pebble bed is described by the dimensionless dispersive Peclet number

(Pe_D), which is physically represents the ratio of the rate of transport by convection to the rate of transport by dispersion. Figure 3.18b shows that dispersive Peclet number increases noticeably with particle Reynolds number at low range of velocities. It was higher for high voidage (higher particle diameter) and this is reasonable while the dispersion is controlled by molecular diffusion mechanism and the lateral spreads is more with more open area (high porosity of bed) and low rate of dispersion at low gas velocity. The low gas velocities could give an asymptote that the dispersive Peclet number goes to a limited value of diffusive (molecular) Peclet number (i.e., $Pe_D \approx Pe_M$). At higher range of velocities and regardless of the particle size, the increase in the Peclet number reduces with respect to the particle Reynolds number. This is because with increasing Reynolds number, the radial velocity profiles in the voids of randomly packed bed become more uniform and possibly spatially presence stagnant zones reduces, therefore, reduction in its dispersion and high rate of dispersion occurs at high gas velocity. In the other words, the hydrodynamic mixing (i.e. convection) becomes the main mechanism of the dispersion phenomena in the bed compared to the molecular diffusion at high Reynolds number.

It is also clear that with the increases in Reynolds number the Peclet number increases to a plateau value of $Pe_D \approx 2$ for fully developed turbulence (i.e., complete mixing in each pore space). This confirms that the contribution is due to the negligible molecular diffusion effect compared to the hydrodynamic mixing (convection) effect. At this limit the bed behaves as a cascade of ideally mixed compartments (Aris and Amundson, 1957), and the axial dispersion is caused by mixing of the fluid in the voids of the packing (Tsotsas, 2010).

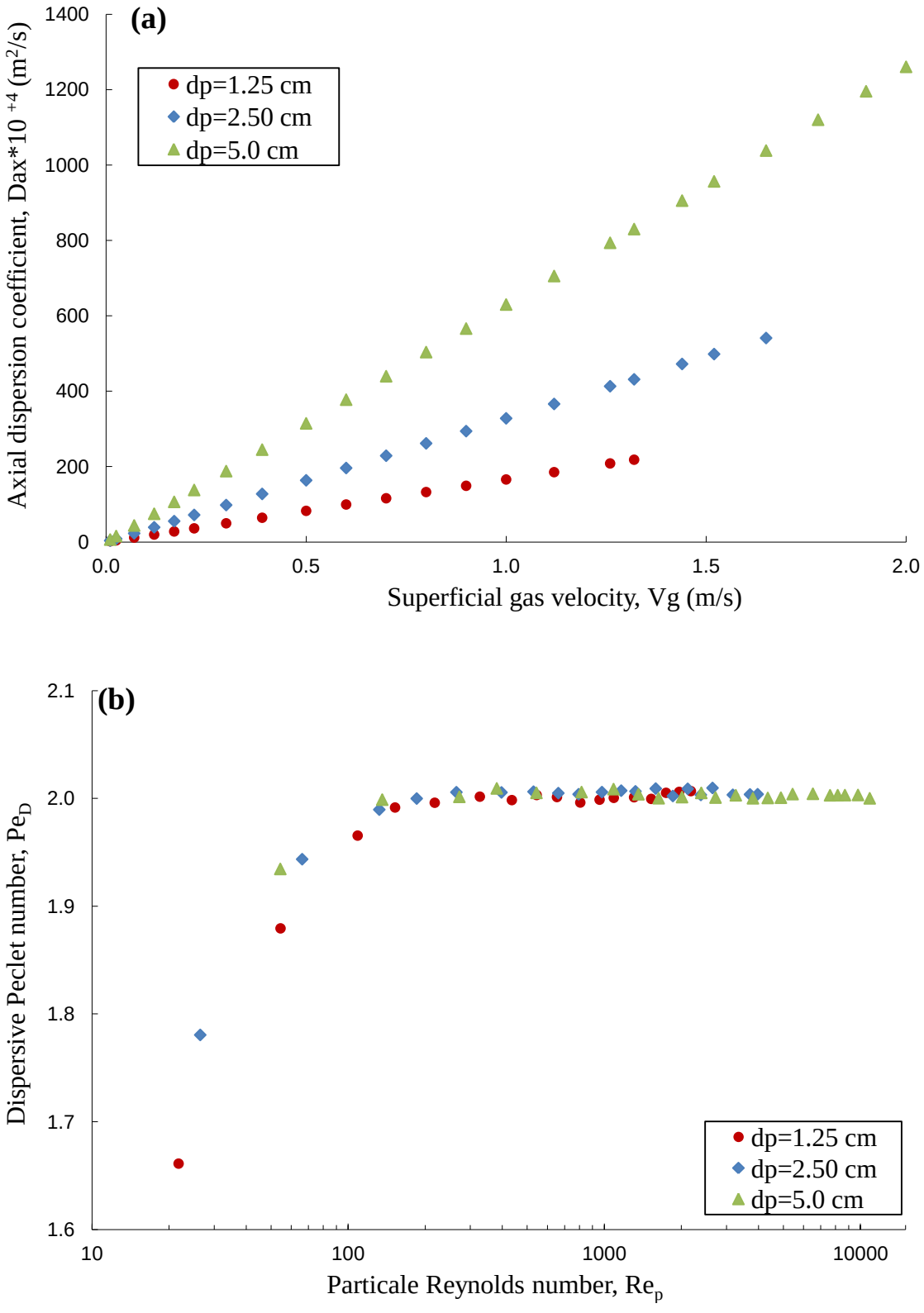

Figure 3.17. a) Variation of the Axial Dispersion Coefficient with Superficial Gas Velocity; and b) Variation of the Dispersive Peclet Number with Particle Reynolds Number

3.7.2. Effect of Pebble Diameter on the Axial Gas Dispersion of the Bed Alone.

In previous sections, it has been concluded that the axial coolant gas dispersion and its extent of mixing are caused by turbulence, radial variation in the gas velocity, and due to the structural properties of packing such as bed geometry and void fraction. Therefore, an investigation of the effect of different pebble sizes on the axial dispersion coefficient has been studied. Three different sizes of pebbles: 1.25 cm, 2.5 cm, and 5 cm diameter having same density have been selected to form a randomly packed pebble-bed with different structure of void distribution. As mentioned earlier the void structure of different particles sizes have been quantified using gamma ray computed tomography (CT) as part of another graduate student work.

Same methodology of data analysis and fitting for ADM which has been discussed in the previous sections is being used in this part. Since the overall tracer signal represents the bed and the experiments external volumes and since the dispersion in the bed alone needs to be investigated for the effect of pebble diameter, the RTD of the normalized gas tracer concentration that is estimated by the ADM has been used to describe the dispersion in the bed. Figure 3.18 shows RTDs obtained by ADM at superficial gas velocity of 0.2 m/s and 92cm bed height for three different sizes of pebble. The increase in the pebble size leads to an increase in the packing porosity of the bed and hence less pressure drop. Therefore, residence time of tracer is found to increase with increase in the pebble size. In addition to that, with the increase in pebble size more dispersion is occurring along the bed. Figure 3.18 also illustrates the effect of pebble diameter on the axial dispersion coefficient (D_{ax}). Axial dispersion coefficient increases with increase in pebble size which means faster (high rate of) dispersion occurs. When

the void increases (increase in d_p) the dispersion rate increases (fast (high rate of) dispersion) and hence D_{ax} increases. In this case larger void structure will help the species to disperse and move fast while flowing with the gas phase (i.e. convection). This helps the flow pattern to have less dispersion and hence the variance of the RTD is 8.61 s^2 with d_p=5 cm compared to 11.7 s^2 with d_p=1.25 cm. For increase in pebbles diameter from a value of 1.25cm to 5.0 cm (increasing the size by four times), axial dispersion coefficient found to be increased by a factor of 1.49 (~ 49%). This can be attributed to an increase in the bed porosity which enhances the rate of dispersion of the tracer. In addition to that, non-homogeneous nature of randomly packed bed plays an important role in the determination of gas flow structure between the pebbles and consequently the axial dispersion. The obtained results indicate that pebbles size strongly affects axial dispersion and mixing in the pebble bed. Therefore, a rigorous measurement of the porosity and its distribution in a packed bed is needed which is part of other study in our laboratory group. This is because the porosity between the particles of the bed helps the diffusion of a tracer and hence affects the rate of dispersion.

From Figure 3.18 it also can be seen that with increases in pebble size, the second moment (variance) is decreasing. A decrease in variance can be attributed to decrease in dispersion around the mean residence time (t_m) value and vice versa. At large pebble size (d_p= 5cm), low values of variance (of about 8.61 s^2, narrow spreading) indicates less dispersion (high rate of "fast" dispersion). It turns out that the gas flow pattern in the studied bed is not much deviated from ideal plug flow behavior and hence ADM can be suitable for such small deviation.

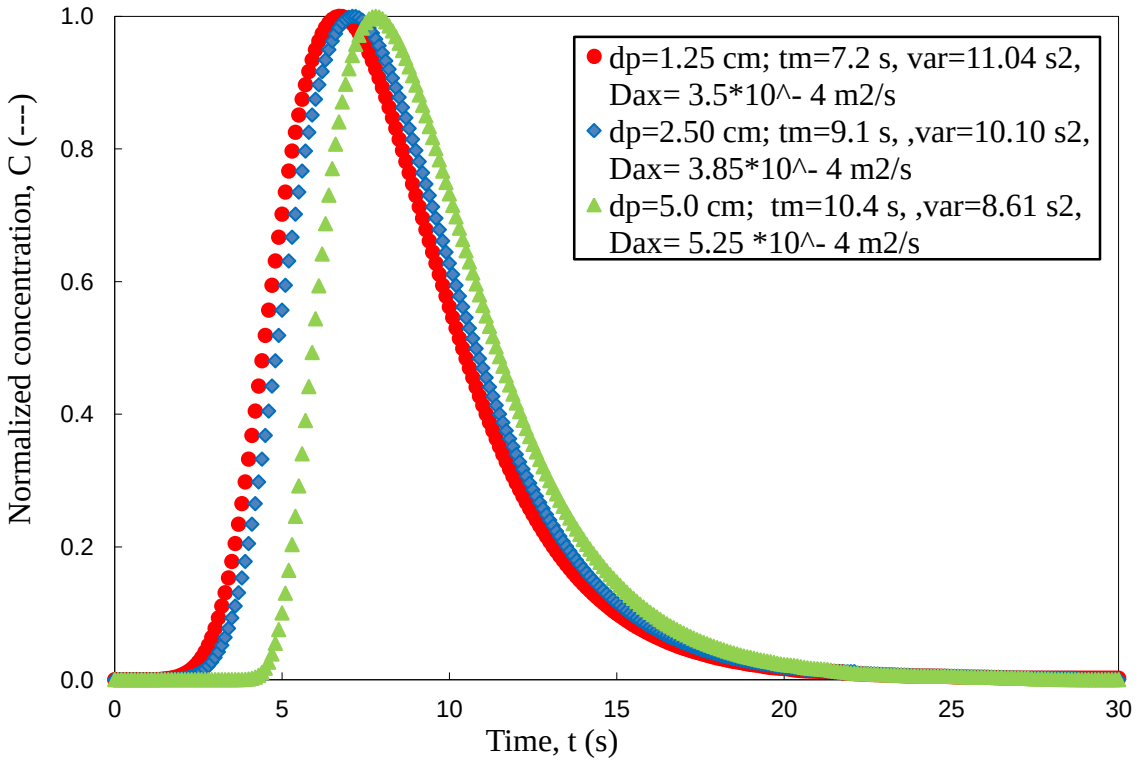

Figure 3.18. ADM Prediction of the Normalized Gas Tracer Concentration (RTD) at the Bed Outlet for Different Pebbles Diameters at Vg=20 cm/s and 92 cm Bed Height

3.7.3. Effect of Bed Height on Axial Gas Dispersion of the Bed Alone.

Investigations of the effect of bed height on the axial dispersion coefficient have been performed. These investigations are being conducted on the same cold-flow packed pebble bed unit. Three different bed heights: 30.5 cm, 61 cm, and 92 cm have been selected to form a randomly packed bed for each. Figure 3.20 shows the residence time distributions (RTDs) of the bed alone which was estimated by the ADM at superficial gas velocity of 0.2 m/s and d_p =5 cm for three different heights (30.5 cm, 61 cm, and 92 cm) of the bed. The mean residence time (t_m) of tracer is found to increase with increase in the height of pebble bed, as expected from the structure of the bed. For increase in the height from a value of 30.5 cm to 92 cm (increasing the height by three times), the mean residence time increases by 29.7%. It has been also noticed that the axial dispersion

coefficient slightly increases with increase in bed height. For increase in the height from 30.5 cm (D_{ax} = 3.5 cm^2/s) to 92 cm (D_{ax} = 3.85 cm^2/s), the axial dispersion coefficient increases by a factor of 1.1 (~ 10%) at 20 cm/s gas velocity. This is due to increase in the tortuosity and local axial voidage of the bed with increase in the bed height which cause faster dispersion of the tracer. In general, the axial dispersion varies slightly with the increase of bed height due to the increase in axial tortuosity at certain range of gas velocity (low range) and particle size (see Figure 3.19). This finding confirms the using of particle diameter instead of bed height as a characteristic length that determines the dimensionless dispersive Peclet number in packed pebble beds.

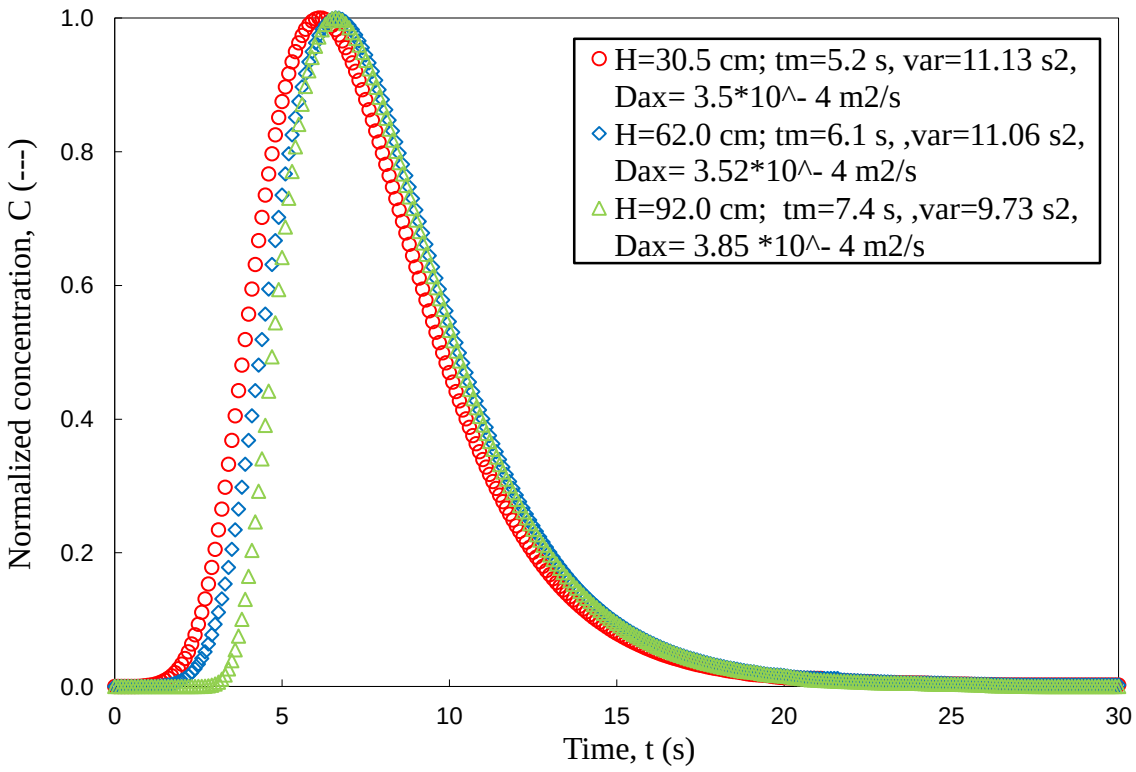

Figure 3.19. ADM Prediction of the Normalized Gas Tracer Concentration (RTD) at the Bed Outlet for Different Bed Heights at Vg=20 cm/s and d_p= 5 cm

Figure 3.20 shows values of axial dispersion coefficients of the bed alone obtained over a wide range of superficial gas velocities (from 0.01 m/s to 1 m/s) using ADM for one pebble sizes (5cm) and three different heights (30.5 cm, 61 cm, and 92 cm) of the bed. Axial dispersion coefficients slightly increase with increase in the height of pebble bed at low superficial gas velocities where large dispersion (slow (low rate of) dispersion exists). This is due to increase in the tortuosity and axial voidage of the bed with the increase in the bed height.

On the other hand, axial dispersion coefficient noticeably increases with increase in gas velocity for three heights of bed. For example at bed height = 61 cm, increase in gas velocity from a value of 0.1 m/s to 1 m/s (increasing the size by ten times), axial dispersion coefficient found to be increased by a factor of ~1.85 (~ 85%). This is due to the increase of gas velocity leads to an increase in the pressure drop along the bed and hence causing fast dispersion which means less amount of dispersion (i.e. high dispersion coefficient exist). This leads to uniform distribution of the gas phase and enhances mixing of the tracer and gradually increases dispersion coefficient. These findings indicate that at high Reynolds numbers (turbulent flow conditions) small deviation from the ideal plug-flow reactor (PFR) model in pebble beds. Hence, ADM can be used to mathematically represent the dispersion occurring in pebble bed at turbulent flow conditions.

It is also seen from Figure 3.20, at high superficial gas velocities (V_g) the differences in axial dispersion coefficients (D_{ax}) increase significantly with the bed height where the dispersion gets faster with the higher bed height due to possible variation in the bed structure with the bed height. For example, when the height increased from 30.5 cm

to 92 cm (increasing the height by three times), the axial dispersion coefficients increase by about 61% and 78% for 0.6 m/s and 1 m/s superficial gas velocities, respectively.

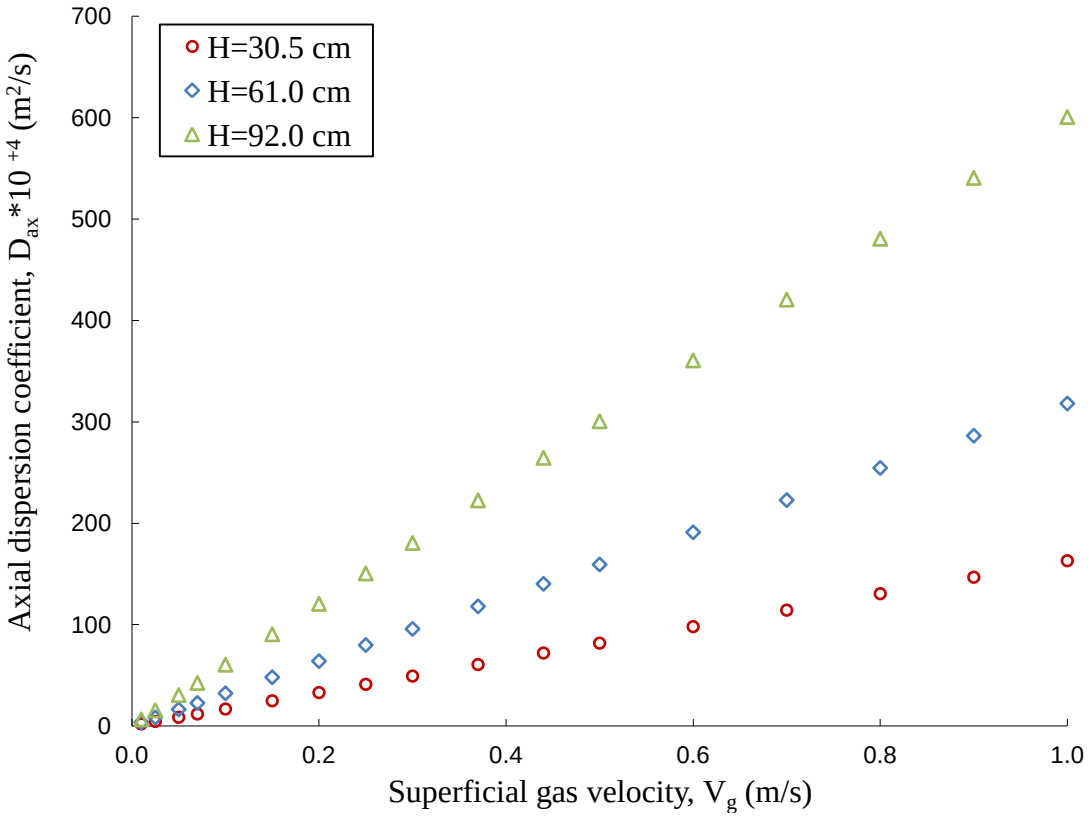

Figure 3.20. Variation of the Axial Dispersion Coefficient (D_{ax}) with the Superficial Gas Velocity (V_g) for Different Bed Heights at dp=5 cm

From Figure 3.21, it is clear that with increases in particle Reynolds number the Peclet number increases to a plateau value of about $Pe_D \approx 2$ for fully developed turbulence (i.e., complete mixing in each pore space). This confirms that the axial dispersion is controlled by the hydrodynamic mixing (convection) and the contribution of the molecular diffusion is negligible.

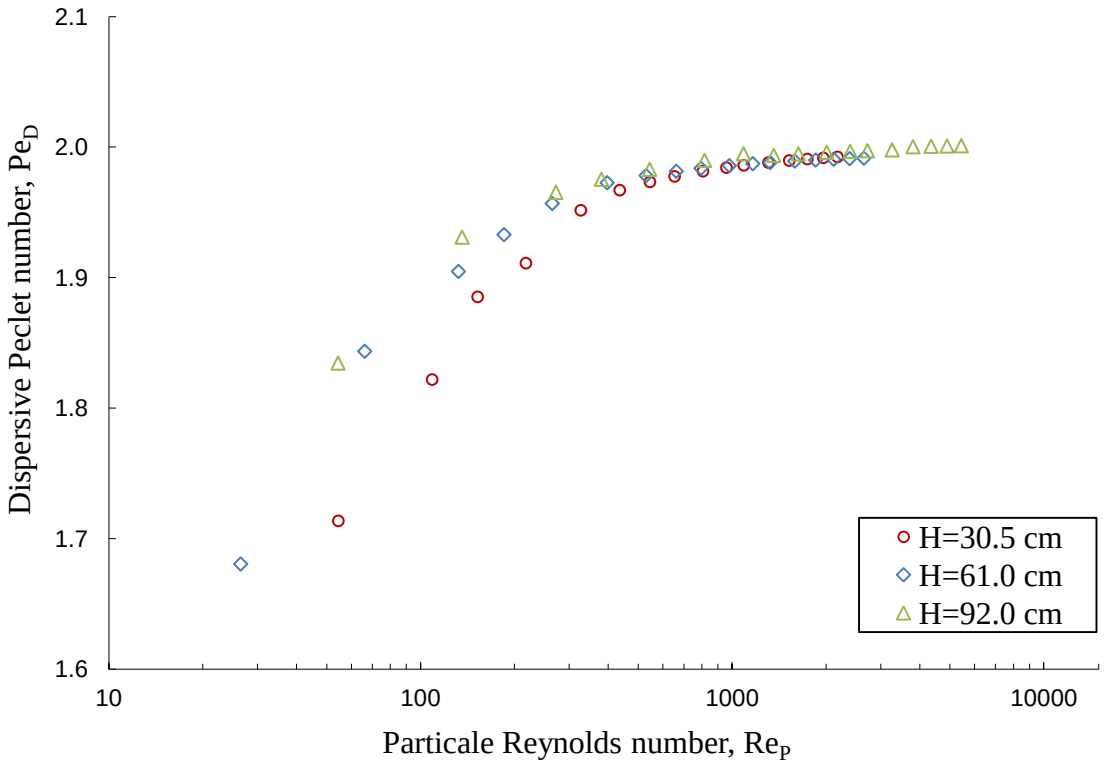

Figure 3.21. Variation of the Dispersive Peclet Number (Pe_D) with Particle Reynolds Number (Re_P) for Different Bed Heights at dp=5 cm

3.8. COMPARISON WITH EMPIRICAL CORRELATIONS

As mentioned earlier, there are no detailed experimental measurements, knowledge and quantification of the gas phase dynamics and its extent of dispersion and mixing for packed-pebble bed reactors. However, there is a large number of studies reported in the literature related to the dispersion of gas phase in the chemical packed bed reactor of smaller particles (1-3 mm diameter). In spite of this large number of studies, the correlations reported in the literature for predictions of the axial gas dispersion in gas-solid packed beds are very few, as they were reported in Section 2. Three different types

of those correlations are selected and used for comparison in this work and recalled here (for clarity).

Gunn, (1987) assumed that diffusive and mixing components of dispersion are additive, as in the following expression:

$$\frac{1}{\mathrm{Pe_D}} = \frac{1}{\tau}\frac{1}{\mathrm{Pe_M}} + \frac{1}{2} \tag{23}$$

In this work, the theoretical model developed by Lanfrey et al. (2010) have been used to calculate the tortuosity of fixed bed randomly packed with identical spherical particles as:

$$\tau = \frac{\varepsilon_b}{\left[\left(1-\varepsilon_b\right)^{4/3}\right]} \tag{16d}$$

Edwards and Richardson (1968) proposed an empirical correlation for the prediction of axial dispersion of gases flowing through a fixed bed of small particles. It accounts for the radial (transverse) dispersion that might be taken place at low Reynolds number. This correlation is expressed as:

$$\frac{1}{\mathrm{Pe_D}} = \frac{0.73}{\mathrm{Pe_M}} + \frac{0.5}{\left[1+9.7\left(\mathrm{Pe_M}\right)^{-1}\right]} \tag{22}$$

Guedes and Delgado (2003) developed a mathematical expression for the longitudinal (axial) dispersion in chemical packed bed and it is recommended only for random packings of spherical particles which are well-packed (Delgado, 2006) and it covers a wide range of values of $\mathrm{Pe_M}$ and Sc. The correlation is as follows:

$$\frac{1}{\mathrm{Pe_D}} = \frac{\mathrm{Pe_M}}{5}\left(1-\mathrm{p}\right)^2 + \frac{\mathrm{Pe_M^2}}{25}\mathrm{p}\left(1-\mathrm{p}\right)^3\left\{\exp\left[-\frac{5}{\mathrm{p}\left(1-\mathrm{p}\right)\mathrm{Pe_M}}\right]-1\right\} + \frac{1}{\tau}\frac{1}{\mathrm{Pe_M}} \tag{26a}$$

with

$$p = \frac{0.48}{Sc^{0.15}} + \left(\frac{1}{2} - \frac{0.48}{Sc^{0.15}}\right)\exp\left(-\frac{75Sc}{Pe_M}\right) \quad (26b)$$

Although these correlations were based on experimental data for upward flow of gas and have been developed for small particles used as catalyst in chemical packed bed reactors, they are evaluated in this work for packed pebble-bed of pebbles diameter of 1.25 cm, 2.5 cm and 5 cm as a first attempt.

Based on the average absolute relative error (AARE), the predictions of the correlations were assessed against the experimental data. AARE between the measured and predicated Peclet numbers is expressed as:

$$AARE = \frac{1}{N}\sum_{1}^{N}\left|\frac{Pe_{pred(i)} - Pe_{exptl(i)}}{Pe_{exptl(i)}}\right| \quad (59)$$

where N is the number of the data points.

Figures 3.22 and 3.23 show values of gas phase dispersion phenomena in terms of dispersive Peclet numbers (Pe_D) and dispersion numbers (reciprocal of Peclet numbers) with respect to molecular Peclet numbers (Pe_M) and particle Reynolds number (Re_P), respectively. The experimental values have been compared with those predicted by the selected correlations of Edwards and Richardson (1968), Gunn (1987) and Guedes and Delgado (2003). The correlation developed by Gunn (1987) seems to provide a good prediction at both low and high superficial gas velocities where the value of AARE is about 2.2%. The prediction based on Edwards and Richardson (1968) correlation is shown in Figures 3.22 and 3.23. At low superficial gas velocities, the trends and the values do not match well, while, the prediction of correlation is better at high superficial gas velocities with AARE of about 1.1%. However, at low superficial gas velocities, there is relatively larger deviation in the prediction but it is still acceptable (AARE is

about 16.7%). In the predictions of Guedes and Delgado (2003) correlation, the trends and the values do not match well for both low and high gas flow conditions. This can be attributed to uncertainties in different measurement techniques used and different operating and design conditions used in the developed of Guedes and Delgado (2003) correlation, such as particle size, tracer type experiment design, etc. In this work, a large pebble diameters (1.25 cm, 2.5 cm and 5 cm) has been used which yields higher values of average bed porosity besides the high molecular diffusivity of helium gas in air of about 0.65 cm^2/sec which leads to low value of Schmidt number, (Sc~ 0.24). However, the trend of measured axial dispersion number is still qualitatively similar to the experimental findings of dispersion of gas phase flowing in fixed beds (Bischoff, 1961; Levenspiel, 1999; Fogler, 2005). The results indicate that with more investigation of mechanisms that govern axial dispersion coefficient and wide range of data at various relevant conditions in the pebble bed would be needed to further improve the predictions of axial dispersion coefficients.

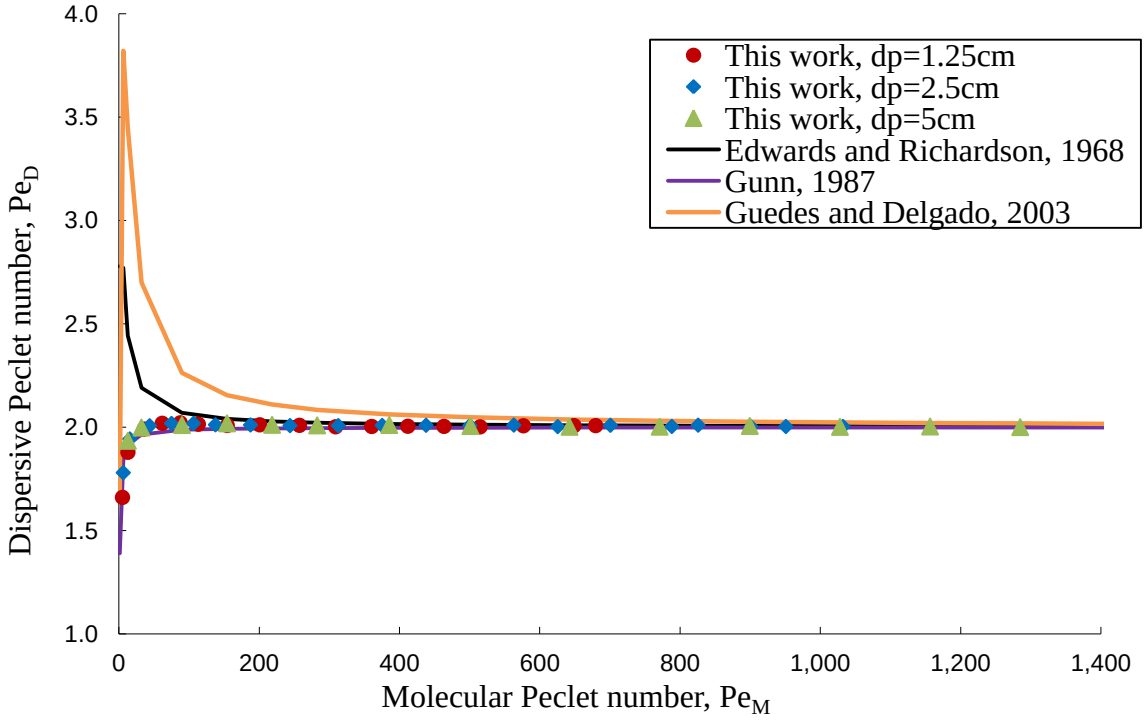

Figure 3.22. Comparison of the Measured Dispersive Peclet Number (Pe_D) with those Estimated by Empirical Correlations

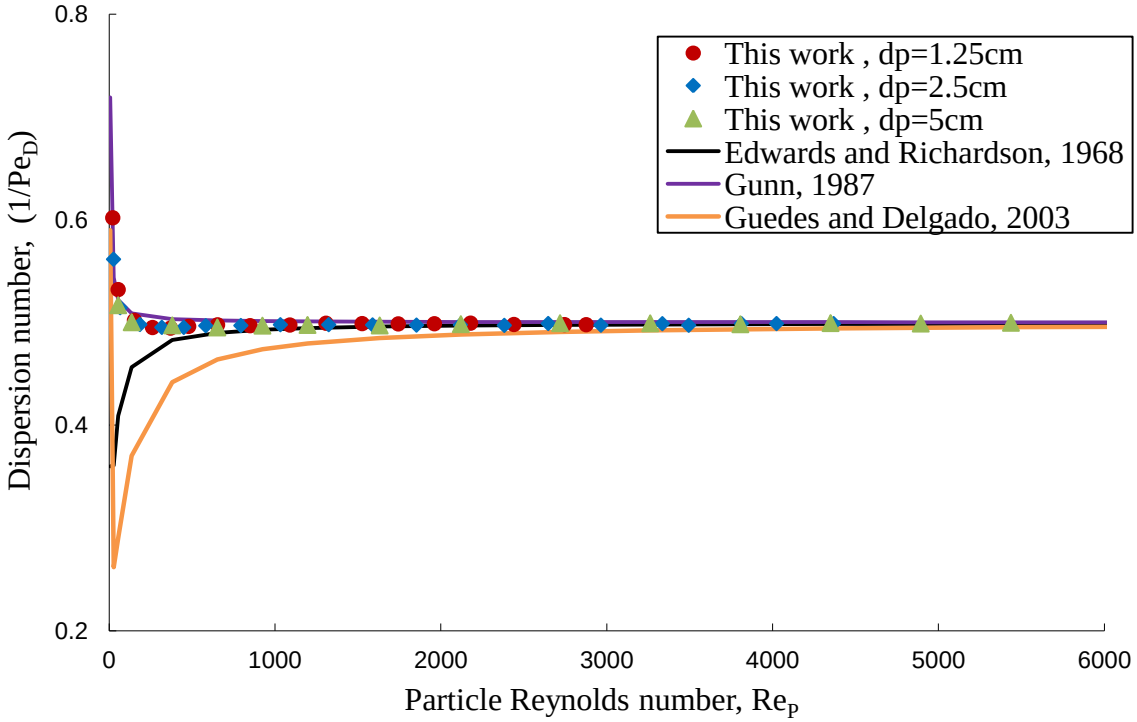

Figure 3.23. Comparison of the Measured Dispersion Number ($1/Pe_D$) with those Estimated by Empirical Correlations

3.9. CONCLUDING REMARKS

1. Quantification of the gas phase dispersion in terms of axial dispersion coefficients and dispersive Peclet numbers in packed pebble-bed has been performed **for the first time** for different gas velocities and particle sizes.
2. The non-uniformity of gas flow in the pebble bed has been described adequately by axial dispersion model at different Reynolds numbers.
3. The mixing in the plenum / distributor zone and sampling lines is significant and causes D_{ax} measurement errors. By using four experiments and the convolution integral method, the extra dispersion was removed from the overall measured axial dispersion in the packed bed to obtain the RTD of the bed alone and its extent of dispersion and mixing.
4. The results show small dispersion with better extent of gas mixing are encountered at higher velocities, while relatively large dispersion are observed at low gas velocities. In addition, these results indicate that the molecular diffusion contributes to gas dispersion phenomena at the low gas velocity, whereas in high gas velocity the hydrodynamics mixing dominates.
5. The effect of bed structure (pebble sizes) on the axial dispersion coefficient has been investigated and the obtained results indicate that pebbles size strongly affects axial dispersion and mixing in the packed pebble-bed.
6. The effect of bed height on the axial dispersion coefficient has been investigated and it is noticed from the obtained results that the axial dispersion coefficient slightly increases with increase in bed height at the low range of superficial gas velocity while at high gas velocity the effect is noticeable.

7. A comparison was made between the measured axial gas dispersion coefficients in terms of Peclet numbers and dispersion numbers (reciprocal of Peclet numbers) at different gas velocities with those predicted by selected correlations. The correlation of Gunn (1987) predicts well the obtained experimental data. However, additional investigations and more data are needed to reach to sound conclusion and to possibly develop a new correlation for packed pebble-bed nuclear reactor.
8. The present work provides insight on the extent of mixing and dispersion of the gas phase in the studied bed using advanced gas dynamics technique and methodology that properly accounts for the external dispersion.

4. GAS DISPERSION AND MIXING PHENOMENA IN THE PEBBLE BED DESCRIBED BY TANKS-IN-SERIES (T-I-S) MODEL

4.1. INTRODUCTION

The tanks-in-series (T-I-S) model or N continuous stirred tank reactor (N-CSTR) model is a one parameter model used to characterize the behavior and describe the non-ideal flow in real reactor. Therefore, it is an alternative to the axial dispersion model for dealing with deviation from ideal plug-flow model. In this model, it is assumed that the actual reactor can be replaced by N identical stirred tank reactor (CSTR) in series, whose total volume is the same as that of the actual reactor. In other words, it consists of a series of N equal volumes (V_i) and completely mixed stages interconnected by the unidirectional main flow stream, as shown in Figure 4.1. In T-I-S model, the measured residence time distribution (RTD) for the pebble bed alone will be analyzed by determining the number of ideal tanks, N, in series that best fit its RTD data. Therefore, the extent of mixing and dispersion of the gas phase in the studied pebble bed reactor (PBR) would be quantified in terms of number of tanks in series using the T-I-S model instead of axial dispersion model (ADM). There are two approaches: one approach is by replacing ADM with T-I-S model in the convolution/deconvolution integral scheme of Figure 3.11and the other approach is to use the dimensionless response of the bed calculated by ADM according to Figure 3.11 and describe it by T-I-S model to estimate the number of tanks that can best represent such response. Therefore, in this work the T-I-S model prediction will be compared with the convoluted ADM response for the bed alone (C_{out}^{*}) (Equation 53, Section 3). This can be achieved by a regression analysis and minimizing the averaged squared error in the time domain. Such comparison will give

further insight on whether the ADM could be used to predict the dispersion occurring in the packed pebble bed reactor, if the number of tanks obtained indicates a small deviation from plug flow pattern. In addition to that, an equivalency between the two models will be assessed as discussed in the next sections.

4.2. PARAMETER ESTIMATION OF THE TANKS-IN-SERIES MODEL

Material balance applied to an injected tracer for each stage in the system leads to set of ordinary differential equations as follows:

For the first tank:

$$\varepsilon_b V_1 \frac{dc_1}{dt} = -Qc_1 \tag{60a}$$

To be consistent with the normalized signals of the ADM model, Equation (60a) is divided by c_{max} as:

$$\varepsilon_b V_1 \frac{d\left(c_1/c_{max}\right)}{dt} = -Q\left(c_1/c_{max}\right) \tag{60b}$$

Since

$$\frac{c_i}{c_{max}} \approx \frac{C_i}{C_{max}} \approx C_{norm} = C_1 \tag{47b}$$

where c is the tracer concentration while C is equivalent mv signal. Therefore, Eqn (60b) becomes:

$$\varepsilon_b V_1 \frac{dC_1}{dt} = -QC_1 \tag{60c}$$

Hence, the rest of the equations will be presented in terms of normalized signal C.

For an intermediate tank:

$$\varepsilon_b V_i \frac{dC_i}{dt} = Q\left(C_{i-1} - C_i\right) \qquad \text{For } 2 \le i \le N-1 \tag{61}$$

For the Nth tank:

$$\varepsilon_b V_N \frac{dC_N}{dt} = Q\left(C_{N-1} - C_N\right) \tag{62}$$

V_i is the identical stirred tank reactor volume (cm^3), Q is volumetric flow rate (cm^3/s), and ε_b is the bed voidage (average void fraction).

Although the set of differential equations (Equations 60-62) are linear in nature, integration of the Nth tank become more complicated, therefore, it is simpler to solve all the set of the above differential equations by Laplace transform (Levenspiel, 1999).

The general expression of the dimensionless tracer response (C(t)) is derived by MacMullin and Weber (1935) and is given in most of the classical chemical reaction engineering textbooks (Levenspiel, 1999; Fogler, 2005), as follows:

$$C_N(t) = \frac{t^{N-1}}{(N-1)!\tau_i^N} e^{-t/\tau_i} \tag{63}$$

where, τ_i is the mean residence time in one of the equal volume tanks and is given by:

$$\tau_i = \frac{\varepsilon_b V_i}{Q} \qquad \text{For } 1 \le i \le N \tag{64}$$

Since all the tanks have the same volume (V_i), the mean residence time in each of them (τ_i) is equal to the total mean residence time (τ) divided by the number of tanks (N), as in the following expression:

$$\tau_i = \frac{\tau}{N} \qquad \text{with} \qquad \tau = \frac{\varepsilon_b V_T}{Q} = \frac{\varepsilon_b L}{V_g} \tag{65}$$

V_T is the packed bed volume (cm^3), Q is volumetric flow rate (cm^3/s), and ε_b is the bed voidage (average void fraction).

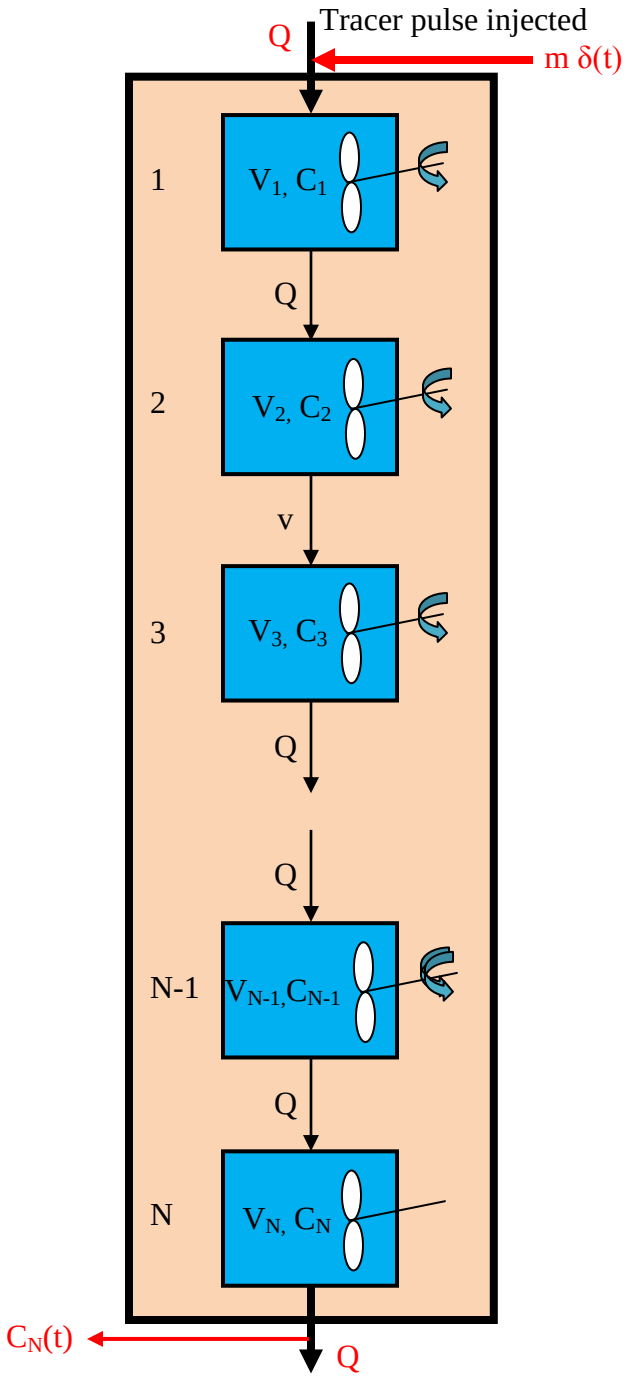

Figure 4.1. Schematic Diagram of the N-CSTR in Series

As mentioned earlier, the predicted response by T-I-S model (C_N (t)) is compared against the convoluted ADM response of the bed alone (C_{out}^*) (Equation 53, Section 3), where N will be fitted by minimizing the averaged squared error in the time domain, defined as:

$$\text{Averaged Squared Error} = \frac{1}{n}\sum_{j=1}^{n}\left[C_N\left(t_j\right) - C_{out}^*\left(t_j\right)\right]^2 \tag{66}$$

In addition to that, the number of tanks in series (N) can be estimated by calculating the dimensionless variance (σ_D^2) value of the measured RTD from a tracer experiment for the bed alone as (Levenspiel 1999; Fogler, 2005):

$$N = \frac{1}{\sigma_D^2} = \frac{t_m^2}{\sigma^2} \qquad \text{For} \quad \text{(plug-flow)} \;\; 0 \le \sigma_D^2 \le 1 \;\; \text{(perfectly mixing)} \tag{67}$$

where, t_m is the measured mean residence time in the bed alone, and σ^2 is the variance of the RTD of the bed alone. If the number of tanks, N, will be small, the gas flow of the pebble bed approaches the flow pattern of CSTR. On the other extreme, when N will be large, the behavior of the gas flow in the pebble bed approaches plug-flow reactor (PFR) pattern. For ideal behaviors, the parameter N is one ($N = 1$) for a single ideal CSTR of completely backmixing and infinite ($N \to \infty$) for a single ideal PFR of no backmixing. It has been reported by Tang et al. (2004) that as a rule of thumb, 10 is generally sufficient to consider the packed bed reactor as close to PFR. In ideal PFR, the RTD becomes symmetrical and Gaussian (Nauman and Buffham, 1983). Another important issue is that the T-I-S model has been defined only for integer values of N; as N= 1, 2, 3$\ldots\infty$. The corresponding values of dimensionless variance (σ_D^2) to these N are as: σ_D^2=1, 1/2, 1/3…0 (Nauman, 2008). Therefore, in fitting experimental data, it is necessary to

consider the case where N is not an integer which then will be approximated to integer value.

4.3. MODEL DISCRIMINATION: AXIAL DISPERSION MODEL VERSUS TANKS-IN-SERIES MODEL

Figure 4.2 a and b show a comparison between the two RTD responses of ADM and T-I-S model for the laminar and turbulent flow regimes. It seems that the ADM and the N-CSTR responses almost match each other through the whole time domain. For laminar-flow regime (Vg=0.08 m/s), the pebble-bed is represented by at least six ideal mixed tanks in series (N≈ 6, σ_D^2 =0.169), see section 5.3, Table 5.5. While for turbulent-flow regime (Vg=0.6 m/s), the pebble-bed is represented by around nine ideal mixed CSTR in series (N≈ 9, σ_D^2 =0.11), see section 5.3, Table 5.5, which reflects small deviation from the ideal plug-flow reactor. The averaged squared error calculated using Equation 66 is found to be 2.29E-04 and 3.85E-04 for the laminar and turbulent flow, respectively. This is a confirmation that the axial dispersion model (ADM) can be used successfully to describe the non-ideal flow behavior in the studied packed pebble beds. In addition, it can be concluded that for a small relative dispersion both models of axial dispersion model (ADM) and tanks-in-series (T-I-S) model give close or similar results. In other words, the relatively small deviation from ideal plug flow which occurs in packed pebble-beds of high flow rate is found to be satisfactory represented by the axial dispersion model or by the tanks-in-series model.

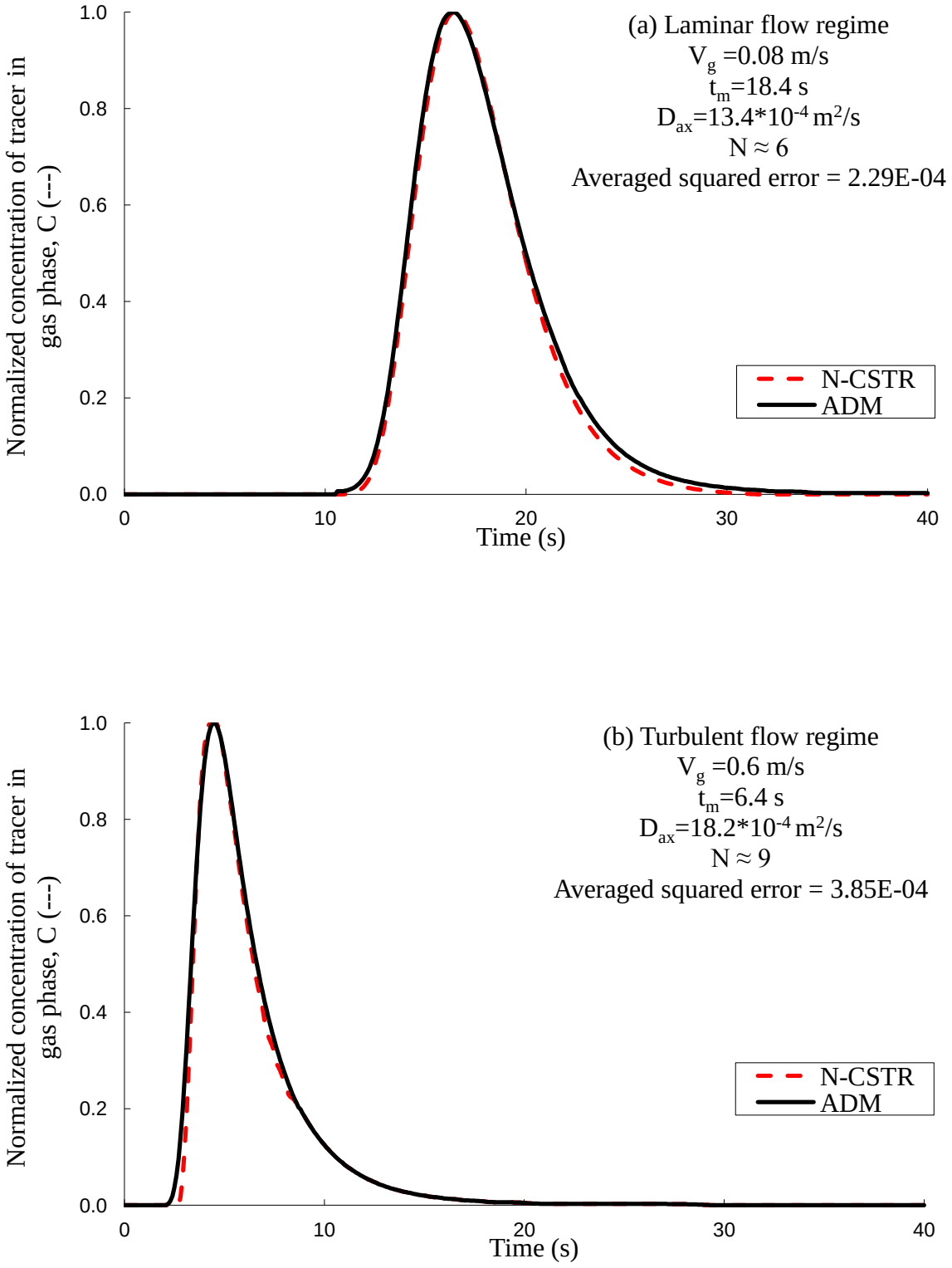

Figure 4.2. Comparison between the ADM Response and the Response Estimated by T-I-S model at Vg=0.2 m/s and dp=5cm for 92 cm Height; (a) Laminar-Flow Regime and (b) Turbulent-Flow Regime

4.4. EQUIVALENCY BETWEEN ADM AND TANKS-IN-SERIES MODEL

The axial dispersion model has advantage in that all available correlations in literature for flow pattern in real reactors invariably use this model (Levenspiel 1999). On the other hand the tanks-in-series model is simple and can be extended without too much difficulty to any arrangement of compartments, with or without recycle. It is possible to apply both of one-parameter models to pebble bed reactor using the definition of dimensionless variance (σ_D^2) of the RTD single of the bed alone. These two models are equivalent when the dispersive Peclet number (Pe_D, the parameter of ADM) is related to the number of tanks in series (N, the parameter of T-I-S model). The two models can be compared quantitatively by equating their variances (Saravanathamizhan et al., 2010). Such equating leads to a relationship between their two parameters, Pe_D and N.

The second dimensionless moment (dimensionless variance, σ_D^2) of a pulse tracer input for the ADM with closed-closed boundary conditions is given by (Levenspiel and Bischoff, 1963):

$$\sigma_D^2 = \frac{\sigma^2}{t_m^2} = \left\{ \frac{2}{Pe_r} - \frac{2}{Pe_r^2}\left[1 - \exp\left(-Pe_r\right)\right] \right\} \tag{68}$$

where Pe_r is the reactor Peclet number ($Pe_r = V_g L/\varepsilon_b D_{ax}$) which uses the reactor length (L) instead of pebble diameter (d_P) as a characteristic length (Fogler, 2005). To replace Pe_r in terms of ($Pe_D = V_g d_p/\varepsilon_b D_{ax}$), Pe_D is multiplied by the ratio of (L/d_P), or ($Pe_r = Pe_D\ (L/d_P)$), therefore Equation (68) becomes:

$$\sigma_D^2 = \frac{\sigma^2}{t_m^2} = \left\{ \frac{2}{Pe_D\left(L/d_P\right)} - \frac{2}{Pe_D^2\left(L/d_P\right)^2}\left[1 - \exp\left(-Pe_D\left(L/d_P\right)\right)\right] \right\} \tag{69}$$

In Equation (69), the dispersive Peclet number (Pe_D) can be found experimentally from the RTD data of bed alone by the curve fitting in the time domain for D_{ax} (where, $Pe_D = V_g\ d_P\ /\varepsilon_b D_{ax}$), as discussed in Section 3.

Recalling the dimensionless variance (σ_D^2) in terms of the number of tanks of the T-I-S model as per Equation (67), σ_D^2 is:

$$\sigma_D^2 = \frac{\sigma^2}{t_m^2} = \frac{1}{N} \tag{70}$$

where N is an integer value. Using Equation (70) for non-integer value of N is possible but destroys the physical basis of the tanks-in-series model (Nauman, 2008).

By using the equality of dimensionless variance for the axial dispersion model (Equation, 69) with the tanks-in-series model (Equation, 70) and this approach is based on exactly matching the tracer response curves, the two models can be related through the value of N for the flow of gas in pebble-bed as:

$$N = \frac{1}{\left\{\frac{2}{Pe_D\left(L/d_p\right)} - \frac{2}{Pe_D^2\left(L/d_p\right)^2}\left[1-\exp\left(-Pe_D\left(L/d_p\right)\right)\right]\right\}} \tag{71}$$

For all studied laminar and turbulent flow conditions, the number of tanks in series can be calculated for the measured value of the dispersive Peclet number (Pe_D), as shown in Figures 4.3 and 4.4. As mentioned earlier, the dispersive Peclet number (Pe_D) controls the level of mixing and quantify it in the pebble-bed. For example at d_P = 1.25 cm, with $Pe_D \to 0.5$ (low V_g), molecular diffusion will be noticeable mechanism and gives (N~6). While $Pe_D \to 2$ (high V_g), the system acts as close to an ideal plug-flow reactor (N~9). This is consisted with the dimensionless variance (σ_D^2) estimation obtained by central moments discussed in Section 5.

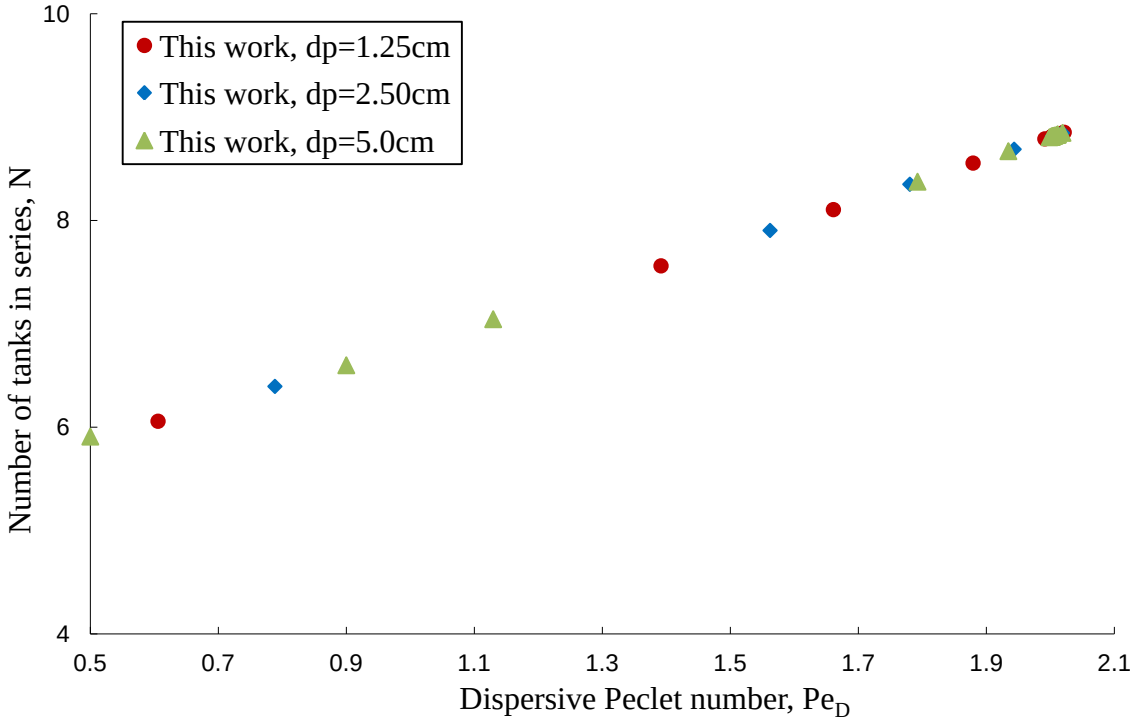

Figure 4.3. Comparison of Fitted Parameters of the ADM and the T-I-S model at Different Pebble Sizes for 92 cm Height

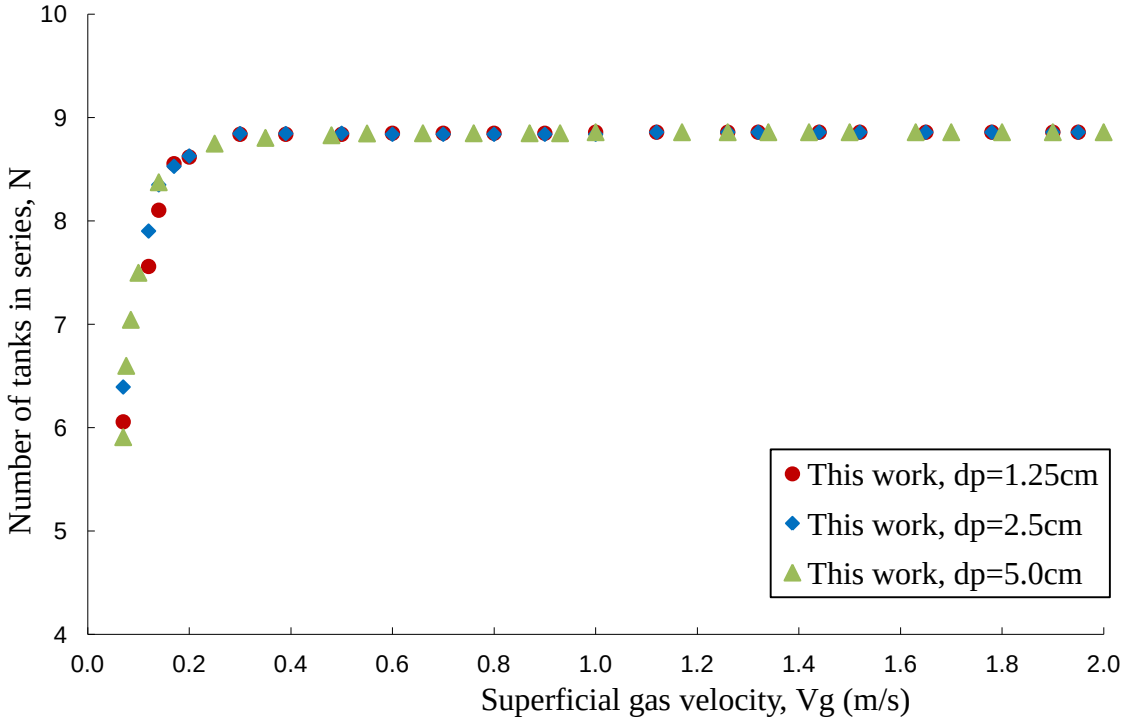

Figure 4.4. Variation of the Number of Tanks in Series (N) with Superficial Gas Velocity at Different Pebble Sizes for 92 cm Height

4.5. CONCLUDING REMARKS

1. The tanks-in-series (T-I-S) model or N continuous stirred tank reactor (N-CSTR) model has been used to characterize the behavior and to describe the non-ideal flow as an alternative to the axial dispersion model (ADM) in packed pebble bed.
2. The results of tanks in series model confirm that the axial dispersion model (ADM) can be used successfully to describe the non-ideal flow behavior in the studied packed pebble bed.
3. Relatively small deviation from ideal plug flow which occurs in the studied packed pebble-beds at high gas flow rate (typical operating conditions of pebble bed reactor) has been found which can be satisfactory represented either by the axial dispersion model or by the tanks-in-series model.
4. To assess for equivalent relationship between the parameters of the axial dispersion model (dispersive Peclet number, $Pe_{D,}$ and σ_D^2) and tanks-in-series model (the number of tanks in series, N) in the studied pebble bed reactors, a comparison of the residence time distributions of both models has been made by equating their dimensionless variance.

5. ANALYSIS OF THE RESDIENCE TIME DISTRIBUTION (RTD) BASED ON THE CENTRAL MOMENTS METHOD

5.1. INTRODUCTION AND OBJECTIVES

It is well known that statistical central moment analyses are among the methods used to quantitatively analyze the residence time distribution (RTD) curves obtained by tracer technique. Since these quantities of moments are additives, the central moments based analyses allow quantifying the gas dispersion and mixing phenomena in the packed pebble-bed reactor without assuming any predefined model for the reactor.

In the previous Sections, the RTD tracer response of the packed pebble bed reactor has been analyzed using axial dispersion and tanks-in-series models and hence the dispersion and mixing phenomena have been quantified. In this Section, the raw RTD tracer response data will be processed to estimate the moments of all components of the set-up based on central moment analyses. In second step, these estimated moments are used to extract the moments of interest for the bed alone. In third step, these extracted moments will be compared with the moments estimated using the ADM response curve. Such comparison will give further insight on whether the ADM could be used to predict the dispersion occurring in the packed pebble bed reactor. In addition, it is possible to use the definition of dimensionless variance (σ_D^2) of the RTD single of the bed alone to calculate the number of tanks in series (N, the parameter of T-I-S model), as discussed in Section 4, and compare it with the results of extracted first and second moments based on the statistical central moment analyses .

5.2. METHODOLOGY OF THE CENTRAL MOMENTS ANALYSES

5.2.1. Overview. It is very common to compare residence time distributions (RTDs) by using their moments instead of trying to compare their entire distributions (Wen and Fan, 1975; Fogler 2005). For this purpose, there are four central moments which will be used for this analysis as follows:

1. The zero moment represents the area under the curve of the time response tracer signal. This moment is useful for mass balance assessment that needs to be carried out in order to ensure that the injected amount of tracer leaves the system.
2. The first moment of the residence time distribution represents the mean age of the tracer (mean residence time, t_m) in the pebble bed, if there is no considerable diffusion transport across inlet and outlet boundaries.
3. The second moment about the mean of residence time is a measure of the dispersion of the distribution and is called the square of the standard deviation (σ^2) or the variance. The magnitude of this moment is an indication of the spread of the distribution around the mean. Greater the value of this moment, wider will be the spread of distribution.

Another very useful parameter which gives an indication on the deviation from the idealized plug-flow model called dimensionless variance (σ_D^2) of moment. It represents the ratio between the variance (2^{nd} moment) and square of the mean residence time (1^{st} moment). Values of the dimensionless variance between close to zero and less than unity represent idealized plug flow model and closer to CSTR model, respectively. Whereas values of the dimensionless variance larger than unity indicate the presence of the stagnant zones and/or the bypassing flow conditions in the system. The two extreme

cases are: $\sigma_D^2 = 0$ for single ideal plug-flow reactor (PFR) of no backmixing and $\sigma_D^2 = 1$ for single continuous stirred tank reactor (CSTR) of completely backmixing.

4. The third central moment of the distribution known as skewness (S^3) will provide the information about the relative weight that the various fractions of feed will have on the total dispersion. The magnitude of this moment measures the extent that a distribution is skewed in one direction or another in reference to the mean.

Table 5.1 summarizes the definition of these four central moments and the relationships used to estimate them in terms of tracer concentration (c(t)) and age distribution function (E(t)) curve for impulse tracer injection. The age distribution function (E(t)) or RTD function can be obtained by changing the tracer concentration c(t) to the normalized concentration (dimensionless signal) ($c/c_{max} \approx C/C_{max} \approx C_{norm} \approx C_{(t)}$) or by using directly the measured quantity in terms of mV, mAmp, etc), if such quantity is linearly correlated with the tracer concentration). These relationships are as follows:

$$E(t) = \frac{c(t)}{\int_0^\infty c(t)\,dt} = \frac{\left(c(t)/c_{max}\right)}{\int_0^\infty \left(c(t)/c_{max}\right)\,dt} = \frac{C_{norm}(t)}{\int_0^\infty C_{norm}(t)\,dt} \qquad (73)$$

where C is the tracer concentration while c is equivalent mv signal.

In this section, all the central moments will be estimated in terms of an age distribution function (E(t)), as expressed in last column of Table 5.1.

Table 5.1. Expressions of the Moments for the Impulse Tracer Response

Central moments	**Physical meaning**	**Relationship in terms of**	
		Outflow concentration, C(t)	**RTD function, E(t)**
Zero moment	Area under the curve, A	$A = \int_0^\infty c(t)\,dt = \left(\frac{M}{Q}\right)$	$\int_0^\infty E(t)\,dt = 1$
First moment	Mean residence time, t_m	$t_m = \left(\frac{Q}{M}\right)\int_0^\infty tc(t)\,dt = \left(\frac{\varepsilon_b V_T}{Q}\right)$	$t_m = \int_0^\infty tE(t)\,dt$
Second moment	Variance, σ^2	$\sigma^2 = \frac{\left(\frac{Q}{M}\right)^2 \int_0^\infty t^2 c(t)\,dt}{t_m^2} - 1$	$\sigma^2 = \int_0^\infty (t - t_m)^2 E(t)\,dt$
	Dimensionless variance, $\sigma_D{}^2$	$\sigma_D^2 = \frac{\sigma^2}{t_m^2}$	
Third moment	Skewness, S^3	$S^3 = \frac{\left(\frac{Q}{M}\right)^3 \int_0^\infty t^3 c(t)\,dt}{t_m^3} - 3\frac{\left(\frac{Q}{M}\right)^2 \int_0^\infty t^2 c(t)\,dt}{t_m^2} + 2$	$S^3 = \frac{1}{\sigma^{3/2}} \int_0^\infty (t - t_m)^3 E(t)\,dt$

E(t) is calculated using the normalized signal as per Eqn (73), V_T is the total bed volume (cm^3), Q is the volumetric flow rate of injected tracer (cm^3/s), M is the total mass of injected tracer (gm), and ε_b is the average bed voidage.

Estimating the above mentioned moments allows quantifying the dispersion and mixing in the system without assuming any predefined flow model for the pebble bed. As mentioned earlier the moment quantities are additives for the components of a system in series. This is applied on the experimental packed pebble bed set-up which has different segments such as sampling line at the top, plenum, the bed and the sampling line at the bottom which are in series, as was shown in Section 3 in Figure 3.5 and identified

in Table 3.2. For clarity, Figure 3.5 is also recalled in this Section and Table 3.2 is re-identified in this section as Table 5.2. As mentioned earlier, the analyses methodology of central moments will be achieved in three steps. In the first step, the moment quantities for the plenum/distributor alone will be extracted from the $E_{(i)}$ and $E_{(ii)}$ functions which represent the measured age distribution function (E(t)) or RTD function (Equation 73). Using the same procedures of the second step, the moment quantities of the RTD function of the bed alone ($E_{(iv)}^{*}$) will be extracted from the RTD response of the whole system ($E_{(iv)}$). In the third step, the extracted moment quantities will be compared with those obtained from the RTD of the bed obtained by ADM based predictions, as described in Section 3.

All positions of different tracer injection ports and sampling ports and extracted quantities are re-identified in Figure 5.1 and Table 5.2.

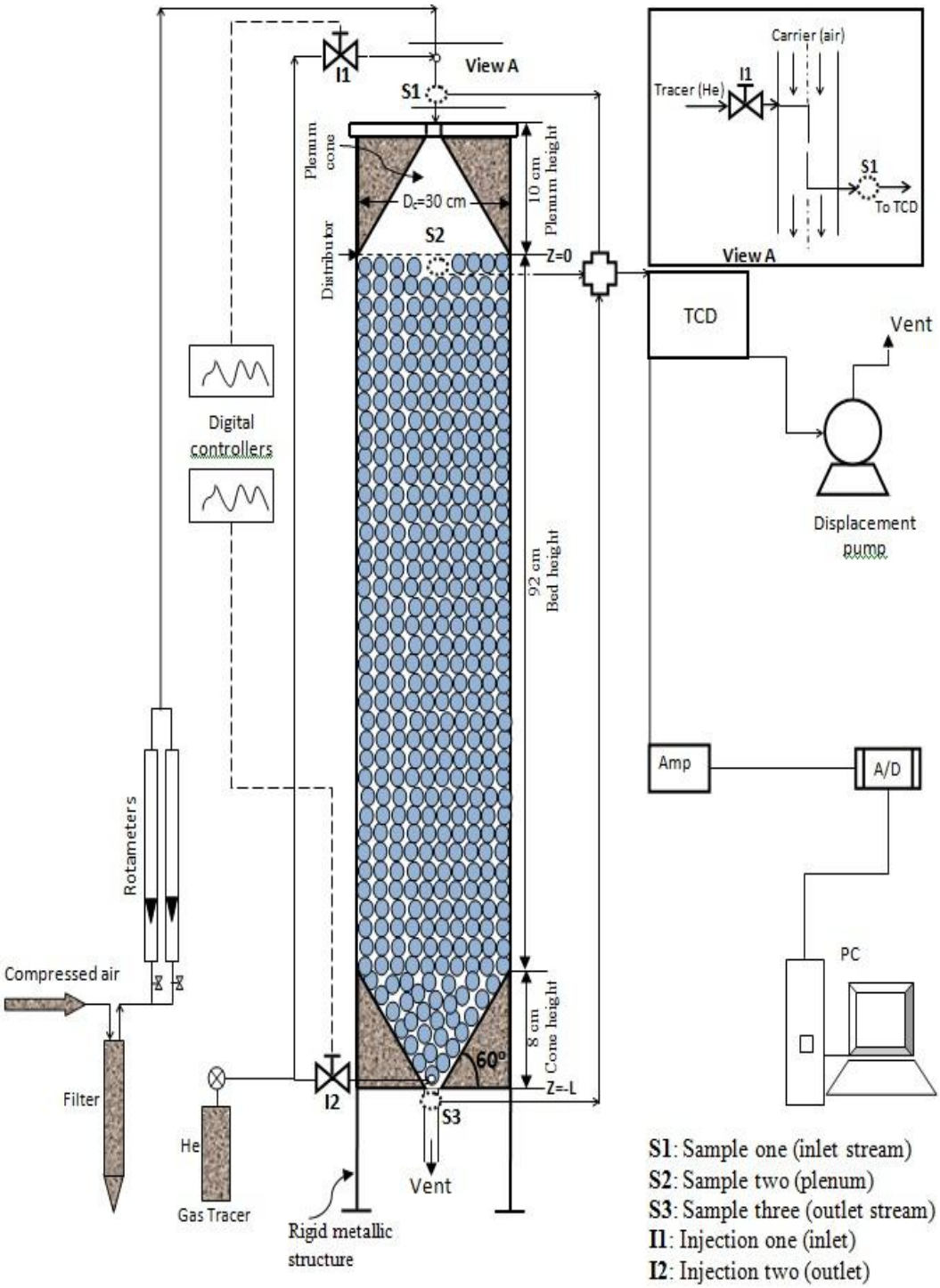

Recalled Figure 3.5 (Page 70). Schematic Diagram of the Advanced Gas Dynamics Experimental Set-Up

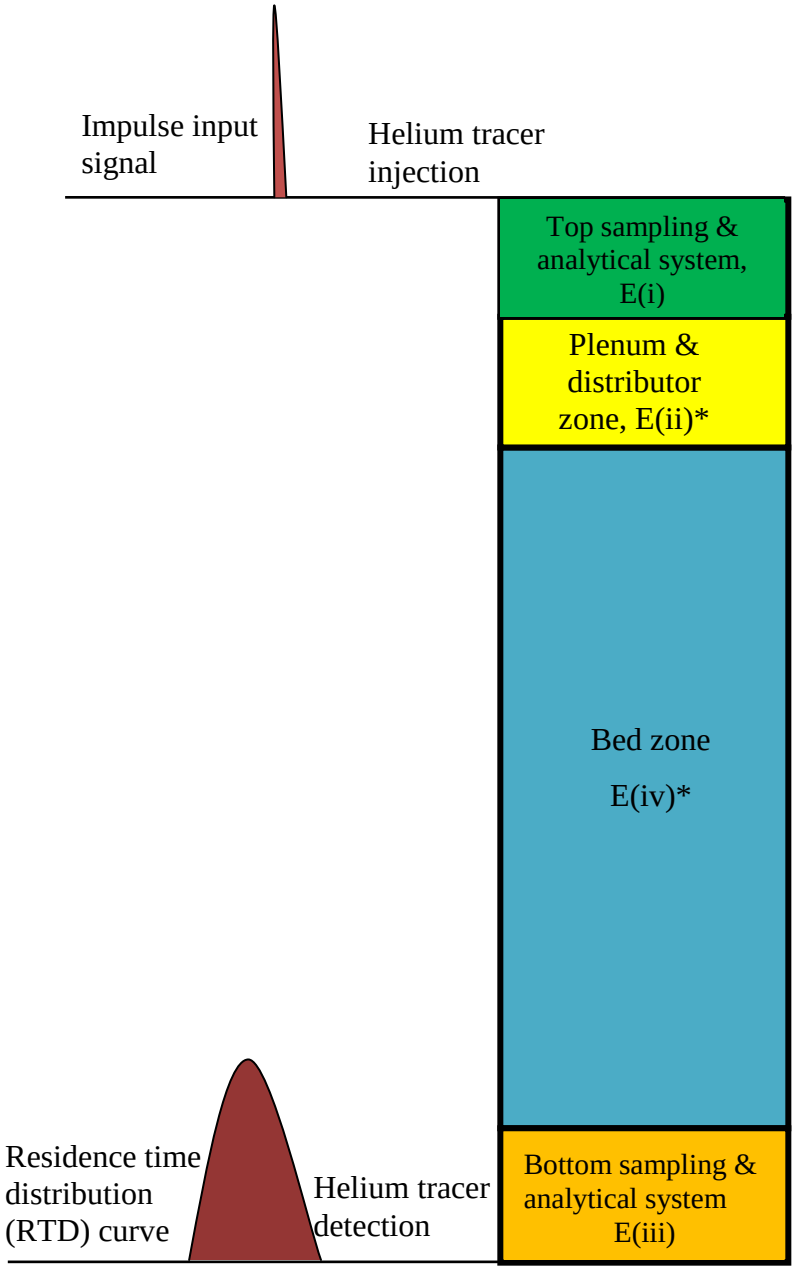

Figure 5.1. Representation of the Experimental Set-Up as Different Components in Series

Table 5.2: Set of Experimental Measurements for the Gaseous Tracer Technique

Measurement	RTD function	Tracer injection	Sampling location	Dispersion zones measured
C(i)	E(i)	I1	S1	Sampling/analytical system from S1
C(ii)	E(ii)	I1	S2	Plenum/distributor zone + sampling/analytical from S2
C(ii)*	**E(ii)***	Extracted plenum/distributor zone response		
C(iii)	E(iii)	I2	S3	Sampling/analytical system from S3
C(iv)	E(iv)	I1	S3	Plenum zone + bed zone +sampling/analytical system from S3
C(iv)*	**E(iv)***	Extracted bed zone response		

I1 and I2: injection ports; while S1, S2 and S3: sampling ports as shown in Figure 3.5

5.2.2. Extraction of the Moments of the Plenum/Distributor Section Alone. In this step, the moment quantities of the plenum and distributor zone alone will be extracted from the E(i) and E(ii) functions. The E(i) and E(ii) functions represent the dispersion occurring in the inlet pipe plus top sampling lines which is measured using the sampling port S1 (at the top of the bed Figure 3.5) and the plenum/distributor section plus the sampling line which is measured using the sampling port S2, respectively (Table 5.2, Figure 3.5). This represents two sections in series, where the sampling lines for ports S1 and S2 are identical in length and fitting. Therefore, the differences between the moments of the E(i) and E(ii) functions provide the central moments for the RTD function of the plenum/ distributor section alone (E(ii)*) alone as follows:

$$\text{E(ii)}^{*}\ \text{moments}_{(\text{plenum})} = \text{E}(\text{ii})\ \text{moments} - \text{E}(\text{i})\,\text{moments} \qquad (74a)$$

$$\left.\begin{aligned} t_{m(\text{plenum})} &= t_{m(\text{plenum+top sampling})} - t_{m(\text{top sampling})} \\ \sigma^2_{(\text{plenum})} &= \sigma^2_{(\text{plenum+top sampling})} - \sigma^2_{(\text{top sampling})} \\ \sigma^2_{D(\text{plenum})} &= \sigma^2_{D(\text{plenum+top sampling})} - \sigma^2_{D(\text{top sampling})} \\ S^3_{(\text{plenum})} &= S^3_{(\text{plenum+top sampling})} - S^3_{(\text{top sampling})} \end{aligned}\right\} \quad (74b)$$

The extracted moments of the plenum/distributor section ($E_{(ii)}^*$) will be compared against the moments of the convoluted plenum CSTR predictions (C_{in}^*) (based on CSTR model, Equation 49, Section 3) after C_{in}^* converted to the RTD function (E_{in}^*) (Equation 73). The average absolute relative error (AARE) between the extracted moments ($E_{(ii)}^*$) by moment analyses will be assessed against the predicated moments by CSTR model for the plenum/ distributor zone alone as:

$$\text{AARE} = \frac{1}{N}\sum_{1}^{N}\left|\frac{E_{(ii)}^{\ *} - E_{(in)}^{\ *}}{E_{(ii)}^{\ *}}\right| \quad (74c)$$

where N is the number of the data points.

5.2.3. Extraction of the Moments of the Pebble Bed Section Alone. Using the same procedures, the moment quantities of RTD response of the bed alone can be extracted from the whole system RTD response. These extracted quantities are compared with those obtained from the RTD of the bed obtained by ADM based predictions. As listed in Table 5.2, E(iii) and E(iv) functions represent the dispersion occurring in the outlet pipe plus sampling line from port S3 (at the bottom of the bed Figure 3.5) and the whole system, respectively. Therefore, the differences between the moments of the E(iv) function and moments of combined E(iii) and extracted E(ii)* can provide the moments of the RTD response of the bed alone (E(iv)*) as follows:

$$\text{E(iv)}^* \text{moments} = \text{E}\left(\text{iv}\right)\text{moments} - \left[\text{E}\left(\text{ii}\right)^* \text{moments} + \text{E(iii)moments}\right] \quad (75a)$$

$$\left.\begin{aligned} t_{m(bed)} &= t_{m(whole)} - \left[t_{m(plenum)} + t_{m(bottom\ sampling)} \right] \\ \sigma^2_{(bed)} &= \sigma^2_{(whole)} - \left[\sigma^2_{(plenum)} + \sigma^2_{(bottom\ sampling)} \right] \\ \sigma^2_{D(bed)} &= \sigma^2_{D(whole)} - \left[\sigma^2_{D(plenum)} + \sigma^2_{D(bottom\ sampling)} \right] \\ S^3_{(bed)} &= S^3_{(whole)} - \left[S^3_{(plenum)} + S^3_{(bottom\ sampling)} \right] \end{aligned}\right\} \quad (75b)$$

In the following section, the moments of the bed alone ($E_{(iv)}^*$) will be compared with the moments of convoluted ADM prediction of the bed (C_{out}^*) (Equation **53**, Section 3) after it converted to the RTD function (E_{out}^*). The average absolute relative error (AARE) between the extracted moments ($E_{(iv)}^*$) by moment analyses will be assessed against the predicated moments by ADM for the bed alone as:

$$AARE = \frac{1}{N} \sum_{1}^{N} \left| \frac{E_{(iv)}^* - E_{(out)}^*}{E_{(iv)}^*} \right| \quad (75c)$$

where N is the number of the data points.

5.2.4. Verification of the Central Moment Analysis (CMA) Methodology.

For verification of the above methodology, analyses of moments have been made on the RTD responses at superficial gas velocity of 0.2 m/s and using pebbles of 1.25 cm diameter. As explained in Section 3, Figure 3.9 shows RTD responses measured at different sampling positions which corresponding to the different components of the studied packed pebble-bed. This figure is also recalled in this section for clarity and the signals (normalized signal C curves) of this figure are converted to RTD functions (E curves) based on Equation 73, as shown in Figure 5.2. Table 5.3 lists the vales of the estimated central moments for all RTD functions based on the Equations in Table 5.1. The moments of E(i) function are smaller than those of E(ii) function. This indicates that smaller residence time and dispersion exist in the sampling line compared to those of the plenum/distributor section. Almost the same values of extracted moments are observed

for the E(iii) and E(i) function due to the identical design of sampling lines at the top and bottom of the bed. The moment's values for E(iv) function are the highest because they represent the whole system. In addition, it can be seen from Table 5.3 that all values of skewness (3rd moment) are positive which indicate an asymmetrical tail extending towards the right side (Figures 3.9 and 5.2). In other words, the gas residence time distribution results show asymmetry about the mean, indicating more uneven distribution of gas.

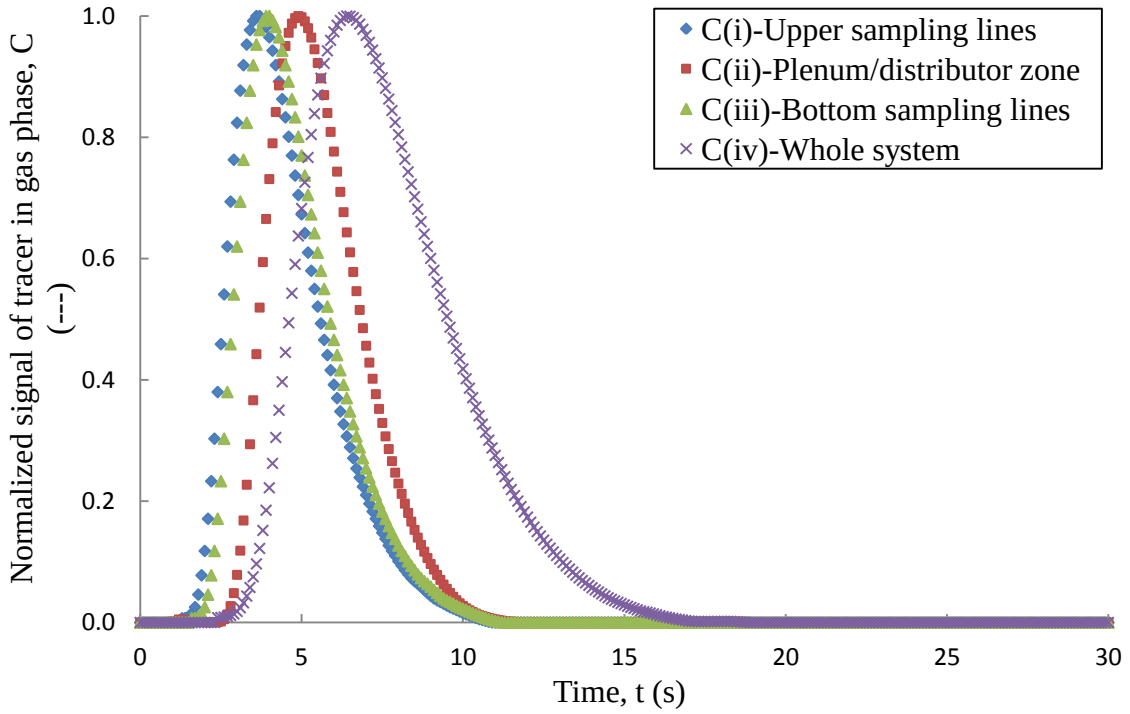

Recalled Figure 3.9 (Page 79). RTD Responses of the Gas Tracer Obtained for Different Sampling Positions at Vg=20 cm/s ($C_{(i)}$, $C_{(ii)}$, $C_{(iii)}$, and $C_{(iv)}$ are defined in Table 5.2)

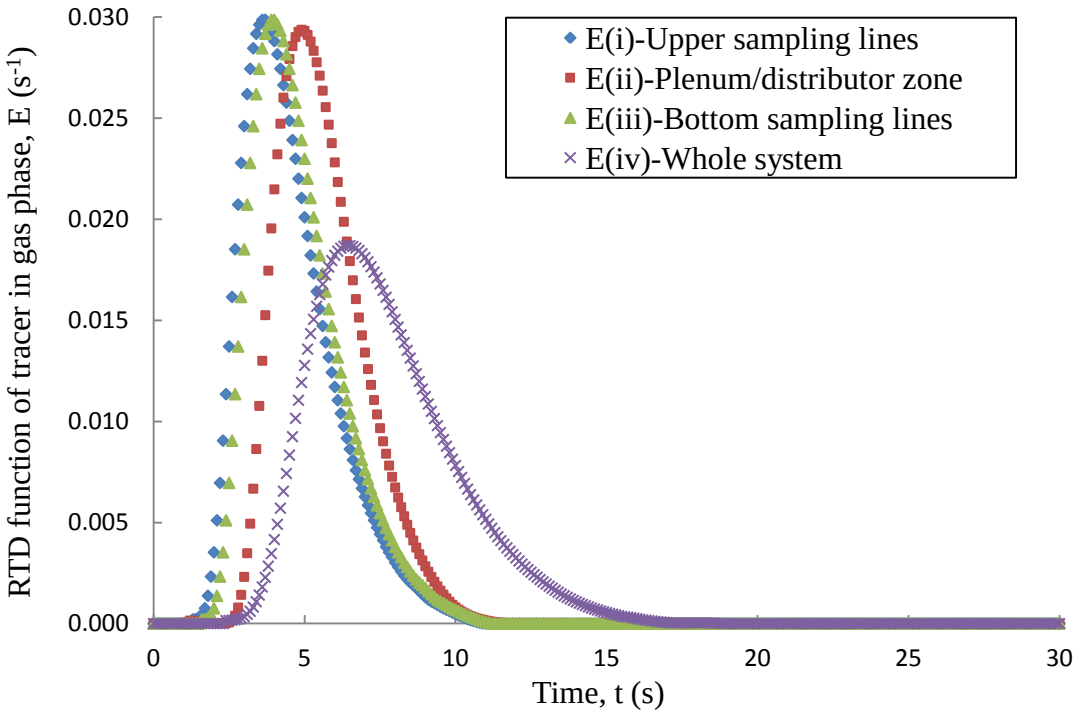

Figure 5.2. RTD Functions of the Gas Tracer Obtained for Different Sampling Positions at Vg=20 cm/s (E(i), E (ii), E (iii), and E (iv) are defined in Table 5.2)

Table 5.3. Moments of the RTD Functions Obtained at Different Sampling Positions

RTD function	**Mean residence time, t_m (s)**	**Variance, σ^2 (s^2)**	**Dimensionless variance, σ_D^2 (---)**	**Skewness, S^3 (--)**
E(i)	1.10	1.06	0.88	2.37
E(ii)	2.20	2.35	0.48	2.41
E(iii)	1.11	1.06	0.88	2.37
E(iv)	9.97	9.48	0.10	5.64

The extracted central moments using CMA have been obtained based on Equations 74a and 75 a, and the results are shown in Table 5.4. The averaged absolute relative error (AARE) between $E_{(ii)}$* (plenum/distributor) and (E_{in}^*) obtained from CSTR model of the plenum/distributor is found to be small (3.1E-02). This small value of

AARE confirms good matching between the estimated moments from the raw data $E_{(ii)}$* and the calculated ones (E_{in}^{*}) using CSTR model.

As listed in Table 5.4, the averaged absolute relative error (AARE) between $E_{(iv)}$* (bed alone) and E_{out}^{*} obtained from ADM of the bed alone is found to be also small (3.8E-03) . The small value of AARE confirms good matching between the estimated moments obtained from the raw data response $E_{(iv)}$* by CMA and those predicted by ADM response (E_{out}^{*}). This also further confirms that the pebble bed can be represented mathematically by ADM at the studied superficial gas velocity of 20 cm/s. Same findings have been obtained for the studied superficial gas velocity that cover both laminar and turbulent flow regimes. The obtained σ_D^2 values also indicate that the gas flow pattern in the studied bed at 20 cm/s gas velocity is not much deviated from ideal plug-flow characteristics.

Table 5.4. Moments of the RTD Functions Obtained for Different Components at Superficial Gas Velocity of 20 cm/s

Measurement	**Mean residence time, t_m (s)**	**Variance , σ^2 (s^2)**	**Dimensionless variance, σ_D^2(--)**	**Skewness, S^3 (--)**	**AARE**
$E(ii)^{*}$(plenum)	1.10	1.09	0.90	0.04	3.1E-02
E_{in}^{*}(CSTR)	1.07	1.02	0.89	0.05	
$E(iv)^{*}$ (bed)	7.86	7.60	0.12	3.23	3.8E-03
E_{out}^{*}(ADM)	7.80	7.23	0.11	3.24	

5.3. RESULTS AND DISCUSSION

Results have been obtained over a wide range of superficial gas velocities (from 0.01 m/s to 1 m/s) which covers both laminar and turbulent flow regimes of the studied packed pebble-bed. As explained in Section 3, Figures 3.14 and 3.15 show the prediction

using CSTR model for plenum/distributor zone and ADM for the bed alone, respectively, at superficial gas velocities of 0.08 m/s and 0.6 m/s. These figures are also recalled in this section for clarity and the signals (normalized signal C curves) of these figures are converted to RTD functions (E curves) based on Equation 73, as shown in Figure 5.3 and Figure 5.4, respectively. As a first step, the corresponding analyses of central moments at superficial gas velocities of 0.08 m/s and 0.6 m/s are tabulated in Table 5.5. This Table also shows the comparison between the extracted moment quantities based on CMA and the corresponding moments predicted using CSTR model for the plenum /distributor and ADM for the pebble bed alone. In the second step, the estimated moments of the plenum and distributor section ($E_{(ii)}^{*}$) using raw data and Equations 74a and 74b are compared with the moments of convoluted plenum CSTR predictions (E_{in}^{*}) (based on CSTR model, Equation 49), as discussed in Section 3. At superficial gas velocities of 0.08 m/s and 0.6 m/s, the averaged absolute relative error (AARE) is found to be relatively small (Table 5.5) which confirms good match between the estimated moments obtained using the raw data $E_{(ii)}$* and the predicted ones (E_{in}^{*}) obtained using CSTR model. The small value of AARE between $E_{(ii)}$ and $E_{(in)}^{*}$ further confirms that the plenum and distributor zone can be modeled as a CSTR over the studied range of superficial gas velocities. In the third step, the estimated moments of the bed alone ($E_{(iv)}^{*}$) using raw data and Equations 75a and 75b are compared with the moments of convoluted ADM predictions of the bed alone (E_{out}^{*}). AARE in this case is also found to be relatively small (Table 5.5) which confirms good match between the estimated moments obtained from the raw data response $E_{(iv)}$* and those predicted by ADM response (E_{out}^{*}). This also further confirms that the pebble bed can be represented mathematically by ADM at the studied conditions.

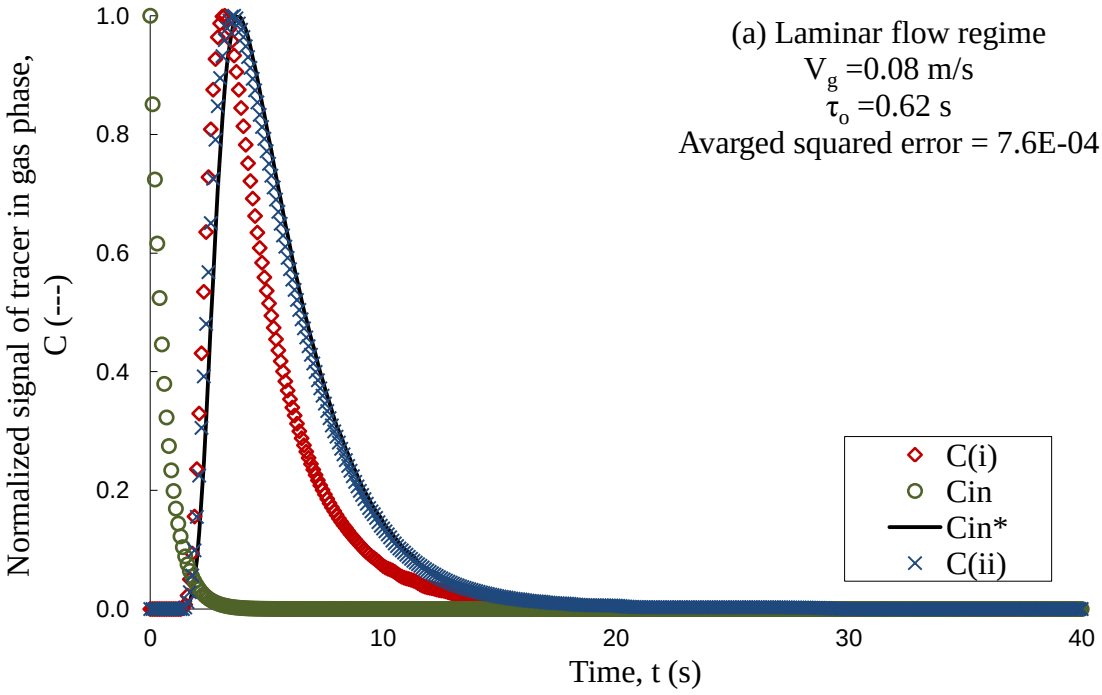

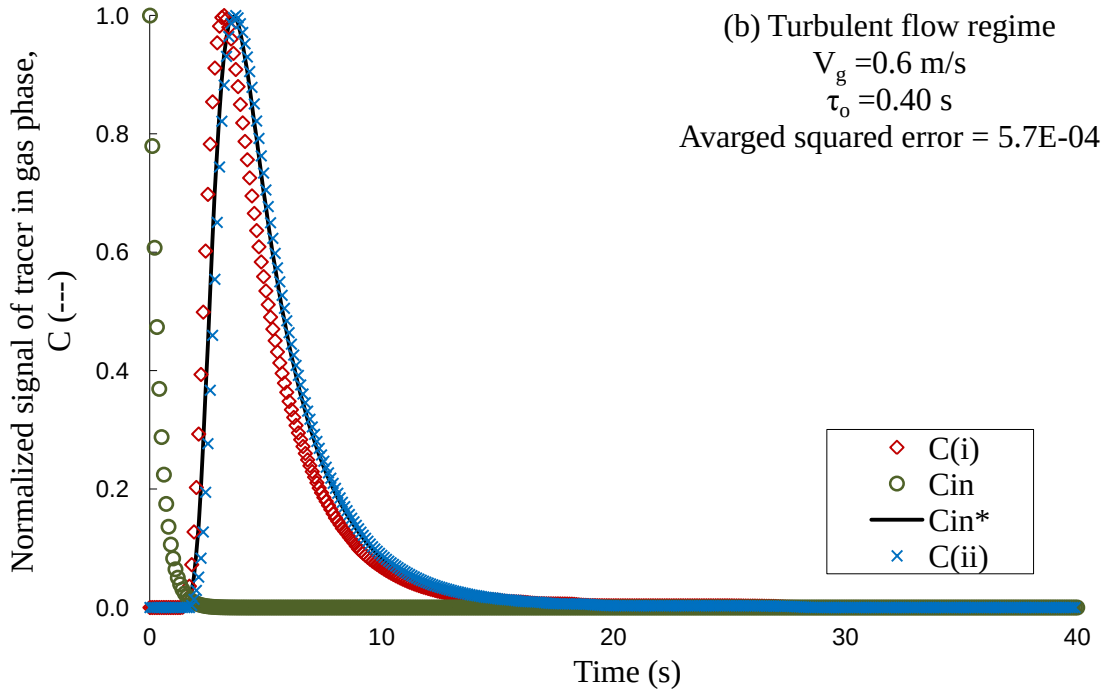

Recalled Figure 3.14 (Page 94). Responses of the Normalized Gas Tracer Signal at the Plenum/ Distributor Zone with CSTR Model Fit: a) Laminar Flow Regime; and b) Turbulent Flow Regime

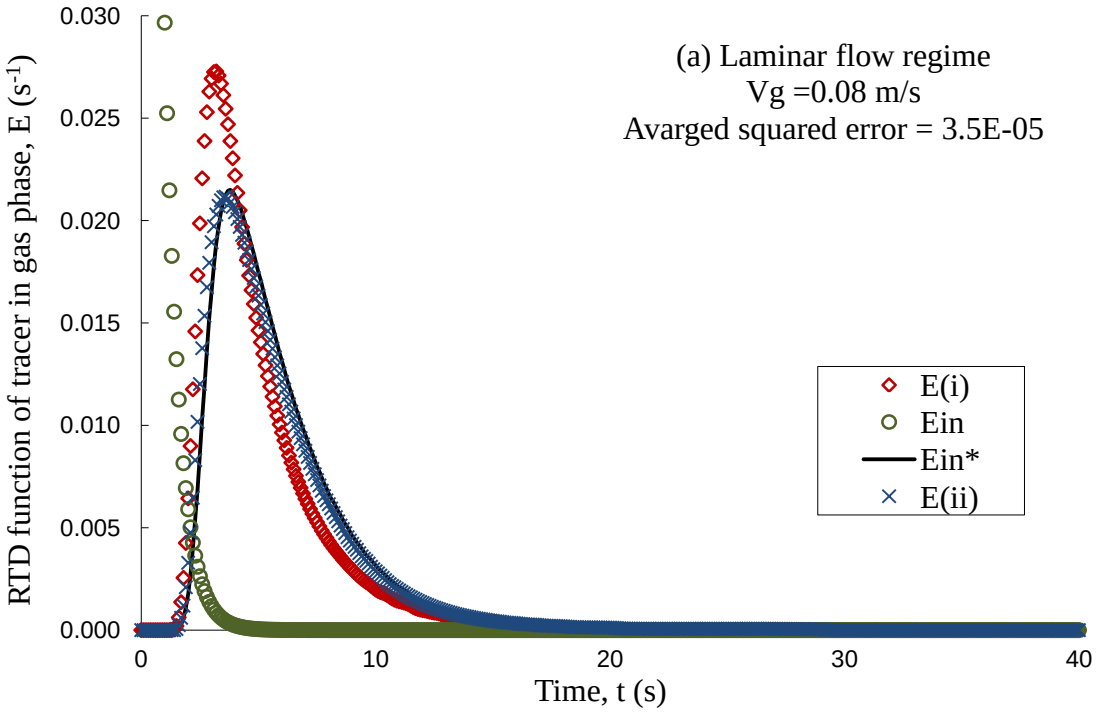

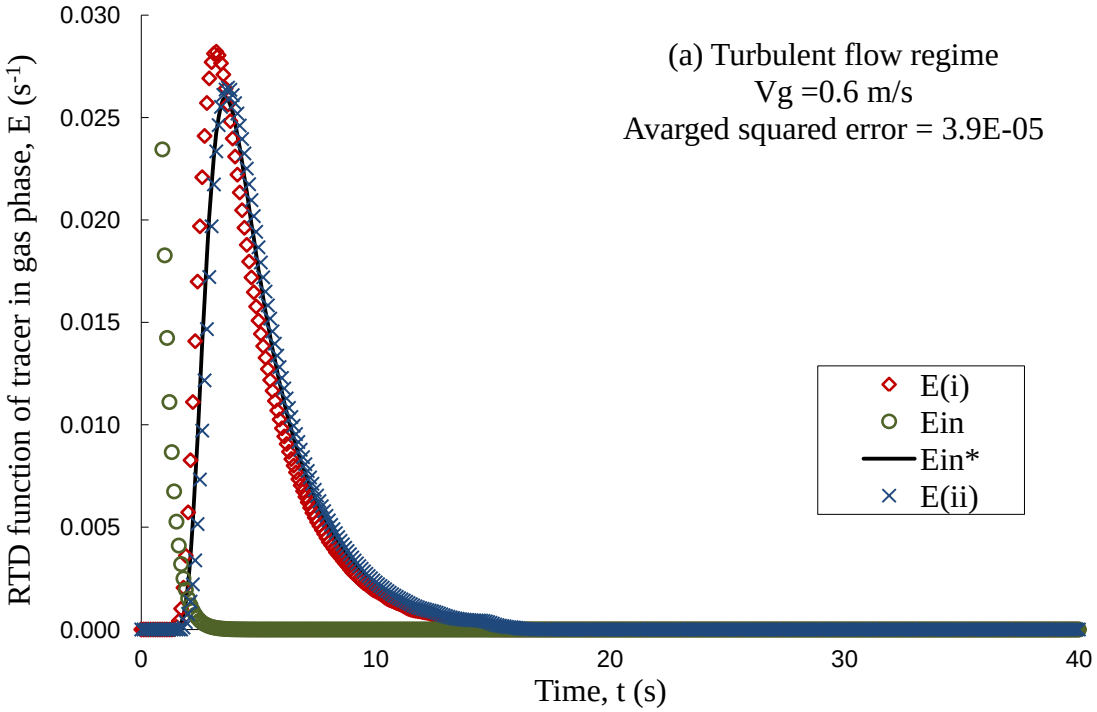

Figure 5.3. RTD Functions of the Gas Tracer Obtained at the Plenum/ Distributor Zone with CSTR Model Fit: a) Laminar Flow Regime; and b) Turbulent Flow Regime

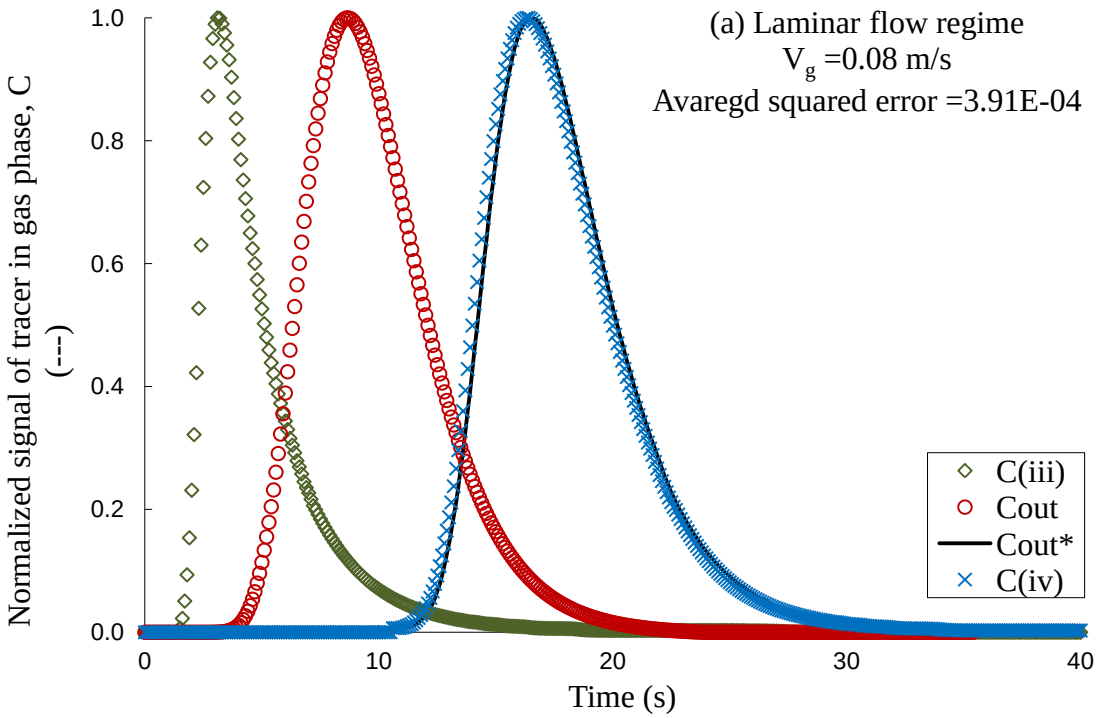

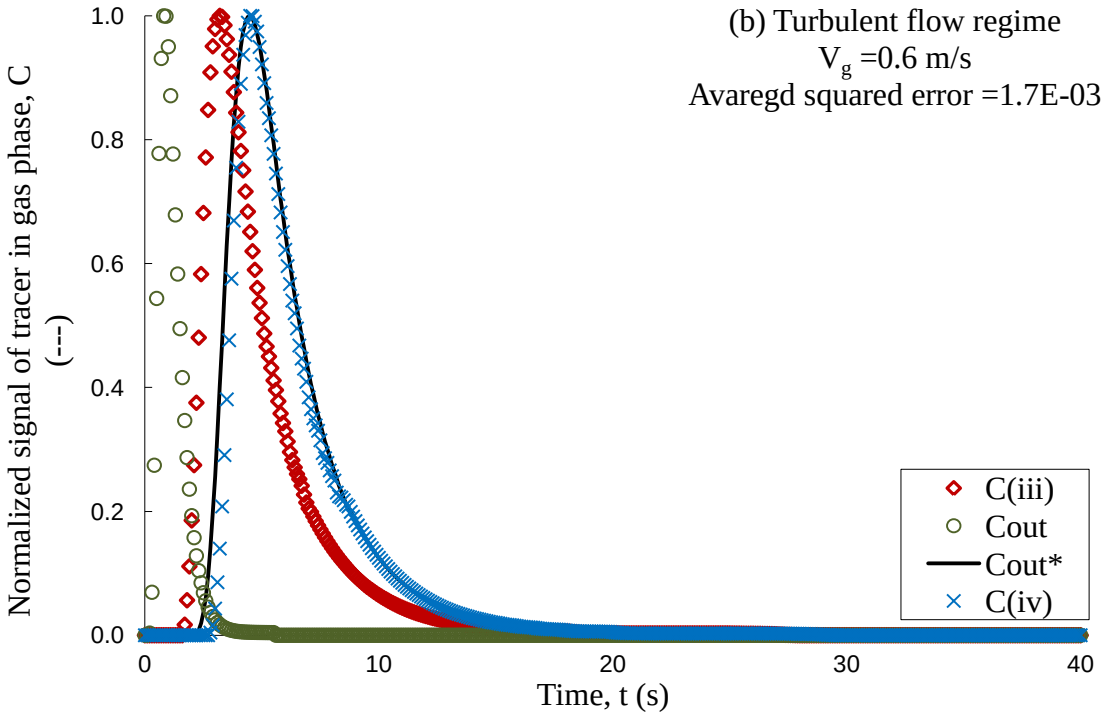

Recalled Figure 3.15 (Page 96). Responses of the Normalized Gas Tracer Signal at the Reactor Outlet with ADM Fit: a) Laminar Flow Regime; and b) Turbulent Flow Regime

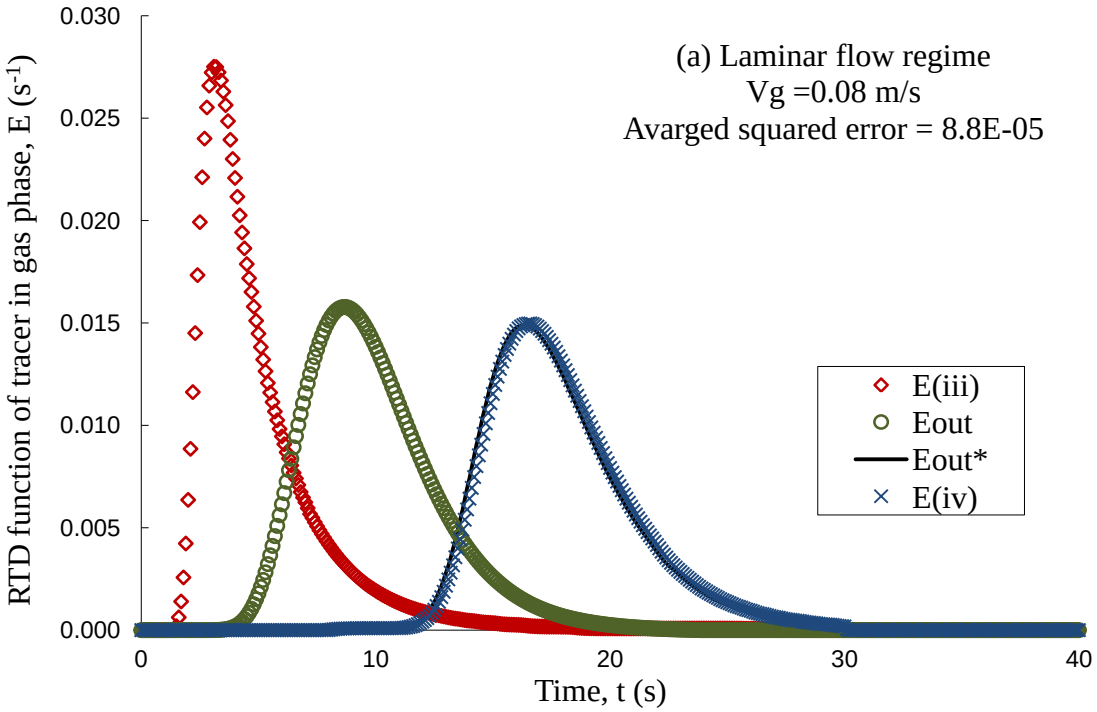

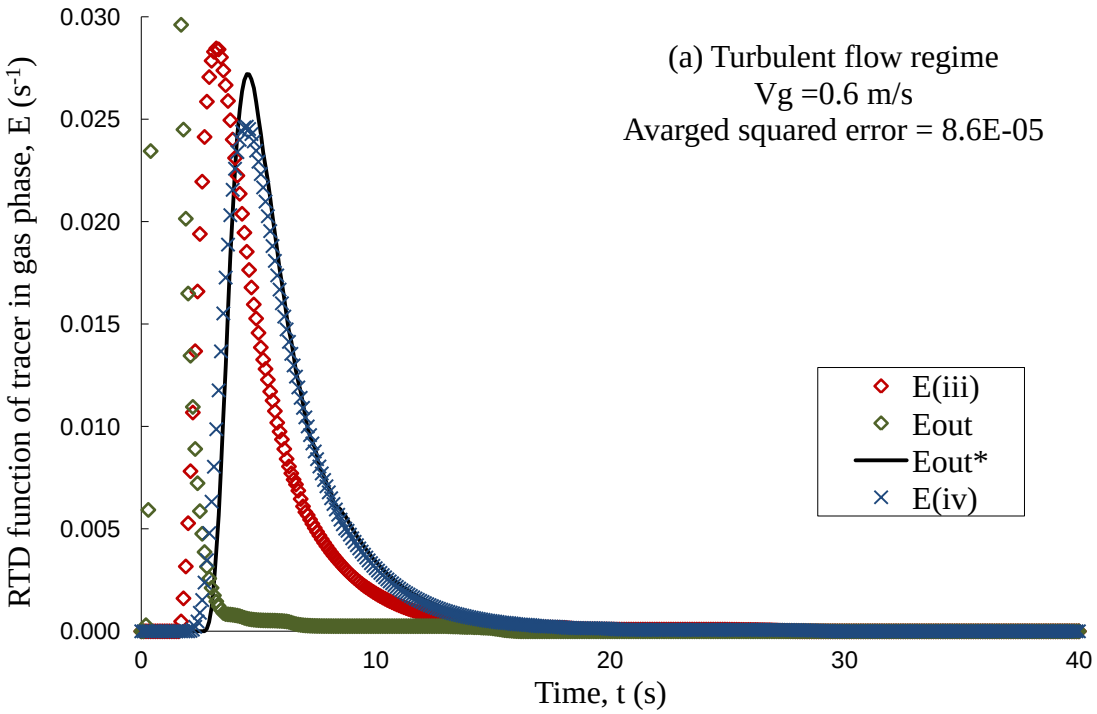

Figure 5.4. RTD Functions of the Gas Tracer Obtained at the Reactor Outlet with ADM Fit: a) Laminar Flow Regime; and b) Turbulent Flow Regime

Table 5.5. Moments Quantities of the RTD Functions Obtained by Two Methods (ADM and CMA)

Velocity / Zone	Vg=0.08 m/s			Vg=0.60 m/s		
Plenum zone	**E_{in}^* using CSTR**	**$E_{(ii)}^*$ using CMA**	**AARE**	**E_{in}^* using CSTR**	**$E_{(ii)}^*$ using CMA**	**AARE**
t_m (s)	5.71	5.68	3.43E-02	5.33	5.21	2.30E-02
σ^2 (s^2)	29.6	29.0	7.37E-03	27.1	26.6	1.84E-02
σ_D^2(--)	0.91	0.92	7.8E-02	0.954	0.960	6.25E-02
S^3 (--)	2.34	2.34	3.0E-03	2.768	2.726	1.56E-02
Bed zone alone	**E_{out}^* using ADM**	**$E_{(iv)}^*$ using CMA**	**AARE**	**E_{out}^* using ADM**	**$E_{(iv)}^*$ using CMA**	**AARE**
t_m (s)	17.4	17.1	1.72E-02	6.22	6.20	3.23E-03
σ^2 (s^2)	51.1	50.3	1.57E-02	4.23	4.25	7.68E-03
σ_D^2(--)	0.168	0.172	2.32E-02	0.11	0.11	1.21E-03
S^3 (--)	1.730	1.734	2.00E-04	2.67	2.67	1.12E-03

Parts a, b and c of Figure 5.5 show the variation with superficial gas velocity of the first moment (mean residence time), second moment (variance) and dimensionless variance, respectively, obtained using the ADM and CMA method. It can be seen from Figure 5.5 that with increase in gas velocity, both mean residence time (t_m) and variance (the measure of the dispersion) are decreasing much faster at low superficial gas velocities as compared to the decrease at high superficial gas velocities. A decrease in variance can be attributed to decrease in dispersion around the mean residence time (t_m) value and vice versa. At high superficial gas velocities, low values of variance (narrow

spread) indicates that the gas flow pattern in the studied bed is not much deviated from ideal plug flow behavior and hence ADM can be suitable for this small deviation. Also, the smaller values of variance imply that there is less dispersion (higher value of coefficient of gas dispersion, D_{ax}) of gas phase in the bed. This also suggests that there is better extent of gas dispersion in the bed at high superficial gas velocities (turbulent flow conditions).

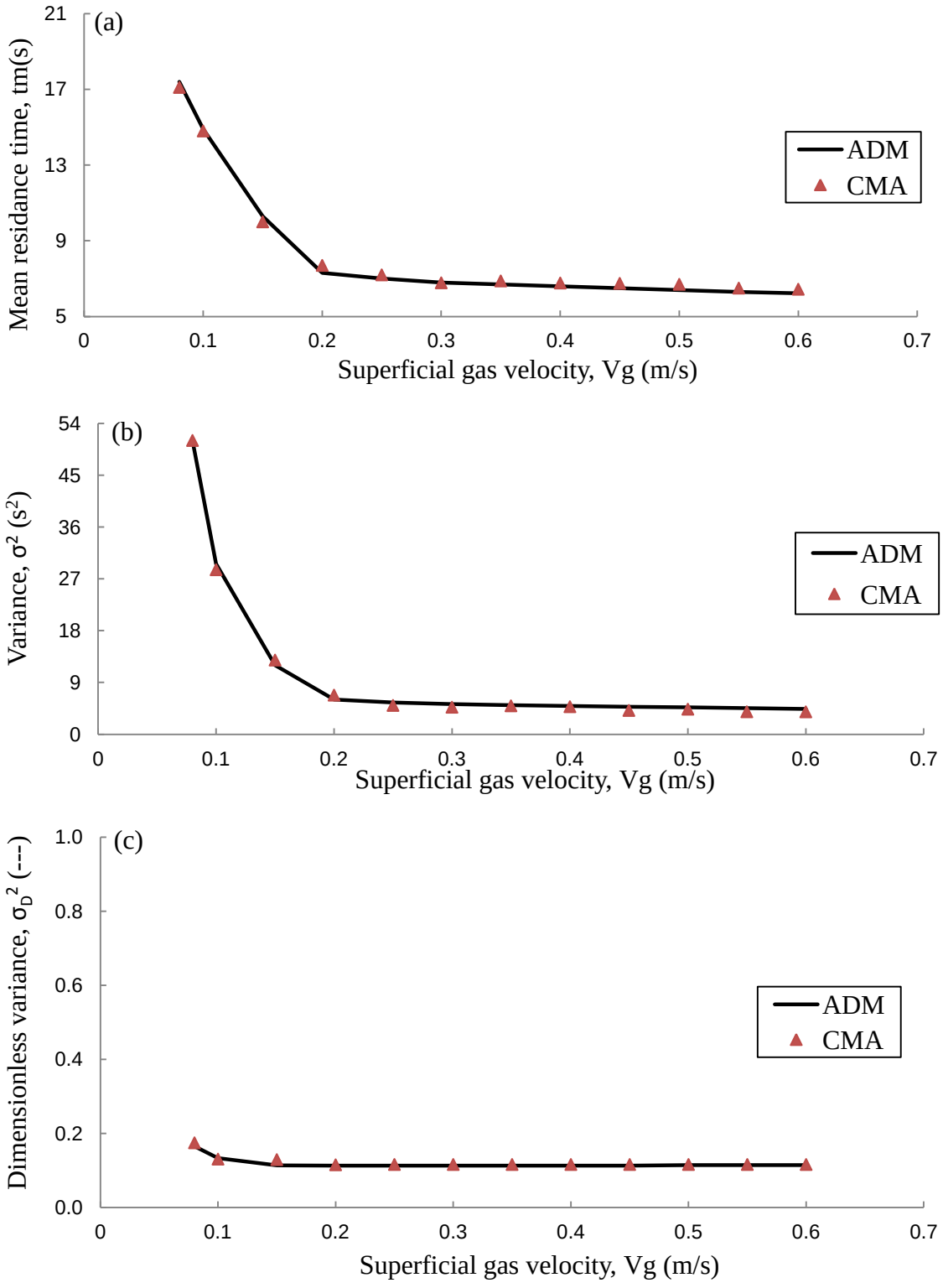

Figure 5.5. Variation of the Predicted and Estimated Moments with Superficial Gas Velocity: (a) Mean Residence Time (t_m), (b) Variance (σ^2), and (c) Dimensionless Variance (σ_D^2)

5.4. CONCLUDING REMARKS

1. The central moment analyses (CMA) have been applied as an alternative to the axial dispersion model (ADM) to characterize the responses of experimental RTDs in terms of the mean residence time (1^{st} moment), degree of spreading (2^{nd} moment) and asymmetry (3^{rd} moment) without proposing a model.
2. Since the central moments are additive in nature, the central moments of the plenum/ distributor zone have been extracted from the plenum/distributor RTD functions which were measured experimentally and compared to those predicated by CSTR.
3. In addition, the central moments of the bed alone have been extracted from the whole system RTD function which was measured experimentally and the results are compared to those predicated by ADM.
4. The results indicate that the gas flow pattern in the studied bed is not much deviated from idealized plug-flow model behavior and hence ADM can be suitable for this small deviation.
5. The results of central moment analyses (CMA) further confirm that the axial dispersion model (ADM) can be used successfully to describe the non-ideal flow behavior in the studied packed pebble bed.

6. PRESSURE DROP IN A PACKED PEBBLE-BED

6.1. MOTIVATION

As mentioned earlier that exact representations of the fluid flow distribution in porous media is a challenging task (Ziolkowska and Ziolkowski, 1993). For flow through packed bed reactors, it is desirable to be able to predict the flow rate obtainable for a given energy input (usually measured as pressure drop) or to be able to predict the pressure drop necessary to achieve a specific flow rate. The flow complexities in fixed beds have so far prevented the detailed understanding of the flow structure in the interstices between the particles (Reddy and Joshi, 2008; 2010). Practically, the complexity of the flow pattern rules out a rigorous analytic solution to the problem; hence, an empirical or semi-empirical correlations have been suggested for the prediction of the pressure drop. Therefore, an experimental data might be very useful to validate these correlations or can be used to benchmark the computational fluid dynamics (CFD) for the prediction of pressure drop through the packed pebble-bed reactors.

Traditionally, packed bed reactors are designed by a trial and error process (Bai et al., 2009). In packed pebble bed reactors, the pressure drop across the bed is a critical parameter for the design of these reactors. Because it is related to the flow distribution, pumping power and operational cost of the reactor, pressure drop in a pebble bed reactor is one of the most important design parameters (Hassan and Kang, 2012). Furthermore, the prediction of the fluid flow within the packing determines the heat transfer characteristics, and hence the performance of these reactors.

Thus, in the present work, the pressure drop in packed pebble bed having different aspect ratios (ratio of the bed diameter to pebbles diameter) has been measured using a

differential pressure transducer. The effects of superficial gas velocity and aspect ratio have been investigated for the studied packed pebble bed. The obtained experimental results have been used to evaluate the predictions of the correlations recommended for pressure drop estimation in packed pebble-bed nuclear reactors.

6.2. EXPERIMENTAL WORK

6.2.1. Experimental Setup. The experimental set up for the pressure drop measurements in packed pebble-bed is similar to the one used for the gas dynamics study as discussed in Section 3.

Figure 6.1 shows the schematic diagram of the experimental setup along with pressure traducer and its components. Compressed air was used as the gas phase flowing downward, while glass bead particles of different diameters were used as the pebbles in a fixed bed. Three different sizes of pebbles: 1.25 cm, 2.5 cm, and 5 cm diameter of the same density have been used to form a randomly packed bed. As mentioned in Section 3, the pebble sizes reflect the aspect ratios (bed-diameter to pebble-diameter, D/dp) of 24, 12 and 6 based on the pebble bed of 30 cm diameter, respectively. The typical value of void fraction (average porosity of the bed) for random packing in each case is measured in our laboratory by direct balance method outlined in Section 3 and found to be around 0.375, 0.384, and 0.397, respectively.

The flow rate of the filtered dry air was adjusted by a pressure regulator and rotameters system, which consists of two rotameters (Omega HFL6715A-0045-14) connected in parallel. The superficial gas velocity (Vg) was varied within the range of 0.02 m/s to 2 m/s which covers both laminar and turbulent flow regimes. A plenum was

placed at the top of the bed to evenly distribute gas phase. Cone type plenum with 0.3m opening and 0.1 m height has been used. The gas distributor used was a perforated plate having 140 holes of 3 mm diameter. These holes were arranged in a square grid of 2.25 cm pitch. The opening area is 2.7% of total cross sectional area. The bottom of the pebble bed consists of a plastic cone shape with an angle of 60^{o} horizontally and 5 cm exit opening.

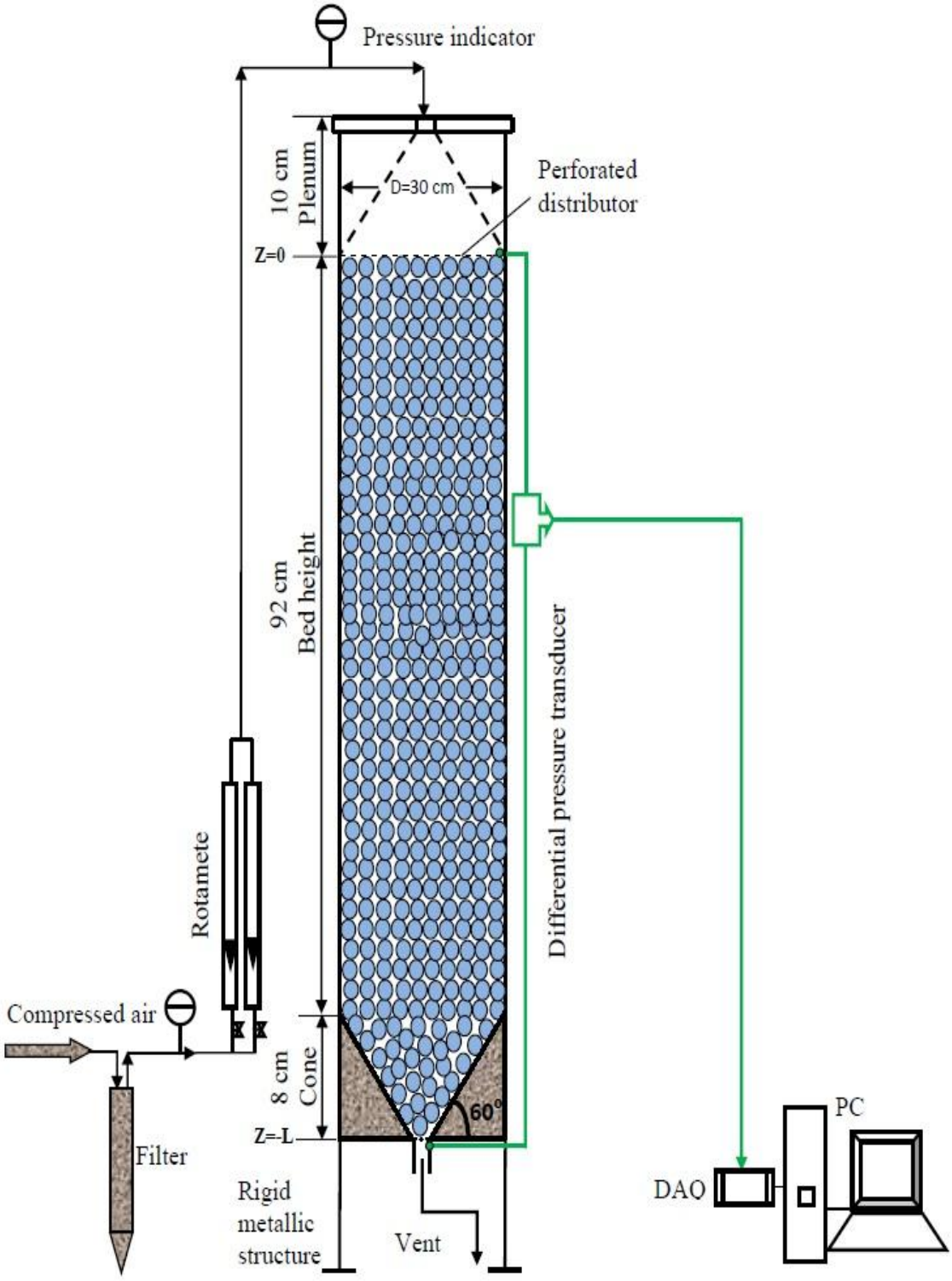

Figure 6.1. Schematic Diagram of the Pressure Drop Cold-Flow Experimental Set-Up

6.2.2. Differential Pressure Transducer. A differential pressure transducer (Omega PX409-005DDU5V) was used to measure the pressure fluctuations along the bed height and it covered the pressure rage from 0-3.35 kPa for measured signal of 0.003-5 V. The pressure transducer was connected to a DC power supply which provides a voltage proportional to the measured differential pressure across the bed. The signal is received by the data acquisition (DAQ) system from OMEGA of model number OMB-DAQ-54. The response time of the pressure transducers was 2 ms and data were recorded for 1000 s at a rate of 60 Hz. The recorded single (in voltage) is averaged and related to the pressure drop based on the following relation:

$$\Delta P\ (\text{kPa}) = 0.68922 \times \text{Voltage} - 0.0917 \tag{76}$$

6.3. RESULTS AND DISCUSSION

6.3.1. Effect of Gas Flow on Pressure Drop. As mentioned earlier, the pressure drop over the core of the pebble bed reactor due to friction is an important parameter that ultimately affects the heat transport effectiveness and hence the performance of the reactor. It is well known that the pressure drop is created by the resistance to flow in the packed-pebble bed and can be varied by varying the coolant flow rate. Therefore, in this work the pressure drop along the packed-pebble bed is measured using differential pressure transducer and plotted against gas velocity (Vg) for three different aspect ratios (D/dp), as shown in Figure 6.2.

The results of Figure 6.2 show the strong dependence of the pressure drop of aspect ratio, and hence the porosity (void fraction) of the bed, and the velocity of the coolant gas. As the size of particles increases, less pressure drop recorded for the same

superficial gas velocity. This is due to a lower interstitial gas velocity existed in the bed at the same flow rate over larger pebbles diameter where the local void fractions are larger compared to those of smaller pebbles diameter. However, for all aspect ratios, the pressure drop increases with superficial gas velocity. The decreasing of either aspect ratio or coolant flow rate would cause a non-uniform flow distribution which would give rise to the by-pass effect across the packed bed. In other words, with decreasing the gas flow rate, the wall effects become more and more important (Hassan and Kang, 2012) while the porosity effect is dominant in the high flow rate (Eisfeld and Schnitzlein, 2001). Contrary to the large aspect ratio (D/d_p=24), the effect of near-wall by-pass flow are small and might be negligibly at higher gas velocities (V_g > 0.3 m/s) which is satisfied the conditions of the turbulent-flow regime (Re_h > 1000) in pebble bed. These observed behaviors are very useful for a successful design and for an efficient operation of the nuclear pebble-bed reactors, where the ratio of core diameter (D) to the pebble diameter (d_p) is very large (Fenech, 1981). For instance, the aspect ratio (D/d_P) of about 33 for the MIT prototype modular pebble-bed reactor (MPBR) (Bazant, 2006).

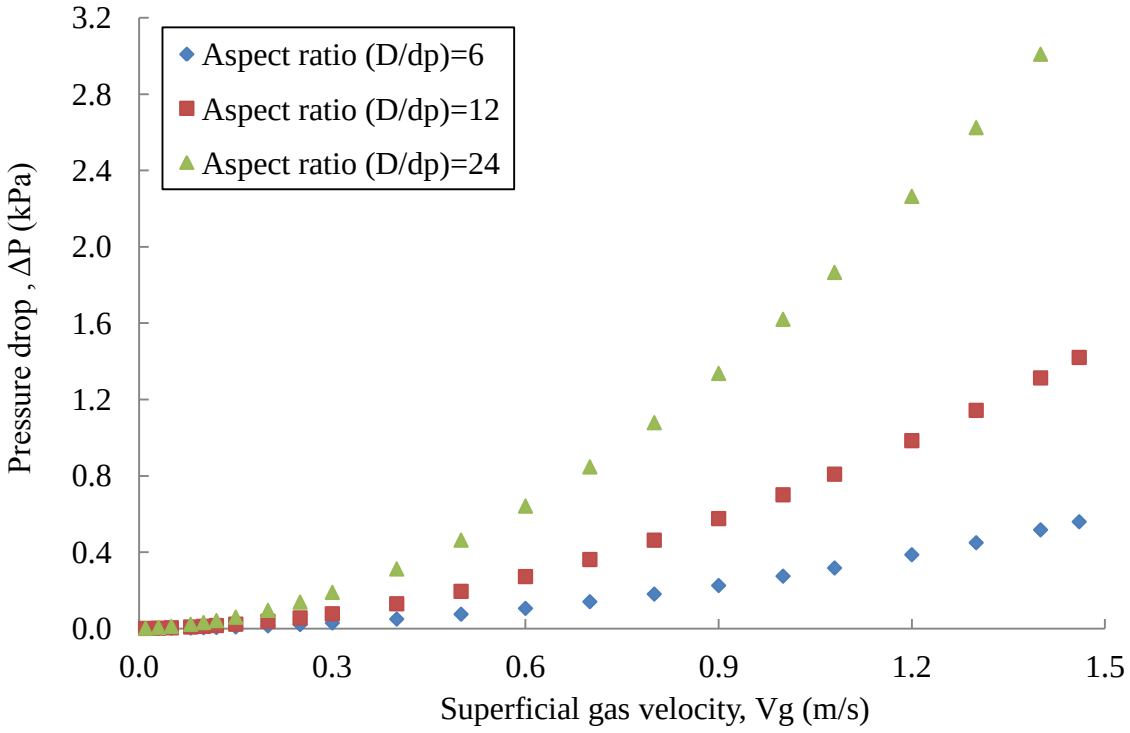

Figure 6.2. Pressure Drop at Various Gas Velocities of Packed Pebble-Bed for Different Aspect Ratios

6.3.2. Comparison of the Measured Pressure Drop Results with the Predictions of the Empirical Correlations.

Generally, in packed pebble-bed reactors, the resistances of flow are usually described in terms of total pressure drop (ΔP) or the pressure drop coefficient, $\left(\psi = \left(\Delta P / \left(\rho/2\right) V^2\right)\left(d_h / L\right)\right)$. The pressure loss due to friction between solid (pebbles) and flowing gas in the core of the pebble bed can be expressed as follows (Fenech, 1981):

$$\Delta P = \psi \frac{L}{d_h} \frac{\rho}{2} V^2 = \psi \frac{L}{d_p} \frac{\rho}{2} V_g^2 \left(\frac{1-\varepsilon_b}{\varepsilon_b^3} \right) \tag{10}$$

where d_h is the equivalent hydraulic (effective) diameter, which is the characteristic length of the packed pebble-bed and defined as follows:

$$d_h = d_p \frac{\varepsilon_b}{(1-\varepsilon_b)} \tag{10a}$$

while V is the interstitial velocity, which is the characteristic or the mean velocity in the gaps between the pebbles and defined as follows:

$$V = \frac{V_g}{\varepsilon_b} \tag{10b}$$

V_g is the superficial gas velocity based on the cross section of the empty column.

In this work the predictions of Ergun (1952), KTA Standards (1981), Eisfeld and Schnitzlein (2001), and VDI (2010) which are four different correlations are evaluated against the experimental results. As discussed in Section 2, these corrections are the most promised and recommended ones for the prediction of the high temperature packed pebble-bed nuclear reactors. For clarity these correlations that are outlined in Section 2 are recalled here along with their equations numbers as follows:

The well-known Ergun equation expresses the friction factor in a packed bed as follows (Ergun, 1952):

$$\psi = \frac{150}{Re_h} + 1.75 \qquad \text{for} \qquad Re_h \le 5\times10^4 \tag{11}$$

where Re_h is an effective or modified Reynolds number that is based on the average interstitial velocity (V) and on the characteristic length scale of the pores (an equivalent hydraulic diameter, d_h) described below:

$$Re_h = \frac{\rho V d_h}{\mu} = \frac{1}{(1-\varepsilon_b)} Re \tag{11a}$$

where Re is the Reynolds number and is defined on the basis of the total mass flow rate through the total cross-sectional area of the packing and on the diameter of the pebbles as follows:

$$Re = \frac{\rho V_g d_p}{\mu} \tag{11b}$$

As mentioned before, the above equation is formed based on the Carmen-Kozeny (Carman, 1937; Kozeny, 1927) equation for purely laminar-flow regime (viscous effect, $\mathrm{Re_h} < 1$), and the Burke-Plummer (Burke and Plummer 1928) equation derived for the fully-turbulent flow regime (inertia effect, $\mathrm{Re_h} \geq 300$). The first term in the expression (Equation 11) refer to viscous energy losses, of importance at low flow rates (i.e. streamline flow), and the second term refer to kinetic energy losses, of importance at high flow rates (i.e. turbulent flow).

Another improved correlation of Ergun-type equation was given by Eisfeld and Schnitzlein (2001) who used Reichelt's approach (Reichelt, 1972) of correcting the Ergun equation to account for the effect of the wall as follows:

$$\psi = \frac{308 A_w^2}{\mathrm{Re_h}} + \frac{2 A_w}{B_w} \qquad \text{for} \qquad \mathrm{Re_h} \leq 2\times 10^4 \tag{12a}$$

The contribution of confining walls to the hydraulic radius was accounted for analytically by the coefficient A_w. Additionally, the coefficient B_w is introduced to describe empirically the porosity effect of the walls at the high Reynolds number. The wall correction terms are given by:

$$A_w = \left[1 + \frac{2}{3} \frac{\left(d_p / D \right)}{(1-\varepsilon_b)} \right] \tag{12a}$$

$$B_w = \left[1.15 \left(\frac{d_p}{D} \right)^2 + 0.87 \right]^2 \tag{12b}$$

The German Nuclear Safety Standard Commission (Kerntechnischer Ausschuss - KTA) has been reviewed about thirty papers relevant to the results of the randomly packed bed with spherical particles (Fenech, 1981). The KTA adopted the following empirical correlation for the pressure drop predictions in the high temperature packed pebble-bed nuclear reactors (KTA Standards, 1981):

$$\psi = \frac{320}{\mathrm{Re_h}} + \frac{6}{\mathrm{Re_h^{0.1}}} \qquad \text{for} \qquad \mathrm{Re_h} \le 5\times10^4 \tag{13}$$

The first term of the above equation (Equation 13), represents the asymptotic solution for laminar flow while the second term represents the same for the turbulent flow.

In addition, the Association of German Engineers (Verein Deutscher Ingenieure-VDI) Heat Atlas provides the following correlation for the coefficient of loss of pressure through friction in fixed beds (Wirth, 2010):

$$\psi = \left(\frac{0.4}{\varepsilon_b}\right)^{0.78} \frac{317}{\mathrm{Re_h}} + \frac{6.17}{\mathrm{Re_h^{0.1}}} \tag{14}$$

The measured pressure drop along the packed-pebble bed and hence pressure drop coefficients (ψ) are plotted against the effective Reynolds number (Re_h), as shown in Figure 6.3. In general for $Re_h > 10^3$, the friction factor decreases slightly with the Reynolds number of coolant gas and its values range between 3 and 2. This is due to that the increase in coolant flow rate reduces the fluid friction between the pebble surface and the gas (coolant) and reduces the wall effects. In other words, at laminar flow regime, the friction is highly affected while at high Reynolds number (turbulent flow regime); the friction effect is less dominates (Eisfeld and Schnitzlein, 2001).

Figure 6.3 also illustrates the predictions obtained by the above mentioned four different correlations and their comparisons with the obtained experimental results for the case of a uniform size spherical packed pebble-bed of $D/d_p = 6$ and void fraction of about 0.397. From Figure 6.3, it has been observed that the measured pressure drop values are in agreement with the KTA and VDI correlations of average errors of about 1.79% and 2.81%, respectively. Hassan and Kang (2012) verified that the KTA correlation could be

used for a gas-cooled pebble bed reactor. The comparison between their experiment of results and the KTA correlations showed that the pressure drop of large bed-to-particle-diameter ratios (D/dp = 19, 9.5, and 6.33) matched very well with the original KTA correlation. However, the authors claimed that the published KTA correlations cannot be expected to predict accurate pressure drop for certain conditions, especially for pebble beds of very low aspect ratio (D/dp < 5).

From Figure 6.3, it has been observed that the dimensionless pressure drop (ψ) is proportional to the reciprocal of effective Reynolds number (Re_h) in the laminar-flow regime and becomes independent of Re_h at higher values for both Ergun- type equations, i.e. Ergun (1952) and Eisfeld and Schnitzlein (2001). Contrary to the prediction of other correlations, i.e. KTA (1981) and VDI (2010), the dependence of pressure drop coefficient on Reynolds number changes gradually with the increasing Reynolds number, indicating a smooth transition from laminar to turbulent flow regimes.

The empirical correlation of Eisfeld and Schnitzlein over predicts the pressure drops within the range of $300 > Re_h > 1500$. The deviations from the measured pressure drops vary dramatically, from acceptable (average error 9.4 % for low effective Reynolds number, $Re_h < 300$) to well prediction (average error 3.3% for intermediate Reynolds number, $300 < Re_h < 1500$) to considerable (average error 19 % for high Reynolds number, $Re_h > 1500$). Although Eisfeld and Schnitzlein (2001) made an improved correlation that accounts for the wall effects where they manipulated the coefficients of the wall correction factor for the inertial pressure loss term, their correlation cannot predict properly the pressure drop coefficients and the trend for certain conditions. This is due to that Eisfeld and Schnitzlein wall correction factor for the inertial pressure loss

term does not come from physical reasoning and it is based on curve-fitting model (Kang 2010).

Although Ergun's correlation was proven to be valid for most of the gas-solid applications in chemical industry, such as chemical/catalytic packed bed reactors, the pressure drop across the core of pebble bed reactor is over-predicts (under predict in terms of dimensionless pressure drop coefficient, ψ) by this correlation, as shown in Figure 6.3. The deviations from the measured pressure drops vary considerably from average error of about 48.51 % for low effective Reynolds number ($Re_h < 1000$) to average error of about 35.69 % for high Reynolds number ($Re_h > 1000$).

However, early pressure drop studies through pebble bed reactors (Stroh et al., 1979; Gerwin et al., 1989; Seker and Downar, 2007) and more recently (Hassan and Kang, 2012) have reported that the Ergun equation considerably over-predicts of the pressure drop in the high Reynolds number range of practical interest. This due to that the mass flow rates, static pressure, and particle diameter and hence the Reynolds numbers in chemical industrial applications are relatively small compared to those used in packed pebble-bed nuclear reactors. In addition to that, Ergun's correlation was based on the model assuming the packing is statistically uniform, so that there is no channeling or bypassing effects (in actual situation, channeling would occur). Therefore, the Ergun's correlation does not predict very well for the randomly packed pebble-bed nuclear reactors. Hence, the obtained experimental results demonstrate the applicability of the VDI and KTA correlations for randomly packed pebble-bed reactors.

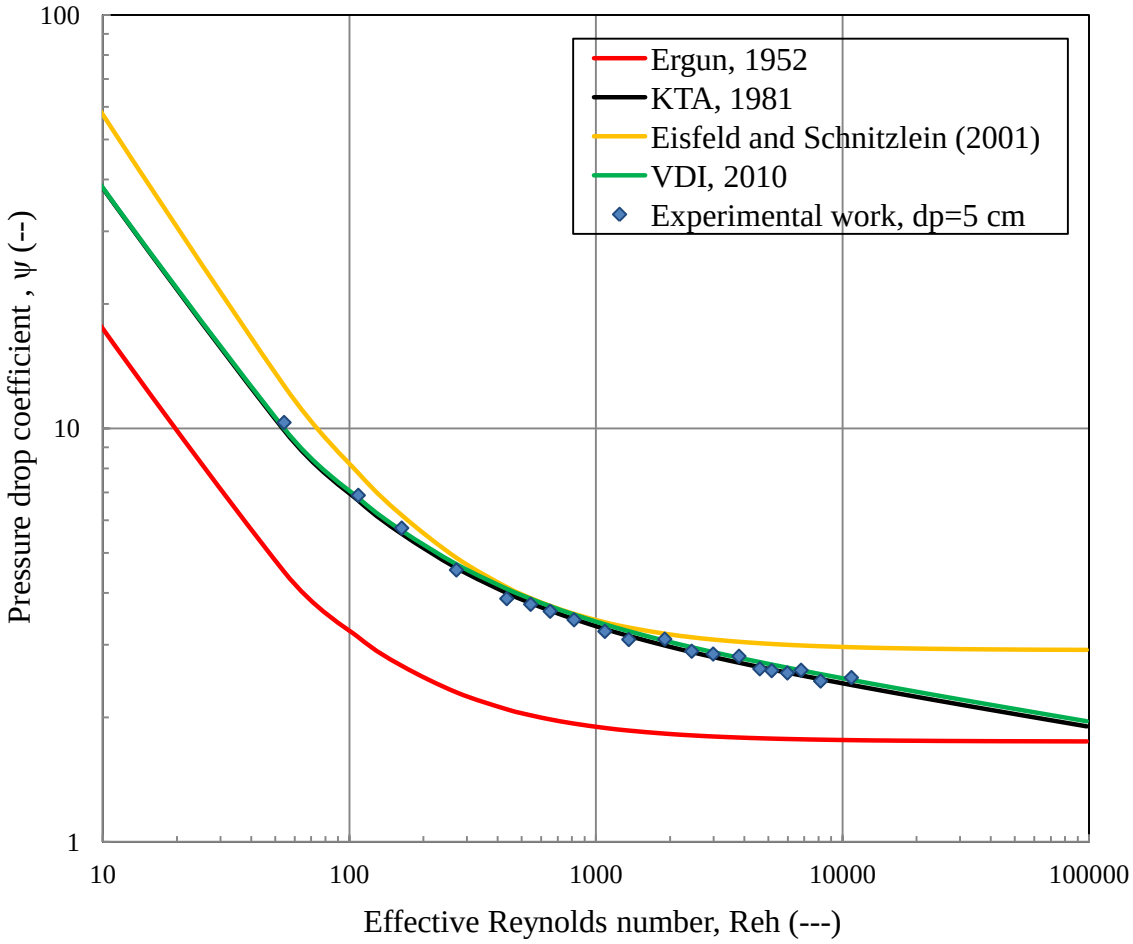

Figure 6.3. Coefficient of Loss of Pressure through Friction (ψ) as a Function of the Effective Reynolds Number (Re/ (1 - ε))

6.4. CONCLUDING REMARKS

The following concluding remarks may be drawn from the present investigation of the pressure drop:

1. The pressure drop along the randomly packed-pebble bed was measured experimentally using differential pressure transducer.

2. The results show the strong dependence of the pressure drop on both the aspect ratio, and hence the porosity of the bed and the coolant gas velocity.
3. The obtained experimental results of pressure drop demonstrate the applicability of the VDI and KTA correlations for prediction of pressure drop in the randomly packed pebble-bed nuclear reactors.
4. In order to test the accuracy of the predictions of pressure drop by the empirical correlations in the literature, a comparison was made with the experimental results. The obtained experimental results of pressure drop confirm that the classical Ergun-type equations, commonly used to estimate pressure drop through chemical packed beds, considerably over-predicts pressured drop of the pebble beds at high Reynolds number.

7. HEAT TRANSFER CHARECTERSITICS IN A PACKED PEBBLE-BED

7.1. MOTIVATION

In the core of pebble bed nuclear reactor, the local fuel temperatures depend not only on the local power generation but on the point heat removal rate. Hence, the detailed information and proper understanding of the transport of heat generated during nuclear fission from slowly moving hot fuel pebbles to the flowing coolant gas are crucial for safe design and efficient operation of packed pebble-bed reactors. All three modes of heat transport (i.e., conduction, convection and radiation) are important for the modeling and predicting the pebble-bed core temperature distribution. During nominal operation of the reactor (relatively high Reynolds numbers), the heat transfer mechanism is governed by forced convection (Fenech, 1981). This heat convection can be quantified and characterized in terms of convective heat transfer coefficient or non-dimensional Nusselt number. At low Reynolds numbers (the case of accident), effects of free convection, thermal radiation, heat conduction, and heat dispersion come into the same order of magnitude as the contribution of the forced convection (Fenech, 1981). However, little information related to pebble bed heat transfer is available in the open literature and has not yet been fully understood (Stainsby et al, 2010b). Furthermore, the quantification of the heat transfer coefficient between the heated pebbles and the flowing coolant gas using models or correlations to predict the temperature distributions for design, scale-up and operation is still lacking.

In the open literature, the heat transfer data have been obtained by direct measurements (in which the component particles are separately heated) and indirect means (by involving transient heating of fluid or mass transfer experiments). On the other

hand, the measurement techniques applied for packed pebble-bed heat transfer are: the electrically heated single sphere buried in the unheated packing (Achenbach, 1982, 1995; Schroder et al., 2006; Rimkevicius et al., 2006; Rimkevicius and Uspuras, 2008; Rousseau and van Staden, 2008); analogy and simultaneous heat and mass transfer (Achenbach, 1982, 1995); regenerative heating technique which is based on the concept of unsteady heat transfer of a heated sphere in a packed pebble bed through which a cooling fluid flows (Hoogenboezem, 2007).

Semi-empirical methods (Gnielinski, 1978;1981) and recently computational and theoretical models (Becker and Laurien, 2002, 2003; Yesilyurt and Hassan, 2003; Lee et al., 2007; Stainsby et al., 2008; Kim et al., 2010; Stainsby et al., 2010a; du Toit and Rousseau, 2012) have been used to predict heat transfer rate and coefficients in pebble-bed reactors. Based on the predetermined criteria or model, it is worthwhile to mention that these experimental/computational determinations of heat transfer coefficients have been made under either steady-state and/or transient conditions.

Unfortunately, in these previous studies, it was found that the experimental results are quite different and show considerable departures from one another, particularly at low Reynolds number. Achenbach (1995) claimed that the reported results cannot be generalized to represent the convective heat transfer in a randomly packed bed. Schroder et al., (2006) pointed out that inhomogeneous interstitial flow velocities are responsible for the scattering of the heat transfer experimental data of other investigators. In fact, this is due to convective heat transfer influenced by many parameters such as local flow condition, bed characteristics, etc. In addition to that, there are inaccuracies in the heat flux and temperature measuring techniques. For instance, the method of single heated

sphere requires that the local heat flux and sphere surface temperature to be measured accurately beside the local gas flow temperature in the gap between the pebbles. While in all previous studies the heat flux is based on the directed energy input method and the boundary condition of constant surface temperature was assumed. This assumption is unreliable for boundary condition. Kaviany (1995) pointed out that the thermal conductivity of the solid is not large enough to lead to an isothermal surface temperature; the thermal conductivity of the solids also influences the temperature field around it. Other important issue is that the surface temperature is approximately obtained and this due to the uncontrolled heat losses via the points of contact with unheated neighboring spheres and the influence of heat transfer by the radiation. The surface temperature was taken to be the arithmetic average of the readings of three or four thermocouples, where their tips were flushed with the sphere surface (Rimkevicius et al., 2006; Hoogenboezem, 2007). In addition to that, the mass transfer analogy experiments are difficult and not an accurate as direct heat transfer measurements. Also, ideal plug flow model was generally assumed in the computational and theoretical approaches, although gas dispersion occurs even at high gas velocities and the actual velocity profile is non-uniform with a pronounced slip at the wall. All these crucial limitations in previous studies inevitably reduce the accuracy of the experimental results. Thus, the selected measurement technique has an important influence on the generated heat transfer data.

It is obvious that extensive investigations are required to further advance the knowledge of heat transport occurring in pebble beds which will provide information for safe and efficient design and operation of packed pebble-bed reactors. Accordingly, in this part, the local pebble-to-gas heat transfer coefficient in a 0.3 m diameter cold-flow

pebble bed unit has been investigated experimentally using two types of fast-response heat transfer probes. One is rod-type probe where its detailed results, development, implementation and discussions are reported in Appendix B. This technique is considered an invasive technique. Another probe is a novel non-invasive spherical type probe where its detailed results, development, implementation and discussions are reported in this section. The novel non-invasive spherical-type probe reduces the integration errors in pervious measurements of local heat transfer in packed pebble-bed due to the invasiveness of the rode type probe. The experimental investigations of this work include various radial locations along the height of the bed. The probe provides the instantaneous heat transfer coefficient measurements over a wide range of superficial gas velocities (0.02–2 m/s) that covers both laminar and turbulent flow conditions. Hence, the effects of the flow characteristics and the nature of the flow regime on the convective heat transfer are studied and analyzed.

7.2. EXPERIMENTAL WORK

7.2.1. Separate Effects Experimental Setup. The experimental set up for the heat transfer investigations in packed pebble-bed is similar to the one used for gas dynamics study discussed in Section 3.

A photo of the cold-flow experimental set-up along with heat transfer technique and its components is shown in Figure 7.1. While Figure 7.2 shows the schematic diagram of the experimental setup. Compressed air was used as the gas phase flowing downward, while glass bead particles of different diameters were used as the pebbles in a fixed bed. Three different sizes of pebbles: 1.25 cm, 2.5 cm, and 5 cm diameter of the

same density have been selected to form a randomly packed bed and used with the rod type heat transfer probe where the results are reported in Appendix B. However, for the novel non-invasive spherical type probe, only pebbles of 5 cm diameter have been used since the developed probe is of 5 cm in diameter that mimics the used pebbles. As mentioned in Section 3, the pebble sizes reflect the aspect ratios (bed-diameter to pebble-diameter, D/dp) of 24, 12 and 6 based on the pebble bed of 30 cm diameter, respectively. The typical value of void fraction (average porosity of the bed) for random packing in each case is measured in our laboratory by direct balance method outlined in Section 3 and found to be around 0.375, 0.384, and 0.397, respectively.

The flow rate of the filtered dry air was adjusted by a pressure regulator and rotameters system, which consists of two rotameters (Omega HFL6715A-0045-14) connected in parallel. The superficial gas velocity (Vg) was varied within the range of 0.02 m/s to 2 m/s which covers both laminar and turbulent flow regimes. A plenum was placed at the top of the bed to evenly distribute gas phase. Cone type plenum with 0.3m opening and 0.1 m height has been used. The gas distributor used was a perforated plate having 140 holes of 3 mm diameter. These holes were arranged in a square grid of 2.25 cm pitch. The opening area is 2.7% of total cross sectional area. The bottom of the pebble bed consists of a plastic cone shape with an angle of 60^{o} horizontally and 5 cm opening.

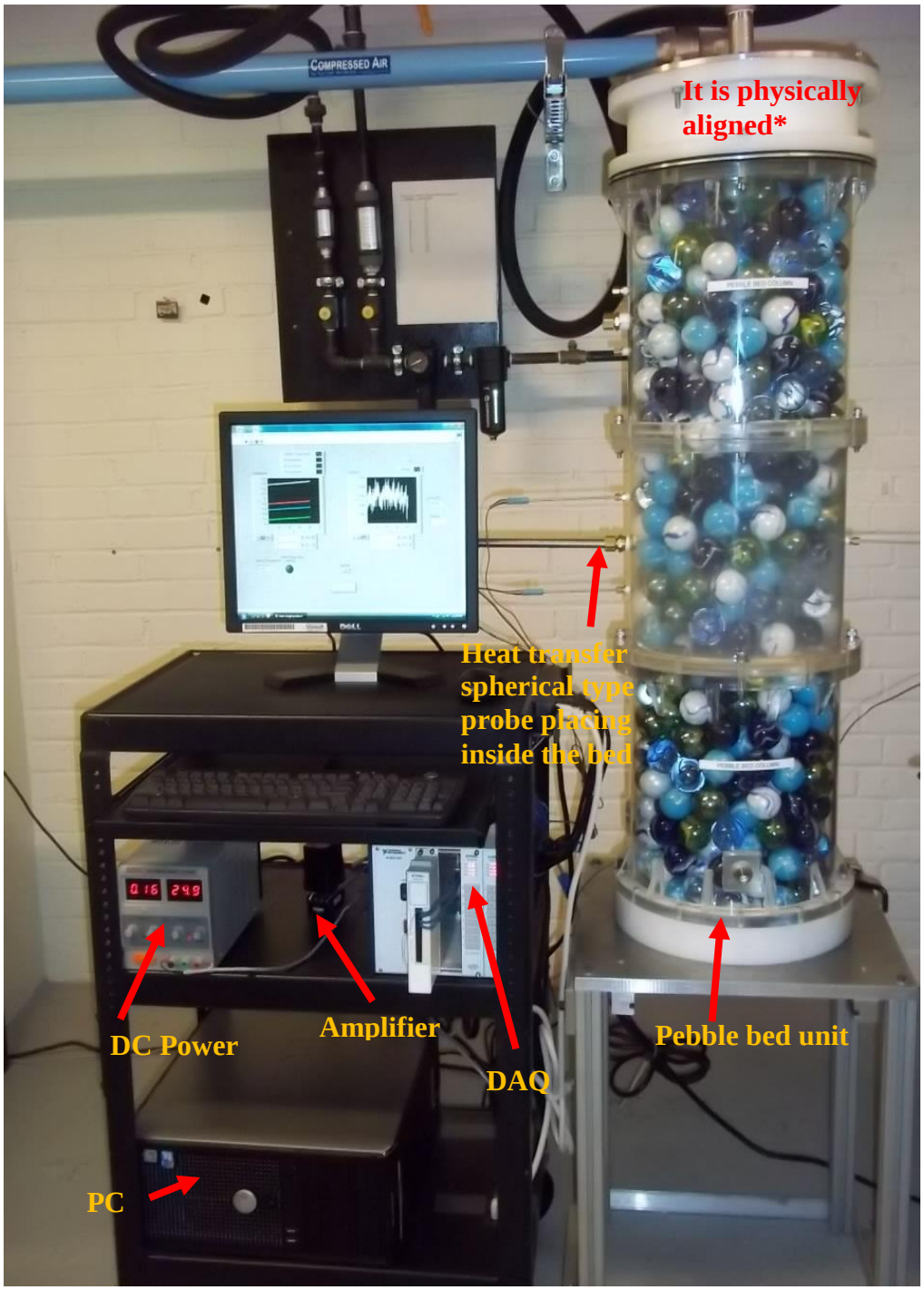

Figure 7.1. A Photo of the Heat Transfer Cold-Flow Experimental Set-Up

* In the photo it is distorted due to the angle of the photo taken (see Figure 3.4 for top plenum alignment)

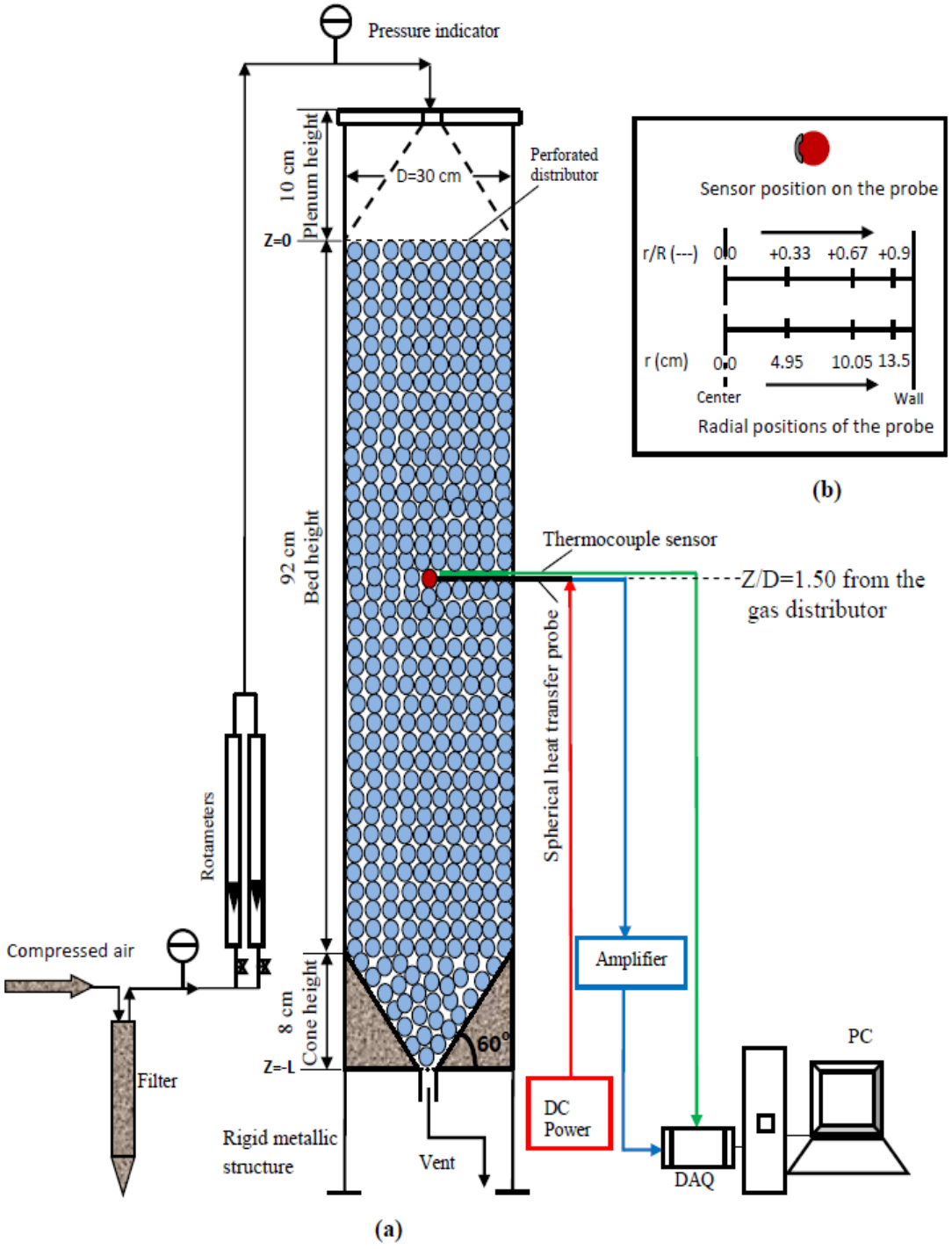

Figure 7.2. (a) Schematic Diagram of the Fast-Response Heat Transfer Probe Used with the Cold-Flow Experimental Set-Up; and (b) Schematic of the Sensor Position and the Spherical Probe Radial Locations Inside the Bed

7.2.2. Development of the Novel Non-Invasive Sophisticated Heat Transfer Spherical Type Probe Technique for Gas-Solid Systems. The developed heat transfer probe is a novel non-invasive fast-response technique of its first time that designed and manufactured to measure properly the heat transfer coefficient in single and multiphase flow systems by measuring simultaneously the local instantaneous heat flux from a hot surface sensor to the adjacent bulk and the surface temperature of the sensor. The bulk temperature is measured by thermocouples placed in the void closer to the sensor. The probe has been used to investigate in more detail the characteristics of heat transfer in pebble bed by placing the probe on a number of axial and radial positions inside the bed.

7.2.2.1 The components of the heat transfer probe technique. Both heat transfer probe techniques (rod and spherical types) consist of fixed heat flux probe, DC power supply, amplifier, thermocouple sensors, and computer with data acquisition (DAQ) system, which is purchased from National Instruments (NI) Corporation, as shown in Figure 7.3. The data acquisition (DAQ) system is including a SCXI-1000 chassis, SCXI-1102 module kit, SCXI-1303 terminal block, SCXI-1349 w/2m cable, and NI PCI-6052E multifunction I/O board. The details of the fast-response heat transfer spherical probe are presented in the next section while the details of the rod type heat transfer probe are discussed in Appendix B.

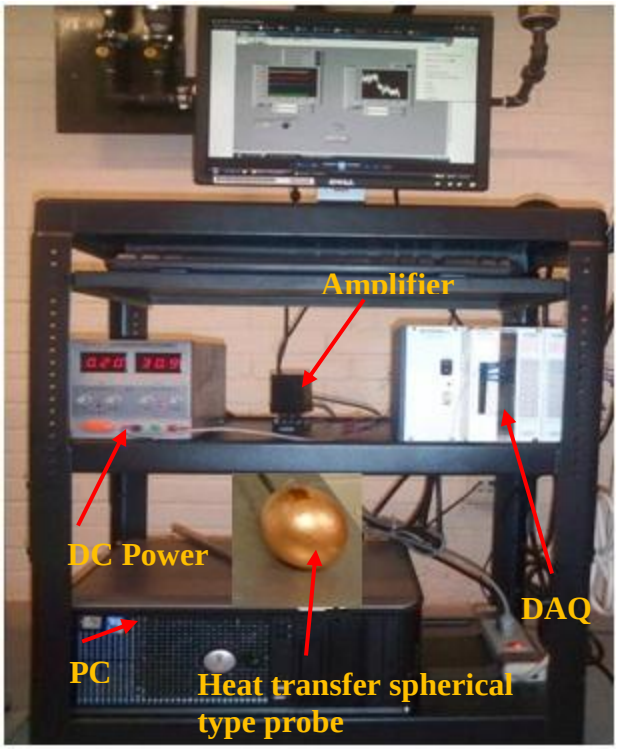

Figure 7.3. The Components of the Fast-Response Heat Transfer Probe Technique

7.2.2.2 The novel non-invasive sophisticated fast response heat transfer probe of spherical-type. The development of the novel non-invasive sophisticated fast response heat transfer probe of spherical-type is based on the electrically heated single sphere buried in an unheated packing. For this purpose, a fast-response heat transfer sensor was flushed mounted on a copper sphere of 5 cm in diameter to measure the heat flux through it and the sensor surface temperature. The copper sphere has heater inside of it to provide the heat through the sensor. This forms the non-invasive spherical-type heat transfer probe. The probe measures the local pebble-to-gas heat transfer coefficient for solid-gas system encountered in packed-pebble bed. It could also measure the solid-solid heat transfer through the contact points between the surface of the sensor and the surface of the contacted pebble. With this novel probe, most of previously mentioned integrated errors in the measurements of local heat transfer in packed pebble-bed using rod type

heat transfer probe could be reduced or eliminated. A photo and schematic diagram of the heat transfer probe are shown in Figure 7.4. A small cartridge heater was installed inside the solid copper sphere which has high thermal conductivity. The DC power was supplied to the cartridge heater through a variac to regulate the supplied power in the range of 20–40V. The micro-foil heat flux sensor (11mm×14mm×0.08 mm, micro-foil heat flow sensor No. 20453 (G161)-1, RDF Corporation) is flush mounted on the copper sphere surface and it can measure accurately and simultaneously the local heat flux (q_i) through it and the probe surface temperature (T_{si}). This forms the spherical-type heat transfer probe. Figure 7.4b shows the design and components of the spherical-type probe. The response time of the sensor is about 0.02 s. As shown in Figure 7.4c, the probe location can be changed both axially and radially at different positions in the bed. The thermocouple sensors are arranged at different axial positions and at radial locations to monitor the flowing gas temperature adjacent to the heat transfer sensor. To properly insert the probes (heat transfer probe and thermocouple sensors) and to prevent any contact effects between the sensor surface and the surface of the pebbles, the test section of the bed has to be structured carefully rather than packing it randomly.

The experimental work was conducted to study the heat transfer in solid-gas packed pebble-bed. In order to get more accurate results and to minimize the experimental error, each of the experimental runs was repeated at least three times. For each run, before any reading was taken, the system was left to equilibrate at the required superficial gas velocity. The experimental steps that were followed in the packed pebble-bed heat transfer system and operating procedures of the heat transfer technique are outlined in Appendix B.

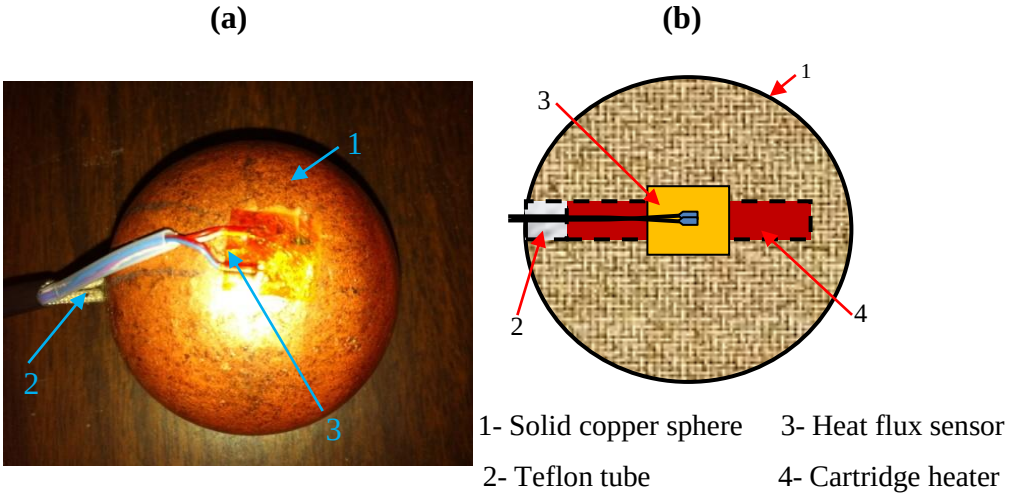

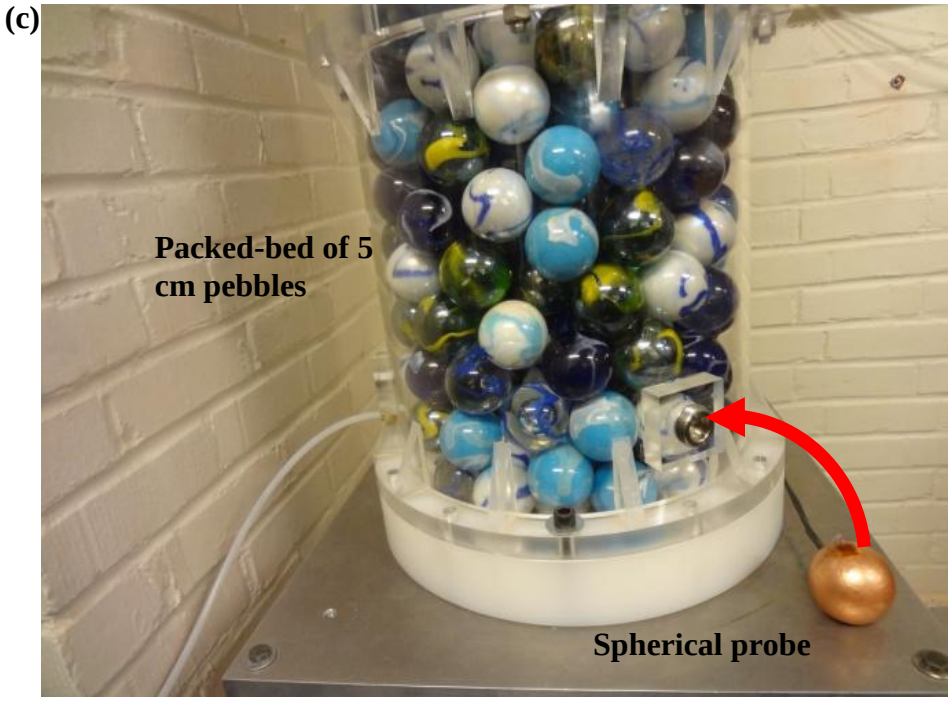

Figure 7.4. Novel Non-Invasive Fast-Response Heat Transfer Probe of Spherical-Type: (a) Picture of the Probe; (b) Schematic Diagram of Probe; and (c) The Pebble-Bed Where the Probe is Placed in it

7.2.3. Data Collections and Analyses. For each experimental run, the surface temperatures and heat flux across the pebble are monitored until the steady state condition is reached. Since the measured signals of the heat flux are in the range of micro-volts, they were amplified before received by the data acquisition (DAQ) system. The heat flux signals and the signals from the thermocouples were sampled simultaneously at 50 Hz for about 40 s. The local instantaneous heat transfer coefficient between the fixed heat flux sensor at surface temperature of T_{si} and the surrounding gas phase dispersion at temperature of T_{bi} is obtained by the following relation:

$$h_i = \frac{q_i}{T_{si} - T_{bi}} \quad ; \quad \Delta T_i = T_{si} - T_{bi} \tag{77}$$

Where h_i is the local instantaneous heat transfer coefficient (kW/ m^2.K), q_i is the instantaneous heat flux across the sensor (kW/m^2), while T_{si} is the instantaneous surface temperature of the probe sensor (K) and T_{bi} is the instantaneous bulk temperature of the media (K).

The local time-averaged heat transfer coefficient (h) at a given location is obtained by averaging the instantaneous heat transfer data over a large number of sampling points as follows:

$$h = \frac{1}{n}\sum_{i=1}^{n}\frac{q_i}{T_{si} - T_{bi}} = \frac{1}{n}\sum_{i=1}^{n} h_i \tag{78}$$

Where n is the total number of experimental data points. In this work n=2050 samples were used to establish a high stable value of heat transfer coefficients for all operating conditions.

Figures 7.5 a,b and c show some of the raw data from the spherical-type heat transfer probe.

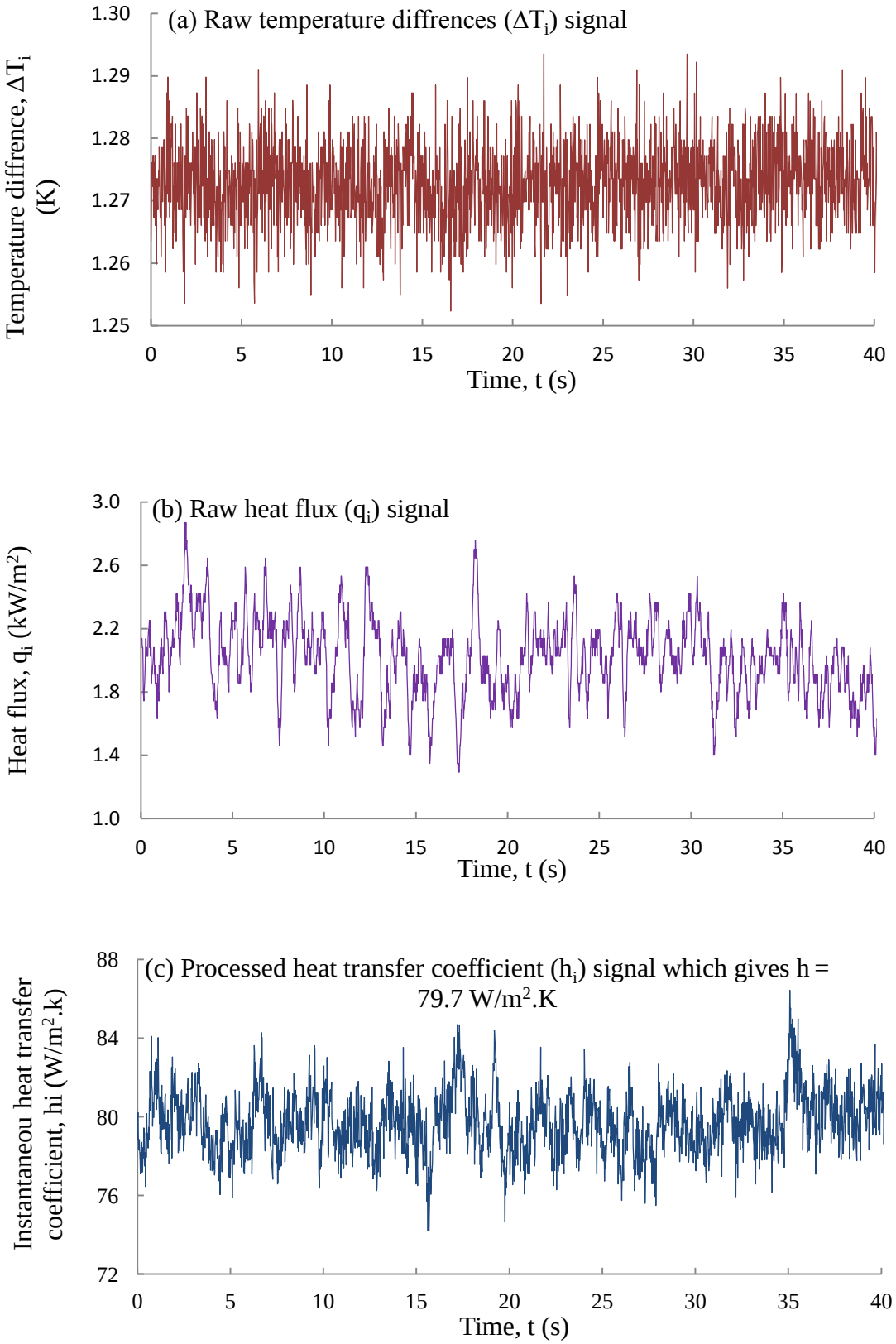

Figure 7.5. Sample of the Time-Series Heat Transfer Data in the Center of the Pebble Bed at V_g= 0.2 m/s

As illustrated in Figure 7.2c and mentioned earlier, the local measurements have been taken at different axial locations and radial positions in the bed. Three different axial heights to column diameter ratios (Z/D) of 0.5, 1.5 and 2.5 from the top distributor were used. At any particular axial location; there have been seven dimensionless radial positions as; $r/R = 0.0$ (center of the bed), ±0.33, ±0.67 and ±0.9 (near wall of the bed). Therefore, the average radial heat transfer coefficients (h_{av}) can be azimuthally averaged based on the cross-sectional area as defined:

$$h_{av} = \frac{2}{R^2}\int_0^R h(r) r dr \qquad (79)$$

Where R is the radius of packed pebble-bed.

Note: All the data of heat transfer coefficient at all studied gas velocity and radial and axial locations are available in the laboratory.

7.3. RESULTS AND DISCUSSION

7.3.1. Effects of Gas Flow on Convective Heat Transfer Coefficients. The effect of coolant gas velocities on the convective heat transfer coefficients were investigated at different axial positions along the bed height with aspect ratio (D/d_p) of 6, as shown in Figure 7.6. For all three axial levels (Z/D =0.5, 1.5, and 2.5), the convective heat transfer coefficients increase gradually with the increase in the gas velocity. It is found that effect of superficial gas velocity on heat transfer coefficients varies from laminar to turbulent flow regimes for all radial positions. At laminar flow regime the change in heat transfer coefficient with respect to change in superficial gas velocity is sharper than that in turbulent flow regime and in between for the transition regime as

depicted from Figure 7.6. In fact, the heat transfer coefficients are continuously increased with the gas velocities and the change in heat transfer coefficient with respect to gas velocity reduces at high range of gas velocity due to not much change encounters in the local flow structure around the pebbles at high range of gas velocity. Furthermore, the increase in the superficial gas velocity 10 times, i.e. from 0.1 m/s ($Re_h \sim 300$) to 1 m/s ($Re_h \sim 3300$) causes an increase in the convective heat-transfer coefficients by about 70%, 72%, and 73% for the cases of top ($Z/D=0.5$), middle ($Z/D=1.5$) and bottom ($Z/D=2.5$) sections, respectively. This is related to the boundary layer which is already very thin in the conditions of turbulent flow regime. In addition, energy transport by heat conduction plays an important role at low Reynolds numbers and will be the dominant transport. This leads to reduce the contributions of the heat transfer by convection at the conditions of laminar flow regime.

The inhomogeneities in the pebble arrangements play an important role in determination the flow structure between the pebbles and consequently the heat transfer (Hassan and Dominguez, 2008).

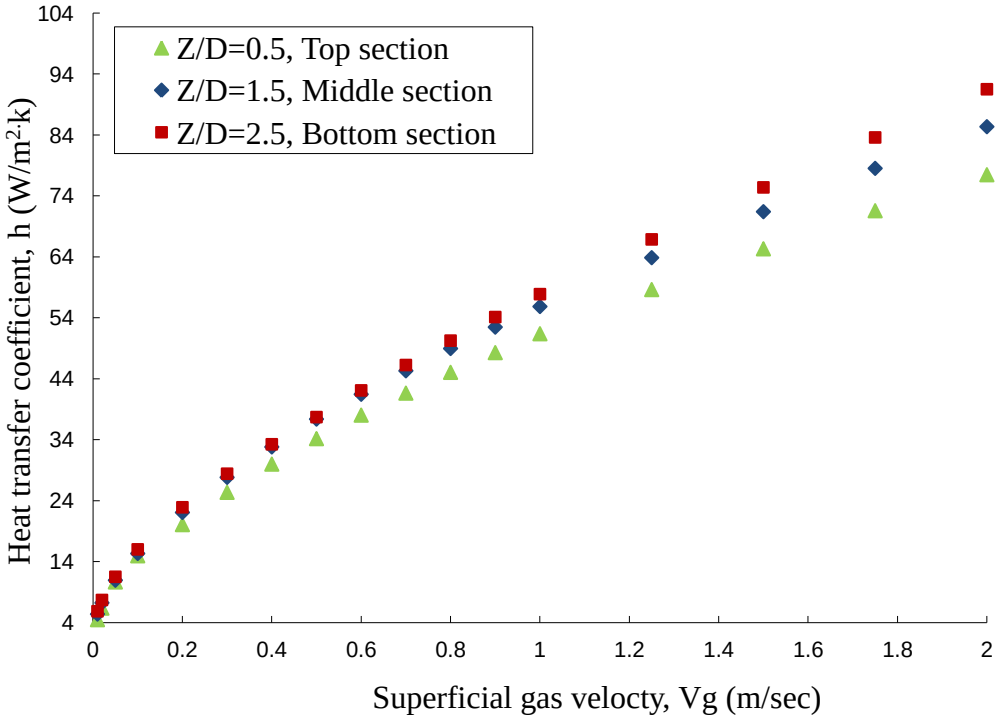

Figure 7.6. Effect of Superficial Gas Velocity on the Convective Heat-Transfer Coefficients at the Bed Center (r/R = 0.0)

Parts a and b of Figure 7.7 show the variation of the measured local heat-transfer coefficients with superficial gas velocity in the center of the bed (r/R = 0.0) and near the bed wall (r/R = 0.9), respectively. The heat transfer coefficients in the central-region of the bed (r/R=0.0, Figure 7.7 a) are smaller than those in the wall-region (r/R=0.9, Figure 7.7 b). The changes in heat transfer coefficient with respect to the changes in superficial gas velocity are sharper near the wall compared to those in the center. The differences between heat transfer coefficient values in the center and those near the wall vary from 33% to 21% with the increase in the superficial gas velocity from 0.05 m/s (laminar flow regime) to 0.6 m/s (turbulent flow regime) at the middle section (Z/D=1.5). In fact, this is due to the strong influence of the radial variations of the porosity (void) in the bed and

hence actual gas velocities would radially vary which affect the radial heat transfer coefficient. In the other words, the behavior of the local heat transfer coefficient is attributed to the reduction of the porosity in the central-region of the bed. This lower porosity in the bed center reduces the velocity of the fluid flow in this region, forcing the fluid to flow through the region of higher porosity, which is close to the bed wall. This consequently results in a higher fluid flow rates and hence higher velocity yielding high heat transfer coefficients near the bed wall. It is very important to mention here that the pressure drop is lower near the wall than in the center of the bed and this is, of course, due to a higher porosity near the wall of the bed. On the other hand, these differences in heat transfer coefficients at low superficial gas velocities are relatively smaller, but at higher superficial gas velocities the differences become larger. This is due to that the heat transfer is slightly influenced by in-homogeneities at low gas velocities ($Re_h < 200$) and the by-pass or the coolant flow channeling effects which increases with decreasing Reynolds number, as mentioned in Section 6.

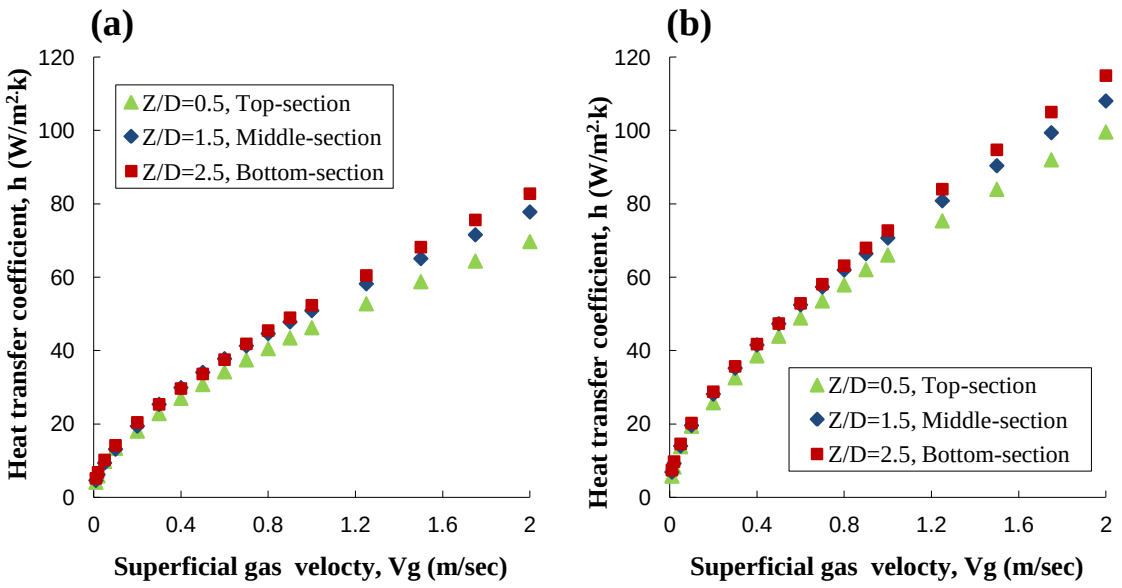

Figure 7.7. Effect of Superficial Gas Velocity on the Heat-Transfer Coefficients: (a) At the Center of the Bed (r/R = 0) and (b) Near the Wall of the Bed (r/R = 0.9)

7.3.2. Radial Profiles of the Local Heat Transfer Coefficients. The local heat transfer coefficients at various radial locations were measured by moving the probe sensor along the bed radius for four different positions, as $r/R = 0.0$ (center of the bed), ± 0.33, ± 0.67 and ± 0.9 (near wall of the bed). Figure 7.8 a and b shows the radial profiles of heat transfer coefficients measured at the three axial locations using high superficial gas velocity (1 m/s, Figure 7.8a) and low superficial gas velocity (0.1 m/s, Figure 7.8b). It can be seen that in the middle section or fully developed flow region (Z/D= 1.5) at the same superficial gas velocity, the local heat transfer coefficient increases from the bed center to the wall by 49.25% for low superficial gas velocity (V_g = 0.1 m/s) and by 38.88% for high superficial gas velocity (V_g = 1 m/s). Figure 7.8a shows that the radial differences in heat transfer coefficients at high superficial gas velocity (V_g > 0.1 m/s) are smaller in the top region (Z/D= 0.5) compared to the fully developed region at the middle

section (Z/D= 1.5). However, Figure 7.8b shows that at low superficial gas velocity (0.1 m/s) about similar trend exists of the radial variation of heat transfer coefficients at all axial levels. This is constituent with the characteristics of creeping flow regime where no turbulence occurs.

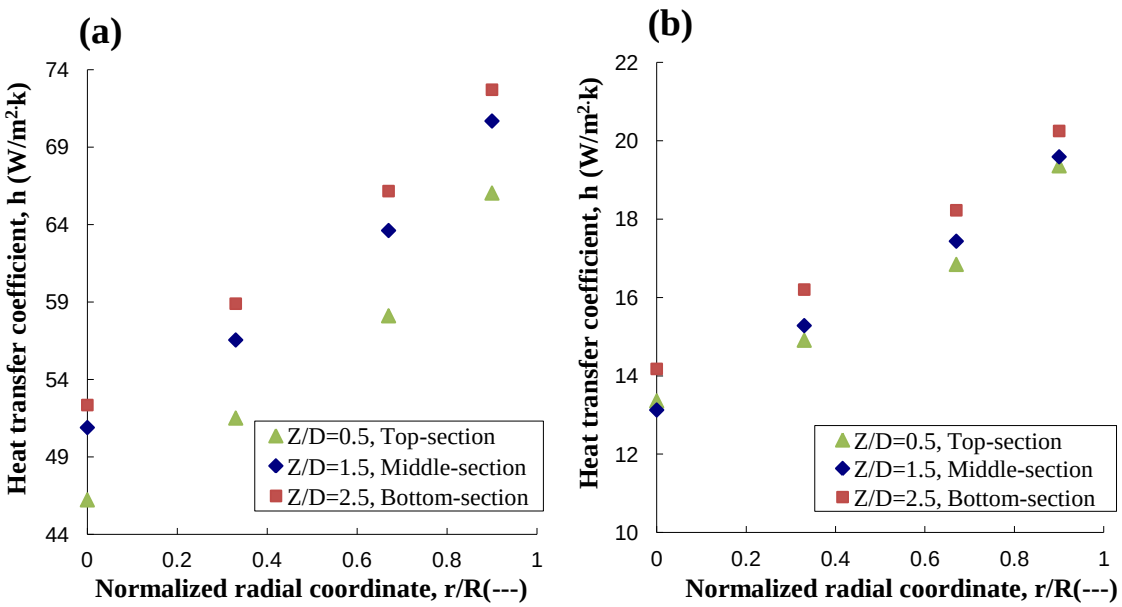

Figure 7.8. Radial Profiles of Local Heat Transfer Coefficients at Different Axial Locations: (a) High Superficial Gas Velocity (V_g = 1 m/s) and (b) Low Superficial Gas Velocity (V_g = 0.1 m/s)

If the radial profiles of the heat transfer coefficients are normalized with respect to value of the radially averaged heat transfer coefficient (as estimated in Equation 58) for each axial level as shown in Figures 7.9 a and b. It can be observed that the radial profiles of heat transfer coefficients are lumped into about single profile or trend for high superficial gas velocities. However, for low superficial gas velocities and for all axial

locations one profile would be not considered. There are some averaged differences of about 1.5 % at high superficial gas velocity (1 m/s) and about 2.7 % at low superficial gas velocity (0.1 m/s).

The results and findings clearly indicate that one value as overall heat transfer coefficient cannot represent the local heat transfer coefficients within the bed and hence correlations to predict radial and axial profile of heat transfer coefficients are needed.

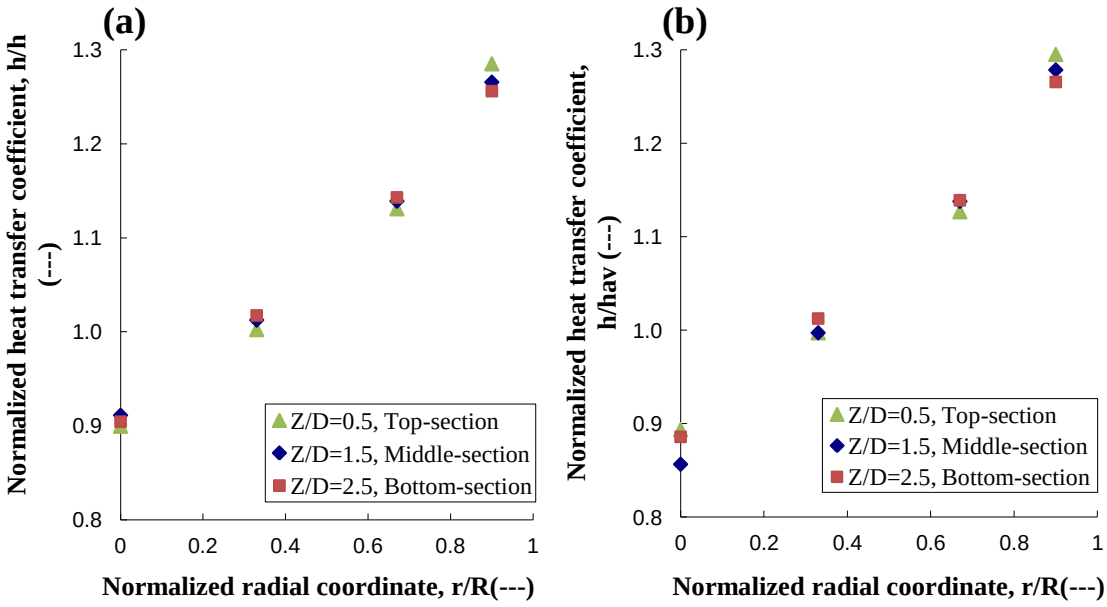

Figure 7.9. Radial Profiles of Normalized Heat Transfer Coefficients at Different Axial Locations: (a) High Superficial Gas Velocity (V_g = 1 m/s) and (b) Low Superficial Gas Velocity (V_g = 0.1 m/s)

7.4. COMPARISON OF THE HEAT TRANSFER RESULTS WITH AVAILABLE EMPIRICAL CORRELATIONS

As mentioned earlier, numerous studies have been conducted around heat transfer in packed bed of spheres of small particles (catalyst). However, for the

convective heat transfer coefficients a number of correlations have been reported in the literature in packed-pebble beds which are given by experimental and semi experimental correlations. The literatures show a great scattering in the heat transfer coefficient predictions of the reported correlations, especially when it comes to fluid of high Prandtl and extremely low flow conditions. This is due to the experiments have been mainly conducted with air and the results are mapped to high Prandtl fluids and to extremely low flow conditions which have been done through analogy with mass transfer experiments.

In this work, four correlations are used to predict the overall average convection heat transfer coefficient in packed pebble-bed nuclear reactor. In this case, since the local heat transfer coefficients have been measured, the overall heat transfer coefficient of the bed has been estimated by averaging these locally measured heat transfer coefficients, as expressed in Equation 79. The correlations have been selected because they were developed based on large experimental database, as discussed in Section 2.

Wakao and Kaguei (1982) gave an overview of the different experimental data existing at that time and proposed the following semi-empirical correlation for the average heat transfer in packed bed as follows:

$$\mathrm{Nu} = 2 + 1.1\mathrm{Pr}^{1/3}\,\mathrm{Re}^{0.6} \tag{27}$$

Where the non-dimensional Prandtl number (Pr) is defined as:

$$\mathrm{Pr} = \frac{\mu \mathrm{C_p}}{\mathrm{k}} \tag{27a}$$

$\mathrm{Nu_h}$ is an effective Nusselt number which is defined based on the average interstitial velocity and on the characteristic length scale for the pores (voids) (an equivalent hydraulic diameter, $\mathrm{d_h}$) as:

$$\mathrm{Nu_h} = \frac{\mathrm{h d_h}}{\mathrm{k}} = \frac{\varepsilon_\mathrm{b}}{\left(1-\varepsilon_\mathrm{b}\right)}\mathrm{Nu} \tag{27b}$$

Where the Nusselt number is defined based on pebble diameter $\left(d_p\right)$ and is given by:

$$Nu = \frac{h d_p}{k} \tag{27c}$$

While, h is the average convective solid-gas heat transfer coefficient in pebble bed and k is the thermal conductivity of flowing coolant gas.

Gnielinski (1978; 1981), evaluated experimental results of about 20 authors and established a relationship among Nusselt number, Reynolds number, Prandtl number and porosity of the packed-pebble bed, in the following form:

$$Nu = f_{\varepsilon} Nu_{sp} \qquad \text{for} \qquad Re/\varepsilon_b \le 2\times 10^4 \tag{29}$$

Where,

$$f_{\varepsilon} = 1 + 1.5(1-\varepsilon) \tag{29a}$$

Nu_{sp} is the Nusselt number of a single sphere (pebble), which can be calculated, according to the following equation:

$$Nu_{sp} = 2 + \sqrt{Nu_{lam}^2 + Nu_{turb}^2} \tag{29b}$$

Nu_{lam} and Nu_{turb} are the Nusselt numbers of the single sphere for laminar and turbulent flow, respectively, and defined as:

$$Nu_{lam} = 0.664\left(Re/\varepsilon_b\right)^{1/2} Pr^{1/3} \tag{29c}$$

$$Nu_{turb} = \frac{0.037\left(Re/\varepsilon_b\right)^{0.8} Pr}{1 + 2.443\left(Re/\varepsilon_b\right)^{-0.1}\left(Pr^{2/3} - 1\right)} \tag{29d}$$

Association of German Engineers (VDI) heat atlas (Gnielinski, 2010), recommended the above equations (29-29d) for the predication of pebble-to-gas heat transfer in the core of the high-temperature packed pebble-bed nuclear reactors. Based on experimental data from several independent studies of heat convection in randomly packed pebble-beds, the German Nuclear Safety Standard Commission (KTA) proposed

a correlation to determine heat transfer coefficient of solid to flowing gas for German high temperature reactor (HTR) as follow (KTA Standards, 1983):

$$\mathrm{Nu} = 1.27\left(\frac{\mathrm{Pr}^{1/3}}{\varepsilon_b^{1.18}}\right)\mathrm{Re}^{0.36} + 0.033\left(\frac{\mathrm{Pr}^{1/2}}{\varepsilon_b^{1.07}}\right)\mathrm{Re}^{0.86} \qquad \text{for} \quad 100 \le \mathrm{Re} \le 10^5 \qquad (30)$$

A similar empirical heat transfer correlation was developed by Achenbach (1995) for a pebble bed heat transfer coefficient in which the Reynolds number range exceeds by one order of magnitude as:

$$\mathrm{Nu} = \left[\left(1.18\,\mathrm{Re}^{0.58}\right)^4 + \left(0.23\left(\mathrm{Re}_h\right)^{0.75}\right)^4\right]^{1/4} \qquad \text{for} \qquad \mathrm{Re}/\,\varepsilon_b \le 7.7\times10^5 \qquad (31)$$

Based on the average absolute relative error (AARE), statistical test was performed to check the fitting of prediction. AARE between the measured and predicated Nusselt numbers is expressed as:

$$\mathrm{AARE} = \frac{1}{N}\sum_{1}^{N}\left|\frac{\mathrm{Nu}_{\mathrm{Pred(i)}} - \mathrm{Nu}_{\mathrm{Exptl(i)}}}{\mathrm{Nu}_{\mathrm{Exptl(i)}}}\right| \qquad (80)$$

Where N is the data point number.

Figure 7.10 shows values of pebble-to-gas heat transfer coefficients in terms of Nusselt numbers $\left(\mathrm{Nu} = \mathrm{hd_p}/\mathrm{k}\right)$ at different effective Reynolds numbers. In this Figure the experimental values of averaged local heat transfer coefficients at the middle section (Z/D=1.5) which explained in Figure (7.6) are compared with those predicted based on the above selected correlations. The prediction of Achenbach's (1995) correlation is relatively better for all flow conditions and the AARE with the experimental data of this work is about 4.4 %. The correlations developed by Gnielinski (1978); KTA Standards (1978) seems to provide a reasonable predictions for turbulent-flow regimes of high flow conditions ($\mathrm{Re_h} > 300$) where the value of AARE are about 3.37% and 2.23%,

respectively. However, both correlations are over-predicts for laminar flow conditions, i.e. $Re_h < 200$. There is relatively larger deviation in the prediction based on the correlation of Wakao and Kaguei (1982) (AARE is about 13 %) for low flow conditions, i.e. $Re_h < 200$. The correlation also gives AARE of about 9 % for high flow conditions of turbulent flow regime hence it cannot be expected to predict accurate convective heat transfer coefficients for these conditions.

At low superficial gas velocities, the trends and the values do not match well for all correlations. This can be attributed to uncertainties in different measurement techniques used and different operating and design conditions of the reported studies. In addition to that, the forced convective heat transfer coefficient is influenced by a number of parameters, for instance, Reynolds number, Prandtl number, local porosity, aspect ratio, local flow conditions, etc. However, the variation of the local porosity and hence local flow conditions remains an important issue for the local heat transfer coefficient. In this work a large pebble diameter (5 cm) has been used which yields higher value of average bed porosity.

The variations in the local values of heat transfer coefficient indicates that more investigations on the mechanisms that govern heat transfer using wide range of relevant conditions in the pebble bed are needed to develop correlations capable of predicting properly the local heat transfer coefficients and to further improve such predictions of the local convective heat transfer coefficients in these reactors.

It is obvious that to obtain a more accurate results and properly understanding of the local heat transfer coefficients and the related mechanism, detailed qualitative and quantitative information of local gas velocity fields and local porosity are needed.

Therefore, special investigations of the local gas velocity fields and local porosity are necessary in packed pebble bed reactors. Since such investigations are not an easy task, the computational fluid dynamics (CFD) are important for predictions of the local flow field for measured or computed local porosity to estimate the local heat transfer coefficient using one of the above mentioned correlations. Hence, developing correlation that is capable to predict local heat transfer coefficient will facilitate using proper integration of hydrodynamics (CFD) and heat transfer computation.

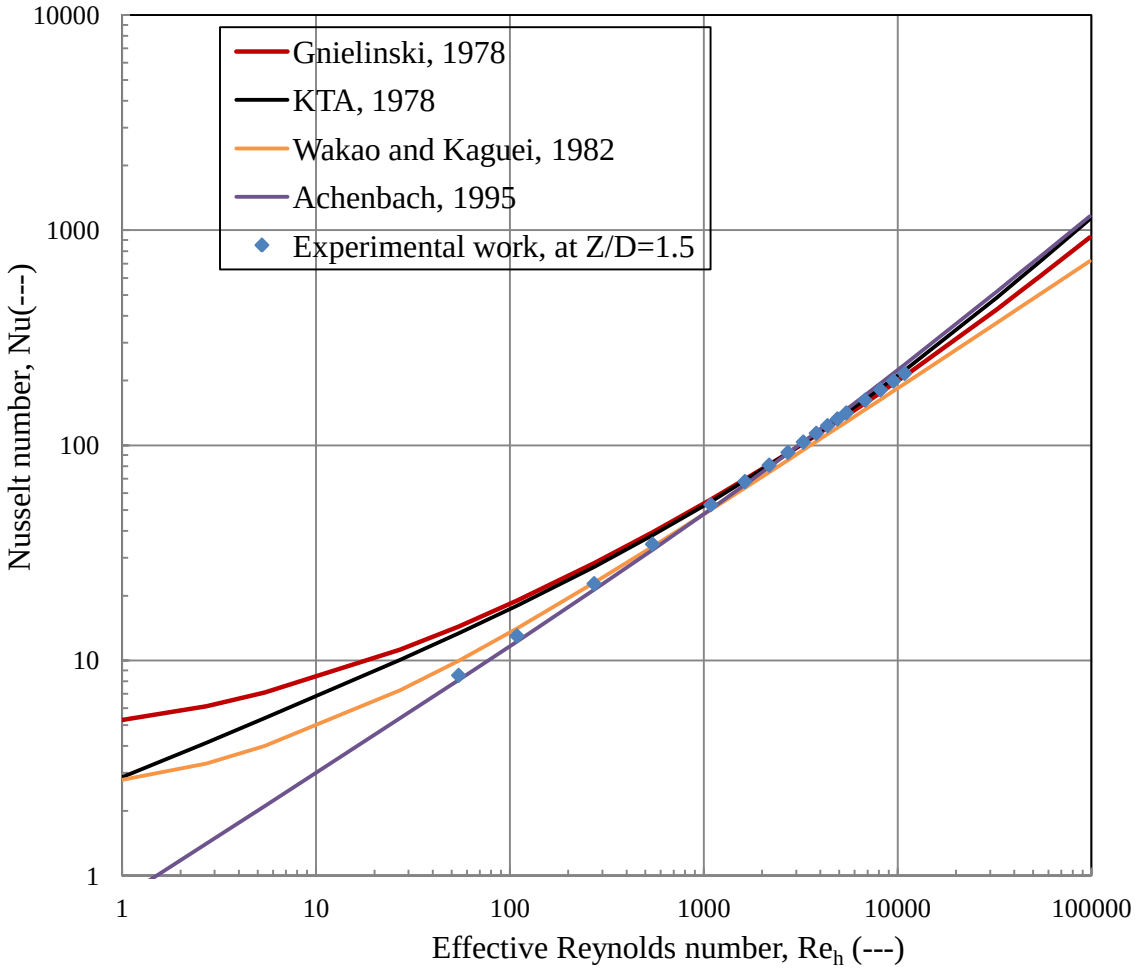

Figure 7.10. Comparison of the Measured Average Heat-Transfer Coefficient with the Empirical Correlations

7.5. CONCLUDING REMARKS

The following concluding remarks may be drawn from the present investigation of heat transfer coefficient:

1. A novel non-invasive sophisticated fast-response heat transfer probe in a spherical type has been developed and used in this work.
2. The local heat transfer coefficients were measured using such sophisticated heat transfer probe of spherical-type and the heat transfer experiments were carried out by applying the method of the electrically heated single sphere buried in an unheated packing.
3. The effect of coolant gas velocities has been investigated at different radial and axial positions along the bed height. The results show that the heat transfer coefficients increase gradually with the increase in the gas velocity and it is found that the effect of gas velocity on heat transfer coefficients varies from laminar to turbulent flow regimes for all radial positions.
4. Heat transfer coefficients at various radial locations were measured by moving the probe sensor along the bed radius for four different positions to get the radial profiles of heat transfer coefficients. The results show that the local heat transfer coefficient increases from the bed center to the wall due to the variation of the bed structure (void) and hence the flow pattern.
5. The convective pebble-gas heat transfer coefficients in terms of Nusselt numbers has been compared with those predicted based on published correlations. The results show that the classical Wakao-equation of chemical packed-bed reactors cannot predict accurate convective heat transfer coefficients for certain conditions, especially for packed pebble-bed nuclear reactors of turbulent flow regime.

6. The obtained experimental results demonstrate the applicability of the Achenbach (1995) correlation for randomly packed pebble-bed nuclear reactors.
7. The results and findings clearly indicate that one value as overall heat transfer coefficient cannot represent the local heat transfer coefficients within the bed and hence correlations to predict radial and axial profile of heat transfer coefficient are needed.
8. The variations in the local values of heat transfer coefficient indicates that more investigations on the mechanisms that govern heat transfer using wide range of relevant conditions in the pebble bed are needed to develop correlations capable of predicting properly the local heat transfer coefficients and to further improve such predictions of the local convective heat transfer coefficients in these reactors.
9. Accordingly, measuring the variation of the local bed structure and the local gas velocity along with the heat transfer coefficient is needed.

8. CONCLUDING REMARKS AND RECOMMENDATIONS FOR FUTURE WORK

This dissertation studied the gas dispersion and mixing and convective heat transport phenomena in packed pebble-bed nuclear reactor of pebbles with different diameters using sophisticated measurement techniques. The following are some of the remarks and findings of this work:

8.1. CONCLUDING REMARKS

8.1.1. Gas Dispersion and Mixing Phenomena Based on Axial Dispersion Model (ADM).

An advanced gas dynamics technique and methodology that properly counts for the external dispersion have been used and therefore, the present work provides insight on the extent of mixing and dispersion of the coolant gas in the studied packed-pebble beds. Quantification of the gas phase dispersion in terms of axial dispersion coefficients and dispersive Peclet numbers in packed pebble-bed has been performed for the first time for different gas velocities and particle sizes. The following are some of the remarks and findings:

1. At flow conditions of interest (high gas flow rate) small deviation from ideal plug flow was observed and hence, axial dispersion model can be applied to describe the flow of coolant gas in packed pebble beds.
2. The results show that small dispersion with better extent of gas mixing exit at higher velocities, while relatively large dispersion are observed at low gas velocities. In addition, these results indicate that the molecular diffusion contributes to gas

dispersion phenomena at the low gas velocity, whereas at high gas velocity the hydrodynamics mixing or convection dominates.

3. The effect of bed structure (pebble sizes) and void distribution on the axial dispersion coefficient has been investigated and the obtained results indicate that the bed structure (pebbles size) strongly affects the axial dispersion and mixing in the packed pebble-bed.
4. The effect of bed height on the axial dispersion coefficient has been investigated and it has been noticed from the obtained results that the axial dispersion coefficient slightly increases with increase in bed height at the low range of superficial gas velocity while at high gas velocity the effect is negligible.
5. Idealized plug-flow behavior cannot be assumed for the normal flow conditions where the dispersion and mixing as well as the wall effects need to be taken in account.
6. A comparison was made between the measured axial gas dispersion coefficients in terms of Peclet numbers and dispersion numbers (reciprocal of Peclet numbers) at different gas velocities with those predicted by selected correlations. The correlation developed by Gunn (1987) provided a good prediction at both low and high superficial gas velocities. However, additional investigations and more data are needed to reach to solid conclusion and possibly to develop a new correlation for packed pebble-bed nuclear reactor.

8.1.2. Tanks-In-Series (T-I-S) Model. The tanks-in-series (T-I-S) model or N continuous stirred tank reactors (N-CSTR) model has been also used to characterize the behavior and to describe the non-ideal flow as an alternative to the axial dispersion model (ADM) in packed pebble bed. The following are some of the findings:

1. The results of tanks in series model confirm that the axial dispersion model (ADM) can be used successfully to describe the non-ideal flow behavior in the studied packed pebble bed. Relatively large number of tanks (~9) describes the residence time distribution (RTD) of the bed at relatively high superficial gas velocity which indicates small deviation from ideal plug flow pattern.
2. Relatively small deviation from ideal plug flow which occurs in the studied packed pebble-beds at high gas flow rate (typical operating conditions of pebble bed reactor) has been found which can be satisfactory represented either by the axial dispersion model or by the tanks-in-series model.
3. To assess for equivalent relationship between the parameters of the axial dispersion model (dispersive Peclet number, Pe_D) and tanks-in-series model (the number of tanks in series, N) in the studied pebble bed reactors, a comparison of the residence time distributions of both models has been made by equating their dimensionless variance.

8.1.3. Residence Time Distribution (RTD) Based on Central Moments Analyses (CMA). The responses of the experimental RTDs in terms of the mean residence time (1^{st} moment), degree of spreading or variance (2^{nd} moment) and asymmetry (3rd moment) has been characterized based on the statistical analysis of the central moments. Since the central moments are additive in nature, the central moments of the plenum/ distributor zone have been extracted from the plenum/distributor RTD functions which were measured experimentally and compared to those predicated by CSTR. In addition, the central moments of the bed alone have been extracted from the whole system RTD function which were measured experimentally and compared to those predicated by ADM.

At high superficial gas velocities, the result indicates that the gas flow pattern in the studied bed is not much deviated from idealized plug-flow model behavior and hence ADM can be suitable to describe the flow behavior for this small deviation.

8.1.4. Pressure Drop and Fluid Flow Characteristics. Differential pressure transducer was used to measure experimentally the pressure drop along the randomly packed-pebble bed.

1. The results show strong dependence of the pressure drop on both the aspect ratio (bed diameter/pebble diameter), and hence the porosity of the bed and the coolant gas velocity.
2. The obtained experimental results of pressure drop demonstrate the applicability of the VDI (Wirth, 2010) and KTA (KTA Standards, 1981) correlations for randomly packed pebble-bed nuclear reactors.

3. The results also confirm that the classical Ergun-type equations, commonly used to calculate pressure drop through small catalyst packed beds, considerably over-predicts for randomly packed pebble-bed of large size pebbles nuclear reactors.

8.1.5. Forced Convection Heat Transport. The heat transfer experiments were carried out by applying the method of the electrically heated single sphere buried in an unheated packing and the local heat transfer coefficients were measured using sophisticated heat transfer probe of spherical-type. The effects of coolant gas velocities were investigated at different axial positions along the bed height. Heat transfer coefficients at various radial locations were measured by moving the probe sensor along the bed radius for four different positions to get the radial profiles of heat transfer coefficients. The following are some of the findings:

1. The results show that the heat-transfer coefficients increase gradually with the increase in the gas velocity and it is found that effect of gas velocity on heat transfer coefficients varies from laminar to turbulent flow regimes for all radial positions.
2. The results show that the local heat transfer coefficient increases from the bed center to the wall. The differences between heat transfer coefficient values in the center and those near the wall vary from 33% to 21% with the increase in the superficial gas velocity from 0.05 m/s (laminar flow regime) to 0.6 m/s (turbulent flow regime) at the middle section (Z/D=1.5). This could be attributed to the distribution of the bed void which affects the flow distribution of the flowing coolant gas and hence heat transfer coefficient.

3. The obtained experimental results demonstrate the applicability of the Achenbach (1995) correlation for randomly packed pebble-bed nuclear reactors.
4. The results show that the classical Wakao-correlation (Wakao and Kaguei, 1982) of chemical packed-bed reactors cannot to predict accurate convective heat transfer coefficients for certain conditions, especially for packed pebble-bed nuclear reactors of turbulent flow regime.
5. The results and findings clearly indicate that one value as overall heat transfer coefficient cannot represent the local heat transfer coefficients within the bed and hence correlations to predict radial and axial profiles of heat transfer coefficients are needed.

8.2. RECOMMENDATIONS FOR FUTURE WORK

Although the current study provides useful knowledge about packed pebble-bed reactors, many questions remain unanswered related to issues of relevance to this work. Below are some recommendations for potential future research opportunities to advance the understanding of the gas dynamics and heat transfer of packed pebble-bed reactors.

8.2.1. Gas Dispersion and Mixing Phenomena.

1. To obtain a further thorough understanding of the gas-dynamic processes, special investigations of the local gas velocity fields and velocity distributions are necessary. These can be performed using a computational fluid dynamics (CFD) simulation which provides an accurate description of the flow pattern. In addition, other different measurements techniques can be used such as a contact-free of laser doppler anemometry (LDA) method and hot-wire anemometry (HWA) which are

fast-response techniques provide detailed information of an instantaneous velocity and other properties like turbulence intensity in one, two or three dimensional gas and/or liquid flows.

2. The radial dispersion (transverse) is very important and needs to be accounted for especially in low flow conditions of accident scenario in packed pebble-bed nuclear reactor. The most popular technique for the measurement of transverse dispersion consists in feeding a continuous stream of tracer from a "point" source somewhere in the bed (usually along the axis) and measuring the radial variation of tracer concentration at one or more downstream locations (Delgado, 2006).
3. The new wave model for axial dispersion of three adjusted parameters can be applied for packed pebble-bed reactors. This model contains three adjusted parameters that depend on the flow conditions, physical properties of the fluid, and the geometry of the system. In this model, the fluid flow is considered to be dependent of variations of the fluid properties, such as density, viscosity, etc. The density effects become more pronounced for gas flow through packed beds with larger tube diameters and at higher pressures (Benneker et al., 1998). The wave model was reported by Westerterp et al. (1995a; 1995b; 1996) as an alternative to the commonly used axial dispersion model (ADM) or dispersed plug-flow model. The model has been applied for the description of longitudinal dispersion in tubular reactors by Benneker et al. (1997). Kronberg and Westerterp (1999) extended the approach to describe two-dimensional heat and material transport processes in fixed-bed reactors.

8.2.2. Heat Transport Process.

1. Natural convection heat transfer mechanism is a source of error in heat transfer measurements in existing literatures (Achenbach, 1995), which may dominate in low flow conditions of accident scenario in nuclear pebble bed reactors. Therefore, this transport is very important and need to be considered in future studies.
2. To generate results that could be used to validate future computational fluid dynamics (CFD) models and heat transfer computation, an additional set of separate effects tests needs to be used to address the following:
   a) The pebble to pebble effective conductivity within the pebble bed reactor.
   b) The effective fluid conductivity due to turbulent mixing.
   c) The pebble effective conductivity in the near-wall region.
3. When the coolant gas flows through the packed pebble-bed, all three modes of heat transfer (conduction, convection and radiation) contribute to the heat transport in the form of various mechanisms which interact by a number of series and parallel paths. Therefore, heat transfer mechanisms of conduction and radiation needs to be evaluated independently of convective effects to assess the contribution of each mechanism for randomly packed pebble-bed reactors.
4. Two general concepts have been used to describe the effects of overall heat transfer mechanisms which include the contribution of conduction, convection and radiation in packed pebble-bed, namely the effective heat transfer coefficient and the effective thermal conductivity. These parameters need to be evaluated in future studies.

APPENDIX A.

THE DEVELOPED ADVANCED GASEOUS TRACER TECHNIQUE

1. Introduction

The gaseous tracer (GT) is a technique that has been used to measure the residence time distribution (RTD) in a complex flow structure of single and multiphase flow systems by injecting an inert chemical, called *tracer,* as an impulse or step change input and monitoring its concentration at the exit. The measured RTD can be utilized to characterize and quantify the gas dispersion (which includes the contribution of both molecular diffusion and turbulent mixing), to identify the degree of mixing in the system and to characterize of any mal-flow distribution.

The RTD response can be further processed using central moments analysis to estimate the mean residence time (1^{st} moment), degree of spreading or variance (2^{nd} moment) and asymmetry (3^{rd} moment) for quantifying the extent of dispersion and mixing and the deviation from ideal flow pattern (plug flow, mixed etc). In addition, it can be used as diagnostic tool for identifying operational problems, such as the presence of bypassing/channeling flow, stagnant regions/dead zones and internal recycling/short recirculation, etc. In this work, the technique that has been developed by Han (2007), has been reproduced to account for and de-convolute the components of all the external mixing and dispersion.

All the mathematical models, algorithms and programs for extracting the signal of any desired part of the system, for statistical analyses of moments, and for signal processing, etc. developed by Han (2007) have been extended to packed pebble-beds and implemented in this work. The GT technique consists of: thermal conductivity detector (TCD), vacuum gas sampling pump, digital controller, signal amplifier, analog/digital (AD) converter, data acquisition (DAQ) software and computer with data acquisition system. All these components of the developed GT technique are discussed below.

2. Components of the Gaseous Tracer Technique

The developed gaseous tracer technique which is shown in Figure A.1 consists of the following components:

1. The 20 series binary gas analyzer

   The gas analyzer consists of thermal conductivity detector (TCD). However, the flame ionization detector (FID) is available as well.

2. Vacuum gas sampling pump

   The gas sampling pump is used to draw the sampling gas under vacuum (Model No.: 59-300 by GOW-MAC).

3. Digital controller

   The digital controllers (timers) are multifunction Dayton time delay relays.

4. Signal amplifier

   The signal amplifier has been designed for the data acquisition chromatography software (DACS). Supplied by a low voltage DC power, the amplifier has two channels (A and B) for both input and output signals.

5. Analog/digital converter

   The A/D converter with an effective 32.5 μV/bit response from 0–5V DC and it has two channels of analog input and an RS-232 port for the digital output.

6. Data acquisition (DAQ) software and computer

   The data acquisition was performed using the DACS Chromatography Software designed by GOW-MAC for MS Windows systems and LabView by national instruments (NI).

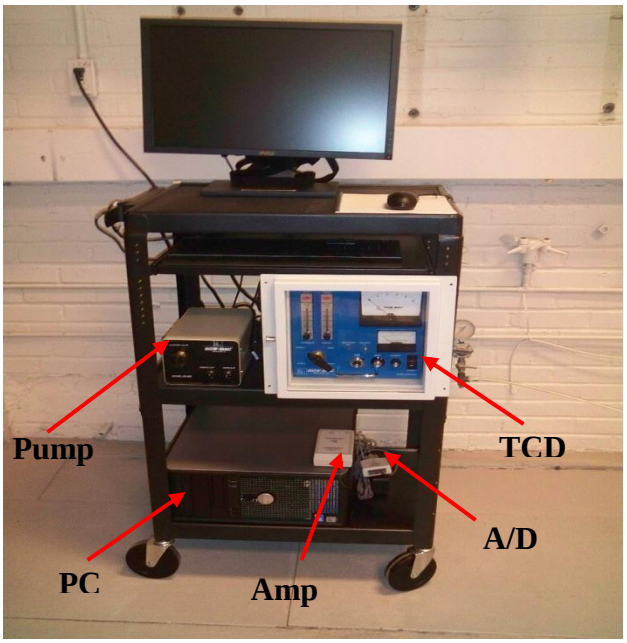

Figure A.1. Components of an Advanced Gas Dynamics Tracer Technique

2.1. Gas Tracer Injection System

The injection system consists of two high pressure (up to 250 psi) gas cylinders as the tracer gas (helium, He) cylinder and reference gas (nitrogen, N_2) cylinder. The tracer gas (helium, He) and reference gas (nitrogen, N_2) cylinders are equipped with two pressure gas regulators to regulate and control the input nitrogen gas and injected helium gas. The tracer gas (helium) line is connected to the solenoid valve and then to the injection points, as shown in part (a) of Figure A.2. The reference gas (nitrogen) line is connected to the thermal conductivity detector (TCD) instrument and then to the outlet, as shown in part (b) of Figure A.2.

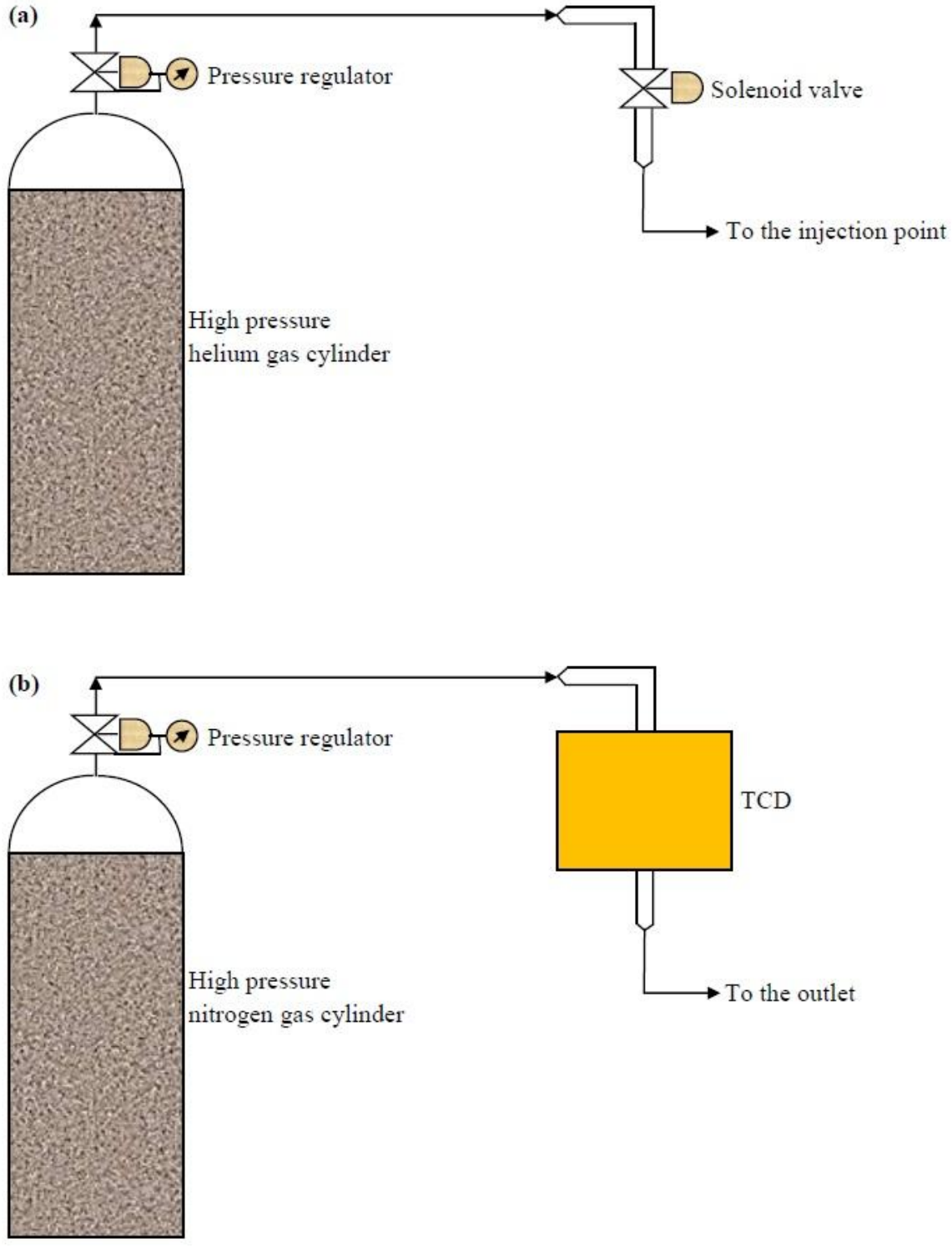

Figure A.2. Schematic Diagram of the Gas Tracer Injection System; (a) The Tracer Gas (Helium) Line and (b) The Reference Gas (Nitrogen) Line

3. Operating Procedure for the Gaseous Tracer Technique

The following step-by-step procedure needs to be followed during measurements of gas tracer signals for the quantification of dispersion and extent of mixing in packed pebble-bed reactor.

1. The gas tracer unit should be set properly along with the connection of the injection and sampling lines. The air is allowed to pass through the bed to purge out any remaining gas tracer from previous experiments. The injection of tracer is controlled by a timer and a valve to give an impulse signal.
2. The packed pebble-bed should be operated at desired operating conditions (air at 80 psi pressure and room temperature) around 30 minutes to reach stable operation.
3. The digital controllers (I and II) should be set at the proper injection time (e.g., ~0.5 sec). The regulation of tracer gas pressure should be carried out to obtain responses as per derived impulse time (i.e. the injected mass should be neither too small as it will be affected by the system noise nor too large as it will exceed the detector range).
4. The sampling pump will be turned on and the sample gas i.e. helium flow rate will be set at 1.0 SCFH (standard cubic feet per hour) by adjusting the sample rotameter to the TCD.
5. The reference gas i.e. N_2 (ultra high purity grade) pressure will be regulated at 50 psi. The reference gas rotameter to the TCD will be adjusted to achieve the flow rate as 1.0 SCFH.
6. After setting both the reference and the sample gas flows to the TCD, the gas analyzer will be powered. The settings on the gas analyzer should be as follows:

- POLARITY nap (positive or negative) is set depending on the thermal conductivity difference of the tracer gas and the reference gas.
- SPAN nap is usually set equal to 10 as long as the signal does not exceed the range of the A/D converter and amplifier.
- ZERO nap is adjusted such that the signal baseline is slightly above the zero reading. This is because the base line can always be adjusted in the data processing, and being slightly above the zero avoids losing data below the zero line during small noise fluctuations.

7. The data acquisition and will be studied turn on the switch of the digital controllers (which starts and repeats the measurements at the pre-set time intervals) will be turned on simultaneously. All the four measurements for given operating conditions should be carried out in one session; one after another (order doesn't matters). It is recommended that same person should perform all the four experimental measurements, shown in Table 3.2, for one set.
8. After the required data is obtained, the data acquisition will be stopped and the digital controllers, gas analyzer, gas pump, and amplifier will be turned off.

APPENDIX B.

THE DEVELOPMENT OF THE INVASIVE FAST RESPONSE HEAT TRANSFER ROD-TYPE PROBE TECHNIQUE, IT'S OPERATING PROCEDURES AND THE OBTAINED RESULTS

1. The Invasive Fast Response Heat Transfer Rod-Type Probe Technique

The developed rod-type heat transfer probe in this work is an invasive fast-response technique that was designed and developed based on the previously made rod-type probe (Wu, 2008) to measure the heat transfer coefficient in single and multiphase flow systems by measuring simultaneously the local instantaneous heat flux from a hot surface sensor to the adjacent bulk, the surface temperature of the sensor and the temperature of the adjacent bulk. The sensor has been selected to be for gas-solid systems (Model No. 20453 (G161)-1, from RDF Corporation). The probe has been used to investigate in more detail the heat transfer coefficient in pebble bed by placing the probe on a number of axial and radial positions inside the bed.

1.1. The Components of the Heat Transfer Technique

A photo of the heat transfer technique components is shown in Figure B.1. The photo shows the fast-response and fixed heat flux sensor heat transfer rod-type probe, DC power supply, amplifier, thermocouple sensor, and data acquisition (DAQ) system and computer. The details of the fast-response heat transfer probe of rode type are presented in the next section and Figure B.2.

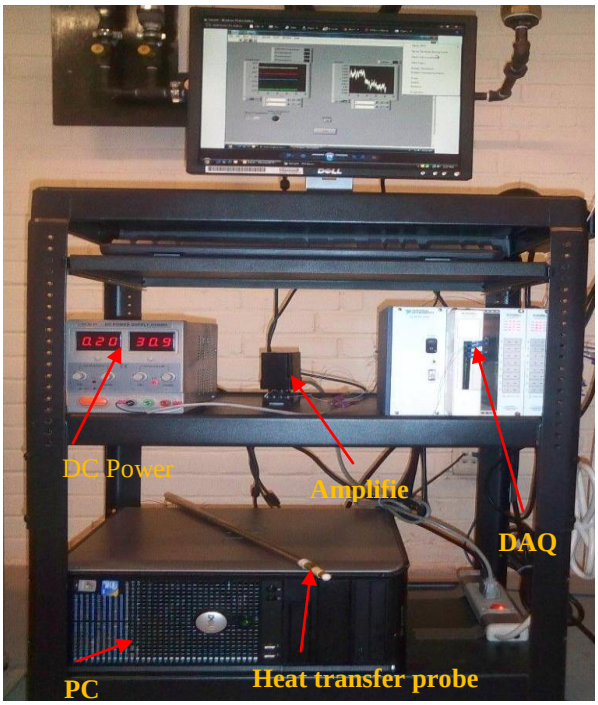

Figure B.1. Components of the Fast-Response Heat Transfer Technique

1.2. The Invasive Fast Response Heat Transfer Rod-Type Probe

A photo and schematic diagram of the fast response heat transfer probe are shown in Figure B.2. A small cartridge heater was installed inside the brass shell of highly thermal conductivity. The DC power was supplied to the cartridge heater by digital variance transformer (Model No. HY-5003, produced by RSR Electronics, Inc) to regulate supplied power in the range of 20–40V. The micro-foil heat flux sensor (11 mm×14 mm×0.08 mm, micro-foil heat flow sensor No. 20453-1, RDF Corporation) for gas-solid system is flush mounted on the brass shell surface and it can measure reliably and simultaneously the local heat flux (q_i) and the probe surface temperature (T_{si}). The two ends of the tube and fittings are Teflon to reduce the heat loss transferred from the heater to the connections. This forms the rod-type heat transfer probe. Figure B.2 b shows the design and components of the rod-type probe. The response time of the sensor is about

0.02 s as given by vendor. The probe location can be changed both axially and radially at different positions in the bed. The thermocouple sensors are arranged at different axial positions and at radial locations to monitor the flowing gas bulk temperature adjacent to the heat transfer sensor.

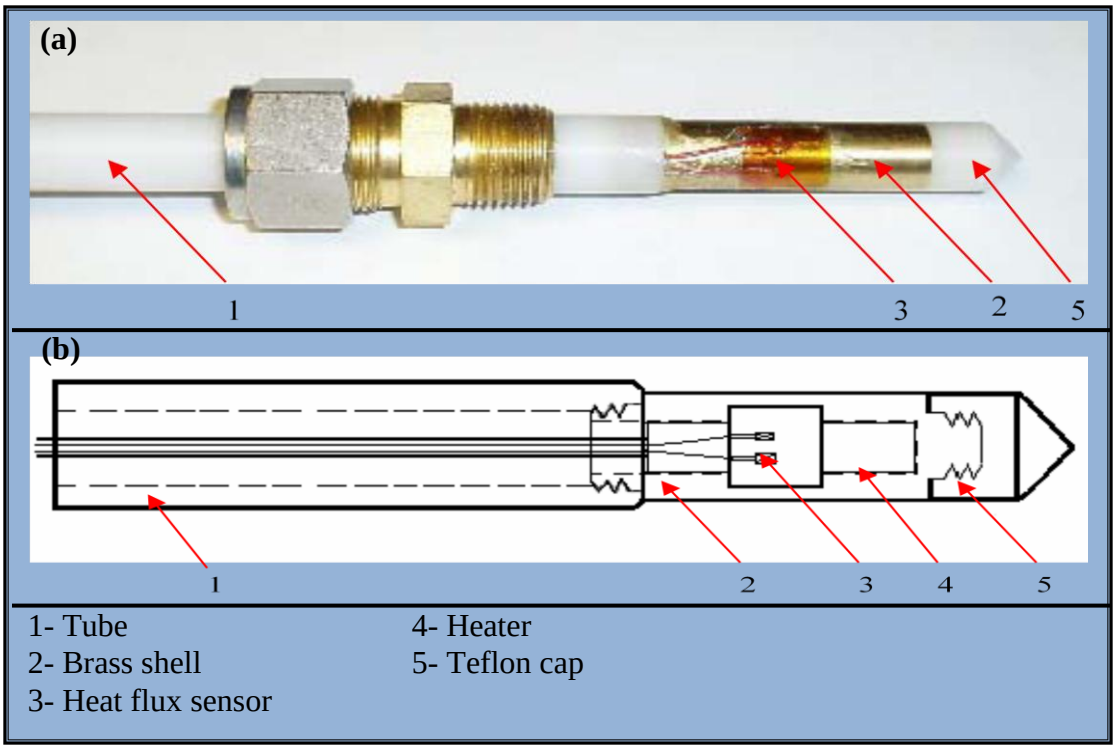

Figure B.2. Fast-Response Heat Transfer Rod-Type Probe: (a) Photography and (b) Schematically

1.3. Data Collections and Analyses

For each experimental run, the surface temperatures and heat flux of the sensor are monitored until the steady state condition is reached. Since the measured signals of the heat flux are in the range of micro-volts, they were amplified before received by the data acquisition (DAQ) system. The heat flux signals and the signals from the thermocouples were sampled simultaneously at 50 Hz for about 40 s. The local instantaneous heat

transfer coefficient between the fixed heat flux sensor at surface temperature (T_{si}) and the surrounding gas phase at temperature (T_{bi}) is obtained by the following relation:

$$h_i = \frac{q_i}{T_{si} - T_{bi}} \quad ; \quad \Delta T_i = T_{si} - T_{bi} \tag{55}$$

Where h_i is the local instantaneous heat transfer coefficient (kW/ m^2.K), q_i is the instantaneous heat flux measured by the sensor (kW/m^2), T_{si} is the instantaneous surface temperature of the probe (K) and T_{bi} is the instantaneous bulk temperature of the media (K).

The local time-averaged heat transfer coefficient (h) at a given location is obtained by averaging the instantaneous heat transfer data over a large number of sampling points as follows:

$$h = \frac{1}{n}\sum_{i=1}^{n}\frac{q_i}{T_{si} - T_{bi}} = \frac{1}{n}\sum_{i=1}^{n} h_i \tag{56}$$

where n is the total number of experimental data points. In this work n of about 2050 sampling points were used to establish a high stable value of heat transfer coefficients for all the operating conditions.

Experimental work was conducted to study the heat transfer in solid-gas packed pebble-bed. In order to assess the experimental error, each of the experimental runs was repeated at least three times. For each run, before any reading was taken, the system was left to equilibrate at the desired superficial gas velocity. The operating procedure of the heat transfer technique is outlined in the next sections.

2. Experimental Setup of Heat Transfer Coefficients based on the Rod-Type Heat Transfer Probe.

The schematic diagram of the heat transfer cold-flow experimental set-up along with the heat transfer technique of rod-type probe and its components are shown in Figure B.3. This experimental set up of the pebble bed for heat transfer measurements is similar to the one used for gas dynamics measurements.

As mentioned in Section 7, a fast-response heat transfer probe of rod-type was developed for gas-solid system to measure the local heat transfer coefficient in the pebble bed. The technique has been developed to meet the experimental work requirements and to provide reliable and detailed heat transfer data. The effect of operating and design conditions on the heat transfer coefficient has been investigated by placing the probe at different axial and radial positions in the bed. The heat transfer probe is introduced horizontally into the pebble bed at different axial locations (Z/D = 0.5, 1.5 and 2.5 from the gas distributor) (Figure B.3). Local probe measurements have carried out at seven radial positions [(r/R): ±0.9 (close to wall of the bed), ±0.60, ±0.3, and 0 (center of the bed)] as illustrated in Figure B.3. The thermocouples are arranged at different axial positions and radial locations to monitor the flowing gas temperature adjacent to the heat transfer probe. To properly insert the probes (heat transfer probe and thermocouples) and to prevent any contact effects between the probe surface and the surface of the pebbles, the test section of the bed has to be structured carefully rather than packed randomly. During the measurements, superficial gas velocity has been varied within the range of 0.01 to 1 m/s which covers both laminar and turbulent flow regimes. The methodology pertinent to heat transfer technique and procedures for obtaining the results were explained in Section 7.

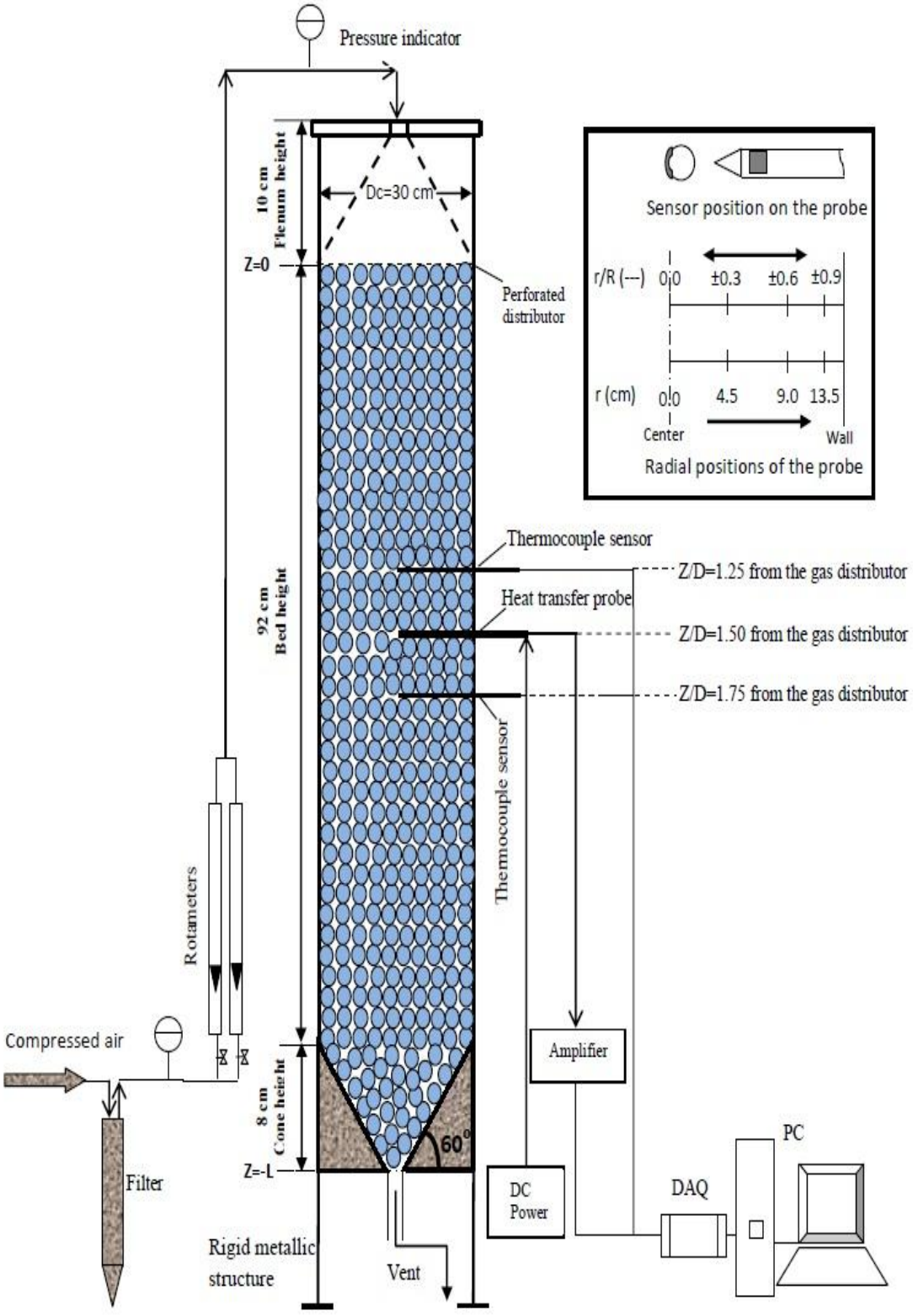

Figure B.3. Schematic Diagram of the Fast-Response Heat Transfer Cold-Flow Experimental Set-Up

3. Operating Procedures for the Heat Transfer Technique

The following steps of operation apply on both heat transfer rod-type and spherical-type probes:

1. Structure carefully rather than packing randomly of the test section of the packed bed and properly insert the heat transfer probe to prevent any contact effects between the surface of the probe sensor and the surface of the pebbles.
2. Mount the temperature thermocouple sensors through the ports of the packed pebble-bed at the desired axial locations and adjusting the radial positions of the probe.
3. Properly connect the power input lines of the heater in the heat transfer probe to the DC power supply.
4. Connect the thermocouple wires of the microfilm sensor to one of the channels numbered from 0 to 7 in the SCXI-1303 terminal block.
5. Connect the heat flux sensor wires to the input of the amplifier, and then connect the output of the amplifier to one of the channels numbered from 8 to 32 in the SCXI-1303 terminal block.
6. Connect the thermocouple wires of the bulk thermocouples to one of the channels numbered from 0 to 7 in the SCXI-1303 terminal block.
7. Operate the packed pebble-bed at the designed condition for 10 minutes, and then switch on the power of the chassis (SCXI-1000) and start the temperature measurement program on the PC.
8. When the system reaches steady state, collect the temperature data several (three) times to obtain the average the temperature difference between the probe surface and the bulk.

9. Switch on the DC power supply of the heater and the power of the amplifier, and then start the heat flux measurement program on the PC.
10. After 10-20 minutes, when the signal of heat flux becomes stable, collect both the heat flux data and the temperature data simultaneously using the heat flux measurement program.

4. Results and Discussion

It is important to highlight here that in this work, the rode-type probe has been successfully used for acquiring the experimental data of the heat transfer measurements. However, based on the comparison with available correlations and the measurement from another probe of spherical type (Figure 6.B), the obtained experimental data were questionable. This is due to the probe shape and geometry, where it disturbs the gas flow around the pebbles and around the probe itself when it is placed inside the bed. This could be obvious from the results where the heat transfer coefficients reach plateau at about 30 cm/s gas velocity. This happens since the flow structure around the sensor remains unchanged at gas velocity of 30 cm/s and higher due to the structure of the bed (void) around the surface of the probe sensor. Therefore, the measurements obtained do not represent the proper heat transfer coefficient inside the bed. For this reason, another novel heat transfer probe of spherical type as a non-invasive technique has been developed and implemented (Section 7). This has also been done in order to mimic an actual heat exchanging surface of heated pebbles in the bubble nuclear packed pebble-bed reactors.

The effect of superficial gas velocity was already investigated at different radial locations at given axial position. Figures B.4 shows the local heat transfer coefficients at

different radial positions from the center (r/R=0.0) of the bed to the near bed wall (r/R=0.9). The heat transfer coefficients in the center region of the bed are smaller than those in the region near wall. The differences vary from 19% to 13% with the increase in the superficial gas velocity from 0.01 to 1 m/s for the center (r/R=0.0) and near the bed wall (r/R=0.9), respectively. The differences at low superficial gas velocities are relatively small whereas at higher superficial gas velocities the differences become larger. At higher gas velocities, heat transfer coefficients reach plateau at about and higher than 0.3 m/s of superficial gas velocity value. In fact, this is not the case of packed- pebble bed reactor, as proven laterally in this work with sophisticated heat transfer technique of a spherical-type probe, that heat transfer coefficients are continuously increased with the gas velocities and the change in heat transfer coefficient with respect to gas velocity reduces at high range of gas velocity due to not much change encounters in the local flow structure around the pebbles at high range of gas velocity. Based on this, it might be the flow around the pebbles was disturbed by the probe geometry and it seems a non flow zone develops where the sensor read a constant surface heat flux and temperature. Hence, the heat transfer coefficients reach a plateau at high range of gas velocities.

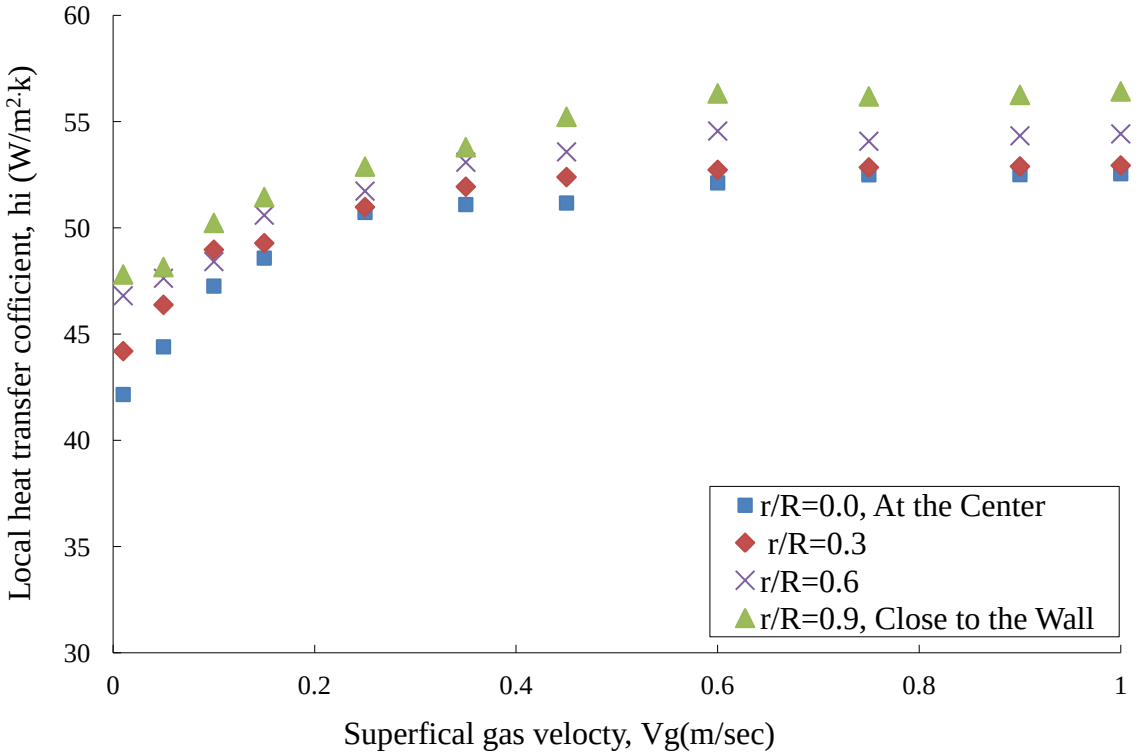

Figure B.4. Radial Profiles of Local Heat Transfer Coefficients at Different Superficial Gas Velocities at Axial Location (Z/D=1.5)

The radial averaged heat transfer coefficient can be obtained from the measured radial heat transfer coefficient profiles, as follows:

$$h_{av} = \frac{2}{R^2}\int_0^R h_i(r)rdr \qquad (1)$$

Figure B.5 shows the radial averaged heat transfer coefficients for different axial positions over a wide range of superficial gas velocities.

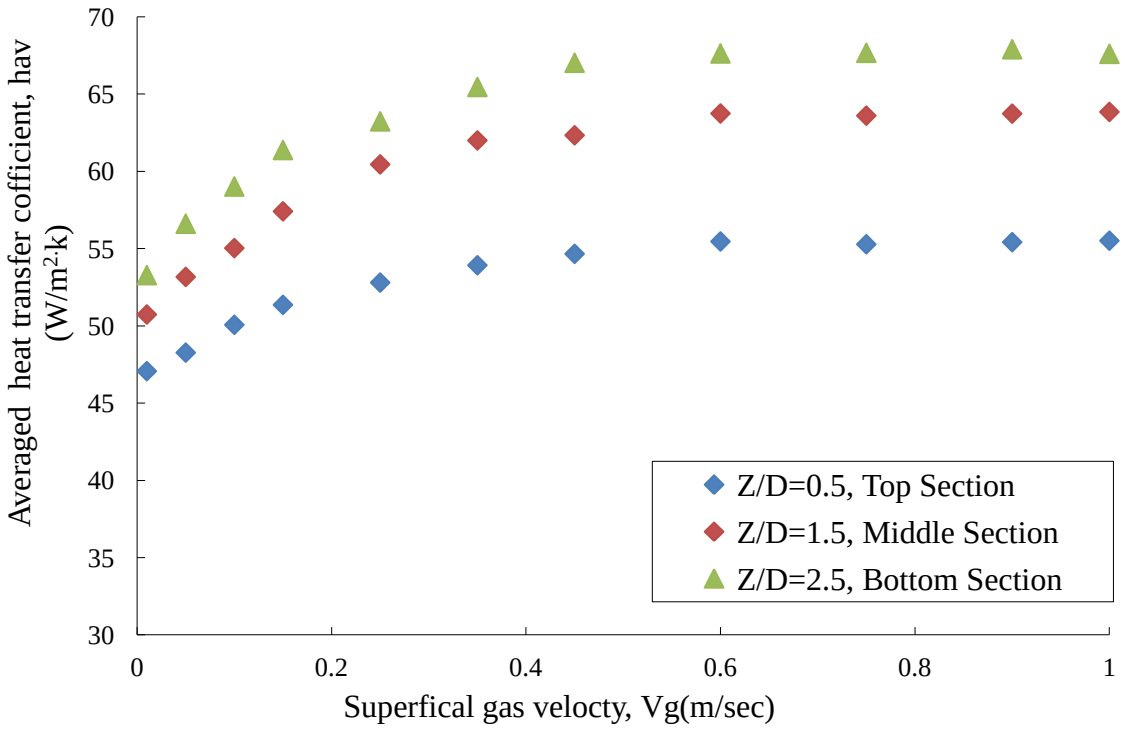

Figure B.5. Effect of Superficial Gas Velocity on the Averaged Heat Transfer Coefficients at Different Axial Locations

It has been found that the effect of superficial gas velocity in terms of trend and magnitude on heat transfer coefficients varies between laminar and turbulent flow regimes for all radial positions. At the middle section (Z/D=1.5) and in the center region of the bed (r/R=0.0), with the increase in the superficial gas velocity (from 0.01 m/s (laminar flow regime) to about 0.4 m/s (turbulent flow regime)) causes an increase in the heat transfer coefficients by about 18%. Not of much change in heat transfer coefficient (about of 3%) has been observed for an increase in superficial gas velocity from 0.4 to 0.6 m/s within turbulent flow regime as the values reach plateau. The change in heat transfer coefficient with respect of the change in superficial gas velocity is large in the

laminar flow regime compared to that in turbulent flow regime. In turbulent regime, such change becomes smaller and reaches plateau at higher superficial gas velocities.

Figure B.6 shows values of pebble-to-gas heat transfer coefficients in terms of Nusselt numbers $\left(Nu = hd_p/k\right)$ at different effective Reynolds numbers. In this Figure the experimental values of averaged local heat transfer coefficients at the middle section (Z/D=1.5) by both rod-type and spherical-type probes which explained in Figure (7.6) and (B.5) , respectively, are compared with those predicted based on four selected correlations, as discussed in Sections 2 and 7. At low flow conditions ($Re_h < 1000$), the values of heat transfer coefficients obtained by rod-type probe do not match well for all empirical correlations and for those obtained by spherical-type probe. In other words, all correlations are under-predicts and there is relatively larger deviation compared with measured heat transfer coefficient by spherical-type probe (AARE is about 74 %) for low flow conditions, i.e. $Re_h < 1000$. However, at high Reynolds numbers ($Re_h > 1000$), the trends and the values of heat transfer coefficients obtained by rod-type probe do not match for all correlations and with those measured by spherical-type probe. The heat transfer coefficients reach plateau at about and higher than 1000 of effective Reynolds numbers (Re_h) value. In fact, this is not the case of packed- pebble bed reactor, as shown in Figure B.6, that heat transfer coefficients are continuously increased with the gas velocities but a lower rate of change at high range of gas velocities. As mentioned earlier, based on this, the obtained experimental data by rod-type probe are unreliable. This is due to the probe shape and geometry and its insertion into the bed which affect the bed structure around the probe sensor and the pebble. Hence, the gas flow disturbs around the

probe and the pebbles. Therefore, the measurements obtained do not represent the proper heat transfer coefficients inside of the studied packed pebble-bed.

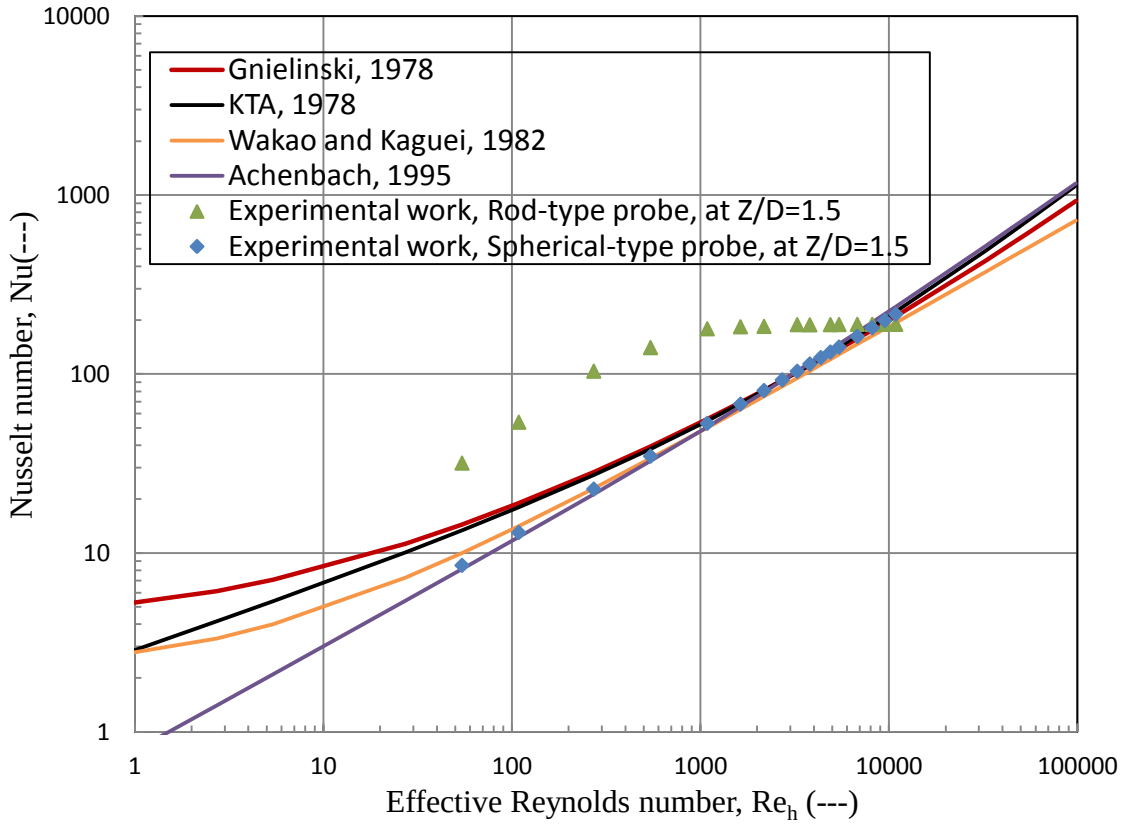

Figure B.6. Comparison of the Measured Average Heat-Transfer Coefficient by both Rod-Type and Spherical-Type Probes with the Empirical Correlations

All the experimental results of the heat transfer coefficients obtained by the rod-type heat transfer probe are reported and tabulated in the next sections.

4.1. Radial Averaged Heat Transfer Coefficients for Pebbles of 5 cm in Diameter.

Table B-1. Averaged Heat Transfer Coefficients ($W/m^2.K$) at Z/D=0.5

V_g (m/sec)	r/R=0.0	r/R=±0.3	r/R=±0.6	r/R=±0.9
0.01	42.15	44.20	46.80	47.80
0.05	44.40	46.38	47.62	48.15
0.10	47.26	48.97	48.40	50.23
0.15	48.57	49.28	50.59	51.44
0.25	50.72	50.98	51.72	52.88
0.35	51.09	51.93	53.08	53.49
0.45	51.17	52.39	53.57	55.22
0.60	52.11	52.73	54.55	56.32
0.75	52.49	52.84	54.07	56.18
0.90	52.50	52.89	54.33	56.25
1.00	52.55	52.93	54.42	56.41

Table B-2. Averaged Heat Transfer Coefficients (W/m2.K) at Z/D=1.5

V_g (m/sec)	r/R=0.0	r/R=±0.3	r/R=±0.6	r/R=±0.9
0.01	44.45	48.14	50.24	51.14
0.05	48.16	51.37	52.72	52.26
0.10	51.49	52.44	55.60	53.57
0.15	53.45	55.66	56.72	56.48
0.25	55.36	57.77	59.47	60.95
0.35	56.17	58.27	61.59	62.96
0.45	56.48	58.82	61.76	63.21
0.60	58.44	61.06	62.60	64.24
0.75	58.57	61.04	62.11	64.46
0.90	58.87	61.21	62.23	64.52
1.00	59.04	61.34	62.32	64.65

Table B-3. Averaged Heat Transfer Coefficients (W/m2.K) at Z/D=2.5

V_g (m/sec)	r/R=0.0	r/R=±0.3	r/R=±0.6	r/R=±0.9
0.01	46.23	50.23	52.86	54.01
0.05	49.16	54.23	56.26	56.09
0.10	51.68	56.29	58.83	58.54
0.15	54.13	58.24	60.21	62.70
0.25	56.86	59.85	62.36	64.31
0.35	58.37	61.32	64.85	67.01
0.45	59.62	63.25	65.98	68.59
0.60	61.17	63.58	66.83	69.17
0.75	61.17	63.94	66.59	69.19
0.90	61.23	64.03	67.04	69.27
1.00	61.33	63.05	67.21	69.23

4.2. Axial Averaged Heat Transfer Coefficients for Pebbles of 5 cm in Diameter.

Table B-4. Averaged Heat Transfer Coefficients ($kW/m^2.K$) at r/R= 0.0

V_g (m/sec)	Z/D=0.5	Z/D=1.5	Z/D=2.5
0.01	42.15	44.45	46.23
0.05	44.39	48.16	49.16
0.10	47.25	51.49	51.68
0.15	48.57	53.45	54.13
0.25	50.72	55.36	56.86
0.35	51.09	56.17	58.37
0.45	51.16	56.48	59.62
0.60	52.11	58.44	61.17
0.75	52.49	58.57	61.17
0.90	52.52	58.58	61.29
1.00	52.49	58.64	61.35

Table B-5. Averaged Heat Transfer Coefficients (kW/m^2.K) at r/R= ±0.3

V_g (m/sec)	Z/D=0.5	Z/D=1.5	Z/D=2.5
0.01	44.19	48.14	50.23
0.05	46.37	51.37	54.23
0.10	48.96	52.44	56.21
0.15	49.27	55.66	58.24
0.25	50.97	57.77	59.88
0.35	51.93	58.27	61.33
0.45	52.37	58.82	63.23
0.60	52.76	61.06	63.53
0.75	52.85	61.04	63.96
0.90	52.97	61.33	64.07
1.00	52.97	61.43	64.08

Table B-6. Averaged Heat Transfer Coefficients (kW/m^2.K) at r/R= ±0.6

V_g (m/sec)	Z/D=0.5	Z/D=1.5	Z/D=2.5
0.01	46.80	50.24	52.86
0.05	47.62	52.73	56.26
0.10	48.40	55.66	58.35
0.15	50.59	56.78	60.23
0.25	51.72	59.43	62.36
0.35	53.08	61.59	64.85
0.45	53.57	61.76	65.98
0.60	54.55	62.67	66.83
0.75	54.07	62.11	66.59
0.90	54.83	62.81	66.63
1.00	54.93	62.91	66.83

Table B-7. Averaged Heat Transfer Coefficients ($kW/m^2.K$) at r/R= ±0.9

V_g (m/sec)	Z/D=0.5	Z/D=1.5	Z/D=2.5
0.01	47.80	51.14	54.01
0.05	48.15	52.26	56.09
0.10	50.23	53.57	58.54
0.15	51.40	56.48	62.70
0.25	52.88	60.95	64.31
0.35	53.49	62.97	67.01
0.45	55.22	63.21	68.59
0.60	56.32	64.24	69.17
0.75	56.18	64.46	69.19
0.90	56.27	64.53	69.23
1.00	56.18	64.46	69.43

4.3. Heat Transfer Results with Pebbles of Different Diameters at Z/D=1.5

Table B-8. Averaged Heat Transfer Coefficients ($kW/m^2.K$) at Center Region (r/R=0.0)

V_g (m/sec)	d_p= 1.25 cm	d_p= 2.5 cm	d_p= 5 cm
0.01	48.23	49.82	54.43
0.05	49.87	50.32	55.23
0.10	51.86	53.54	57.64
0.15	53.28	54.32	59.39
0.25	55.54	56.53	60.43
0.35	57.81	58.65	61.74
0.45	58.91	59.45	62.39
0.60	59.23	61.32	64.76
0.75	61.65	62.24	66.43
0.90	61.75	62.26	66.49
1.00	61.67	62.25	66.59

Table B-9. Averaged Heat Transfer Coefficients ($kW/m^2.K$) at Wall Region (r/R= ±0.9)

V_g (m/sec)	d_p= 1.25 cm	d_p= 2.5 cm	d_p= 5 cm
0.01	45.23	49.81	55.33
0.05	56.54	59.63	62.61
0.10	58.67	60.32	64.32
0.15	63.42	64.32	66.54
0.25	64.40	66.13	66.84
0.35	65.01	67.44	70.21
0.45	65.37	68.61	71.51
0.60	66.12	69.12	72.72
0.75	68.29	71.23	73.54
0.90	68.32	71.34	73.57
1.00	68.31	71.48	73.59

BIBLIOGRAPHY

Abdulmohsin R, and Al-Dahhan M, Characteristics of Heat Transfer in a Packed Pebble-Bed Reactor. Transactions of the American Nuclear Society 2012, Vol 107, pp. 1330-1332.

Abdulmohsin R, and Al-Dahhan M, Axial Gas Dispersion and Heat Transfer Coefficient in a Pebble Bed Reactor. Transactions of the American Nuclear Society 2011a, Vol 105, pp. 972-974.

Abdulmohsin R, and Al-Dahhan M, Axial Gas Dispersion in a Pebble Bed Reactor: Effect of Pebble Size. Transactions of the American Nuclear Society 2011b, Vol 104, pp. 987-989.

Abdulmohsin R, Ali N and Al-Dahhan M, Heat Transfer Coefficient in a Pebble Bed Reactor (PBR). Transactions of the American Nuclear Society 2011, Vol 104, pp. 984-986.

Achenbach E, Heat Transfer and Pressure Drop of Pebble Beds Up to High Reynolds Number. 7th International Heat Transfer Conference 1982, pp. 3–8.

Achenbach E, Heat and Flow Characteristics of Packed Beds. Experimental Thermal and Fluid Sciences 1995, Vol 10, pp. 17–27.

Aris R, and Amundson N, Some Remarks on Longitudinal Mixing or Diffusion in Fixed Beds. AIChE Journal 1957, Vol.3, pp. 280-282.

Bai H, Theuerkauf J, Gillis P, and Witt P, A Coupled DEM and CFD Simulation of Flow Field and Pressure Drop in Fixed Bed Reactor with Randomly Packed Catalyst Particles. Ind. Eng. Chem. Res. 2009, Vol 48, pp.4060–4074.

Barthels H, Pressure Drop in Pebble Beds. Fuel Combined Heat and Power 1972, Vol.24, pp.233- 236.

Barthels H, Flow Rate in the Boundary Zone of Pebble Beds. Internal Report IB-8-77 1977, KFA Jülich / IRB

Barjaktarovic B, Sovilj M, and Popovic S, Hydrodynamics and Axial Mixing in a Packed Gas-Liquid Column. BIBLID 2003, Vol 34, pp. 33-48.

Bazant, M, Modeling and Simulation of Granular Flow in Pebble Bed Nuclear Reactors. Final Report, MIT 2006.

Becker S and Laurien E, Numerical Simulation of the Convective Heat Transport in Pebble Beds at High Temperatures. Proceedings of the Annual Meeting Nuclear Technology 2001, Dresden, Germany, May 14–17.

Becker S and Laurien E, Three-Dimensional Numerical Simulation of Flow and Heat Transport in High-Temperature Nuclear Reactors. Nuclear Engineering and Design 2003, Vol 222, pp. 189–201.

Benenati R, and Brosilow C, Void Fraction Distribution in Beds of Spheres. AIChEJ 1962, Vol 8, pp. 233-236.

Benneker A, Kronberg A, and Westerterp K, Longitudinal Mass and Heat Dispersion in Tubular Reactors. Industrial and Engineering Chemistry Research 1997, Vol 36, pp. 2031-2041.

Bird R, Stewart W, and Lightfoot E, Transport Phenomena. 2nd Ed, John Wiley& Sons Inc, 2002 New York, USA.

Bischoff K, Fluid Dispersion, Generalization and Comparison of Mathematical Models, Illinois Institute of Technology 1961, PhD thesis, Chicago, IL.

Bischoff K and Levenspiel O, Fluid Dispersion-Generalization and Comparison of Mathematical Models-I: Generalization of Models. Chem. Eng. Sci. 1962a, Vol 17, pp. 245-255.

Bischoff K and Levenspiel O, Fluid Dispersion-Generalization and Comparison of Mathematical Models-II: Comparison of Models. Chem. Eng. Sci. 1962b, Vol 17, pp. 257-264.

Bischoff K and McCracken E, Tracer Tests in Flow Systems. Ind. Eng. Chem. 1966, Vol 58, pp. 18–31.

Blackwell R J, Rayne J R, and Terry W M, Factors Influencing the Efficiency of Miscible Displacement. Petroleum Transactions AIME 1959, Vol 216, pp.1–8

Boudreau B, The Diffusive Tortuosity of Fine-Grained Unlithified Sediments. Geochimica et Cosmochimica Acta 1996, Vol 60, pp. 3139–3142.

Burke S, and Plummer W, Gas Flow through Packed Columns. Ind. Eng. Chem. 1928, Vol 20, pp. 1196–1200.

Carberry J J, and Bretton R H, Axial Dispersion of Mass in Flow through Fixed Beds. AIChE Journal 1958, Vol 4, pp.367–375

Carman P, Fluid Flow through Granular Beds. Trans. Inst. Chem. Engrs. 1937, Vol 15, pp.150–166.

Carman P, Flow of Gases through Porous Media. Butterworths Scientific Publications 1956, London-UK.

Chao R and Hoelscher H, Simultaneous Axial Dispersion and Adsorption in Packed Beds. AIChE Journal 1966, Vol 12, pp. 271–278.

Cheng P, and Hsu C, Fully-Developed, Forced Convection Flow Through an Annular Packed-Sphere Bed With Wall Effects. International Journal of Heat and Mass Transfer 1986, Vol 29, pp.1843–1853.

Claxton K, A Review of Pebble Bed Reactors and the Characteristics of Packed Beds. Journal of Nuclear Energy Parts A/B 1966, Vol 20, pp. 735-777.

Cohen, Y., Metzner, A.B., 1981.Wall Effects in Laminar Flow of Fluids through Packed Beds. AIChE J. 8, 359–361.

Danckwerts P, Continuous Flow Systems: Distribution of Residence Times. Chem. Eng. Sci. 1953, Vol 2, pp. 1-15.

de Klerk A, Voidage Variation in Packed Beds at Small Column to Particle Diameter Ratio. AIChE Journal 2003, Vol 49, pp. 2022–2029.

Degaleesan, S, Turbulence and Liquid Mixing in Bubble Columns. D.Sc. Thesis 1997, Washington University in St. Louis, Saint Louis, Missouri, USA.

Delgado J, A Critical Review of Dispersion in Packed Beds. Heat Mass Transfer 2006, Vol 42, pp. 279–310.

du Toit C, The Pebble-Bed Reactor: Effect of Wall Channeling on The Flow in the Core, Kruger Park 2002, South Africa .

du Toit, C, Radial Variation in Porosity in Annular Packed Beds. Nuclear Engineering and Design 2008, Vol 238, pp.3073–3079.

du Toit C, and Rousseau P, Modeling the Flow and Heat Transfer in a Packed Bed High Temperature Gas-Cooled Reactor in the Context of Systems CFD Approach. Journal of Heat Transfer 2012, Vol 134, pp. 031015-1.

Edwards M, and Richardson F, Gas Dispersion in Packed Beds. Chem. Eng. Sci. 1968, Vol 23, pp. 109–123.

EIA, International Energy Outlook 2011. Energy Information Administration (EIA), 2011.

Eisfeld B, Pseudo-Continuous Modeling of the Flow in Packed Bed Reactors. PhD Dissertation 1999, Brandenburg University of Technology Cottbus, Germany.

Eisfeld B, and Schnitzlein K, The Influence of Confining Walls on The Pressure Drop in Packed Beds. Chem. Eng. Sci. 2001, Vol 56, pp. 4321–4329.

Ergun S, Fluid Flow through Packed Columns. Chemical Engineering Progress 1952, Vol. 48, pp.89-94.

Evans E V, and Kenney C N, Gaseous Dispersion in Packed Beds at Low Reynolds Numbers. Trans Inst Chem Engr 1966, Vol 44, pp.T189–T197.

Fan L-S, and Zhu C, Principles of Gas-Solid Flows. 1st Ed, Cambridge University Press 1998, New York, USA.

Fenech H, Heat Transfer and Fluid Flow in Nuclear Systems. 1st Ed. Pergamon Press 1981, New York, USA.

Frewer, H, Keller, W, and Pruschek, R, The Modular High-Temperature Reactor. Nucl. Sci. Eng. 1985 , Vol 90, pp.411–426.

Fogler H, Elements of Chemical Reaction Engineering. 4th Ed. John Wiley & Sons Inc 2005, New York, pp. 867-1005.

Gerwin H, Scherer, W, and Teuchert, E , The TINTE Modular Code System for Computational Simulation of Transient Processes in the Primary Circuit of a Pebble Bed High-Temperature Gas-Cooled Reactor. Nuclear Science and Engineering 1989, Vol 103, pp. 302-312.

Gnielinski V, Formula for Calculating the Heat and Mass Transfer In Through Flow of a Fixed Bed at Medium and Large Peclet. Process-Technology 1978, Vol 12, pp. 63-366.

Gnielinski V, Equations for the Calculation of Heat and Mass Transfer during Flow through Stationary Spherical Packings at Moderate and High Peclet Numbers. Int. Chem. Eng. 1981, Vol 21, pp. 378-383.

Gnielinski V, Fluid-Particle Heat Transfer in Flow through Packed Beds of Solids. VDI Heat Atlas 2010, 2nd Ed, Springer, Heidelberg, Vol G9, pp. 743–744.

Goodjohn, A, Summary of Gas-Cooled Reactor Programs. Energy 1991, Vol. 16, pp. 79–106.

Goodling J, Vachon R Stelpflug W, and Ying S, Radial Porosity Distribution in Cylindrical Beds Packed with Spheres. Powder Technology 1983, Vol 35, pp.23–29.

Gougar H, The Application of the PEBBED Code Suite to the PBMR-400 Coupled Code Benchmark – FY 2006 Annual Report. Idaho National Laboratory 2006, INL/EXT-06-11842.

Gougar H, Ougouag A, Moore R and Terry W, Conceptual Design of a Very High Temperature Pebble-Bed Reactor. ANS Winter Meeting 2003, Idaho National Engineering and Environmental Laboratory (INEEL)/CON-03-00792.

Guedes J, and Delgado J, Overall Map and Correlation of Dispersion Data for Flow through Granular Packed Beds. Chem. Eng. Sci. 2005, Vol 60, pp. 365 –375.

Guedes J, and Delgado J, The Effect of Fluid Properties on Dispersion in Flow Through Packed. AIChE Journal 2003, Vol 49, pp. 1980 –1985.

Gunn D, Theory of Axial and Radial Dispersion in Packed Beds. Trans IChemE. 1969, Vol 47, pp. T351–T359.

Gunn D. Axial and Radial Dispersion in Fixed Beds. Chem. Eng. Sci. 1987, Vol 42, pp. 363–373.

Gunn D, an Analysis of Convective Dispersion and Reaction in the Fixed-Bed Reactor. International Journal of Heat and Mass Transfer 2004, Vol 47, pp. 2861-2875.

Gunn D and Pryce C, Dispersion in Packed Beds. Trans IChemE 1969 , Vol 47, pp. T341–T350

Gupta S, Chaube R and Upadhyay S, Fluid Particle Heat Transfer in Fixed and Fluidized Beds. Chem Engineering Science 1974, Vol 29, pp 839–843.

Hahn W, and Achenbach E, Determination of the Wall Heat Transfer Coefficient in Pebble Beds. Research Center Jülich (KFA) report 1986, Juel-2093, Jülich, Germany.

Hamed M, Hydrodynamics, Mixing, and Mass Transfer in Bubble Columns with Internals. Washington University in St. Louis, PhD Dissertation 2012, St. Louis MO, USA.

Han L, Slurry Bubble Column Hydrodynamics. Washington University in St. Louis, D.Sc. Dissertation 2007, St. Louis MO, USA.

Hassan Y, Large Eddy Simulation in Pebble Bed Gas Cooled Core Reactors. Nuclear Engineering and Design 2008, Vol 238, pp. 530–537.

Hassan Y, and Dominguez-Ontiveros, E, Flow Visualization in a Pebble Bed Reactor Experiment Using PIV and Refractive Index Matching Techniques. Nuclear Engineering and Design 2008, Vol 238, pp. 3080-3085.

Hassan Y and Kang C, Pressure Drop in a Pebble Bed Reactor under High Reynolds Number. Nuclear Technology 2012, Vol. 180, pp. 159-173.

Hiby J W, Longitudinal Dispersion in Single-Phase Liquid Flow through Ordered and Random Packings. Interact between Fluid &Particles (London Instn Chem Engrs), pp.312–325.

Hlushkou D and Tallarek U, Transition from Creeping Via Viscous-Inertial to Turbulent Flow in Fixed Beds. Journal of Chromatography A 2006, Vol 1126, pp.70-85.

Hoogenboezem T, Heat Transfer Phenomena in Flow through Packed Beds. North-West University, PhD Dissertation 2007, South Africa.

Huda M and Obara T, Development and Testing of Analytical Models for the Pebble Bed Type HTRs. Annals of Nuclear Energy 2008 , Vol 35, pp.1994-2005.

Hunt M, and Tien C, Non-Darcian Flow, Heat and Mass Transfer in Catalytic Packed Bed Reactors. Chemical Engineering Science 1990, Vol 45, pp.55–63.

Jess A, Kragl U and Wasserschei P, Chemical Technology: An Integral Textbook. Vch Pub, 2013, 1st Ed. England UK.

Johnson G W, and Kapner R S, The Dependence Of Axial Dispersion on Non-Uniform Flows in Beds of Uniform Packing. Chem Eng Sci 1990, Vol 45, pp.3329–3339.

Kadak, A, and Berte, M, Modularity in Design of the MIT Pebble Bed Reactor. Winter American Nuclear Society Meeting 2001, Reno, Nevada, USA.

Kang C, pressure drop in a pebble bed reactor. MS Thesis 2010, Texas A&M University, Texas.

Kaviany W, Principles of Heat Transfer in Porous Media. 2nd Ed, Springer 1995, New York.

Kim H, Lee J, and No H, Thermal Hydraulic Behavior in the Deteriorated Turbulent Heat Transfer Regime for a Gas-Cooled Reactor. Nuclear Engineering and Design 2010, Vol 240, pp. 783–795

Kramers H, and Alberda G, Frequency Response Analysis of Continuous Flow Systems. Chem. Eng. Sci. 1953, Vol 2, pp. 173-186.

Kronberg A and Westerterp K, Nonequilibrium Effects in Fixed-Bed Interstitial Fluid Dispersion. Chemical Engineering Science 1999, Vol. 54, pp. 3977-3993.

Koster A, Matzner H and Nicholsi D, PBMR Design for the Future. Nucl. Eng. Des. 2003, Vol 222, pp.231–245.

Kozeny J, Uber Kapillare Leitung Des Wassers in Boden. Sitzungsber Akad, Wiss. Wien Math. Naturwiss. Kl. 1927, Vol 13: pp. 271–306 (in German).

KTA Standards, Reactor Core Design of High-Temperature Gas-Cooled Reactors. Nuclear Safety Standards Commission 1986: 3102.1 (1978), 3102.2 (1983), 3102.3 (1981).

KTA Standards, Reactor Core Design of High Temperature Gas-Cooled Reactors, Part 1: Calculation of the Material Properties of Helium. Nuclear Safety Standards Commission 1978, 3102.1, Salzgitter, Germany.

KTA Standards, Reactor Core Design of High Temperature Gas-Cooled Reactors, Part 2: Heat Transfer in Spherical Fuel Elements. Nuclear Safety Standards Commission 1983, 3102.2 Salzgitter, Germany.

KTA Standards, Reactor Core Design of High-Temperature Gas-Cooled Reactors, Part 3: Loss of Pressure through Friction in Pebble Bed Cores. Nuclear Safety Standards Commission 1981, 3102.3 Salzgitter, Germany.

Langer G, Roethe A, Roethe K P, and Gelbin D, Heat and Mass-Transfer in Packed-Beds-III. Axial Mass Dispersion. Int J Heat Mass Transfer 1978, Vol 21, pp.751–759

Lanfrey P, Kuzeljevic Z, Dudukovic M, Tortuosity Model for Fixed Beds Randomly Packed with Identical Particles. Chem. Eng. Sci. 2010, Vol 65, pp.1891–1896.

Lee J, and Lee, S, Flow Visualization in the Scaled Up Pebble Bed of High Temperature Gas-Cooled Reactor Using Particle Image Velocimetry Method. J. Eng. Gas Turbines Power 2009, Vol 131, pp. 064502(1-4).

Lee J, Park G, Kim K, and Lee W, Numerical Treatment of Pebble Contact in the Flow and Heat Transfer Analysis of a Pebble Bed Reactor Core. Nuclear Engineering and Design 2007, Vol 237, pp. 2183–2196.

Levenspiel O, Chemical Reaction Engineering. 3rd Ed. John Wiley & Sons Inc 1999, New York, pp. 255-365.

Levenspiel O, and Bischoff K, Patterns of Flow in Chemical Process Vessels. Adv. Chem. Eng. 1963, Vol. 4, Academic Press, New York, USA.

Levenspiel O, and Smith W, Notes on The Diffusion-Type Model for the Longitudinal Mixing of Fluids in Flow. Chem. Eng. Sci. 1957, Vol 6, pp. 227–233.

Li Y, Xu Y and Jiang S, DEM Simulations and Experiments of Pebble Flow with Mono-Sized Spheres. Powder Technology 2009, Vol 193, pp. 312-318.

Liao H-T,and Shiau C-Y, Analytical Solution to an Axial Dispersion Model for the Fixed-Bed Adsorber. AIChE Journal 2004, Vol. 46, pp. 1168-1176.

Lohnert G, and Reutler H, The modular HTR – a New Design of High-Temperature Pebble-Bed Reactor. Nucl. Energy 1983, Vol 22, pp.3.

MacMullin R and Weber M, The Theory of Short-Circuiting in Continuous-Flow Mixing Vessels in Series and Kinetics of Chemical Reactions in Such Systems. Trans. AIChE 1935, Vol 31, pp. 409–458.

Martin H, Low Peclet number Particle-To-Fluid Heat and Mass Transfer in Packed Beds. Chemical Engineering Science 1978, Vol 33, pp. 913–919.

Melese G, and Katz R, Thermal and Flow Design of Helium-Cooled Reactors. ANS 1984.

Molerus O, Principles of Flow in Dispersive Systems. Chapman and Hall 1993, London UK.

Mueller G, Prediction of Radial Porosity Distributions in Randomly Packed Fixed Beds of Uniformly Sized Spheres in Cylindrical Containers. Chemical Engineering Science 1991, Vol 46, pp.706–708.

Mueller G, Radial Void Fraction Distribution in Randomly Packed Fixed Beds of Uniformly Sized Spheres in Cylindrical Containers. Powder Technology 1992, Vol 72, pp. 269–275.

Mueller G, Radial Void Correlation for Annular Packed Beds. AIChE Journal 1999, Vol 45, pp. 2458–2460.

Mueller G, Narrow Annular Packed-Bed Radial Void Fraction Correlation. AIChE Journal 2002, Vol 48, pp. 644–647.

Mueller G, Numerically Packing Spheres in Cylinders. Powder Technology 2005, Vol 159, pp.105–110.

Mueller G, Radial Porosity in Packed Beds of Spheres. Powder Technology 2010, Vol 203, pp. 626–633.

Mueller G, A Simple Method for Determining Sphere Packed Bed Radial Porosity. Powder Technology 2012, Vol 229, pp.90–96.

Nelson P and Galloway T, Particle-to-Fluid Heat and Mass Transfer in Dense Systems of Fine Particles. Chem. Eng. Sci. 1975, Vol. 30, pp. 1-6.

Nield D, Alternative Model for Wall Effect in Laminar Flow of Fluid through a Packed Column. AIChE Journal 1983, Vol 29, pp.688-689.

Nauman E, Chemical Reactor Design, Optimization, and Scale up. 2nd Ed, John Wiley & Sons 2008, New York, USA.

Nauman E, and Buffham B, Mixing in Continuous Flow Systems. 1st Ed, John Wiley & Sons 1983, New York, USA.

Perkins T K, Johnston O C, A Review of Diffusion and Dispersion in Porous Media. Soc Petrol Engrs 1963, Vol J, pp.70–84

Ranz W, Friction and Transfer Coefficients for Single Panicles and Packed Beds. Chem. Eng. Progr. 1952, Vol 48, pp. 247-53.

Reddy R, and Joshi J, CFD Modeling of Pressure Drop and Drag Coefficient in Fixed and Expanded Beds. Chemical Engineering Research and Design 2008, Vol 86, pp. 444-453.

Reddy R, and Joshi J, CFD Modeling of Pressure Drop and Drag Coefficient in Fixed Beds: Wall Effects. Particuology 2010, Vol 8, pp. 37-43.

Reichelt W, Calculation of Pressure Drop in Spherical and Cylindrical Packings for Single-Phase Flow. Chemie-Ingenieur-Technik 1972, Vol 44, pp. 1068-1071.

Reitsma F, Thermal Fluid Characteristics for Pebble Bed HTGRs. IAEA Course on High temperature Gas Cooled Reactor Technology 2012, Beijing, China

Ridgway K, and Tarbuck K, Radial Voidage Variation in Randomly-Packed Beds of Spheres of Different Sizes. Journal of Pharmacy and Pharmacology 1966, Vol 18, pp.168S–175S.

Ridgway K, and Tarbuck K, Voidage Fluctuations in Randomly-Packed Beds of Spheres Adjacent to a Containing Wall. Chemical Engineering Science 1968, Vol 23, pp.1147–1155.

Rimkevicius S, Vilemas J, and Uspuras E, Experimental Investigation of Heat Transfer and Flow Mixing in Pebble Beds. Heat Transfer Engineering 2006, Vol 27, pp. 9–15.

Rimkevicius S, and Uspuras E, Experimental Investigation of Pebble Beds Thermal Hydraulic Characteristics. Nuclear Engineering and Design 2008, Vol 238, pp. 940–944.

Roblee L, Baird R, and Tierney J, Radial Porosity Variations in Packed Beds. AIChE Journal 1958, Vol 4, pp.460-464.

Rousseau P, and Van Staden, M, Introduction to the PBMR Heat Transfer Test Facility. Nuclear Engineering and Design 2008, Vol 238, pp. 3060–3072.
Rowe P, and Claxton K, Heat and Mass Transfer from a Single Sphere to Fluid Flowing Through an Array. Trans. Inst. Chem. Engr. 1965, Vol 4, pp. T321-T328.

Rycroft C, Multi-scale Modeling in Granular Flow. Massachusetts Institute of Technology (MIT), PhD Thesis 2007.

Saravanathamizhan R, Balasubramanian N and Srinivasakannan C, Comparison of Tanks-In-Series and Axial Dispersion Models for an Electrochemical Reactor. Journal of Modeling and Simulation of Systems 2010, Vol.1, pp. 171-175.

Seker V and Downar T, Multi-physics Methods Development for High Temperature Gas Cooled Reactor Analysis. International Conference on Emerging Nuclear Energy Systems (ICENES) 2007, June 3 – 8, Istanbul, Turkey.

Schroder E, Class A, and Krebs L, Measurements of Heat Transfer between Particles and Gas in Packed Beds at Low to Medium Reynolds Numbers. Experimental Thermal and Fluid Science 2006, Vol 30, pp. 545–558.

Schulten R, Pebble-Bed HTRs. Ann. Nucl. Energy 1978, Vol 5 , pp.357–374.

Scott D S, Lee W, and Papa J, The Measurement of Transport Coefficients in Gas–Solid Heterogeneous Reactions. Chem Eng Sci 1974, Vol 29, pp.2155–2167

Sherwood T, Pigford R, Wilke C, Mass Transfer. International Student Edition. McGraw-Hill 1975, Kogakusha.

Sinclair R J and Potter O E, The Dispersion of Gas in Flow through a Bed of Packed Solids. Trans IChemE 1965, Vol 43, pp.T3–T9

Sodre J, and Parise J, Fluid Flow Pressure Drop through an Annular Bed of Spheres with Wall Effects. Experimental Thermal and Fluid Science 1998, Vol 17, pp.265–275.

Stainsby R, Worsley M, Dawson F, Dennier A, Baker J, Grief A, and Coddington P, Development of Local Heat Transfer Models for Safety Assessment of Pebble Bed High Temperature Gas-Cooled Reactor Cores. Proceedings of the 14th International Topical Meeting on High Temperature Reactor Technology 2008, HTR2008-58293, Washington DC, USA.

Stainsby R, Worsley M, Dawson F, Baker J, Grief A, Coddington P, and Dennier A, Development of Local Heat Transfer Models for the Safety Assessment of High Temperature Gas-Cooled Reactor Cores- Part I: Pebble Bed Reactors. Journal of Engineering for Gas Turbines and Power 2010a, Vol 132, 012906-1-9.

Stainsby R, Worsley M, Dawson F, Baker J, Grief A, Coddington P, and Dennier A, Development of Local Heat Transfer Models for The Safety Assessment of High Temperature Gas-Cooled Reactor Cores- Part II: Prismatic Modular Reactors. Journal of Engineering for Gas Turbines and Power 2010b, Vol 132, pp. 012907-1-8.

Stroh K, Jiacoletti R, and Olson H, Thermal-hydraulic Analysis Techniques for Axisymmetric Pebble Bed Reactor Cores. Nuclear Engineering and Design 1979, Vol 52, pp. 343-347.

Szomanski E and Aust M, Paced Beds, Their Dynamics, Structure, Fluid Flow, Heat Transfer and other Characteristics. The Third Australian Conference on Hydraulics and Fluid Mechanics 1968, 25th-29th November, Sydney-Australian.

US DOE. A Technology Roadmap for Generation IV Nuclear Energy Systems. Nuclear Energy Research Advisory Committee and the Generation IV International Forum, 2002.

Tang D, Jess A, Ren X, Bluemich B, and Stapf S, Axial Dispersion and Wall Effects in Narrow Fixed Bed Reactors: A Comparative Study Based on RTD and NMR Measurements. Chemical Engineering & Technology 2004, Vol 27, pp. 866–873.

Tsotsas E, Heat and Mass Transfer in Packed Beds with Fluid Flow. VDI Heat Atlas 2010, 2nd Ed, Springer, Heidelberg, Vol M7, pp. 1327–1341.

Tsotsas E, and Martin H, Thermal Conductivity of Packed Beds: A Review. Chemical Engineering and Processing 1987, Vol 22, pp. 19-37.

Tsotsas E, and Schlunder E, On Axial Dispersion in Packed Beds with Fluid Flow. Chem. Eng. Process. 1988, Vol 24, pp. 15–31.

Terry W, Modular Pebble-Bed Reactor Project. Annual Report INEEL/EXT-01-01623, 2001.

Terry, W, Gougar, H, and Ougouag, O, Novel Method for the Deterministic Design, Analysis, and Optimization of the In-Core Fuel Cycle of a Recirculating Pebble-Bed Reactor. Ann. Nucl. Energy 2001, Vol 29, pp.1345–1364.

Theuerkauf J, Witt P, and Schwesig, D, Analysis of Particle Porosity Distribution in Fixed Beds Using the Discrete Element Method. Powder Technology 2006, Vol 165, pp. 92–99.

van Antwerpen W, Du Toit C, and Rousseau, P, A Review of Correlations to Model the Packing Structure and Effective Thermal Conductivity in Packed Beds of Mono-Sized Spherical Particles. Nuclear Engineering and Design 2010, Vol 240, pp. 1803-1818.

Vortmeyer D, and Schuster J, Evaluation of Steady Flow Profiles in Rectangular and Circular Packed Beds by a Variational Method. Chemical Engineering Science 1983, Vol 38, pp.1691–1699.

Wakao N, and Kaguei S, Heat and Mass Transfer in Packed Bed. 1st Ed, Gordon and Breach Science Publishers 1982, New York.

Wang D and Lu Y, Roles and Prospect of Nuclear Power in China's Energy Supply Strategy. Nucl. Eng. Des. 2002, Vol 218, p.3-12.

Wen C, and Fan L, Models for Flow Systems and Chemical Reactors. Marcel Dekker 1975, New York, pp. 113–208.

Westerterp K, Dil'man V, and Kronberg A, Wave Model for Longitudinal Dispersion: Development of the Model. AIChE Journal 1995a, Vol 41, pp.2013-2028.

Westerterp K, Dil'man V, and Kronberg A, Wave Model for Longitudinal Dispersion: Analysis and Applications. AIChE Journal 1995b, Vol 41, pp.2029-2039.

Westerterp K, Kronberg A, Benneker A,and Dil'man V, Wave Concept in the Theory of Hydrodynamical Dispersion. Transactions of the Institution of Chemical Engineers 1996, Vol 74, pp. 944-952.

White S, and Tien C, Analysis of Flow Channeling Near the Wall in Packed Beds. Warme- und Stoffubertragung 1987, Vol 21, pp.291–296.

Wirth K, Pressure Drop in Fixed Beds. VDI Heat Atlas 2010, 2nd Ed, Springer, Heidelberg , Vol G9, pp. 1106–1110.

Wu C, Heat Transfer and Bubble Dynamics in Slurry Bubble Columns for Fischer–Tropsch Clean Alternative Energy. Washington University in Saint Louis, Ph.D. Thesis 2008.

Xu Y, and Sun Y, IAEA TCM on High Temperature Gas Cooled Reactor Application and Future Prospects ECN. Petten 1997, the Netherlands, November.

Yesilyurt G,and Hassan Y, LES Simulation in Pebble Bed Modular Reactor Core Through Randomly Distributed Fuel Elements. Proceedings of the International Conference on Global Environment and Advanced Nuclear Power Plants 2003, Kyoto, Japan, September.

Zhang W, Thompsona K, Reed A, and Beenkena, L, Relationship between Packing Structure and Porosity in Fixed Beds of Equilateral Cylindrical Particles. Chemical Engineering Science 2006, Vol 61, pp. 8060 – 8074.

Ziòlkowska I and Ziòlkowski D, Modeling of Gas Interstitial Velocity Radial Distribution over a Cross-Section of a Tube Packed With a Granular Catalyst Bed. Chemical Engineering Science 1993, Vol 48, pp.3283-3292.

VITA

Rahman Shnain Abdulmohsin

Rahman Abdulmohsin was born in Thi-Qar province, Republic of Iraq. He received his Bachelor Science (B.Sc) degree in Chemical Engineering from University of Technology-Baghdad, Iraq in July 1996. He worked for the General Company for Petrochemicals/North Area- Iraq for two years (Oct.1996 – July 1998). He worked as a design engineer of the heat transfer equipments in the State Company for Design & Consultant Industries/Baghdad-Iraq for three years (Aug 1998-Sep 2001). In parallel with that, he also received his Master Science (M.Sc) degree in Chemical Engineering from University of Technology-Baghdad, Iraq in September 2001.

After teaching in University of Technology/Baghdad- Iraq for 6 years, he received his first Doctor of Philosophy (PhD) degree in Chemical Engineering from University of Technology-Baghdad in December 2008. The PhD research has been conducted in the Chemical Reaction Engineering Laboratory (CREL) at Washington University in St. Louis (WUSTL). Since the coursework have been completed at University of Technology-Baghdad/Iraq, the degree had been offered by this university.

Rahman Abdulmohsin entered the PhD program in Department of Chemical and Biochemical Engineering at Missouri University of Science and Technology in the spring of 2010. His main area of research is the gas dynamics and heat transfer of multiphase flow systems. He received his PhD in December 2013.

Rahman Abdulmohsin worked as a senior member of the Very High Temperature Reactor (VHTR) consortium for 5 years (Jan 2009- Dec 2013) in the Department of Chemical and Biochemical Engineering at the Missouri University of Science and Technology.

Rahman Abdulmohsin has published conference and journal papers, some of which are listed in references of this work.

Rahman Abdulmohsin has been a member of the Iraqi Engineers Association (IEA) and Iraqi Scientists Society (ISS) since 1996 and 2010, respectively. He also has been a member of the American Institute for Chemical Engineers (AIChE) and American Chemical Society (ACS) since 2010 and 2011, respectively.